Denny Creek Bridge Stress Investigation

WA-RD 58.1

Final

June 1983

Washington State Department of Transportation
Planning, Research and Public Transportation
in Cooperation with
United States Department of Transportation
Federal Highway Administration

TECHNICAL REPORT STANDARD TITLE PAGE

1. Report No.	2. Government Accession No.	3. Recipient's Catalog No.

4. Title and Subtitle
INVESTIGATION OF THERMAL AND LIVE LOAD STRESSES IN DENNY CREEK VIADUCT

5. Report Date
June, 1983

6. Performing Organization Code

7. Author(s)
Neil M. Hawkins and John H. Clark

8. Performing Organization Report No.
63-1080

9. Performing Organization Name and Address
Department of Civil Engineering
University of Washington, FX-10
Seattle, WA 98195

10. Work Unit No.

11. Contract or Grant No.
Y-2198

12. Sponsoring Agency Name and Address
Washington State Department of Transportation
Highway Administration Building
Olympia, WA 98504

13. Type of Report and Period Covered
Final
October 1980-June 1983

14. Sponsoring Agency Code

15. Supplementary Notes
Study conducted in cooperation with U.S. Department of Transportation, Federal Highway Administration

16. Abstract

The span by span, stage constructed, prestressed concrete box girder bridge, known as the Denny Creek Viaduct, was instrumented during construction with Carlson gages. This report describes information on long term creep and shrinkage strains, and on live load and thermal strains collected using those gages in a two-year period starting approximately two years after completion of the bridge. Relevant literature on creep and shrinkage deformation predictions, live load stress predictions, and thermal load predictions for stage constructed bridges is reviewed. The predictions of accepted state-of-the-art procedures are compared with the strains and temperatures recorded by the Carlson gages. Significant temperature gradient strains, caused by diurnal temperature changes, are reported. A procedure is developed for predicting those temperature-induced strains based on environmental and material property parameters and design scenarios recommended for critical temperature events. The stage constructed cross-section responded to live loads similarly to a homogeneous section. However, tension strains still existed in regions where compression strains were predicted as a result of creep and shrinkage effects.

17. Key Words	18. Distribution Statement
Bridges, box girders, live load stress, thermal stress, creep, shrinkage	

19. Security Classif. (of this report)	20. Security Classif. (of this page)	21. No. of Pages	22. Price
unclassified	unclassified	337	

Form DOT F 1700.7 (8-69)
HWY FORM 341-004 6/72

AN INVESTIGATION OF
THERMAL AND LIVE LOAD STRESSES
IN DENNY CREEK VIADUCT

by
Neil M. Hawkins and John H. Clark

A report to the Washington State Department of Transportation
on Contract No. Y-2198

Department of Civil Engineering
University of Washington
Seattle, Washington 98195

April 1983

TABLE OF CONTENTS

LIST OF TABLES

LIST OF FIGURES

SUMMARY

Purpose

The purpose of this investigation was to improve procedures for the design of large-scale, span-by-span, stage constructed, concrete box girder bridges by investigating, for the Denny Creek Viaduct, the redistribution of construction stresses through shrinkage, and the response of the completed structure to live loads and the stresses caused by diurnal and long-term temperature variations.

Scope

This investigation included (1) a review of archival literature; (2) a review of strain and temperature data collected by Construction Technology Laboratories (CTL) and the Washington State Department of Transportation (WSDOT) during the construction of the Denny Creek Viaduct; (3) the collection of additional data including strain, temperature and environmental data during the period 1980-1982; (4) the collection of strain data during live load tests; (5) interpretation of the significance of the long-term strain data, the live load data, and the environmental data; and (6) the development of recommended procedures for predicting the stresses induced in box girder bridges by temperature variations.

Methodology

This investigation utilized Carlson strain gages installed by CTL during construction of the bridge. The long-term deformation measurements, initiated by CTL with those gages, were continued for two more years in this project. Those gages were also used to monitor the response of the bridge to known truck loads and daily temperature fluctuations. Continuous measurements were made of air temperature and wind speed at the bridge site during periods when

the temperature and strains in the bridge were being recorded. Those temperature and wind speed results were compared to data collected concurrently at the Stampede Pass National Weather Station. Considerable effort was devoted to developing an automatic recording system for the Carlson gages and other sensors. However, that system failed to operate as planned due to electrical noise problems, and strain gage and temperature data were therefore collected by manual techniques.

The significance of the long-term creep and shrinkage data, collected in this study and in the CTL study, was evaluated by comparing observed strains with those expected for the known construction history of the bridge; and the CTL report on their creep and shrinkage studies was reviewed in light of the additional creep and shrinkage studies and temperature studies made in this investigation. Heat flow analyses were made to determine the practicality of predicting the measured temperature in the bridge from environmental data and to establish the critical weather scenarios governing the temperature gradients which should be used for design. Temperatures predicted by the heat flow analyses were compared to the observed temperatures. Temperature distributions obtained from the heat flow analyses were used in conjunction with procedures proposed by the CTL and Priestley to predict concrete strains for a homogeneous uncracked analytical model of the bridge. The strains predicted by those procedures were compared to the strains measured during known temperature scenarios.

Findings

Creep and shrinkage deformations for the instrumented span of the bridge had stabilized by about two years after completion of that span. The degree of redistribution of stresses within the cross-section due to those deformations could be determined only in a qualitative and not a quantitative

sense. Wide differences were found between actual construction procedures and schedules, and those assumed by CTL for their shrinkage and creep studies. Further, in several instances, actual procedures could not be definitively established. Significant tensile strains were still found to exist in the bridge in regions where analyses, that utilized the most likely construction schedule and the measured modulus parameters, indicated that compression strains should have developed as a result of creep and shrinkage effects. It is concluded that the analyses customarily used to predict long-term stress redistribution effects do not adequately account for the redistributions occurring in a structure built by complex methods such as those used for the Denny Creek Viaduct.

The live load tests showed that the span-by-span, stage constructed Viaduct responded to applied loads in the same manner as a homogeneous unit. The live load strains and deformations were in good agreement with those predicted using conventional frame analysis and an uncracked and fully effective cross-section. Under live loads, the deck slab performed well at its discontinuous, transverse edges in spite of the absence of an edge beam. The barrier rail was effective in distributing, in the longitudinal direction, wheel loads placed on the cantilever slab overhang.

Daily changes in ambient air temperature and solar radiation induced stresses in the Viaduct as large as the stresses predicted for full live load. Significant tensile stresses develop daily during periods of warm sunny weather in late summer. Air temperature variations of the same magnitude as those in summer occur during other times of the year. However, those variations are accompanied by lesser amounts of solar radiation and therefore induce lesser tensile stresses than in summer.

Unidimensional heat flow analyses were effective for predicting the magnitude and the variation in the temperatures induced in the bridge by known

weather conditions. Temperatures measured in the bridge agreed reasonably well with those predicted using the observed air temperatures, theoretical solar radiation values for a clear sky adjusted for local topography, an assumed wind speed of 40 mph, and a heat flow analysis based on the numerical integration of the one-dimensional diffusion equation with convective boundary conditions. The heavy traffic on the Viaduct necessitated the use of a wind speed substantially higher than the calm conditions postulated in most analyses. Thus, the temperature gradient appropriate for design is less than that for calm conditions. The strains induced in the bridge due to its observed temperature variations agreed reasonably well with those predicted using Priestley's method for calculating temperature gradient effects. Those effects must be applied to an analytical model of the bridge that includes the restraints provided by frame action.

Recommendations

It is concluded from this study of the Denny Creek Viaduct that the following design recommendations are appropriate for span-by-span, stage constructed, concrete box girder bridges.

1. Creep and Shrinkage Redistribution of Construction Stresses

   1.1. Analyses of the redistribution of construction stresses due to creep and shrinkage effects are subject to large uncertainties in the basic parameters that define those effects and are dependent upon a construction schedule that can only be assumed during the design stage. Any analysis must therefore be interpreted with conservative engineering judgment and should include a variation of at least $\pm$ 33% in the characteristic values of the creep and shrinkage parameters. Testing of

samples of the concrete to be used in the bridge will not reduce the uncertainties in creep and shrinkage effects imposed by the unknown construction schedule. Such testing is, however, desirable to define the characteristic parameters about which the basic variations should be taken.

1.2. The response of stage constructed cross-sections to applied live loads can be calculated similarly to cross-sections cast as a homogeneous unit.

2. Thermal Stresses

2.1. Stresses caused by temperature gradients are significant only at the service load levels. They do not alter the ultimate flexural capacity of the bridge. However, those stresses can, if not considered, induce flexural and diagonal tension cracking, and reduce the durability and repeated load performance of the bridge.

2.2. Temperature gradients develop in concrete bridges in response to daily changes in ambient air temperature and solar radiation.

2.3. Highly simplified methods of analysis for temperature effects, such as those utilized in the CTL report, give a distorted picture of the stresses at the interface between the portions of the structure assumed to be at different temperatures.

2.4. Priestley's method of analysis is an appropriate procedure for determining the response of a bridge to non-uniform temperature distributions over its depth. The reduction in stresses possible due to cracking should be considered, at least qualitatively, when interpreting the results of Priestley's analysis.

2.5. Sufficient mild steel reinforcing should be provided to control changes in steel stress, for both deformed bar and prestressing steels, as a result of cracking of the concrete. Crack width and fatigue behavior will thereby be controlled. As a rule of thumb, approximately 0.3 to 0.5 per cent steel will be required to achieve this control. Additional prestressing steel is not recommended for control of temperature stresses calculated according to methods based on a homogeneous, elastic section.

2.6. The temperature profiles recommended by Priestley are, in general, appropriate for non-uniform temperature analyses. However, the limiting values should be made site-specific through consideration of the known long-term air temperature variations for the site, theoretical solar radiation values adjusted for topography, and wind speed adjusted for traffic and site conditions. For the Denny Creek Viaduct site, a temperature increase over the reference temperature of 40 degrees F (22 degrees C) is appropriate for extreme weather events and 20 degres F (11 degrees C) for weather events combined with partial live load. A temperature decrease from the reference temperature of 15 degrees F (8 degrees C) is appropriate for extreme weather events and 8 degrees F (4 degrees C) for weather events combined with partial live load.

3. Live Loads

3.1. Design procedures for cantilever slabs should be adjusted to include the beneficial distributing effect of the edge beam inherent in the New Jersey barrier curb. Joints in the barrier curb should be eliminated on large scale concrete bridges.

Homberg's influence surface charts (2.15), the "Ontario" method, finite element plate analysis, or empirical distribution factors, for the design of cantilever slabs, are all suitable if applied with good engineering judgment. Finite element plate analysis is the only method which satisfactorily provides for all possible variations in slab and edge beam configuration. Finite element analyses and the "Ontario" method are appropriate for studying the influence of the free edge at expansion joints.

3.2. Conventional frame analysis, in which members are modeled as line elements, will provide satisfactory results for the global response of stage constructed bridges to live loads. Good engineering judgment is required to interpret results at boundary points and in the vicinity of concentrated loads. More elaborate analytical models should be used for detailed studies of behavior in such regions.

3.3. Longitudinal analysis should be performed on the basis of the full cross-section loaded with the total live load, and if appropriate, the effects of torsional shear, and the additional longitudinal moment that accompanies torsion, should be examined by applying an eccentric live load.

4. Future Research

4.1. Temperature distributions in concrete box girder bridges and the accompanying environmental conditions should be measured for a wide variety of bridge sites.

4.2. The temperature distributions that developed for fresh concrete placed against hardened concrete should be measured for a variety of field conditions.

4.3. Available weather recorded for representative weather stations should be analyzed and the statistical parameters characterizing the critical differential temperature event defined probabilistically.

4.4. The load factors appropriate at service levels for combined live load and differential temperature effects should be established through a probabilistic analysis that insures a level of risk compatible with that for the combinations used for design.

4.5. Any research program involving substantial instrumentation under field conditions should be two-phased. The first phase should be a detailed planning and development study for the instrumentation. That phase should be completed prior to any hardware commitment or commitment to the subsequent utilization phase. That planning phase should be funded separately from the hardware acquisition and utilization phase.

1. INTRODUCTION

1.1. Description of the Structure

The Denny Creek Viaduct is located approximately two miles west of the summit of Snoqualmie Pass on Interstate 90, which is the main east-west route in Washington State across the Cascade Mountains. The location of the viaduct is shown in Figure 1.1 and its form in Figure 1.2. The structure's site is on the west slope of the Cascades at an elevation of approximately 2600 feet above sea level. The 20-span, 3620-feet long viaduct traverses a steep, forested, south-facing slope crossing a deep ravine and an avalanche path. A plan and elevation of the structure are shown in Figure 1.3. The typical span length is 188 feet and the height above the ground level varies from 40 feet to 160 feet. The viaduct cross-section is shown in Figure 1.4. It is a single cell concrete box girder of 9-foot depth, which carries a 52-foot wide roadway. The roadway slab varies in thickness from 10 inches to 21 inches and cantilevers 14 feet 6 inches from the exterior face of the web. The distance between the exterior faces of the web is 23 feet at the top and 16 feet at the bottom. The structure is post-tensioned longitudinally and the roadway slab is prestressed transversely. Web reinforcing is mild steel.

The structure was constructed segmentally in a "span-by-span" mode as illustrated in Figures 1.4 and 1.5. The full cross-section was placed in three segments with each segment being constructed in sequence over all or part of a span at different times and even in different construction seasons. Segments were prestressed as soon as they had the necessary strength and could carry the weight of the falsework and the concrete of succeeding stages. A mobile falsework truss was employed to place the initial U-shaped segment that was the bottom slab and webs. That truss was supported from the front of the previously placed and stressed structure and the next foward pier. After this

Stage I segment had been cured and stressed, the truss was moved ahead to the next span. The roadway slab between the webs was then cast as the Stage II segment on formwork supported by the Stage I structure. The cantilever roadway slabs of Stage III were cast on forms supported by falsework riding on the Stage II roadway slab. Stage III concrete was placed in 94-foot lengths and simultaneously on both sides of the bridge centerline. Transverse prestress was applied to the Stage III construction as soon as the concrete reached adequate strength. Non-structural barrier curbs and a 2-inch concrete overlay for the roadway surface completed the construction.

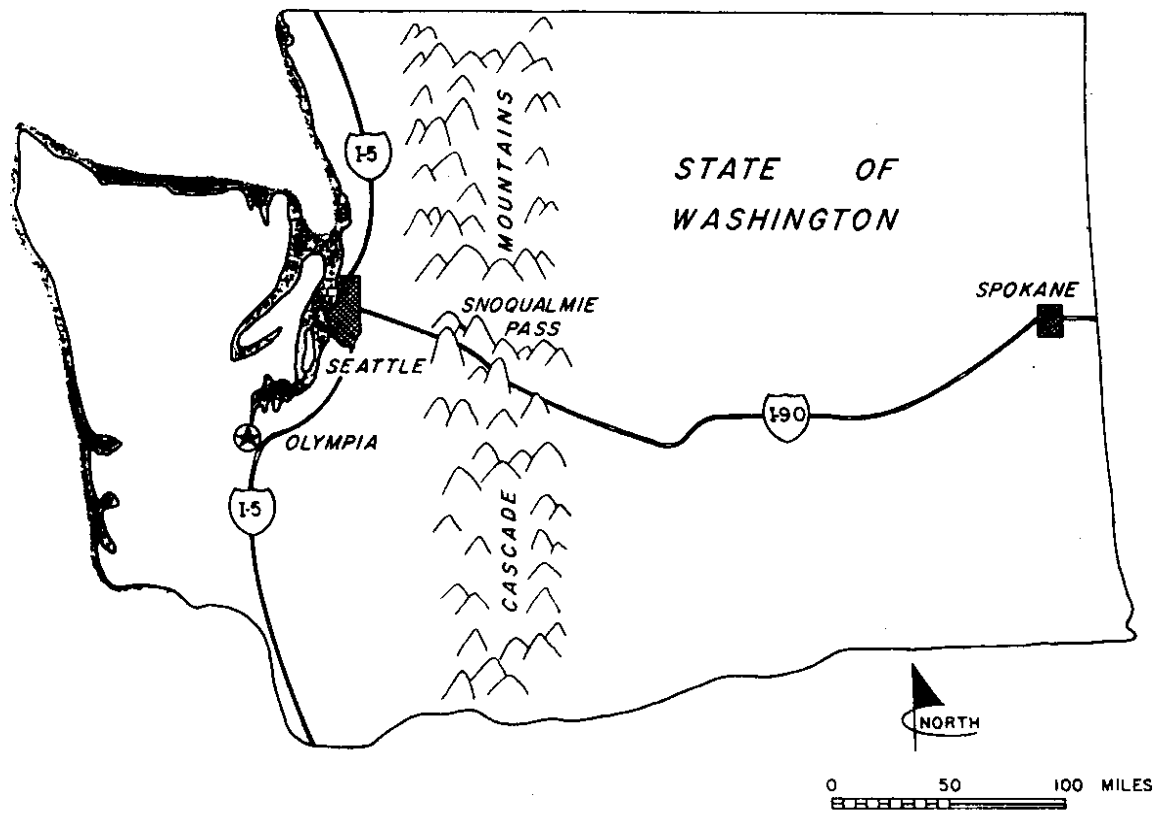

Figure 1.1. Location Map

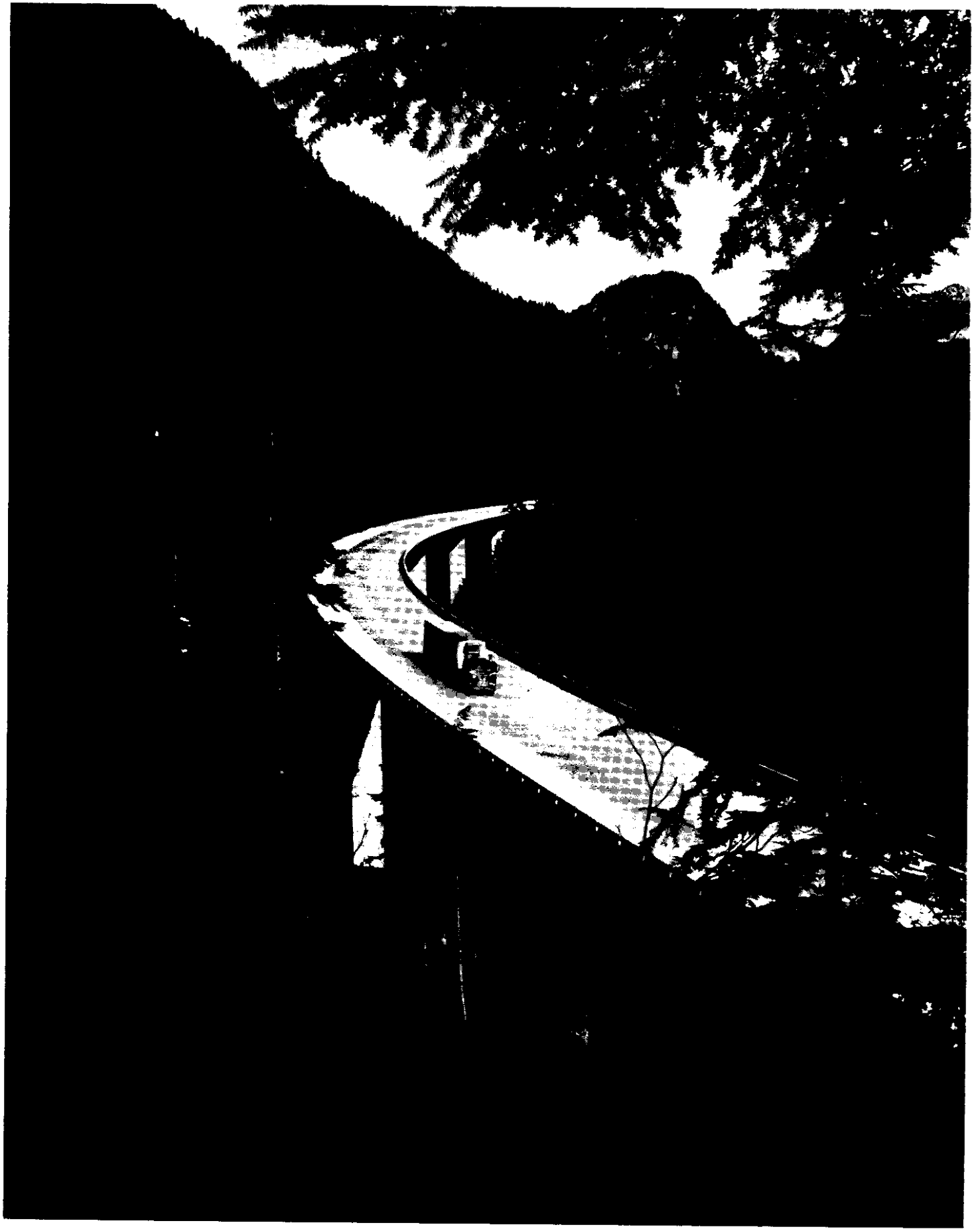

Figure 1.2. Denny Creek Viaduct

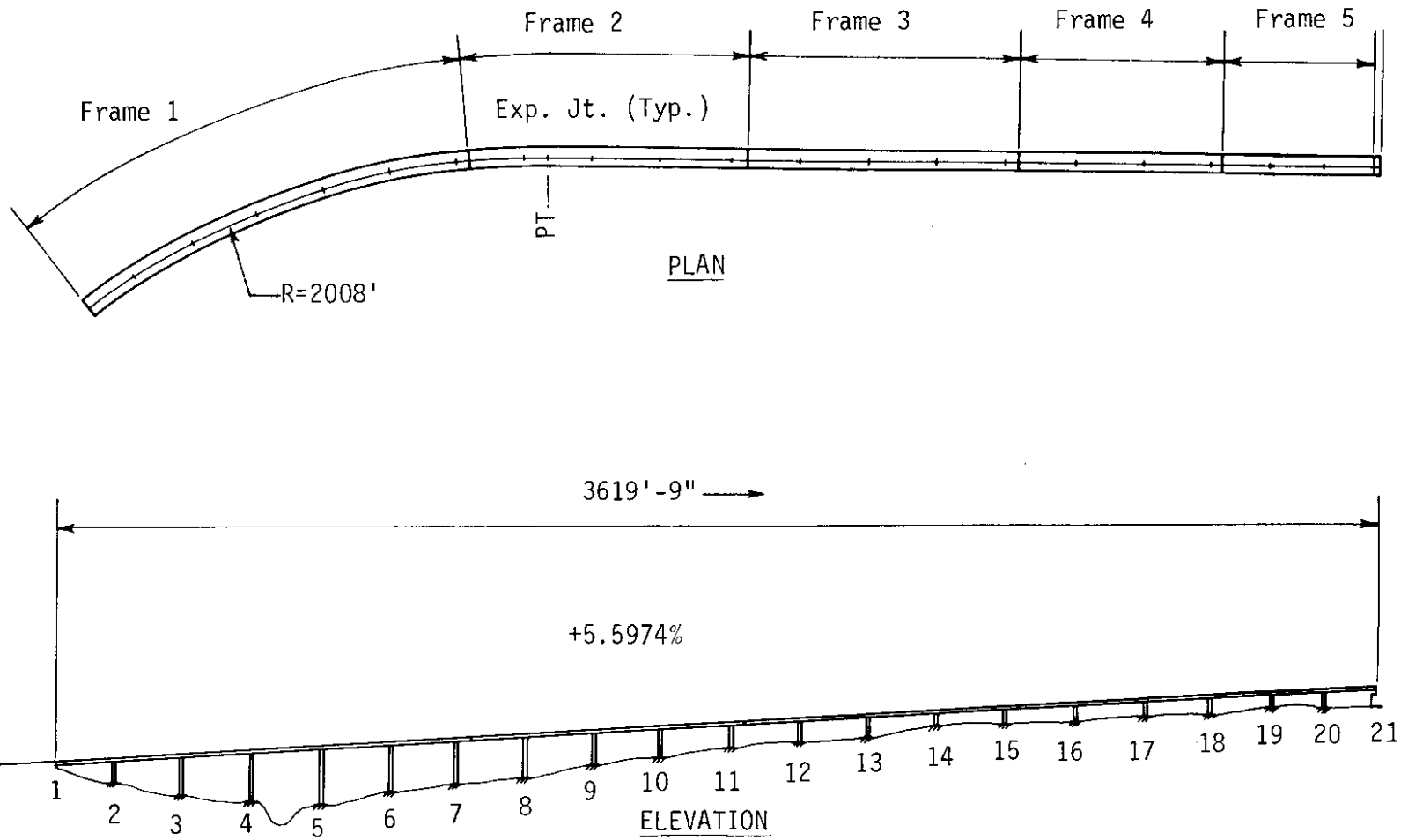

Figure 1.3. Plan and Elevation, Denny Creek Viaduct

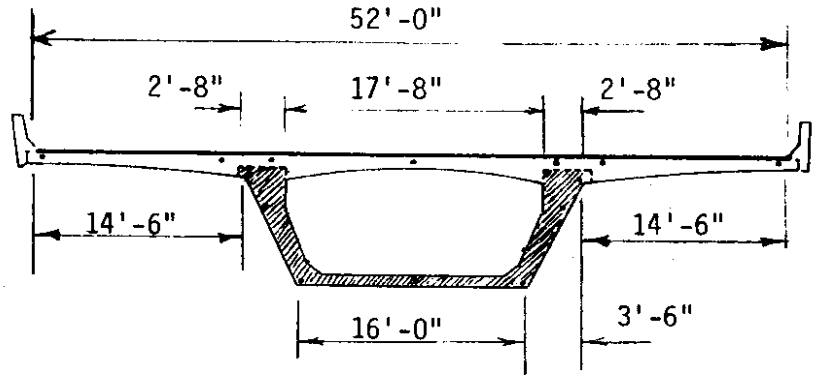

Stage I Hatched

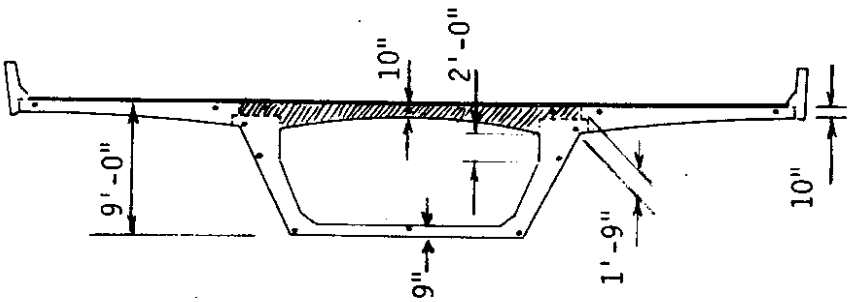

Stage II Hatched

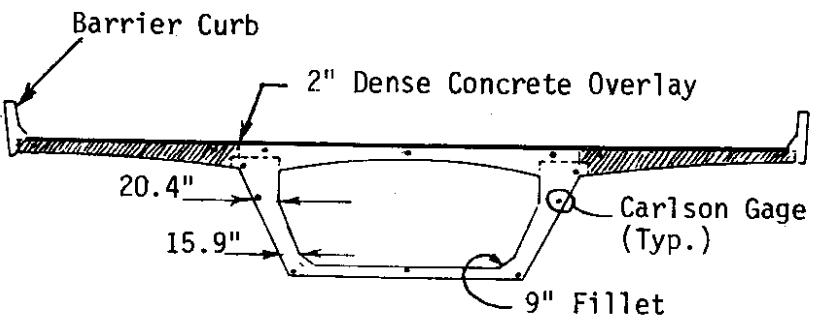

Stage III Hatched

Figure 1.4. Stage Construction of Cross-Section and Section Dimensions

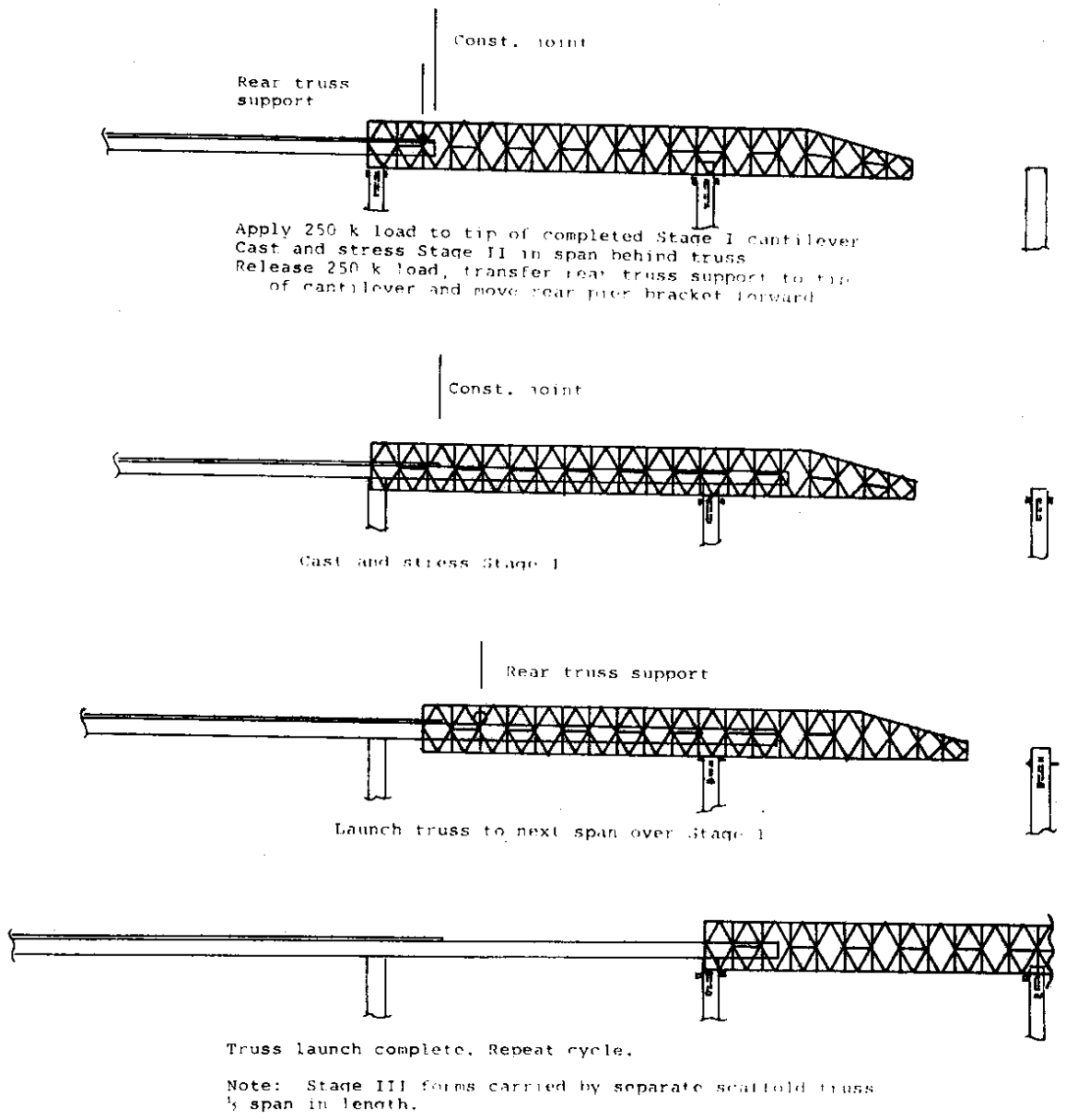

Figure 1.5. Span-by-Span Construction Procedure

1.2. Issues in the Design of Stage Constructed Concrete Box Girders

Issues in the design of single cell post-tensioned concrete box girder bridges built by stage construction concern primarily three areas:

1. The effects of shear lag in the top flange and in the bottom flange of the girder near the reactions;
2. The stress distributions for different stages of construction and the effects of creep and shrinkage on those distributions; and
3. The magnitude and distribution of the stresses due to thermal gradients arising from environmental causes and from construction techniques.

These three issues are interrelated and therefore it is necessary to study all three effects in order to correctly interpret any measured strain and deformation data for such bridges.

1.2.1. Load Distribution and Shear Lag

The current AASHTO bridge code (1.1) design provisions governing the distribution of load were developed primarily for use with multi-cell girder bridges. It is customarily assumed that for the distribution of live load, the bridge can be modeled by a line element analysis that considers an explicit distribution of torsion. Provision for shear lag in the flanges is not, however, customarily covered by such analyses. Single cell box girders are of such a size that the complete width of the roadway can be expected to participate fully in resisting forces at some distance from any concentrated load. However, the factors that determine the distance and the consequences of such actions are ill-defined. Live load studies can produce information on shear lag, or effective flange width. Current design code provisions for shear lag do not adequately cover large single cell box girders. Shear lag is

primarily of concern for such structures in the bottom slab adjacent to the piers. The concentrated reaction loads must be distributed from the bearings into the webs and flanges of the box. The high compressive stresses indicated by beam theory often result in the designer thickening the bottom slab adjacent to the pier. Such thickening may be unnecessary if significant shear lag effects are present.

The current AASHTO Code requirements for minimum bottom flange thickness may also be unnecessarily restrictive for positive moment regions. Those provisions require a thickness equal to or greater than the clear span between webs but not less than 5 1/2 inches. In box girders with a large span between webs this requirement can lead to an unnecessarily thick bottom slab. The bottom slab must be of adequate thickness to accommodate the longitudinal post-tensioning tendons and provide the necessary cover to the transverse and longitudinal mild steel. In addition, the stress requirements for the slab spanning between the webs and carrying dead load, possible construction live loads, and any curvature forces from the tendons must be satisfied. AASHTO Interim 1979 allows use of the full top flange width for stress calculations in lieu of effective width concepts. This provision needs experimental verification on full-scale structures.

1.2.2. Creep and Shrinkage Stress Redistribution

The stage construction, span by span, that was used for the Denny Creek Viaduct, offers important economy in falsework for construction in difficult terrains. The staging of the construction minimizes the need for expensive temporary supporting falsework trusses or ground supported falsework. However, the technique imposes high temporary stresses in the previously completed portions of the structure. For design, it is assumed that the resulting peak stresses are redistributed by creep over a period of a few

months to a few years and that for the completed structure, the response to dead load and post-tensioning is eventually similar to the response which would be found for the same structure cast-in-place on falsework and post-tensioned as a single unit. In a previous contract, the Washington State Department of Transportation (WSDOT) commissioned the Construction Technology Laboratories (CTL) of the Portland Cement Association to install strain gages during the construction, make strain measurements and laboratory tests, and collect other data bearing on the issue of stress redistribution. The results of the CTL study are reported in reference (1.2) and are further discussed in Chapter 3.

1.2.3. Thermal Effects

The AASHTO Bridge Code does not require consideration of thermal gradients in the design of a bridge structure. That Code provides guidance only for the effects of overall thermal expansions and contractions for annual or longer temperature cycles. The ACI-ASCE Committee (1.3) on concrete bridges has recommended that both stresses and movements due to temperature changes and temperature differentials be considered in design. They have recommended, in the absence of temperature data, consideration of temperature changes in a moderate climate that rise by 30 degrees F and fall by 40 degrees F from those at the time of construction. They have also recommended consideration of a linear temperature differential of 20 degrees F between the top and bottom of the bridge.

Studies of thermal effects in bridges have revealed that significant stresses are possible due to thermal gradients (1.4-1.8). Priestly (1.6) has outlined a method for taking account of thermal stresses in design and a design temperature gradient appropriate for New Zealand. Similar data for the development of design guides for thermal gradients for U.S. conditions are not

available, in spite of the recommendation in reference (1.3) that account be taken of thermal gradients. Leonhardt (1.5) has reported a case in which severe cracking in a box girder was attributable to thermal stresses. That result demonstrates the significance of the thermal stresses in assessments of a bridge's durability. Obviously, such stresses can exceed the tensile capacity of the concrete, even though the structure is post-tensioned. Thermal loadings are not likely to affect the ultimate strength of a bridge. However, it is possible that they could significantly affect the bridge's service load response, its fatigue strength, and its durability.

It is necessary to be able to separate the stresses and deformations due to thermal effects from those due to creep and shrinkage, and those due to live load in any stress and deformation study of an actual bridge. Because of the instrumentation installed by CTL for strain gage studies during construction, there was a unique opportunity with the Denny Creek Bridge for collection of basic data not only on the relation of temperature gradients to normally available environmental data, but also on the gross structural effects of thermal gradients.

1.3. Objectives

The objectives of this research were to:

A. Analyze the creep and shrinkage data collected in the CTL study. correlate that data with predicted stresses and deflections, and interpret the significance of that data for design.

B. Document the strain and deformation response of the structure to live loads and compare that response with predictions based on current design codes and available analytical methods.

C. Document the relationship between environmental parameters and thermal gradients in the structure.

D. Document the response of the structure to thermal gradients and compare that response with predictions obtained from heat transfer analyses.

E. Recommend methods of analysis for live loads appropriate for single-cell box girders.

F. Recommend procedures for design for thermal gradients in box girders.

1.4. Scope

In this study, a review is made of the strain and temperature data collected during the construction of the Denny Creek Viaduct by Construction Technology Laboratories and the Washington State Department of Transportation; the results of additional strain and environmental data collected and the bridge site are reported; the significance of those results interpreted; and design recommendations made for the prediction of the stresses induced in a bridge by non-uniform temperature gradients over the depth of that bridge.

This study covers three separate but interrelated topics for the Denny Creek Viaduct: redistribution of stresses through creep and shrinkage, live load response, and thermal stress response. Chapter 2 contains a review of the literature relevant to stage constructed concrete box girder bridges for each of these three topics. Chapter 3 reviews the Construction Technology Laboratories' report on the results of their creep and shrinkage studies and correlates their data with additional data collected as part of this investigation. Chapter 4 describes the results of a series of live load tests made on the structure and the correlation between those results and the predictions of customary methods of analysis. Chapter 5 describes the investigation of the thermal response of the bridge to non-uniform temperature distributions, and Chapter 6 examines the research methodology adopted for this project, its

limitations and the changes that would be proposed in that methodology for future studies of this kind.

Appendix A details the construction chronology for the Denny Creek Bridge extracted from the WSDOT resident engineer's records. Appendix B tabulates the Carlson strain gage readings that extend the CTL data on creep and shrinkage and were taken as part of this study. Appendix C reports the results of measurements of the expansion joint movements with time and temperature. Appendix D tabulates creep and shrinkage data required for understanding the review in Chapter 3 of the CTL study. Appendix E contains critical extracts from the body of the CTL report. Appendix F contains the computer program for Priestley's analysis and an example of the application of that analysis.

1.5. Strain Measuring Devices

In the previous study by CTL, instrumentation was installed in Span 4 between Piers No. 4 and No. 5 as shown in Figure 1.6. Three bridge sections designated as A, B and C were each instrumented with 13 Whittemore mechanical strain gage points and 14 Carlson meters. The three sections A, B and C were selected to represent sections next to the pier, near the quarter span, and mid-span, respectively. The locations of the Carlson meters within each section are shown in Appendix E, Figures E1, E2 and E3. Those Carlson meters were used for the live load studies, creep and shrinkage studies, and thermal stress studies reported here. Although every effort was made to properly utilize the Whittemore Strain instrumentation, readings taken from that instrumentation were found ineffective. Other strain instrumentation was also installed on the bridge, but climatic and traffic conditions soon rendered that instrumentation ineffective also.

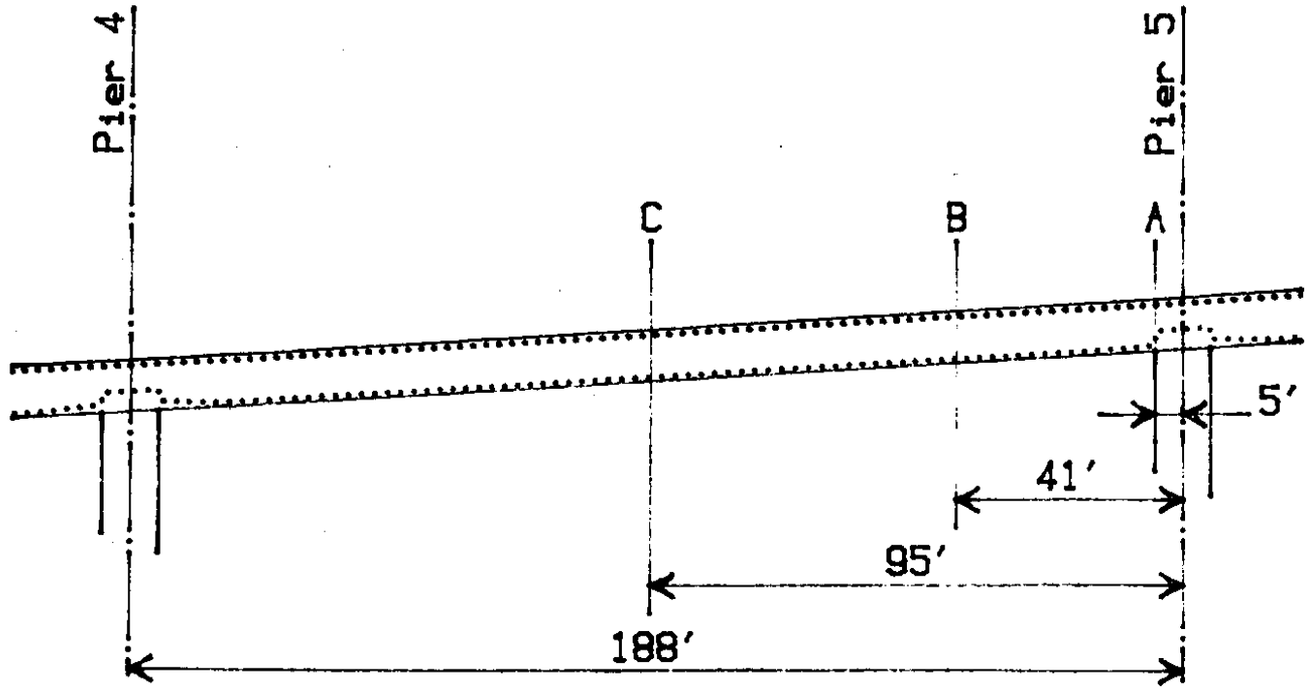

Figure 1.6. Location of Instrumented Sections

2. LITERATURE REVIEW

2.1. Creep and Shrinkage

The extant literature on creep and shrinkage deformations in concrete is very extensive and continues to proliferate. This fact is a clear indication of the complexity of the subject and is also an indication that no simple method has yet been found to represent this phenomenon in terms of one or two parameters of general applicability.

The pioneering work by Ross (2.1) is still very much applicable today. Ross describes the three basic approaches to the problem of time dependent deformations in concrete, presents the results of analyses, and compares those results to experimental data for some simple cases of variable stress history. The basic differential equation which is assumed to govern this phenomenon is

$$f - \frac{c}{\alpha} - \frac{1}{\phi}\frac{dc}{dt} = 0 \qquad (2.1)$$

where f = concrete stress

c = creep strain

α, ϕ = constants determined from tests

t = time

Ross describes the effective modulus, the rate of creep, and the superposition methods. The effective modulus method gives the deformation in terms of the secant modulus at any time t after application of the stress. The rate of creep method assumes that the time rate of change of deformation at any time, dc_1/dt, is known, where c_1 is the specific creep under 1 psi at the appropriate time. The superposition method is analogous to the other two methods except that the age at first loading is accounted for by separate

creep curves for each age.

Mattock (2.2) applied Ross's method to prestressed precast beams made continuous for live load and showed the equivalence of the rate of creep and effective modulus method for that case. He also derived a solution for the stresses and restraint moments which arise due to differential shrinkage between the slab and the girder. He compared the predictions of his analyses with measured experimental data and demonstrated good agreement. His procedures have now become standard practice in bridge design.

Branson (2.3) has written a particularly comprehensive text on the subject of time dependent deformations in concrete. His text covers current formulations of the problem, presents numerous examples on the use of those formulations, and provides a wealth of experimental data on creep and shrinkage. The text also compares the predictions of several analytical methods.

Tadros, Dilger and Ghali (2.4, 2.5) have shown the importance for deflection calculations of including the redistribution of stresses between the concrete and the reinforcing steel with time. They report a theory and develop a comprehensive computer program to track the stresses and deformations in a segmentally constructed bridge. Their program has recently been made commercially available and is in use in the construction analysis of several major concrete box girder bridges. It shows promise in its ability to account for most of the more important aspects of creep phenomena and appears capable of extension to other creep laws as those laws become available.

One standard reference currently used in the profession for prediction of creep and shrinkage is the CEB-FIP Recommendations (2.6, 2.7). Those Recommendations are well described by Branson (2.3). They give a single parameter representation of creep which may be used with either the rate of creep or the effective modulus method. The parameter is defined with

reference to the major influences which have been shown experimentally to be effective in determining creep and shrinkage. These influences include ambient relative humidity, age at first loading, concrete mix design including unit content of cement and cement sized particles, and water cement ratio, theoretical thickness of the concrete, reinforcing steel ratio, and time rate of development of creep. The formulation is based on the ratio of the creep strain to the elastic strain calculated with respect to the elastic deflection computed as the stress divided by the modulus of elasticity at 28 days. This dependence of the formulation on the 28 day modulus of elasticity is not always recognized and results in some misleading comparisons when the creep is referred to the measured elastic strain at the time of loading or calculated using the modulus of elasticity appropriate to the time of loading instead of the modulus of elasticity at 28 days.

The CEB-FIP 1970 Recommendations were updated in 1978 to include a more refined evaluation of the creep phenomena. The creep strain is separated into three parts. The creep coefficient is still taken as a single parameter and defined with respect to the elastic deformation for a constant stress operating on a linearly elastic specimen characterized by the 28 day modulus of elasticity and stresses are assumed to be in the range where superposition is valid. The basic parameters in the determination of the creep coefficient remain as described previously but the different effects are assumed to influence different portions of the creep than that predicted with the 1970 recommendation. The creep strain is taken as the sum of three strains; an irreversible strain which occurs within the first few days of the application of the first load, a delayed elastic (i.e., recoverable) strain which develops with time, and a flow (nonrecoverable) component that expresses delayed plasticity. These components are related to one or more of the governing parameters and

their values given by tables and graphs. The application of the method is complex enough to have generated a 400-page manual with examples and commentary (Chiorino (2.8)).

The difficulties of the various available methods in treating creep under a variable stress regime are emphasized by the predictions of the various methods of the creep caused by removal of a load, or creep recovery. The effective modulus method predicts full recovery of both the elastic and creep deflection. The rate of creep method predicts no recovery of the creep deflection upon removal of the load. The superposition method predicts results intermediate between the rate of creep and the effective modulus method but still seems to overestimate the recovery of the creep deflection, at least for simple stress regimes. It appears that there is an unrecoverable component of deflection associated with each load application, as well as an elastic component and a flow component.

In the case of precast, prestressed beams with a composite cast-in-place slab there is essentially one change in the stress regime, at least for stresses of long duration. Thus, the various methods all make acceptable predictions. However, for a stage constructed cross-section, constructed span by span, there are many changes in the stress regime of varying duration. The presence of concretes of different ages in the same cross-section complicates the choice of an appropriate single creep parameter representative of the whole cross-section.

2.1. Analytical Methods for Design of Box Girders

The literature on the design of box girder bridges is extensive. Comprehensive surveys have been presented by Kristek (2.9) and Maisel et al. (2.10). Only a few of the more important publications will be reviewed here.

The general categories of available design methods are listed below in order of increasing complexity.

1. Elementary beam theory, torsion neglected
2. Elementary beam theory, torsion considered
3. Finite strip methods
4. Finite element methods with plate elements
5. Finite element methods with "brick" ((3-dimensional) elements

The elementary beam theory is the most commonly used method of analysis in the design office. It is simple and easy to apply and thousands of bridges of all sizes have been built using beam theory as a guide. The principal deficiencies are typically covered in design codes by distribution factors on live loads and effective width concepts for shear lag. The theory is not appropriate for problems associated with transverse analyses of the cross-section and the simplifications that are usually made to permit application of simple beam theory to transverse analysis must be applied with care. Elementary beam theory does not give a correct picture of the stresses at support points nor those in the vicinity of concentrated loads. Distribution of a concentrated load, such as a wheel load, prestress, or support reaction, by assuming that the load spreads through a cone of some known vertex angle (for example, 52 degrees, a 2:1 distribution or 90 degrees, a 1:1 distribution) can often give satisfactory approximations for design. Most importantly, elementary beam theory can provide a simple, well-understood means for checking the results predicted by more elaborate analytical models.

The next level of sophistication in analysis is the inclusion of the torsional properties of the line elements making up the model for the frame analysis, as well as the third dimension. A modest level of improvement in accuracy is achieved in certain cases at the cost of much labor. It is usually necessary to resort to a general purpose computer program, such as

STRUDL, to process such an analysis. Transverse load distribution effects can be calculated by using such a program to analyze a grid model of the deck system. Hambly (2.11) discusses the application of these methods in some detail and gives effective guidance on the interpretation of results and modeling.

The finite strip method divides the bridge section as a whole into longitudinal strips which effectively represent portions of the section with similar longitudinal stiffness. Equations are written for the vertical shear forces required between the elements to restore deflection compatibility. Loads on the strips are expressed by means of Fourier series expansion and the simultaneous equations for the deflections are solved in terms of the harmonics of the Fourier series. This method can predict the lateral distribution of wheel loads to the different cross-sectional elements and provides information on the distortion of the cross-section. The method can be used without a special purpose computer program, but for each analysis it is necessary to set up and solve the equations for several harmonics. Interpretation of the results must be done with judgment, but the general concept is clear and easy to understand. Hambly also discusses this method in some detail.

Finite element methods, employing general purpose computer programs such as STRUDL, SAP, ANSYS, and others, can be used to model the structure. The drawback to this approach is the enormous labor involved in setting up, reviewing, checking, and coding the required input, the significant amount of computer time, and the considerable effort required to properly interpret the voluminous output. The results obtained depend entirely upon the erudition and experience of the engineer performing the analysis. Experience is necessary in structural analysis, finite element methods, and bridge design.

The program presented by Meyer and Scordelis (2.12) is a special purpose program developed especially for bridge design. It combines the simplicity of elementary frame analysis with the ability to model critical portions, or all parts of the structure, with plate elements in which account is taken of both in-plane and out-of-plane behavior. There are some limitations on mesh size changes but they are not restrictive. One of the principal advantages of this program is that it contains a maximum amount of programmed element generation. In other words, the input data are minimized to those required by the program to generate the coordinates of each node and describe the properties of each element. Compared to an elementary plane frame analysis, the input and output are significantly greater. The program was developed over time as part of an extensive study into the behavior of concrete box girder bridges. It has the benefit of parallel calibration through tests on fairly large scale models. Transverse behavior, shear lag, and lateral load distribution are handled by theoretically correct methods in the model.

The authors are unaware of any finite element programs, utilizing shell elements, which have been developed specifically for bridges. General finite element programs containing shell or solid elements could, in theory, be used at the cost of large amounts of computer time and much labor in preparing input and interpreting output. However, the cases where such models would be appropriate are few for bridge design. One such case would be for the Three Sisters Bridge proposed to carry I-66 over the Potomac River near Washington, D.C. That large scale concrete box girder structure is planned to have curved exterior webs as well as the usual haunched soffit. The advantages and disadvantages of using a finite element program with shell elements for that structure can be readily calibrated by reference to the results of the 1:10 scale model of the structure tested by CTL and reported by Corley and Carpenter (2.13).

2.2. Analytical Methods for Slab Design

Determination of roadway slab design moments for this type of structure is commonly done by means of influence surface charts such as those by Pucher (2.14) and Homberg and Ropers (2.15). An example of such a chart is shown in Figure 2.1. Pucher's charts are limited to constant thickness slabs with various aspect ratios and boundary conditions. Homberg and Ropers present charts for cantilever and interior slabs with different soffit profiles (either parabolic or linear variation of thickness) for selected ratios of minimum to maximum thickness. A separate chart is required for each point of interest and direction of moment. The influence surface for moment in a plate is expressed analytically by a Green's function which simultaneously satisfies the partial differential equation for plate bending, the associated boundary conditions, and the conditions for a unit impulse applied at the point of interest. This unit impulse is a slope discontinuity for moment which integrates to unity across the point of interest (see Hildebrand (2.16)). These surfaces are the two-dimensional analog of the influence line familiar to structural analysts. The closed form analytical expressions representing these surfaces are very complicated and lengthy and not suitable for general design use. Closed form expressions have not yet been developed for the case of variable slab thickness. Homberg and Ropers influence surface charts are therefore prepared by use of finite element analysis.

These influence surface charts are easy to use, practical for use in the design office, and give adequately accurate results within the limitations inherent in the assumptions upon which they are based. The principal limitation is that the charts cannot be prepared to cover every possible point of interest or variation in form and proportion of soffit profile. Homberg and Ropers' charts are also out of print and not readily available in the U.S. In the design of a given structure, moments in the slab are determined at the

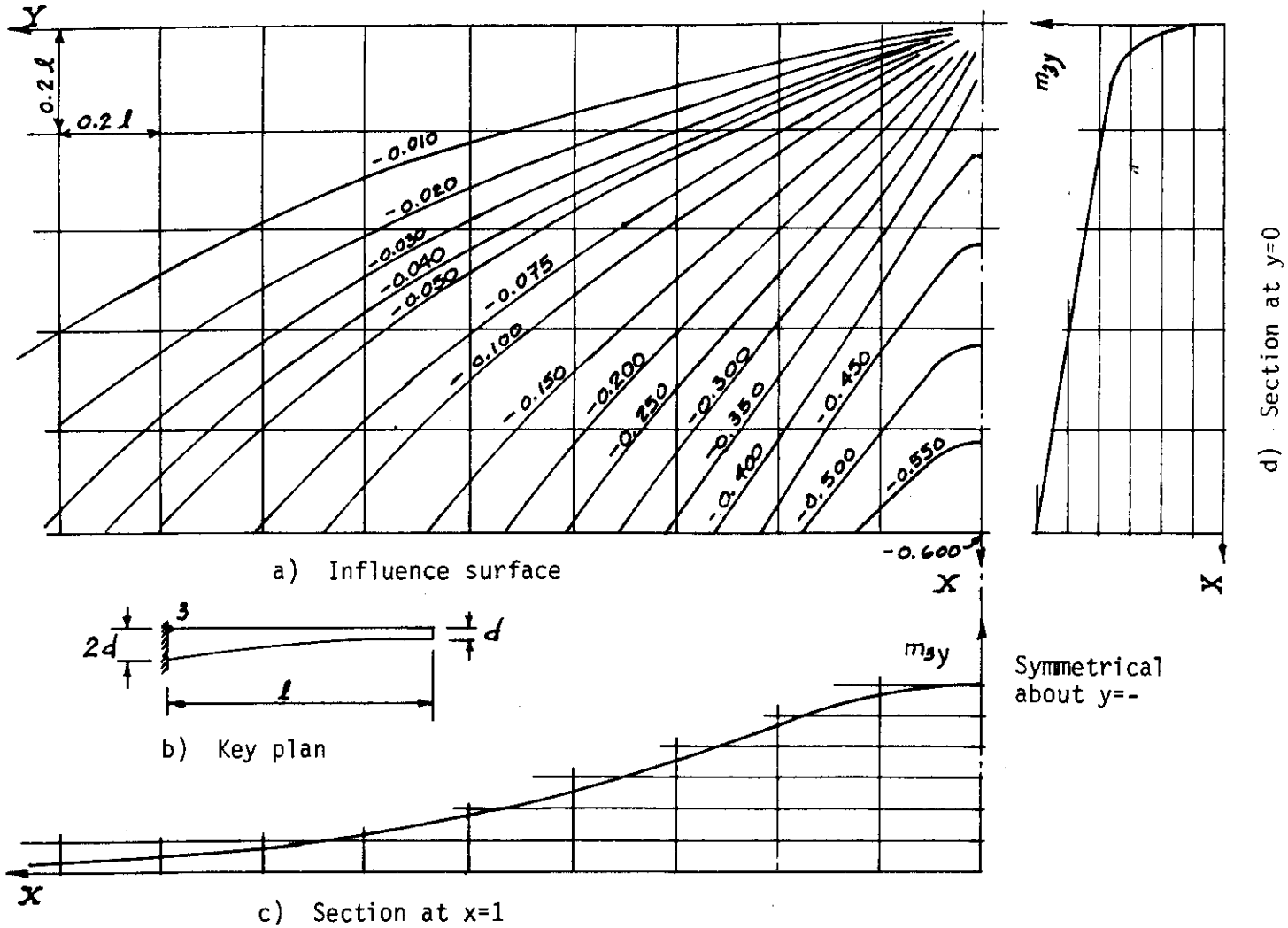

Figure 2.1. Influence Surface for Moments at Root of Cantilever (from Homberg and Ropers (2.15))

web, midway between the web and the edge of the cantilever and midway between the webs as shown in Figure 2.2. These moments at these locations are used to draw envelope curves using straight line interpolation. Figure 2.3 shows envelope curves given by Schlaich and Sheef (2.17) as typical of European practice. Guyon (2.18) has outlined a method for combining the results of the influence surfaces for plates of constant thickness with results of stiffnesses determined from frame analysis and fixed end moment factors for haunched beams. This method is somewhat contrived and subject to judgmental errors but it does serve as a means of adapting the influence charts for constant thickness plates to the case of variable thickness plates.

Several authors have addressed the problem of the influence of the edge beam on the distributions of moments in the cantilever slab. In general, these methods are summaries of the results of finite element analyses. Kawai and Thurlimann (2.19) present a closed form analytical method for constant thickness slabs with cross beams which could be used with appropriate assumptions and modeling to be a portion of a larger slab with specified boundary conditions. Bahkt (2.20) presents the only treatment which addresses the problem of the influence of the free edge and which most nearly represents the conditions present for the live load test on the Denny Creek Viaduct. However, he has given results only for a slab with a linear variation in thickness over the full span. This method is also called the "Ontario" method.

Bahkt's method is based on the results of a finite element analysis which utilizes plate elements. Schaich and Scheef (2.17) give curves attributed to Menn (2.21) showing the influence of both the edge beam and the profile of the slab soffit on the distribution of the moment at the root of the cantilever

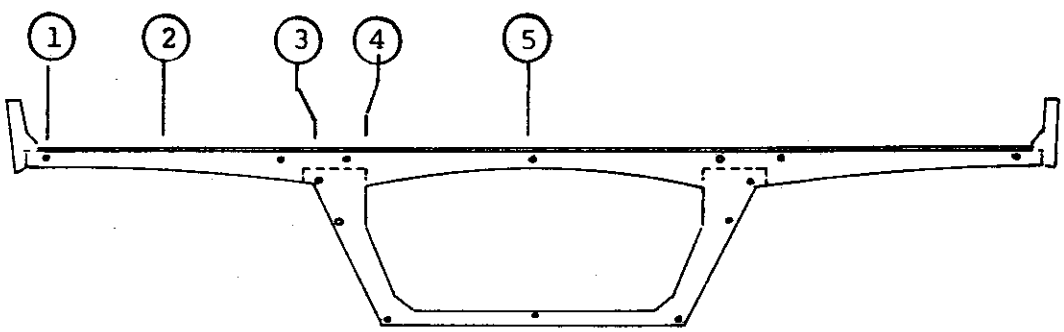

Figure 2.2

Reference Sketch for Slab Design Sections

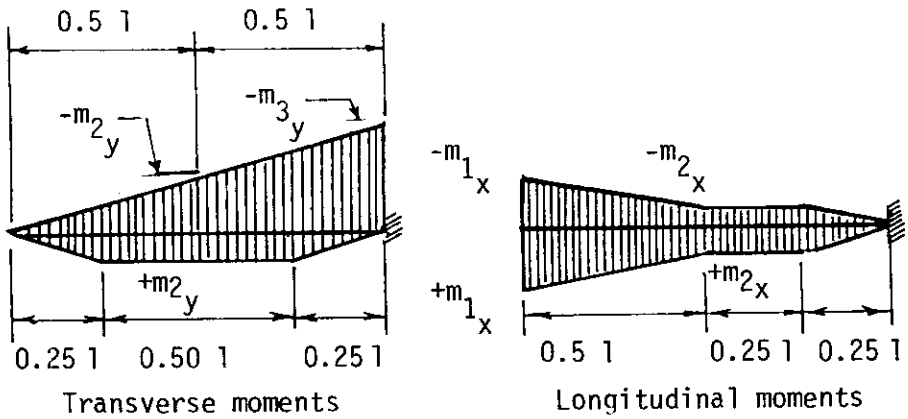

cantilever slab

m_2 = moment at location 2, Figure 2.2

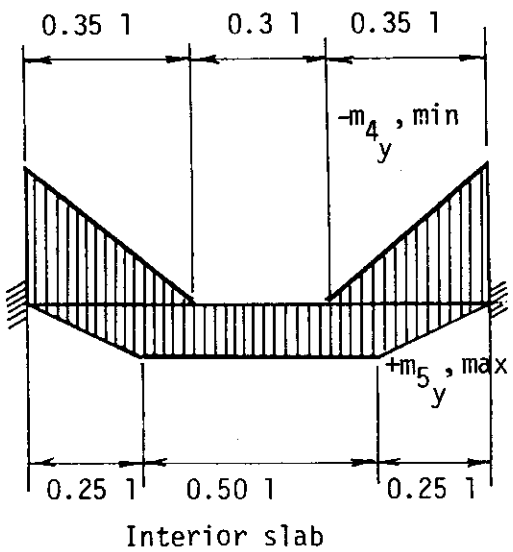

Figure 2.3. Live Load Moment Envelopes for Slab Design

for several different slab soffit profiles and edge beam stiffnesses. These curves are shown in Figure 2.4.

General purpose finite element analyses utilizing plate elements can be used to analyze any configuration of slab soffit profile and edge beam stiffness. Several programs are available for use on larger computer systems. The principal disadvantage for routine design office use is the amount of time necessary to code, edit, verify, and check the input for such a program and to interpret the output. These considerations generally limit the use of such programs to final checks of designs developed using simpler methods.

The simplicity of the procedure upon which the standard AASHTO distribution factors, given in Paragraph 1.3.2 (C) of reference (1.1), are based should not be overlooked, especially for preliminary design. Those distribution factors are based on an assumed minimum width of 3.75 feet and thence spreading of the load at a constant angle, 39 degrees, for determining the width of the slab which participates in resisting the moment generated by a given wheel load. No distinction is made between dual wheels or single wheels; therefore, it is assumed that this distribution is applicable to either situation. This method becomes overly conservative for long cantilevers where the distribution cones for adjacent axles overlap and where more than one set of wheels can be placed between the edge and root of the cantilever. An adaptation of this method, which accounted for the free edge, was used to calculate the moments to be anticipated for the test load applied adjacent to the expansion joint in the live load tests reported in Chapter 4.

The same calculation was repeated using Bahkt's analysis. The maximum transverse moments at the root of the cantilever were predicted to be as follows:

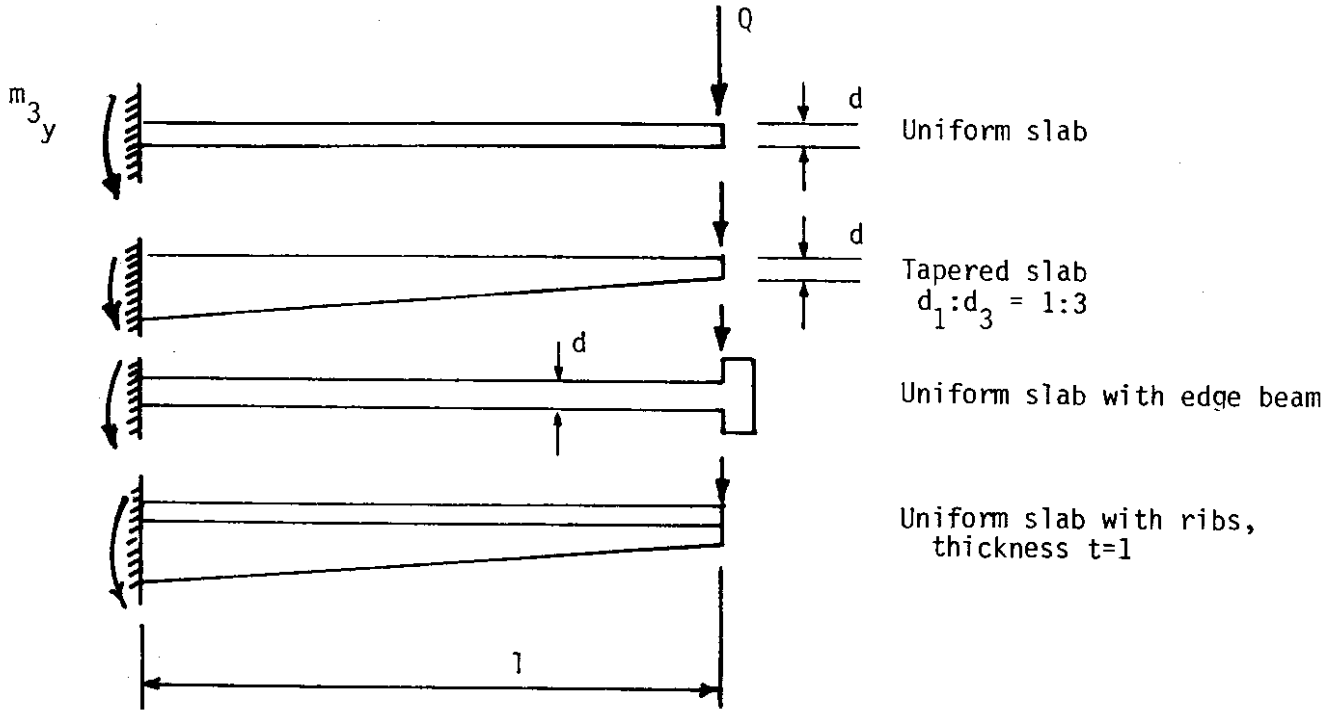

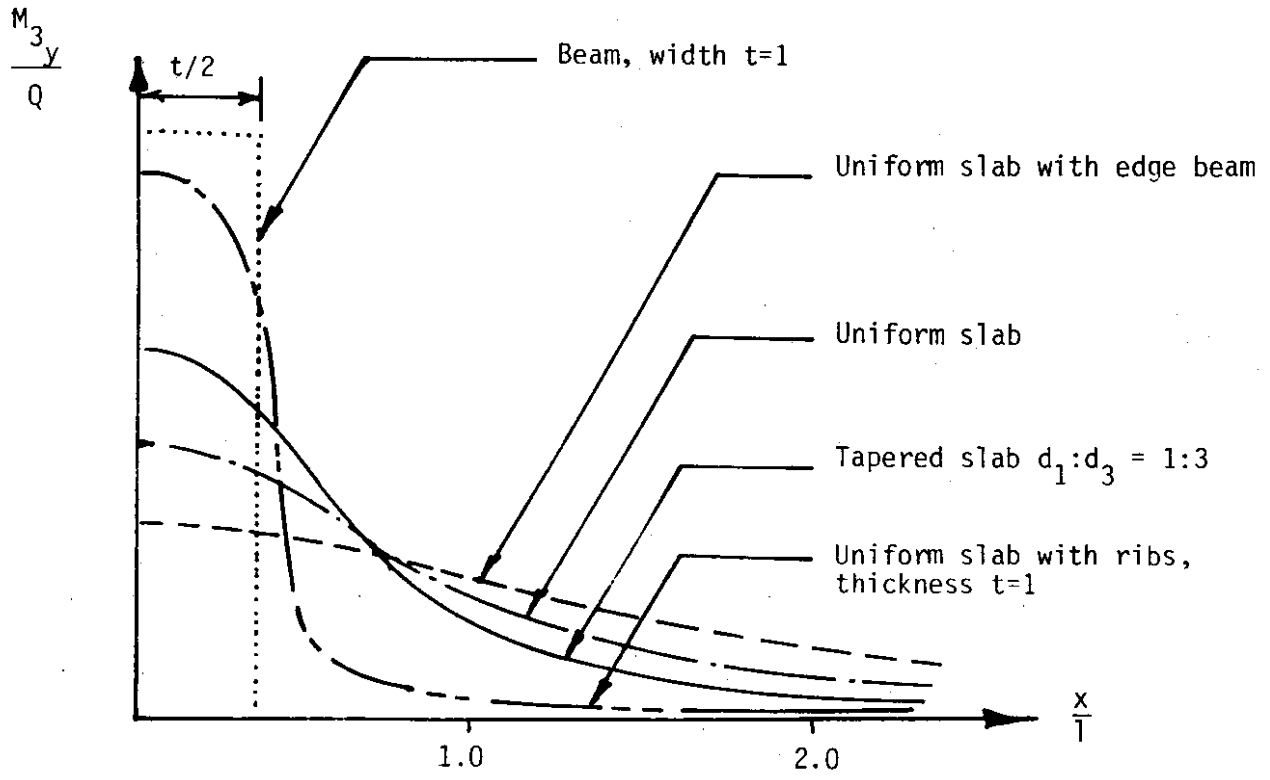

Figure 2.4. Longitudinal Distribution of a Concentrated Wheel Load for Cantilever Slabs of Differing Forms (2.17)

Method	Maximum mx k-ft per 1ft
Modified AASHTO	37.0
Bahkt 2:1 taper	
Ib:Is = 1.0	22.0

The value used for the stiffness of the edge beam assumed that the edge beam participated fully in resisting loads. Hence, no reduction was made for joints in the barrier rail. Also, the parabolic taper for the Denny Creek Viaduct's cantilever slab means that the slab is less effective in distributing loads longitudinally than a linearly tapered slab with the same root and edge thicknesses.

2.4. Thermal Stresses

Emerson (2.22, 2.23, 2.24, 2.25) studied bridge temperatures in the British Isles extensively, producing recommendations for predicting bridge temperatures from environmental parameters and typical distributions of temperatures with depth. The methods and parameters presented by Emerson have been calibrated only against data collected for bridges in the British Isles. However, those methods should be able to give reasonable results in widely divergent climatic conditions.

Jones (2.26) developed a computer program for prediction of the mean effective temperature of a bridge based on site observations of certain environmental parameters. His program is intended for use in establishing a reference temperature for longitudinal expansion, as would be required for proper installation of expansion joints and bearings during construction.

Reynolds and Emanuel (1.8) surveyed studies of thermal stresses in bridges prior to 1971. They discussed the various factors involved in estimating the magnitude of the temperature differential between the top and

bottom of the structure and reported the results of various theoretical studies and measurements of temperatures in bridges.

Radioli and Green (1.7) used nonlinear gradients to study the possible stresses in two typical bridge structures, a beam and slab system and a box girder. They assumed a temperature distribution represented by a sixth order parabolic variation with depth as follows:

$$t(y) = T\,(y/d)^6 \qquad (2.2)$$

where: $t(y)$ = temperature as a function of depth measured from the soffit

T = surface temperature

y = height above the soffit

d = total depth of section

Their analyses showed stresses of 200 psi tension and 800 psi compression in a typical two-span concrete box girder for an apparent temperature gradient of 20 degrees Fahrenheit.

Priestley (1.6, 2.29) has studied the problem of the form of the thermal gradient and the stresses produced in structures by such gradients. He proposed a form for the gradient based on his observations and investigations in New Zealand. His gradient has a form similar to the gradient proposed by Radioli and Green. His distribution also covers the case of slabs over enclosed cells and the temperature distribution in the bottom slab of such cells (see Figure 2.5). Priestly also studied one of the few cases of reported damage from thermal effects. Built et al. (2.28) give details of the Newmarket Viaduct in Auckland. This structure experienced severe cracking, triggered by temperature stresses, which provided the impetus for Priestley's research.

Hambly (1.4) discussed the implications of the various proposed temperature distributions for design. He includes analyses of reinforced

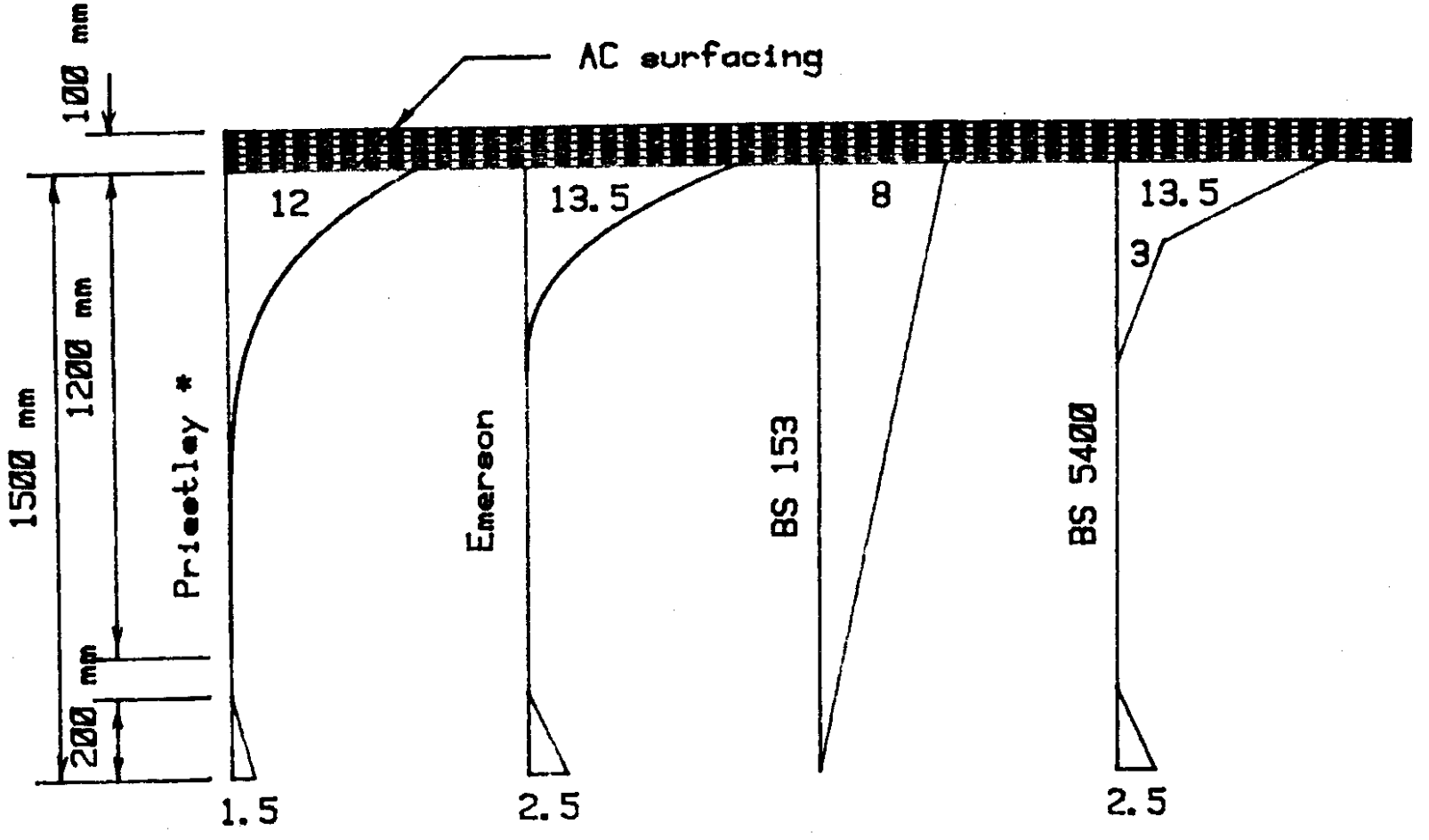

Fig. 2.5 Temperature profiles (Deg C) recommended for design

* Modified for section w/o surfacing, See Ref 1.6

concrete sections illustrating the influence of cracking in relieving restraint induced stresses.

White (2.29) has reviewed the available literature on non-linear differential temperature distributions in concrete bridges through 1978 and identified the various distributions that are suitable for use in design (see Figure 2.5).

Richmond (2.30) has raised the question of whether there is a creep component related to temperature and suggested that this phenomenon may explain the apparent discrepancy between the relatively high stresses predicted by the analyses described previously and the relatively few documented cases of substantial damage to existing bridges as a result of such stresses.

Aguado, Mari and Penon (2.31) have described an iterative method for the analysis of frames composed of members with arbitrary moment-curvature diagrams and presented examples of the analysis of frames subject to both gravity loads and imposed deformations. Their approach indicates the ductility required in the various members.

Aparicio and Arenas (2.32) have described the application of the general method developed by Aguado, Mari and Penon to the problem of highway bridges subjected to linear temperature gradients and live loads that are progressively increased until failure occurs. Their analyses predict a decrease in the restraint moments caused by thermal gradients as the imposed live load increases, and that the thermal gradient affects only the ductility required at failure and not the ultimate capacity of the structure.

Emerson (2.33) has reported the results of heat flow studies based on the one-dimensional heat flow model developed at the British Transport and Road Research Laboratory. The influence was documented of several parameters,

including resultant temperature profiles. This paper is significant because it identifies the relative importance of each of those parameters. The overriding influence of solar radiation is obvious from these results. The temperatures resulting from the incoming solar radiation depend on the emissivity and absorptivity coefficients of the surface. However, the range of the emissivity is such that its influence is small compared to the influence of the range of the incoming radiation.

The second most important parameter is the wind speed, which affects the surface coefficient of convective heat transfer. Two values were examined in Emerson's study: 9 kilometers per hour, which gives heat flow of 23 watts per meters^2 degrees C; and 53 kilometers per hour, which gives heat flow of 70 watts per meters^2 degrees C. The higher value resulted in lesser input temperatures when the upper surface was being heated by radiation. The variation in this coefficient was less important for determining lower surface temperature. Thus, the surface heat transfer by convection is more important for cooling the deck than for heating the lower surface. This implies that the increase in soffit temperature used by Priestley is likely to develop in response to a change in ambient air temperature for the range of wind conditions normally observed. This study also demonstrated the beneficial effect of asphalt overlays for reducing the effective temperature gradients in the structural concrete. As confirmed by other researchers, surfacing acts as an insulator.

Zichner (2.34) has described analytical studies and field observations of temperature effects for German bridges. Those studies were similar to the studies reported here. A two-dimensional explicit formulation of the finite difference approximation to the partial differential equation for heat flow was used in his analysis. The results are similar to those obtained by others with a one-dimensional analysis. The paper reports on cracking,

attributed to temperature effects, in the bottom slab and webs of a seven-span single cell box girder with spans of approximately 26.6 m (87 feet). The cracks were in general confined to the central half of each span and ranged in width from less than 0.2 mm (0.008 in) average to 0.4 mm (0.016)maximum. The web cracks were in general vertical and extended from the bottom of the web to the neutral axis. Bottom slab cracks extended completely across the slab. Both web and slab cracks were evenly spaced and numbered from four to eight per span. The bridge was curved in plan with a radius of about 145 m (476 ft). Zichner emphasized the importance of the boundary conditions to the results of a heat flow analysis. He recommended use of a surface coefficient of heat transfer of

$$h = 5.58 + 3.95\ w \qquad (2.3)$$

where: h = coefficient $W/m^2\ ^\circ C)$

w = wind speed m/s

He also suggested that the starting temperature value, assumed to be constant initially, will not influence the results beyond the first two days. He took the emissivity coefficient for short wave radiation as 0.65. The values he used for other thermal properties were similar to those used in the calculations made for this study. Curves of predicted versus observed temperatures are shown and agreement is excellent. Observations were taken during a summer period of extended fine weather and a difference observed between the response for a single cell box girder and twin webbed tee-beam bridges. The effective gradients, after the correction for self-equilibrating stresses converted back to temperatures, were approximately 8 degrees C and 5 degrees C, respectively, for tee-beam and box girders. The mean temperatures were only slightly greater for the tee-beam, daily range 9 degrees C, than for the box girder, daily range 7.5 degrees C. Eigenstress values computed assuming a modulus of

elasticity of 35000 MN/m (5100 ksi) and a coefficient of thermal expansion of 10E-06, deg C (5.6E-06, deg F) for an interior span exhibited a daily range of between +1.2 MPa and -1.9 MPa (+180 psi and -280 psi) for the bottom and top of the top slab, respectively. It is assumed that these stresses do not include the stresses due to flexural restraint. The stress values quoted above were nearly identical for the tee-beam and box girder bridges. It is inferred from the context of the discussion that these stresses were for the longitudinal direction. In another example, the daily temperature ranges observed for three thermocouples in the top slab of a single cell box girder were compared with the calculated values for the same location. The girder had a slab depth of 25 cm (10 inches) and there was a 6 cm (2.4 inch) asphalt surfacing on the deck. The concrete cover on the top and bottom thermocouples was 1.5 cm (0.6 in). The observed daily temperature ranges for the top, middle and bottom gages were 12.5, 6.8 and 5.4 degrees C, respectively, and calculated values were approximately 15 per cent less. Zichner also reports observations on the midspan deflections of a simple span twin web tee-beam of 39.3 m (129 feet) span. The midspan deflection was measured as 7.8 mm (0.31 inch) maximum. That value corresponded to an effective differential temperature of 8.1 degrees C and was in good agreement with the results predicted by the heat flow analysis. Measured strains in the prestressing strand in the bottom slab of a single cell box girder were also given. The daily range due to an effective differential temperature of 3.4 C degrees was 153 microstrain. That change would be equivalent to a stress change of approximately 31.0 MPa (4.5 ksi).

The "state of the art" for calculation of differential temperature stresses in concrete box girder bridges is a two-dimensional heat flow analysis with arbitrary boundary conditions and including both convective and radiative heat transfer at the surfaces, coupled with a non-linear iterative

analysis to determine the stresses produced by a given temperature distribution. Such an analysis is time-consuming, beyond the capabilities of most design offices, and often unnecessarily complex. The "state of practice," meaning the best practical procedure, is a unidimensional heat flow analysis with both radiative and convective heat transfer at the boundaries, coupled with a homogeneous linear elastic analysis for thermal stresses due to a given temperature distribution in one direction. Non-linearity would be considered qualitatively by choosing the moment of inertia and area of the section with due regard for the state of stress after application of the thermal stresses. It is concluded that any reasonable procedure for considering thermal stresses would result in the designer taking definite measures to provide for those stresses. The designer would either provide mild steel reinforcing to distribute potential cracks or increase the level of prestress to attempt to prevent them.

The important point is that cracking can only be prevented by the application of prestress if the designer can be very confident that all loadings have been taken into account as well as all local stress concentration factors. This is seldom the case. Therefore, it would appear that the most prudent design approach would be to provide prestressing on a "load balancing" approach for dead load plus frequently occuring live load. The required ultimate moment would be provided by the prestressing steel plus additional mild steel. Crack width and change in steel stress should be controlled to insure proper durability and fatigue resistance.

3. CREEP AND SHRINKAGE STUDIES

This chapter reviews the report entitled "Instrumentation of the Denny Creek Bridge" dated August 1981 and prepared by the Construction Technology Laboratory (CTL) for the Washington State Department of Transportation (1.2). The observations, findings, and recommendations of the CTL report are included as Appendix E of this report for reference. Additional creep and shrinkage data collected in this study are presented. The correlation between the two sets of data is examined and their significance for design assessed. An estimate of the stresses is developed for the current stress levels at the instrumented sections of the bridge and that estimate compared with the currently measured strain values.

3.1. CTL Observations, Findings and Recommendations

Observation No. 1 states, "In the first 100 days, longitudinal deformations in the bridge were caused primarily by instantaneous strains." Table 3.1 lists creep strain and specific creep values for each of the laboratory specimens at 100 days and 600 days. These values were obtained by linear interpolation between values given in the CTL report and reproduced in Appendix D to this report. Approximately 80 per cent of the creep at 600 days occurred in the first 100 days. The CEB-FIP curves for time rate of development of creep (i.e., k) show that even if correction is made for the greater thickness of the Denny Creek Viaduct concrete than that of the laboratory specimens, 35 to 50 per cent of the creep strain due to a given load increment would have occurred in the first 100 days. Load history was the major cause of the differences in creep behavior for the specimens tested by CTL in the laboratory and those observed in the bridge. The laboratory specimens were subjected to a constant stress history, whereas the bridge concretes experienced a highly variable stress history. The linearized creep

theory utilized by CTL to predict the measured strains provides acceptable results for essentially constant stress histories but is less effective for variable stress histories. Ross (2.1) has discussed the various creep theories and their reliability for relatively simple stress histories. The prediction of behavior for decreasing stresses is particularly difficult. The dead load of the structure was added in several stages and was not complete until approximately 100 days or more after casting the first stage. CTL's Observation No. 1 would not seem easily defensible given the known difficulty in predicting creep behavior in concrete experiencing as complex a stress history as that for the construction of the Denny Creek Viaduct.

Table 3.1.

Percentage of 600 Day Specific Creep Developed in First 100 Days

Concrete from Stage	Age at Loading	Creep at 100 Days [1]		Creep at 600 Days [1]		Per cent of 600 day crp in 1st 100 days
2	days	3	4	3	4	5
I @ 1200	4	852	0.710	1063	0.886	80
I 1900	27	1228	0.646	1556	0.819	80
I 2000	90	1138	0.569	1422	0.711	80
II 1500	5	795	0.530	980	0.653	81
II 1200	28	596	0.497	745	0.621	80
II 2000	91	971	0.486	1240	0.620	78
III 1200	8	701	0.584	909	0.758	77
III 2000	29	1101	0.551	1480	0.740	74
III 2000	92	931	0.466	1267	0.634	74

Notes:
1. Linear interpolation from data in CTL Report
2. Load in psi
3. Creep strain in microstrain
4. Specific creep in microstrain/psi
5. 100(Sp crp at 100/Sp crp at 600)

Observations No. 2 & 6 are cited by CTL as primary evidence of the redistribution of stresses in the cross-section due to creep and shrinkage. That observation, however, conflicts with the sign of the strains recorded at several locations. The measured strains for gages C-11 and C-14 were still tensile strains even after correction for the temperature difference between the new Stage III concrete and the previously cast stages. The issue of how to correct the readings for this differential temperature is discussed in more detail later. Even so, the strains indicated by gages 11, 12, 13 and 14, located in the Stage III concrete, were still found to be tensile in measurements made for this study. It is believed that the discrepancy is due to the relaxation factor applied by CTL to the calculated corrections. CTL used a relaxation factor appropriate to a slowly applied load rather than the factor appropriate to a suddenly applied load. This difference is significant, as is discussed in more detail later.

Observation No. 3, Finding No. 2 and Recommendation No. 3 all concern tensile stresses generated in Stage III by the temperature difference between the new concrete and the previously placed concrete. In the CTL report, tensile stresses for Stage III concrete were apparently calculated by applying the method described in that report to the difference in the average temperature for the new concrete and the old concrete at each section and using the modulus of elasticity and coefficient of thermal expansion measured on the laboratory specimens. The stresses calculated by CTL are tabulated in Appendix D of their report after modification by the relaxation factor shown in Figure 15 of that report. These CTL stresses appear to be the stresses appropriate for a simple span, and apparently neglect the compensating stresses caused by flexural restraint furnished by the monolithic piers and adjacent span. Those compensating stresses are large compared to the primary stresses.

The actual temperature distribution is also much more complex than that assumed for the CTL analysis due to conduction of heat from the new to the older concrete. Conduction eases the apparent peak temperatures, especially at the interface between the two concretes. Peak concrete temperatures occur in the first two days for sections of the thickness used in the Denny Creek Viaduct. Thus, the appropriate relaxation factor is closer to that for suddenly applied loads rather than that for loads applied in a time scale commensurate with the development of creep and shrinkage. Leonhardt (3.1) gives the relaxation factor for suddenly applied loads as $e^{-\phi}$ and the factor for slowly applied loads as that shown in Figure 15 of the CTL report. The former factor gives a much more rapid decay of the stresses for the same ratio of creep strain to elastic strain (i.e., same ϕ). The CTL report focused on creep and shrinkage and stress redistribution effects. Therefore, a correction for "locked in" temperature stresses was appropriate. However, the magnitude of the correction utilized by CTL is highly questionable.

Stresses due to restraint of cooling contractions are augmented by stresses generated by the restraint of differential shrinkage between the new and the old concrete. In Span 4 of the Denny Creek Viaduct, the potential differential shrinkage between the Stage II and III concrete is 60 microstrain, based on the data given in Appendix B of the CTL report, corrected for the difference in properties between the laboratory specimens and field concrete, and the difference between the as-built and as-designed construction schedule. That strain is equivalent to an additional cooling of 12 degrees F for a coefficient of thermal expansion of 5 microstrain per degree F. The time scale for those two effects is, however, quite different. From the temperature records it can be seen that cooling was probably complete within the first week after the pour. By contrast, the differential shrinkage strains

must have developed slowly over several months. Currently, the soffit of the Stage III concrete is cracked in most spans of the Denny Creek Viaduct. Similar cracks are also visible in isolated locations in the soffit of the Stage II concrete that forms the interior of the box girder. Those Stage II soffit cracks in Span 2 near Pier 3 were measured and found to have widths at the surface less than 0.1 mm (0.004 in). Personnel from the WSDOT Resident Engineer's office mapped the cracks observed in Stage II and classified the extent of cracking in the various spans. Shown in Figure 3.1a are the cracks and prestress for Spans 5 and 6. The cracks in Stage II roughly correlate with the location of the post-tensioning tendons in Stage II. For example, cracks are more numerous in that portion of the Stage II slab extending from the construction joint to the forward, in the sense of the direction of construction, 3/4 point of the span than in the portion of the slab between the pier and forward construction joint. The number of tendons in the Stage II slab for the former region were significantly greater than for the latter region. The data on the Stage II cracking were received as this manuscript was in preparation and therefore were not available for extended study. No reason is readily apparent for the differences in the extent of cracking in the Stage II slab from span to span. However, the cracking in both Stages II and III would be influenced by differences in temperature between the new and the old concrete at the time of casting and during subsequent curing, restraint of differential shrinkage between the two concretes, and possibly tensile stresses induced by the stage construction methods. All three factors were present to varying degrees in each span and would contribute to the potential for cracking. No cracking was noted by the authors of this study on the deck surface prior to placement of the overlay and the cracks in the Stage II soffit appeared to have sealed.

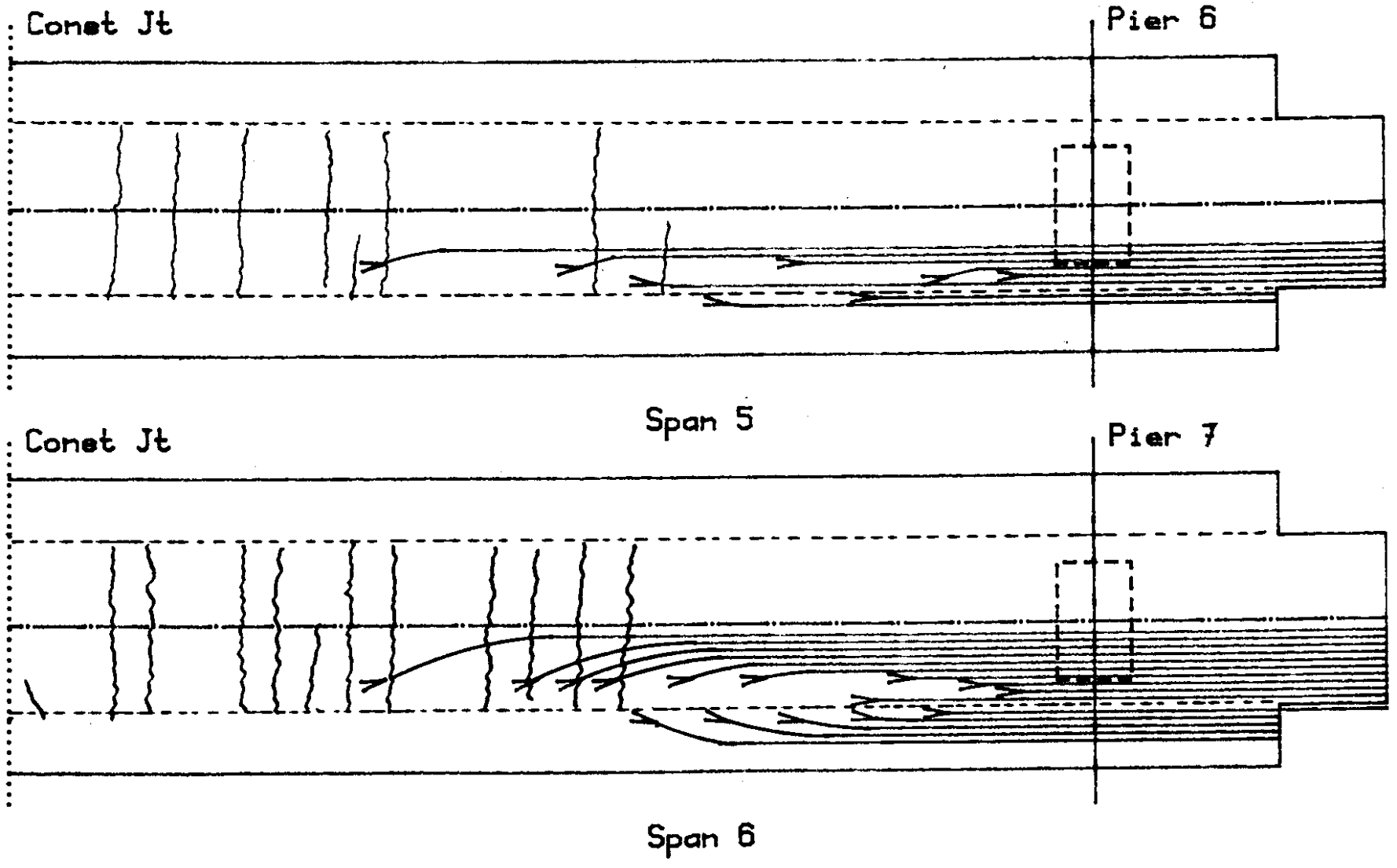

Fig. 3.1a Stage II cracking and Stage II and III prestress tendons, Spans 5 and 6

The development of a complete stress history with full accounting for all changes in loading, support and member properties is beyond the scope of the current investigation. In order to fully account for all changes, it would be necessary to take incremental creep and shrinkage effects into account. Further, in light of the known inability of the various methods for analyzing creep effects to accurately predict measured results, and the uncertainties in the basic parameters to be used in such analyses, that effort would be questionable. However, in order to give a feeling for the significance of these effects and for the stresses due to temperature gradients, an approximate calculation was made of the stresses due to permanent loads and creep and shrinkage effects. The results are presented in Tables 3.2 to 3.4. Table 3.5 describes the entries in those tables.

For generation of Tables 3.2 through 3.4, creep and shrinkage parameters were estimated using a combination of the laboratory test data contained in the CTL report and the procedures and graphs given in the 1970 CEB-FIP report (2.6). The CTL data for 6 x 12 inch cylinders tested at 70 per cent relative humidity and 20 degrees C temperature were used to determine basic values for shrinkage and creep parameters. Those values were adjusted to account for differences betwen the properties and conditions for the test cylinders and the bridge. Those differences include the greater theoretical thickness for the bridge, the annual average relative humidity at the bridge, about 75 per cent, duration of loading from the event under consideration to the final condition, age since cessation of curing, and reinforcement. A cylindrical specimen with sealed ends was assumed to be the shrinkage and creep specimen used by CTL. The theoretical thickness, volume divided by twice the surface area, for such a specimen is 3.8 cm (1.5 in), for which the CEB-FIP correction factor is 1.3 for k_e, the partial factor for theoretical thickness. The theoretical thickness of the bridge members, calculated in a similar manner,

Table 3.2

Calculation of Existing Stress Levels in the Denny Creek Viaduct with correction for creep, differential shrinkage, and differential temperature at casting of succeeding stages
Section A near Pier 5

Load	M	Stage I		Stage II		Stage III	
		fcb	fct	fcb	fct	fcb	fct
	kip-ft	psi	psi	psi	psi	psi	psi
DL1	-37914	-1344	469	469	696	469	696
DL2	-5163	-183	64	64	95	64	95
0.86(PT + PT2)	30210	1296	-1312	-1312	-1638	-1312	-1638
Sum DL+0.86PT	-12867	-231	-779	-779	-847	-779	-847
Sum const		-1022	-1238	-472	-456	44	78
phi = 1.00		-522	-948	-666	-703	-476	-507
phi = 2.00		-338	-841	-737	-794	-668	-722
DT12 *		5	-67	55	51	0	0
DS12		-1	-37	30	28	0	0
DT23 *		-85	-80	-80	-79	225	231
DS23		-38	-36	-36	-35	101	104
Sum DT+DS		-119	-220	-31	-35	326	335
Sum perm loads		-641	-1168	-697	-738	-150	-172
LL+I +M	1458	52	-18	-18	-27	-18	-27
-M	-8429	-299	104	104	155	104	155
Sum perm +M		-589	-1186	-715	-765	-168	-199
Sum perm -M		-940	-1064	-593	-583	-46	-17
+ 40F DT		-133	60	60	-813	60	-813
- 15F DT		-445	113	113	451	113	451
Sum perm +M+DT		-722	-1126	-655	-1578	-108	-1012
Sum perm -M-DT		-1385	-951	-480	-132	67	434

Note: tension +

*See Figure B.1 for stress before relaxation and continuity moment.

Table 3.3.

Calculation of Existing Stress Levels in the Denny Creek Viaduct with correction for creep, differential shrinkage and differential temperature at casting of succeeding stages
Section B at 1/4 point

Load	M	Stage I		Stage II		Stage III	
		fcb	fct	fcb	fct	fcb	fct
	kip-ft	psi	psi	psi	psi	psi	psi
DL1	223	11	-3	-3	-5	-3	-5
DL2	30	1	0	0	-1	0	-1
0.86(PT + PT2)	1565	-315	-228	-228	-213	-228	-213
Sum DL+0.86PT	1818	-303	-231	-231	-219	-231	-219
Sum const		-733	-934	-137	-117	46	74
phi = 1.00		-461	-490	-196	-181	-129	-111
phi = 2.00		-361	-326	-218	-205	-194	-179
DT12*		-3	-88	63	57	0	0
DS12		-1	-39	28	25	0	0
DT23*		-58	-59	-59	-60	143	146
DS23		-39	-40	-40	-79	95	98
Sum DT+DS		-101	-226	-8	-57	238	244
Sum perm loads		-562	-716	-204	-238	-109	133
LL+I +M	1786	90	-22	-22	-36	-22	-36
-M	-1768	-89	21	21	35	21	35
Sum perm +M		-472	-738	-226	-274	87	97
Sum perm -M		-651	-695	-183	-203	130	168
+ 40F DT		-133	60	60	-813	60	-813
- 15F DT		-445	113	113	451	113	451
Sum perm +M+DT		-605	-678	-166	-1087	147	-716
Sum perm -M-DT		-1096	-582	-70	248	243	619

Note: tension +

*See Figure B.2 for stress before relaxation and continuity moment.

Table 3.4.

Calculation of Existing Stress Levels in the Denny Creek Viaduct with correction for creep, differential shrinkage, and differential temperature at casting of succeeding stages
Section C at CL Span 4

Load	M	Stage I		Stage II		Stage III	
		fcb	fct	fcb	fct	fcb	fct
	kip-ft	psi	psi	psi	psi	psi	psi
DL1	20619	1040	-250	-250	-411	-250	-411
DL2	2809	142	-34	-34	-56	-34	-56
0.86(PT + PT2)	-21686	-1681	-106	-106	90	-106	90
Sum DL+0.86PT	1742	-499	-390	-390	-377	-390	-377
Sum const		-1102	-1391	-186	-237	39	63
phi = 1.00		-721	-758	-315	-325	-232	-215
phi = 2.00		-581	-525	-362	-358	-332	-317
DT12*		17	-139	83	70	0	0
DS12		5	-43	26	21	0	0
DT23*		-31	-91	-91	-98	154	152
DS23		-17	-52	-52	-56	87	86
Sum DT+DS		-26	-325	-34	-63	241	238
Sum perm loads		-747	-1083	-349	-388	9	23
LL+I +M	6579	332	-80	-80	-131	-80	-131
-M	-2174	-110	26	26	43	26	43
Sum perm +M		-415	-1163	-429	-520	-71	-108
Sum perm -M		-856	-1057	-323	-345	35	66
+ 40F DT		-133	60	60	-813	60	-813
- 15F DT		-445	113	113	451	113	451
Sum perm +M+DT		-548	-1103	-369	-1333	-11	-921
Sum perm -M-DT		-1301	-944	-210	106	148	517

Note: tension +

*See Figure B.3 for stress before relaxation and continuity moment.

Table 3.5.

Calculation of Existing Stress Levels in the Denny Creek Viaduct with correction for creep, differential shrinkage, and differential temperature at casting of succeeding stages

Load	Description of Entries in Tables 3.2, 3.3, and 3.4	
DL1	Dead load structural concrete	D&W Jun 77
DL2	Dead load curbs, overlay	Final frame
0.86(PT +PT2)	Post-tension incl 2ndry mnts	built at one
Sum DL+0.86PT	Mf = summation permanent loads	time
Sum const	Mo = summation construction stresses	D&W June 77
phi = 1.00	Mo * exp(-0) + Mf * (1-exp(-0))	
phi = 2.00	" " " "	
DT12	Stresses due to DT casting Stg II * exp(-1.00)	
DS12	Stresses due to DS I/II * relaxation, phi=1.00	
DT23	Stresses due to DT casting Stg III * exp(-1.00)	
DS23	Stresses due to DS II/III * relaxation, phi=1.00	
Sum DT+DS	Summation stresses due to diff temp ad shrink	
Sum perm loads	Summation perm loads and DT&DS for phi = 1.00	
LL+I +M	Design live load and impact 3 lanes HS-20	
-M	" " " " " " " "	
Sum perm +M	Service load stresses w/o add'l diff temperature	
Sum perm -M	" " " " " " "	
+ 40F DT	Stresses due to diff temp Priestley's method	
- 15F DT	" " " " " " "	
Sum perm +M+DT	Service load stresses w/add'l diff temperature	
Sum perm -M-DT	" " " " " "	

is approximately 40 cm (16 in), for which the k_e factor is 0.55 for shrinkage and 0.72 for creep. The average value of the steel reinforcing ratio is approximately 0.7 per cent when both the mild steel reinforcing and prestressing steel are included. The partial factor on shrinkage, k_p, is thus 0.88. There is no corresponding partial factor on creep. The laboratory specimens were also assumed to be made from the actual concrete used on the project or from a similar mix. Thus, the partial factor for concrete composition, k_b, was already taken into account in the laboratory specimens. CTL results for tests on three sets of creep specimens were used to develop partial factors for creep, dependent on the age of the concrete at first loading, k_p. It is recognized, of course, that the stress history for the bridge concrete was far from constant as implied by this approach. The creep and shrinkage values at the termination of the laboratory tests were taken as the ultimate values for the CEB-FIP graph for calculation of the partial factor on load duration for creep or age after curing for concrete with a theoretical thickness of 5 cm (2 in). A single parameter for creep and shrinkage, applicable for all three stages, was developed by averaging the data from all CTL tests. The anomalous result for creep in the Stage II concrete, loaded at 28 days, was disregarded for this estimate. That concrete showed much more creep than the same concrete loaded at 7 days amd much more creep than the two other concretes loaded at 28 days. The resulting partial factors and calculated shrinkage values are as follows:

Partial Factor	As Measured in Laboratory ($k = 1.3$)	As Corrected to Bridge Site ($k = 0.55$)
(1) Basic creep for		
load at 7 days	2.38	1.26
load at 28 days	2.06	1.09
load at 90 days	1.83	0.97
(2) Shrinkage potential ($\times 10^6$)	800	300
(3) Differential shrinkage ($\times 10^6$), k_t, for Stage I when Stage II cast (19 days) ($\times 10^6$)		27
for Stage I, II when Stage III cast (80 days) ($\times 10^6$)		60

The differential temperature at casting of the new concrete against the existing concrete was relaxed by the factor $e^{-\phi}$ and the loading was assumed to occur at 7 days. The appropriate creep factor, ϕ, was therefore estimated as 1.00. The differential shrinkage potential between the new and the old concrete was relaxed by the factor $\frac{1-e^{-\phi}}{\phi}$ using the same creep factor. The analysis in Appendix A of the CTL report was used to compute the stresses, before relaxation, attributable to those two effects. For this calculation, the modulus of elasticity of the concretes was assumed to be 3500 ksi for the new concrete and 4800 ksi for the old concrete. Flexural restraint stresses were calculated for the structural configuration effective at the time, as taken from the Resident Engineer's records (see Construction Chronology, Appendix A).

In lieu of a separate calculation of the stress history, the stresses due to dead load and prestressing were estimated by Dischinger's method using the results presented in Dyckerhoff and Widmann's check analysis of the contractor's construction scheme. In that analysis, two stress conditions are reported: a summation of the stresses at each point for all elastic effects taken on the appropriate statical system without modification for creep redistribution or loss of prestress, and the stresses at the same points calculated as if the structure were constructed at one time on falsework and post-tensioned. The summation of the construction stage stresses is designated f_o,

and the summation of the stresses as if built on falswork is designated f_f. Stresses f_f are calculated with an assumed 14 per cent loss in prestress. The adjusted stresses due to the permanent loads existing at the time of the July-August 1982 observations is calculated as the sum

$$f = f_o e^{-\phi} + f_f (1-e^{-\phi}) \qquad (3.1)$$

Live load plus impact stresses for the positive and negative envelope values at each section, differential temperature stresses calculated using Priestley's method, and the summation of those stresses, the permanent load stresses, the calculated stresses due to the concrete temperature differences at placement, and the calculatd shrinkage stresses are listed in Tables 3.2, 3.3 and 3.4.

Comparison of these tabulated stresses with the allowable stresses for a concrete with the minimum specified strength of 5000 psi shows that, at Section A near Pier 5 (Table 3.2), only the stress at the top surface of the Stage III construction, for the case of permanent load, full negative live load, differential shrinkage, and a negative differential temperature of 15 degrees F, is greater than the allowable tensile stress of 212 psi ($3\sqrt{f'_c}$) and while that stress exceeds the allowable by a considerable amount, it is still less than the likely stress for cracking. At Section B, the quarter point of Span 4(Table 3.3), the live load stresses are small in comparison to the differential temperature stresses. The effective centroid of the post-tensioning force is near the neutral axis, and thus, stresses due to permanent loads are smaller in absolute value than at the other two sections. The stresses due to differential temperature are substantially the same as at the other two sections, and thus, the resultant stresses under the dead load, live load, and differential temperature are significantly higher. Tensile stresses exist at the top of the Stage II and III construction and at the bottom of the Stage

III construction. The maximum tensile stress of 619 psi exceeds the cracking strength of 531 psi ($7.5\sqrt{f'_c}$) normally anticipated for this concrete. A similar situation exists at Section C except that the maximum tensile stress, 517 psi, is somewhat lower.

From Tables 3.2 through 3.5 it can be concluded that for the condition of permanent stresses, live load stresses, and differential temperature stresses:

1. The maximum tensile stresses are very local, reducing quickly with depth in accordance with Priestley's fifth order parabola.

2. These high tensile stresses will be significantly reduced by any cracking.

3. The stresses have been computed neglecting the concrete overlay, which would have the effect of reducing extreme temperatures while simultaneously increasing overall stresses by contributing more area subject to the extreme temperature.

4. The tensile stresses predicted here have no influence on the ultimate flexural capacity of the bridge.

The strain distributions over cross-sections A, B and C, predicted by this analysis, are compared with the results measured during Event No. 77 on 5 August 1982 in Figure 3.1b. The predicted stresses are converted to strains using an effective modulus one-half the instantaneous modulus (ϕ=1). The measured strains are significantly greater than the predicted strains, particularly in compression in the bottom fiber near the piers.

Observation No. 4 draws attention to large strains due to shear in the bottom slab of the box girder near the support. The difference between the strains indicated by gage 4 and those indicated by gages 3 and 5, for all three sections, is taken as evidence of shear lag. Gage 4 was attached to the top mat of deformed reinforcing steel in the bottom slab, whereas gages 3 and 5 were attached to the bottom reinforcing steel of the same slab. At Section A for that difference in distance from the neutral axis, the ratio of the bending stress at gages 3 and 5 to that at gage 4, for three different construction stages, should be as follows:

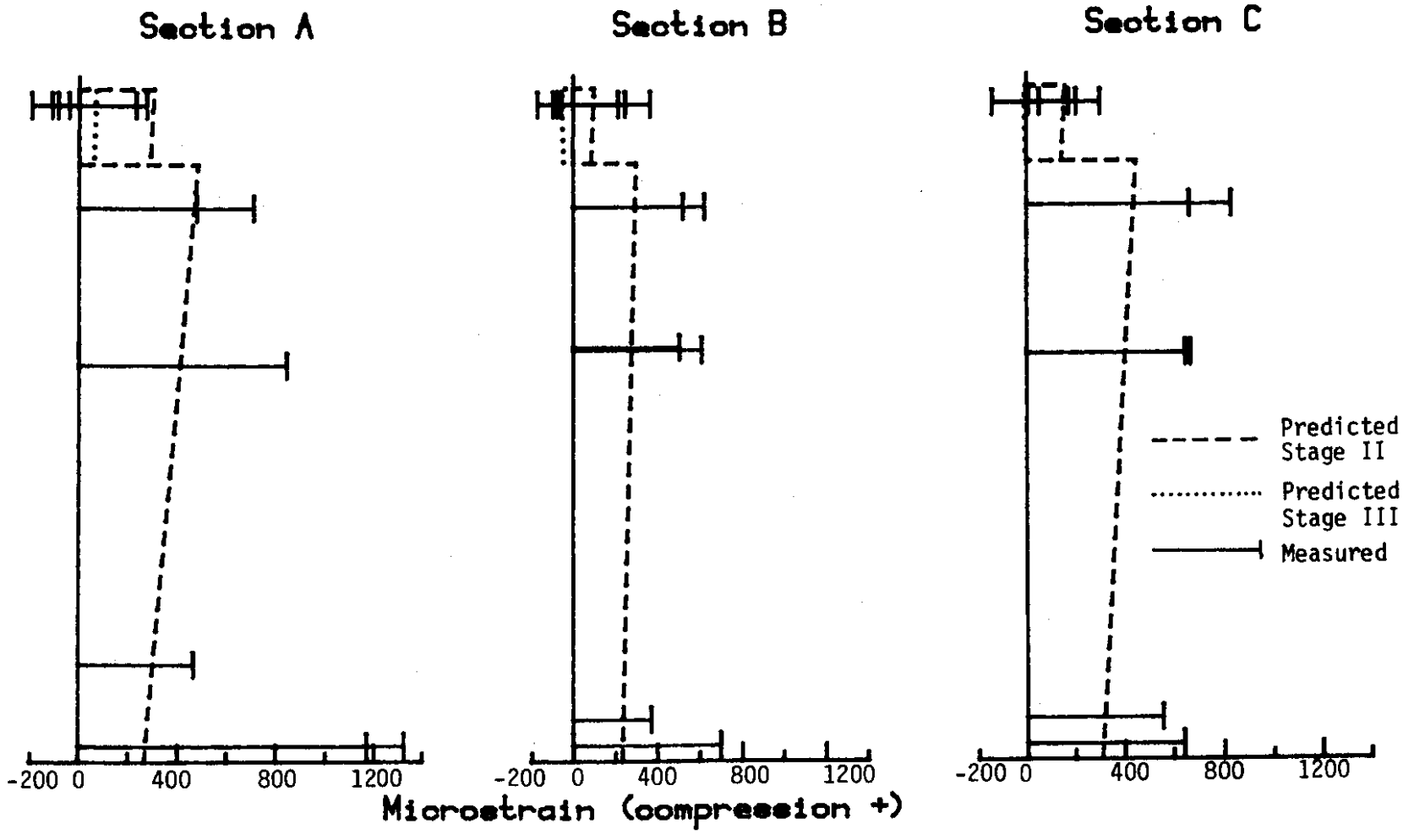

Fig. 3.1b Comparison of measured and predicted strains Event 77 AM 9 Aug
(No differential temperature effect)
See Tables 3.2-3.4 for predicted values, Table B 1 for measured values

Stage I: y_{bcgc}=36.7" $y_{b3,5}$=2.5" y =15.8"

$(y_{bcgc}-y_{b3,5})/(y_{bcgc}-y_{b4})=(36.7-2.5)/(36.7-15.8)=1.64$

Stage II: y_{bcgc}=59.2"

$(y_{bcgc}-y_{bc,5})/(y_{bcgc}-y_{b4})=(59.2-2.5)/(59.2-15.8)=1.31$

Stage III: y_{bcgc}=71.4"

$(y_{bcgc}-y_{bc,5})/(y_{bcgc}-y_{b4})=(71.4-2.5)/(71.4-15.8)=1.24$

Thus, the bending stresses at gages 3 and 5 should overall be higher than that at gage 4. Figures 21, 22 and 23 of the CTL report are reproduced in Appendix E. It can be seen that the differences cited above are sufficient to account for the differences in results for gages 3, 4 and 5 for Sections B and C. Figures 21, 22 and 23 also show CTL's predicted strains. Those strains are less than the measured strains for all three gages and all three locations. If the differences in the measured strains for gages 3, 4 and 5 were primarily due to shear lag, it is reasonable to expect the strains predicted by beam theory to be intermediate between those measured for gages 3 and 5 and those measured for gage 4. When torsional effects are also considered, then it is obvious that the strains of gage 5 should be greater than those at gage 3 and the difference should diminish with increasing distances from the pier. Finally, Poisson's effect due to vertical stresses caused by pier reactions would also affect the gages at Section A. Those effects could amount to 15 to 20 per cent of the column stress. Thus, the difference in strains for gages 3 and 5 as opposed to gage 4 cannot be explained solely by shear lag.

Finding 4 refers to the method of analysis used by CTL to calculate the deformations caused by creep, shrinkage and temperature, and it is claimed that with the exception of the results for gages 3 and 5 there is excellent agreement between measured and predicted strains. The CTL method of analysis was presumably based on the enforcement of strain compatibility at the interface between the different stages for the four different deformation

conditions: instantaneous creep, shrinkage, and temperature, for which independent relationships are described in the CTL text on page 26. CTL developed a computer program for predicting the resultant strains. Details of that program are not given. Without those details it is unclear how the multiple construction stages were taken into account and which creep factors were used when the concretes were of differing ages. Based on the corrections made to measured strains to account for the observed differential temperatures when succeeding stages were cast, it appears that flexural restraint effects were also neglected.

Recommendation 1 states that "use of concretes with comparable elastic properties will minimize strain or stress redistribution within cross-sections." The reason for that recommendation is unclear. The design of the Denny Creek Viaduct relied on strain and stress redistribution for satisfaction of the service load design criteria at all stages of construction and service. A more appropriate recommendation would be for designers to state on the plans or in the specifications precisely what assumptions have been made in this regard and, therefore, what limitations should be imposed upon construction schedules and concrete mix designs.

The CTL report notes, page 23, that "measured strains cannot be used directly to calculate stress levels because of time-dependent behavior and redistribution of stresses caused by different end conditions." It is stated that an iterative procedure was developed to estimate stress levels. That iterative procedure is presumed to be the procedure derived from the analytical method discussed with reference to Finding 4. A vital question for assessing the appropriateness of that procedure would be the sensitivity and stability of the iterations to the accuracy of the assumed stress history. The CTL study used stress histories based on the erection stress calculations

made by Dyckerhoff and Widmann and dated 22 June 1977. Those were the stress calculations available to WSDOT at the onset of the CTL study. Some of the limitations and assumptions are stated in Appendix C of the CTL report, which is reproduced in this report in Appendix E. During this study, it was found that some construction procedures differed from those assumed in the Dyckerhoff and Widmann calculations, and not all of these limitations were considered in CTL's predictions of the stress histories. Changes were as follows:

(A) The load on the tip of the cantilever, due to the casting of Stage I in the span ahead of the point under consideration, was assumed in the erection calculations to be 518 kips. Revisions in the erection procedure resulted in that load being 625 kips and in a 250 kip load being applied to the tip of the cantilever prior to the casting of Stage II for the span under consideration. Although both loads were temporary loads, they must have caused at least some residual effect.

(B) The erection stress calculations assumed that Stage III construction followed behind Stage II construction by two spans in a regular sequence. In the actual construction, Stage III concreting lagged Stage II by more than two spans and the lag was not constant from span to span. At the time Stage I and II were cast in Span 4, Stage III construction had not progressed beyond Span I. That lag would have a small effect on the final stresses.

A more severe limitation than those changes in construction procedures is the fact that the erection calculations did not account for time dependent changes in support moments due to changes in the structural system and loss of prestress. In the absence of additional information on CTL's iterative procedure, it is impossible to assess the significance of such changes and limitations in the assumed strain history for matching the predicted and

measured strains. Further, the Dyckerhoff and Widmann erection calculations grouped several separate events together in one step. Some of those separate events were not of a negligible character. For example, the Stage III falsework truss at 211 kips was comparable in weight to the concrete in Stage III at 477 kips. The dates on which the falsework were moved on and off Span 4 lie between the readings shown in the erection calculations. Yet that event is not reflected in the erection calculations separately from the concrete placement event. The construction chronology taken from WSDOT's Resident Engineer's records is shown in Appendix A. Comparison of that chronology with the chronology assumed for the CTL study (Appendix E) shows that difference clearly. These observations are made from the vantage point of hindsight and considerable investigation. A stress analysis of sufficient detail to eliminate most of the discrepancies between the stress history assumed by CTL and the more likely stress history would be a major undertaking. Such an investigation would be more comprehensive than the investigation undertaken for the original design, and that for the erection review and the CTL report. It was also beyond the scope of this study.

Equation 2, page 30 of the CTL report (Appendix E), defines a reduction factor for creep dependent on the amount of reinforcement in the section. Additional comments and/or an example are needed to clarify the application of that equation. The appropriate value for the specific creep factor is not obvious when there are three concrete segments, all of roughly equal area, having different ages and different specific creep values. The CEB-FIP Recommendations (2.6, 2.7) do not include a reduction factor on creep for reinforcement and recommend use of a simpler, but more approximate, formula for reduction of shrinkage due to the presence of reinforcing steel.

3.2. Extended Strain Histories

The strain histories presented in Tables A1, A3 and A5 of the CTL report are reproduced in Appendix B of this report. Those strain histories were extended by strains measured during the course of this study and the extended histories are shown in Appendix B immediately after the CTL data. Additional readings were taken in this study on the following dates:

24 October 1980

8 July 1981

23 July 1981 Live load tests, average of before and after readings

9 August 1981

9 July 1982

12 July 1982

15 July 1982 through 14 August 1982

The CTL and University of Washington data provide a total of 89 separate readings spanning four years. Some of the readings taken under this study were made late in the day, when the effects of differential temperature due to solar heating of the top slab were present. These differential temperature effects have not been removed, nor has the correction for the differential temperature immediately after casting the subsequent stage been removed, as was the case in the CTL report. As discussed previously, there is no agreed procedure on how best to select the specific creep factors to be used in calculating the relaxation of the differential temperature strains. Nevertheless, it is apparent from Figures 3.2 through 3.16 that the data collected in this study conforms to the trends of the CTL data and that the endpoints for the CTL data are representative of the final creep values obtained in the bridge. It should be noted that the data taken on 24 April, 1 August, and 24 October 1980 were all obtained with a Carlson gage measuring bridge that provided readings with only three significant digits. Thus, those readings

are all subject to approximately $\pm$ 30 microstrain error. That reduced sensitivity was traced to a broken connection for the bridge amplifier in the readout device. The broken connection was repaired for the readings made subsequently in this study. Some of the connections in the switch boxes were damaged during installation of lead wires for the attempted automatic data collection system. While those connections were repaired prior to the collection of data in the summer of 1982, it is still possible that an additional component of lead resistance was introduced by the alteration of the connection. Some of the gages operated intermittently and sometimes there was a reappearance of signals from gages previously inoperative.

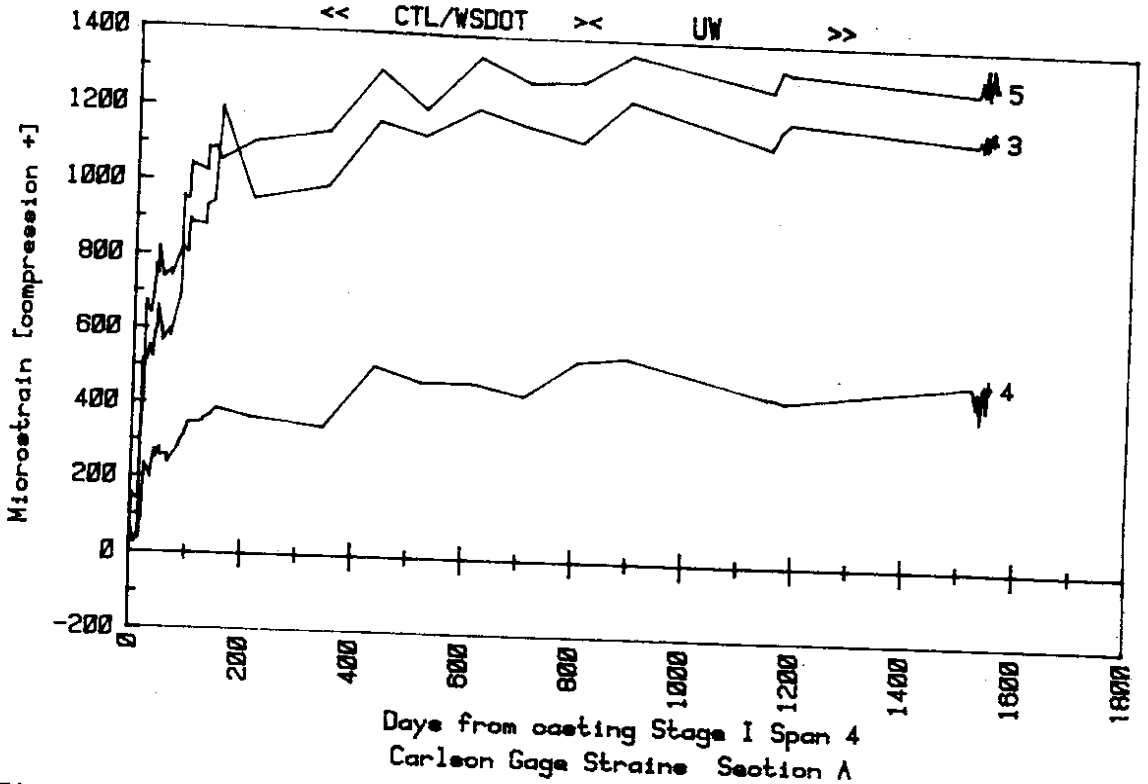

Figure 3.2. Carlson Gage Strains - Section A, Gages 3, 4, 5

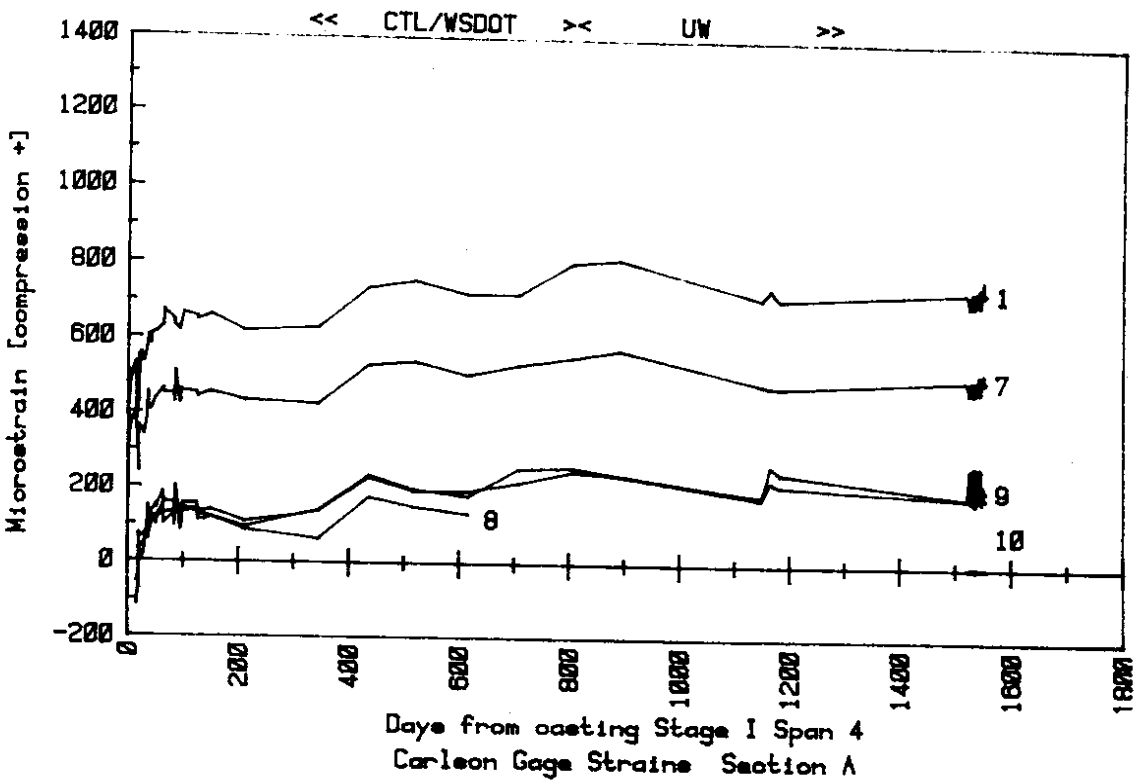

Figure 3.3. Carlson Gage Strains - Section A, Gages 1, 7, 8, 9, 10

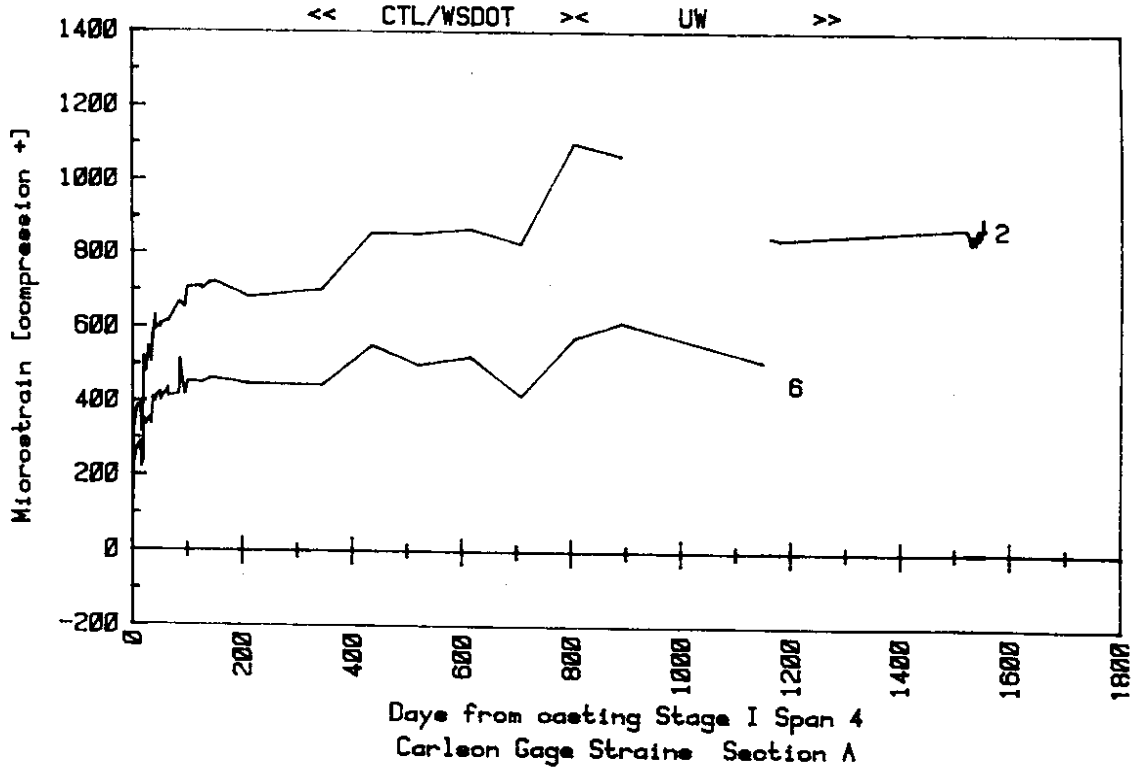

Figure 3.4. Carlson Gage Strains - Section A, Gages 2, 6

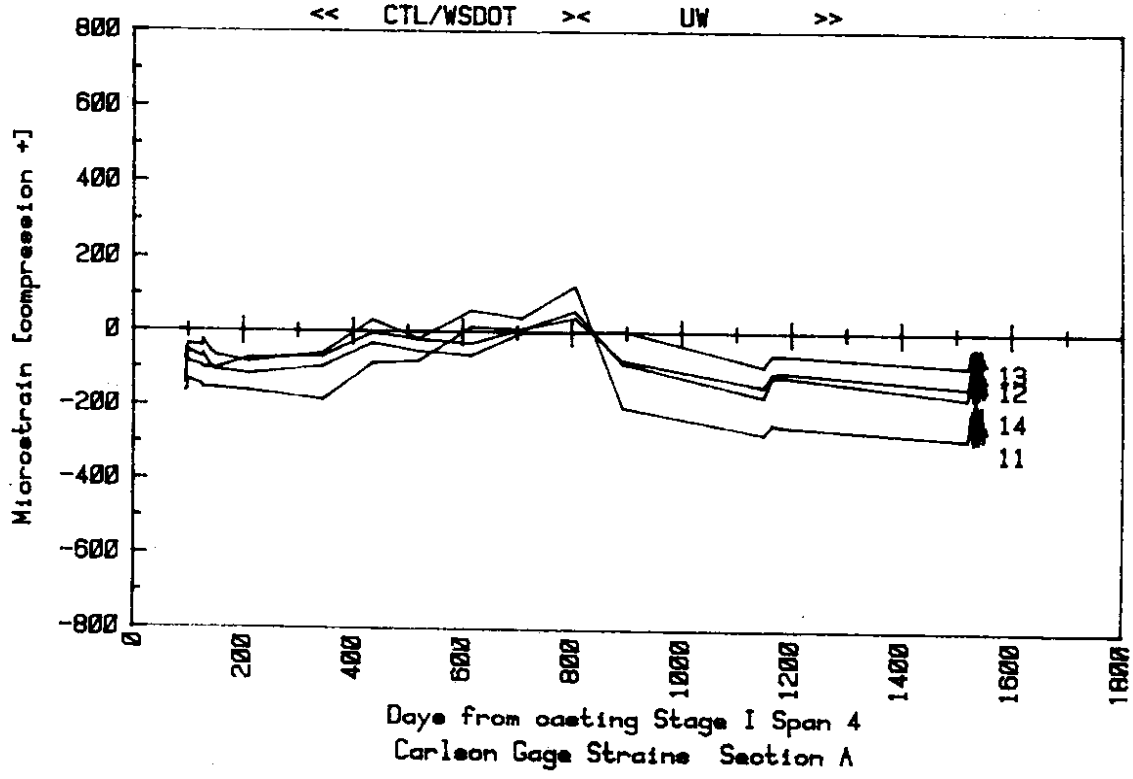

Figure 3.5. Carlson Gage Strains - Section A, 11, 12, 13, 14

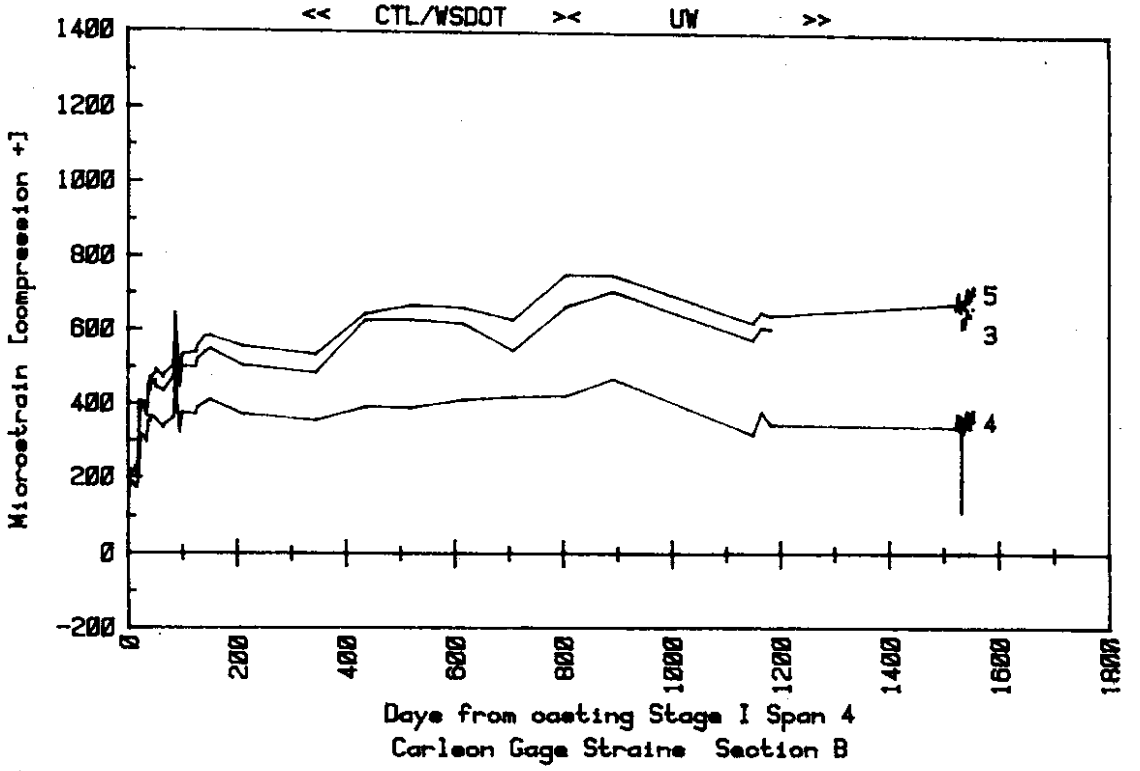

Figure 3.6. Carlson Gage Strains - Section B, Gages 3, 4, 5

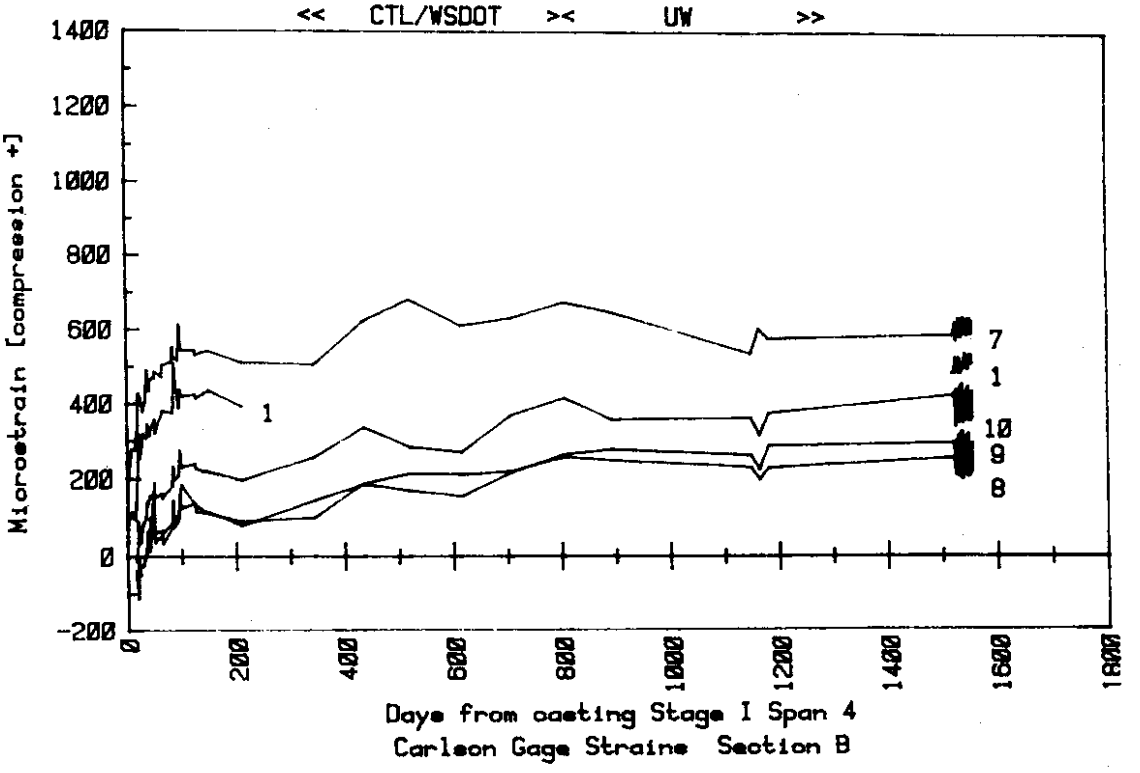

Figure 3.7. Carlson Gage Strains - Section B, Gages 1, 7, 8, 9, 10

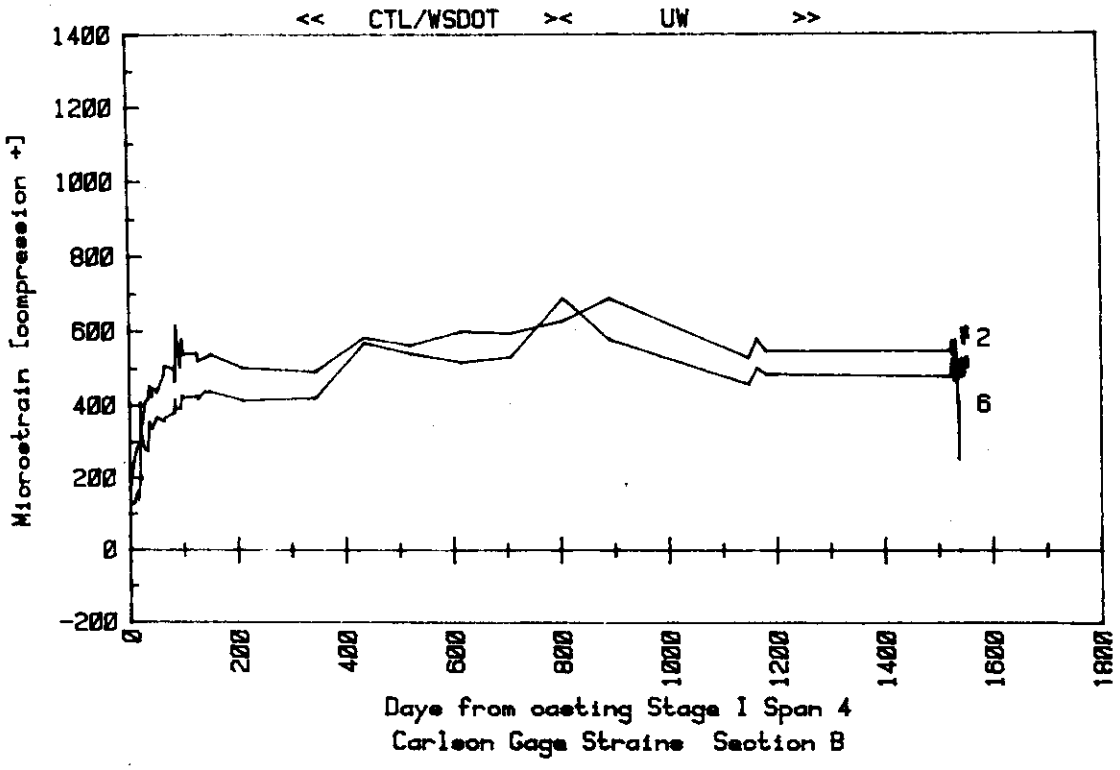

Figure 3.8. Carlson Gage Strains - Section B, Gages 2, 6

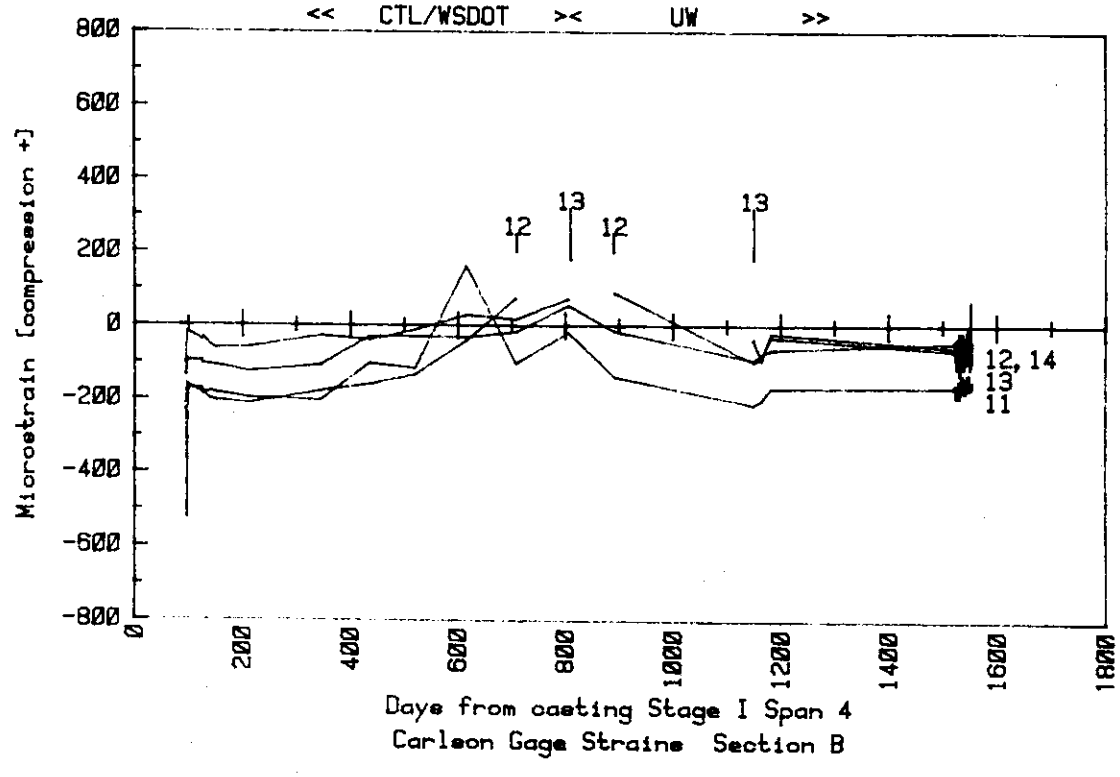

Figure 3.9. Carlson Gage Strains - Section B, Gages 11, 12, 13, 14

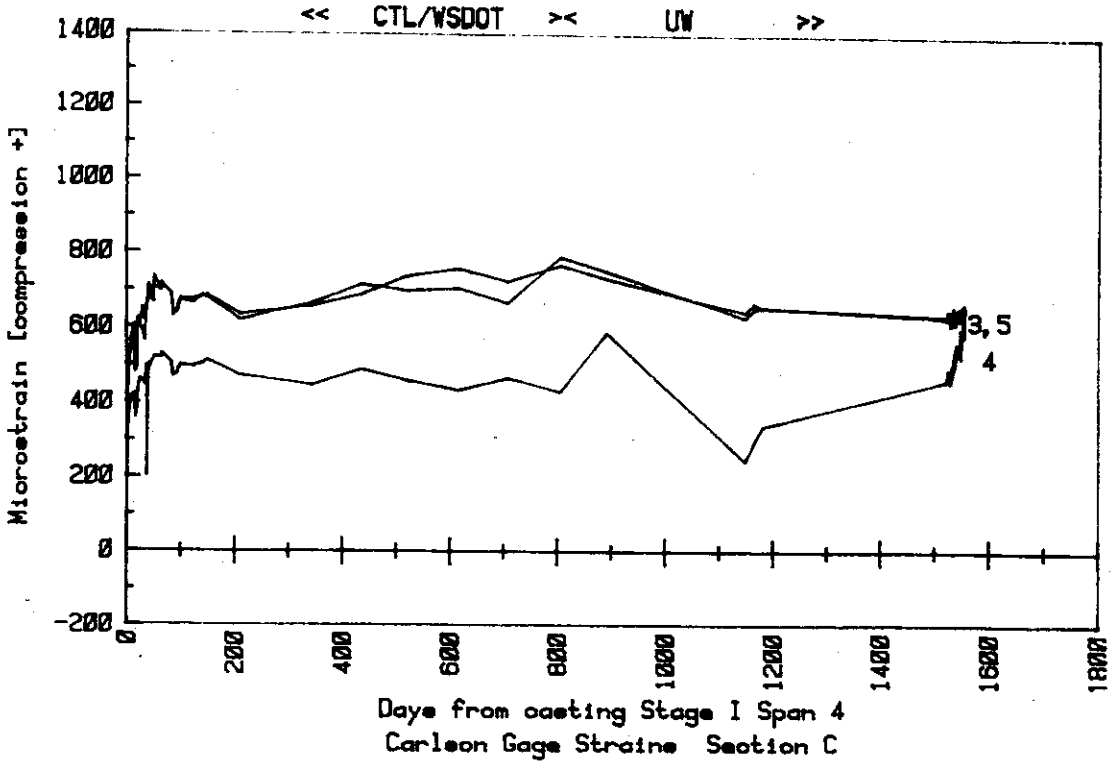

Figure 3.10. Carlson Gage Strains - Section C - Gages 3, 4, 5

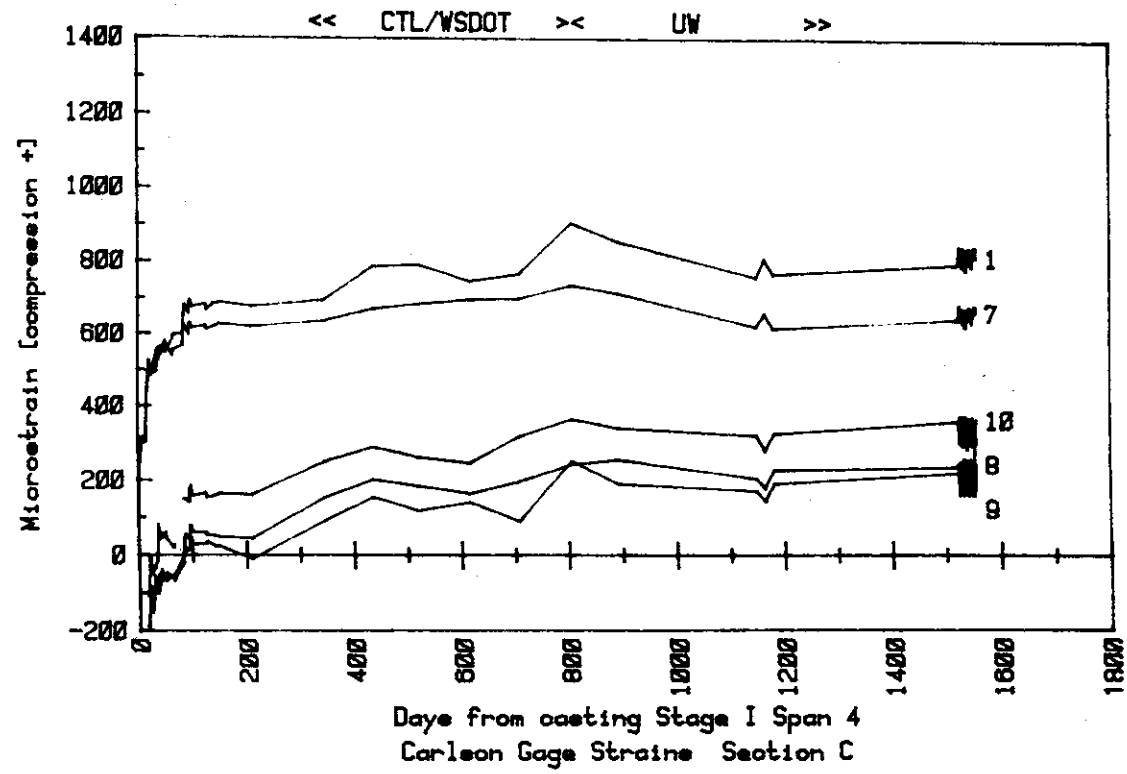

Figure 3.11. Carlson Gage Strains - Section C, Gages 1, 7, 8, 9, 10

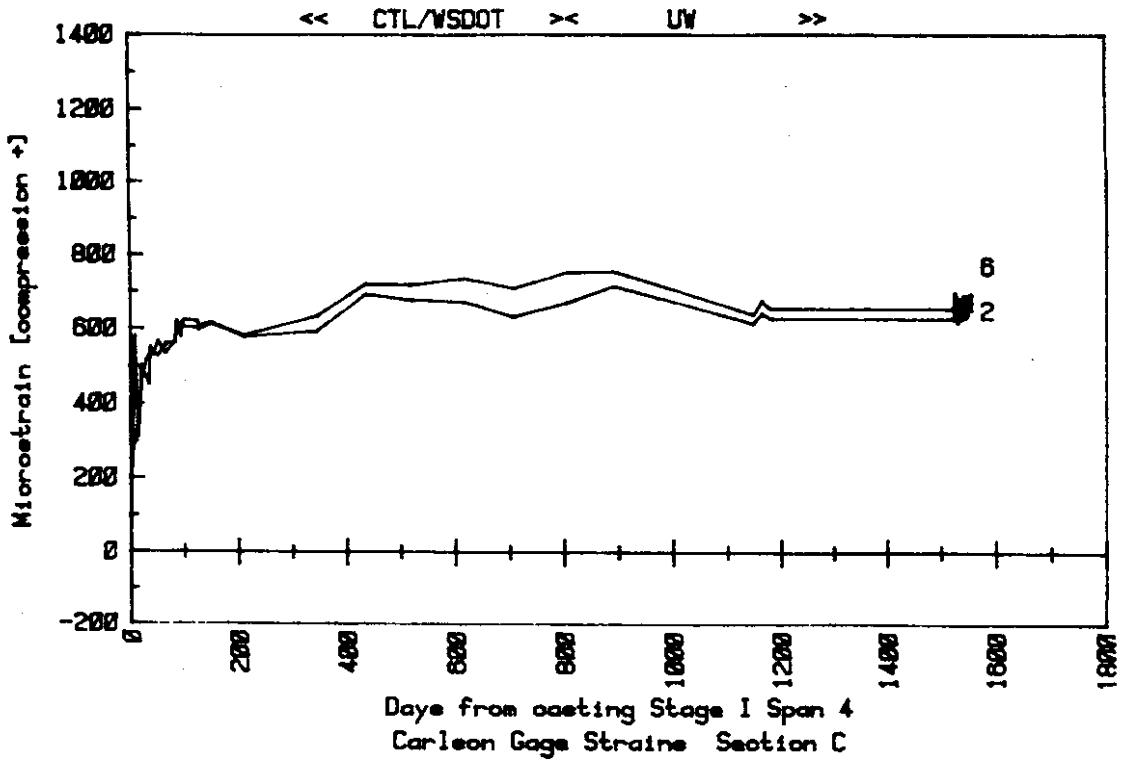

Figure 3.12. Carlson Gage Strains - Section C, Gages, 2, 6

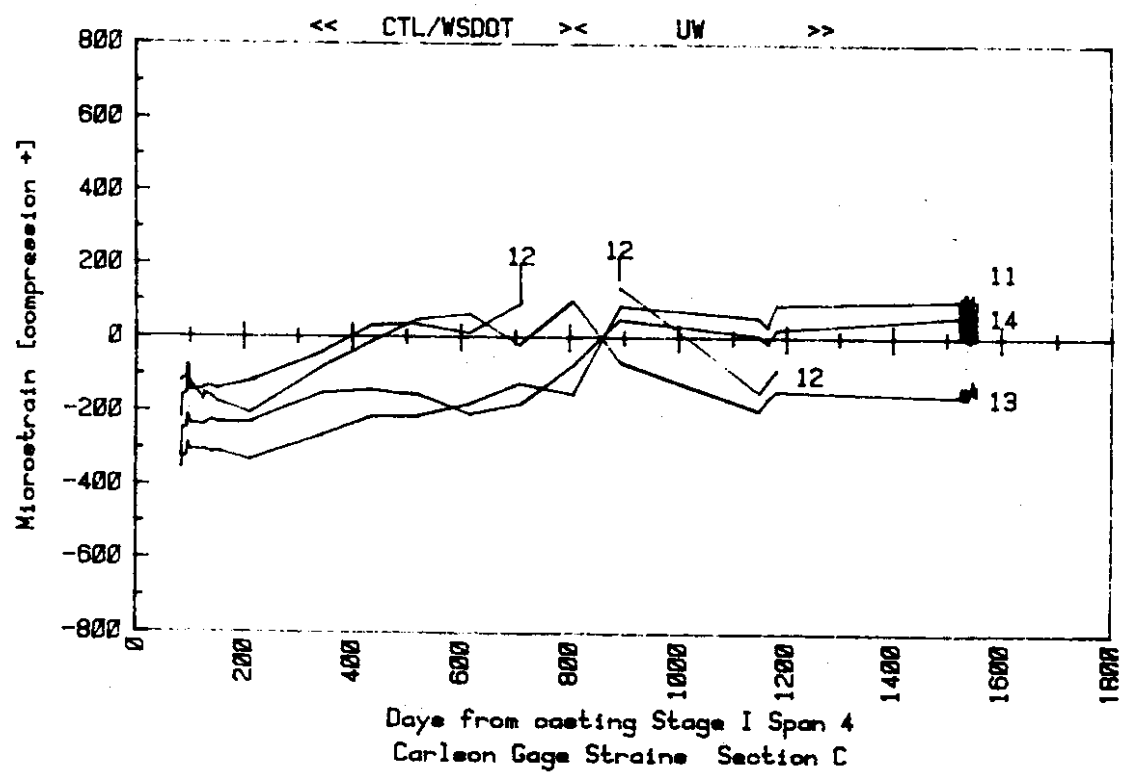

Figure 3.13. Carlson Gage Strains - Section C, Gages 11, 12, 13, 14

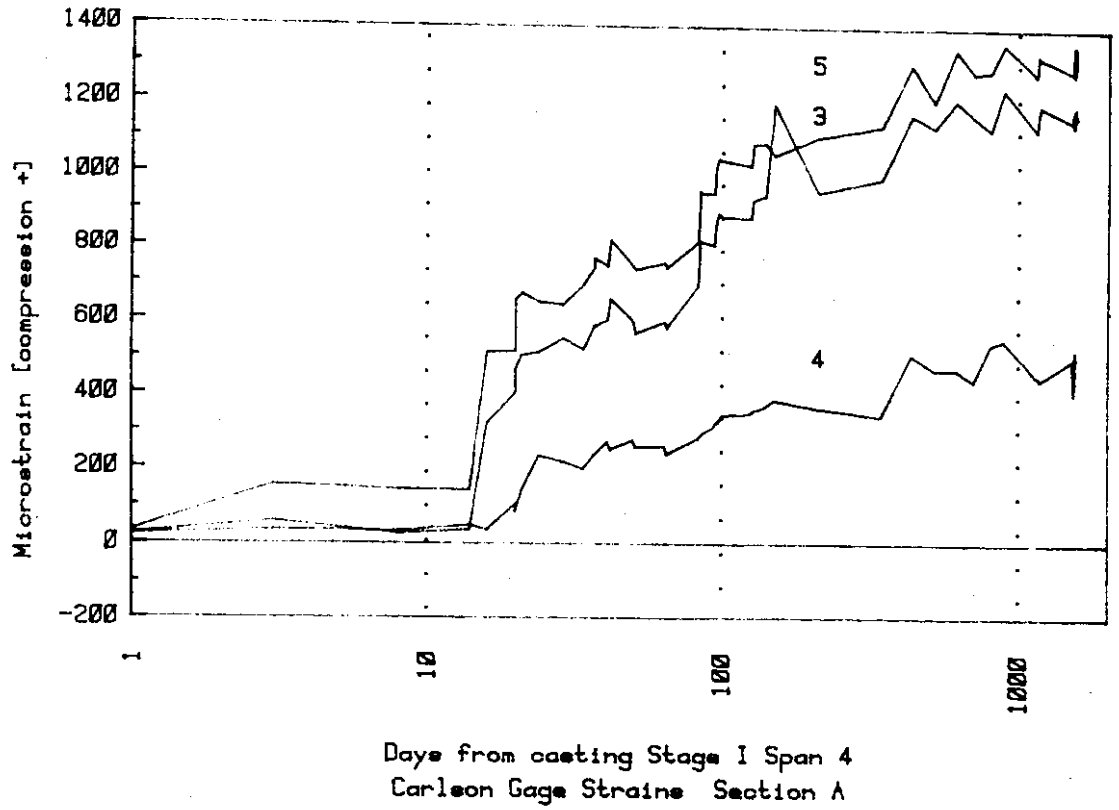

Figure 3.14. Carlson Gage Strains - Section A, Gages 3, 4, 5

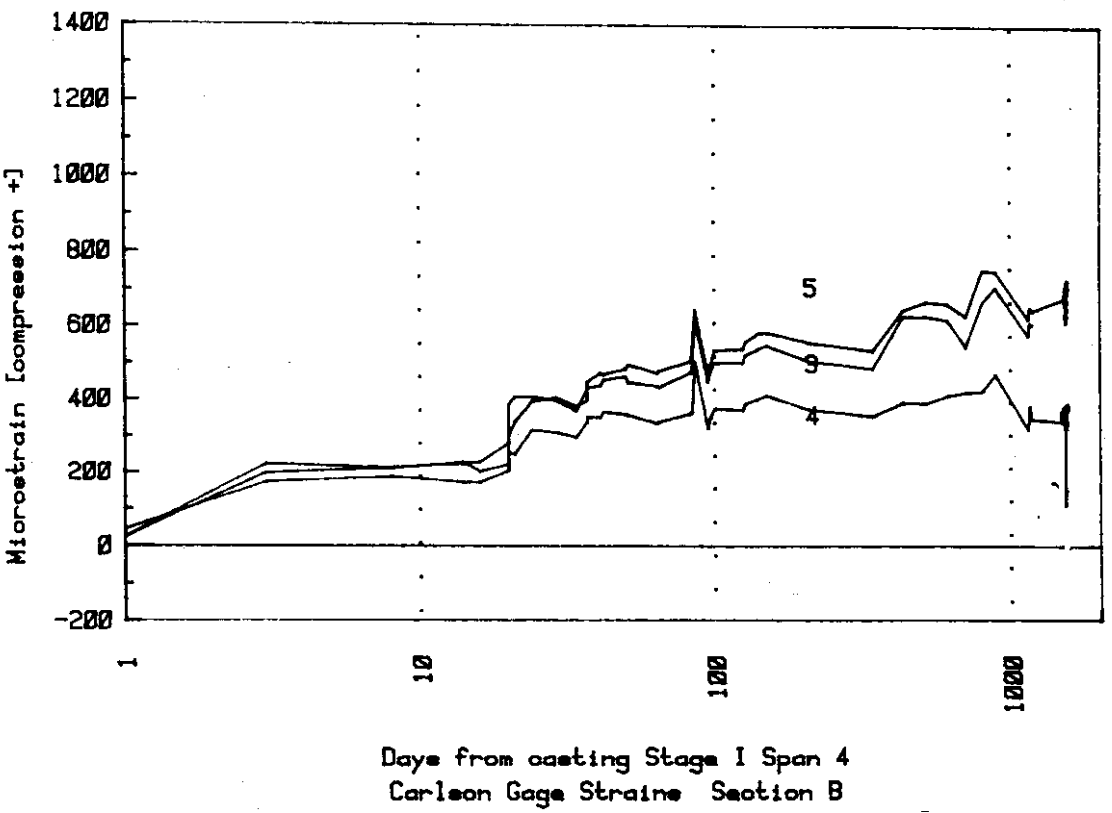

Figure 3.15. Carlson Gage Strains - Section B, Gages, 3, 4, 5

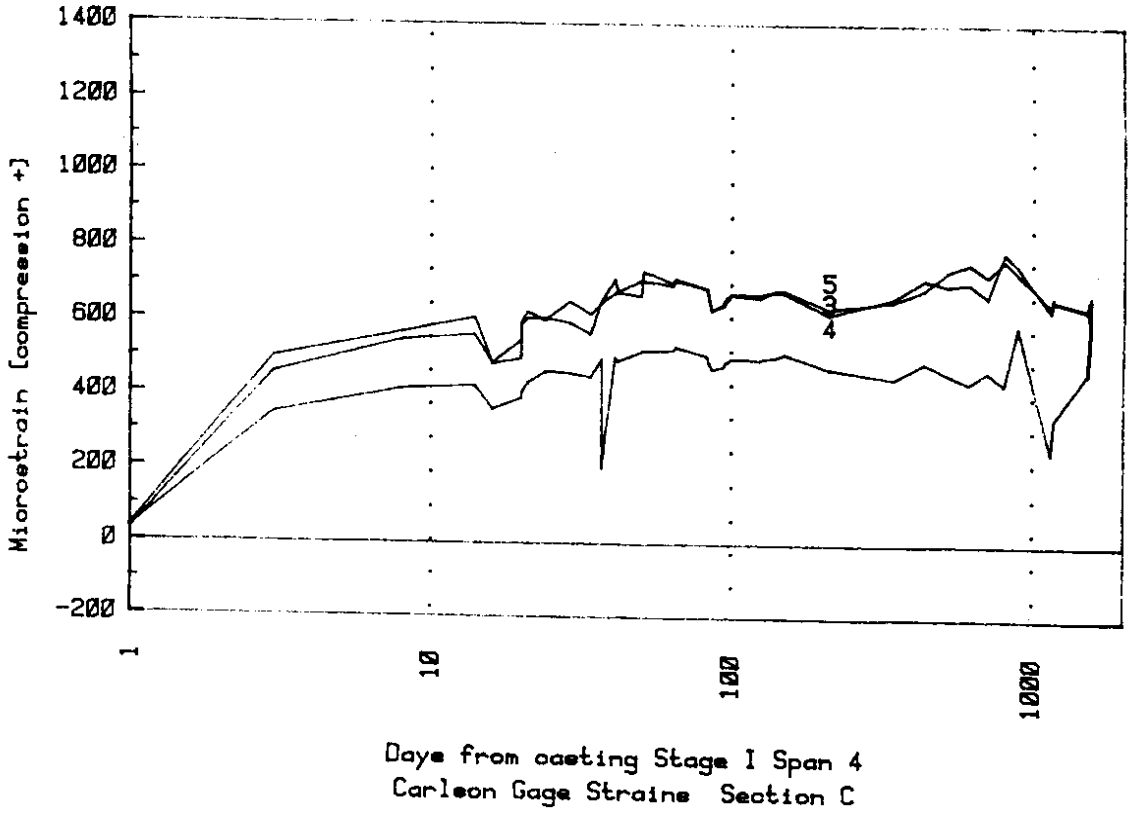

Figure 3.16. Carlson Gage Strains - Section C , Gages 3, 4, 5

3.3. Expansion Joint Movement

Movements of the superstructure with respect to Abutment 1 were measured by the WSDOT Resident Engineer's staff during the construction period. Details of the bearing at that abutment are shown in Figure 3.17. The Resident Engineer's staff measured the displacement between the portion of the sliding bearings attached to the superstructure and the portion attached to the abutment. The nature of the bearings permitted a simple but relatively precise measurement of the movement. Those measurements were continued in this study. An attempt was made to compensate for the temperature component of those measurements and thus measure the overall average creep and shrinkage shortening of the bridge. This correction for temperature was complicated by the fact that the fixed point, point of zero movement, for the bridge for axial strains changed as the support conditions changed and was also dependent on the magnitude of the movement involved. This dependence of the location of the fixed point on the magnitude of the movement was due to friction in the expansion bearings. A column with an expansion bearing acts as though it were pinned to the superstructure until the displacement of the top of the column has generated a shearing force sufficient to overcome friction. Further superstructure movement occurs at a constant friction force so long as the movement is in the same direction. However, when the direction of the movement reverses, then the "pinned" condition is reestablished. This action results in a shifting of the fixed point. That shifting of the fixed point has been neglected in the presentation of the resulting data on movement of the expansion bearings in Figures 3.18 and 3.19. The total data, corrected to a constant temperature of 73 degrees F, are shown in Figure 3.18. Uncorrected data for a period during the present study, when clear and sunny conditions prevailed, are shown in Figure 3.19. The fixed point was assumed to be at Abutment 1 prior to release of the sliding bearings at that location, at Pier 4 from December 1977 through

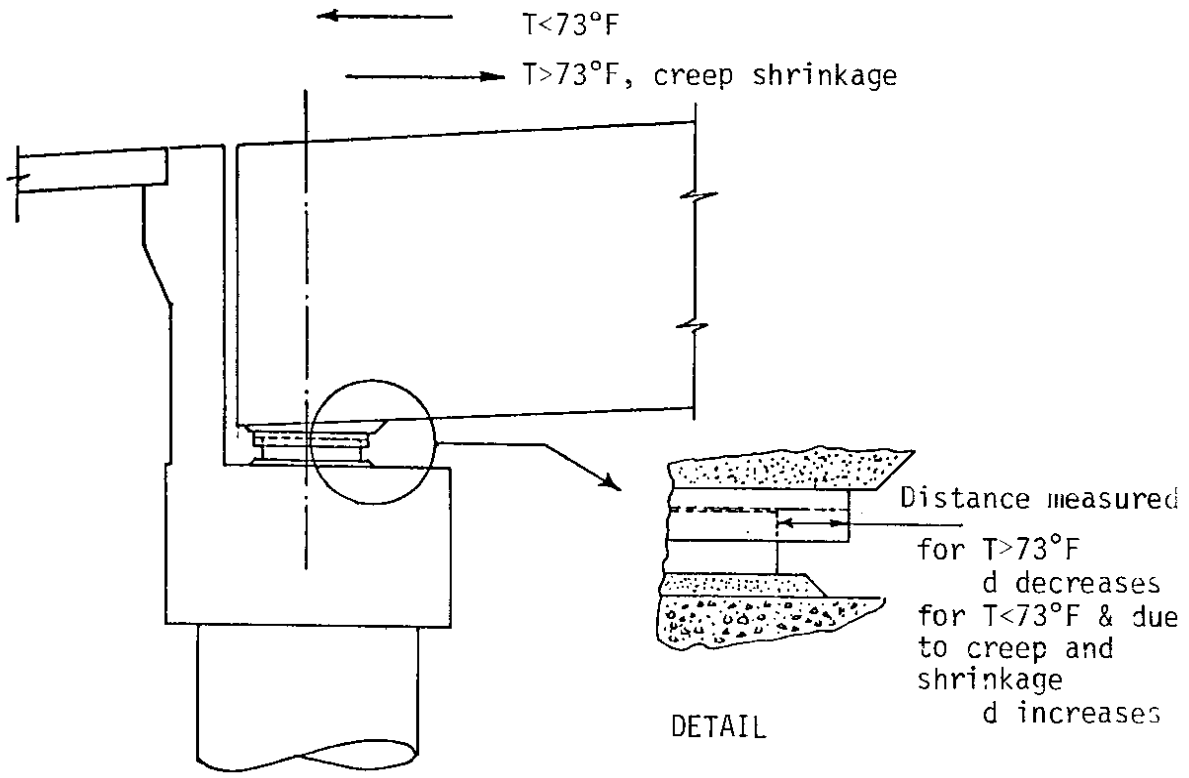

Figure 3.17. Expansion Bearing Details

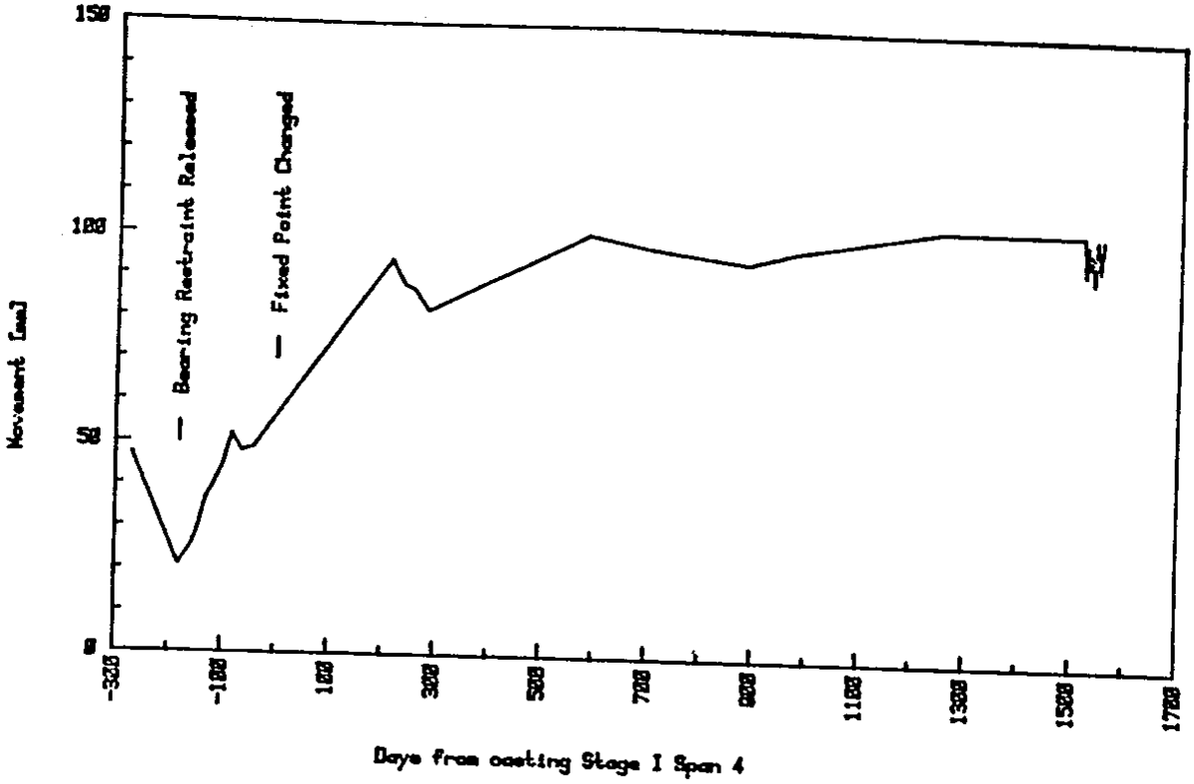

Figure 3.18. Expansion Bearing Movement at Abutment 1 Corrected to 73 Degrees F

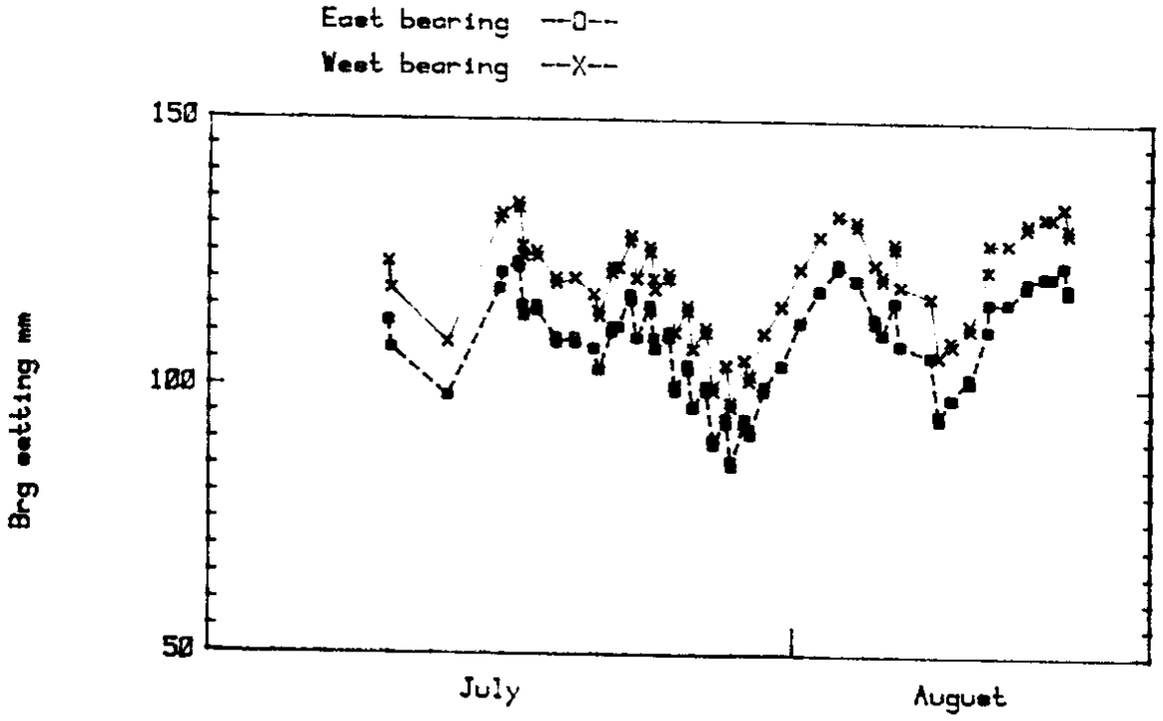

3.19. Expansion Bearing Movements July, August 1982

May 1978, and at Pier 5 after December 1978. Examination of the corrections for temperature indicates that a location between Pier 4 and Pier 5 is probably correct for the final condition. The only temperatures for which results were reported prior to the summer of 1982 were the outside air temperatures at the time of the Carlson observations. Those temperatures may or may not have been representative of the average temperature of the concrete in the bridge. For the data gathered during this study in the summer of 1982, there was a movement of up to 6 mm (0.25 inch) between morning and afternoon readings on sunny days. The response of the structure to the daily temperature cycle is clearly apparent in Figure 3.19. The 6mmm (0.25 inch) movement represents a change in the average bridge temperature of 2.4 degrees C. Data taken by WSDOT staff prior to this study, and the data collected during this study, are tabulated in Appendix C to this report.

3.4. Creep and Shrinkage Plots

In their study, CTL reported that creep and shrinkage data obtained from tests in their laboratories on control cylinders taken during construction of the bridge were plotted against time on a logarithmic scale in order to derive values for the ratio of creep to elastic strain. The CTL data are tabulated in Appendix D and plotted in Figures 3.20 through 3.25. Creep to shrinkage strain ratios calculated from that data are also tabulated in Appendix D. The creep coefficients at the completion of loading at 720 days varied from 4.14 for Stage II concrete loaded at 28 days to 2.80 for Stage II concrete loaded at 91 days. Further, there was a considerable difference in the modulus of elasticity derived from the creep specimen results and that determined in the modulus of elasticity tests reported in Table 2 of the CTL report. Differences as large as $\pm$ 30 per cent are reported when essentially similar results are to be expected. Those moduli of elasticity results are summarized in Table 3.6.

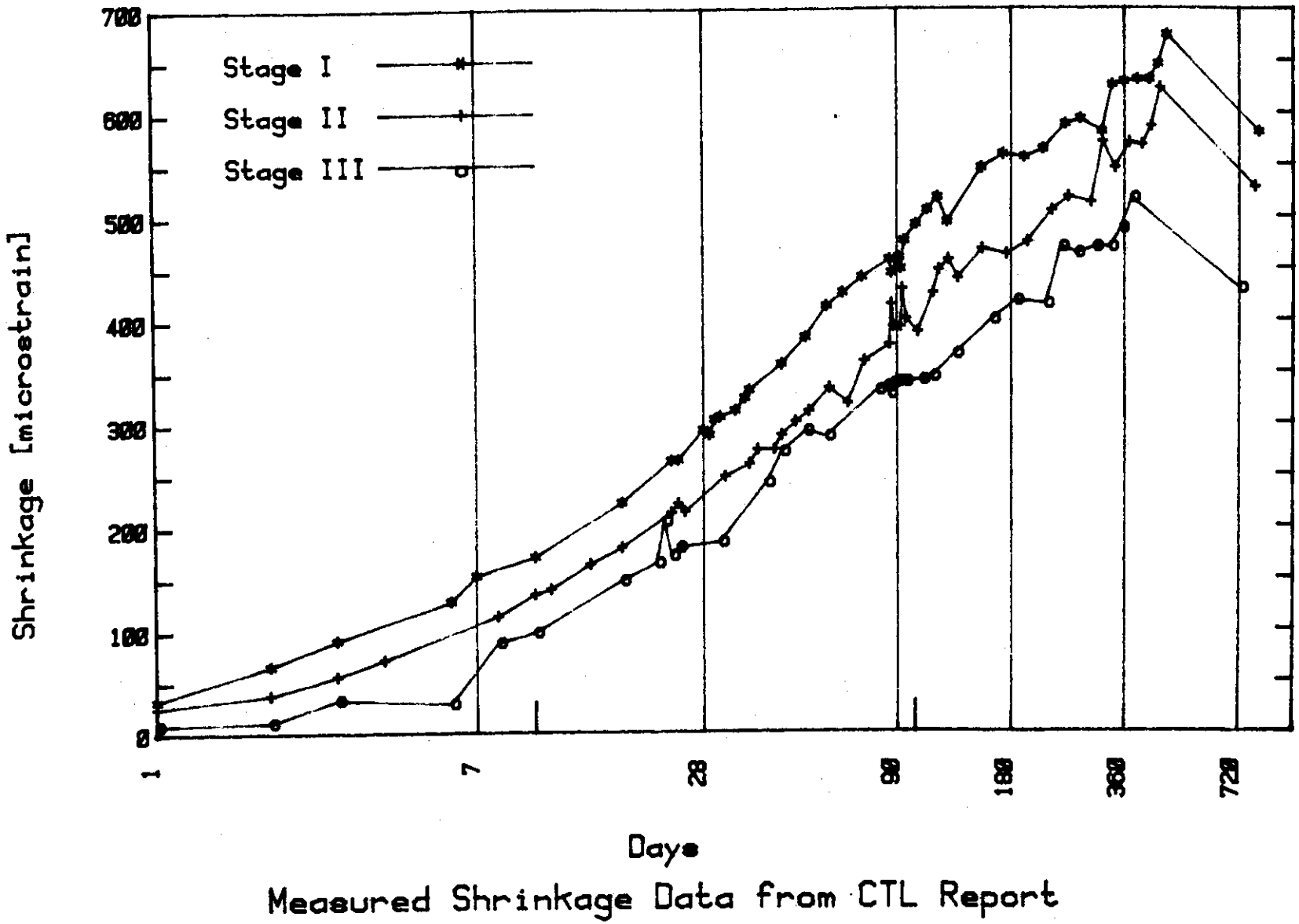

Figure 3.20. Time Development of Shrinkage (CTL) Data

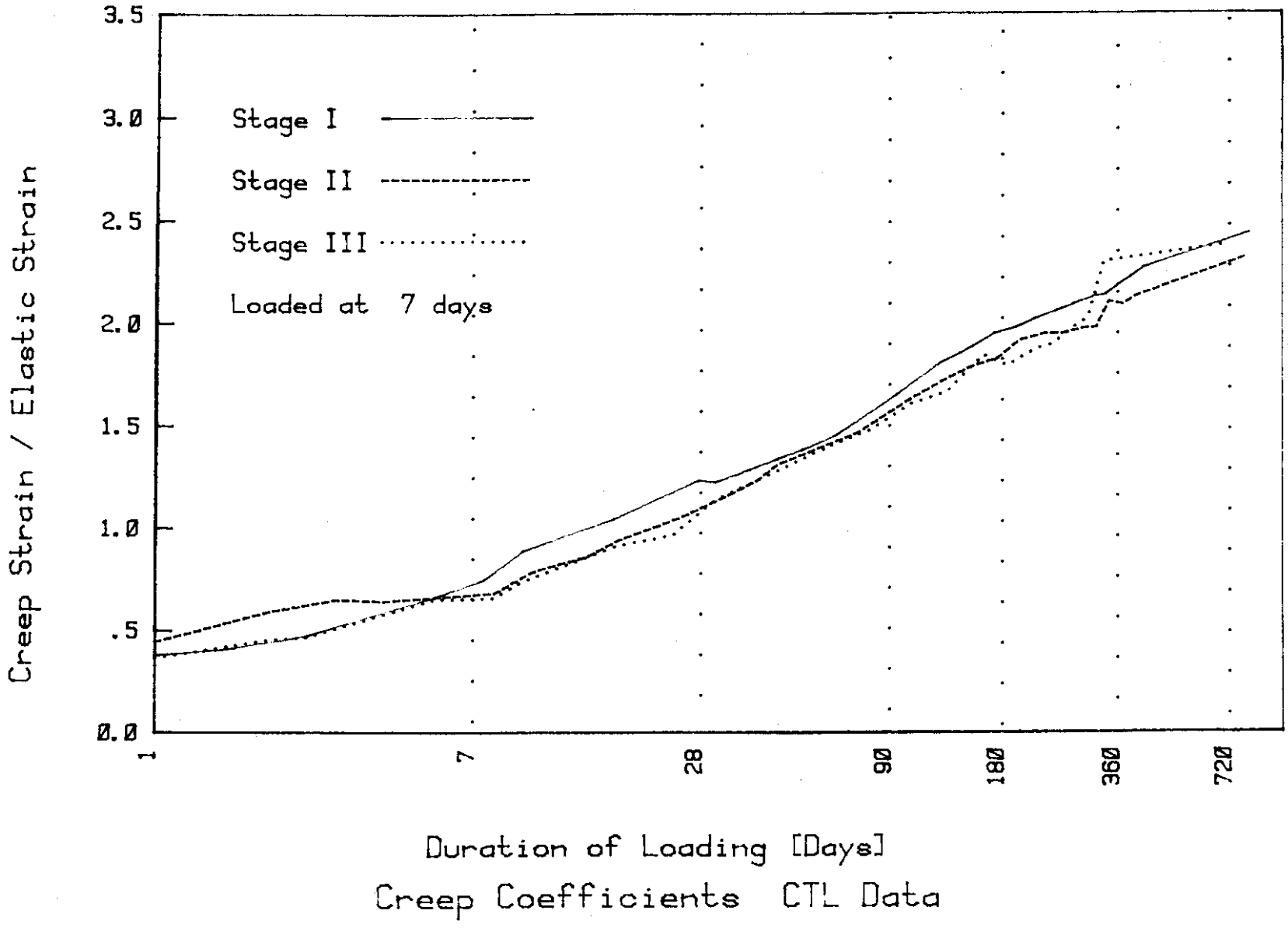

Figure 3.21. Time Development of Creep (CTL Data) Stage I

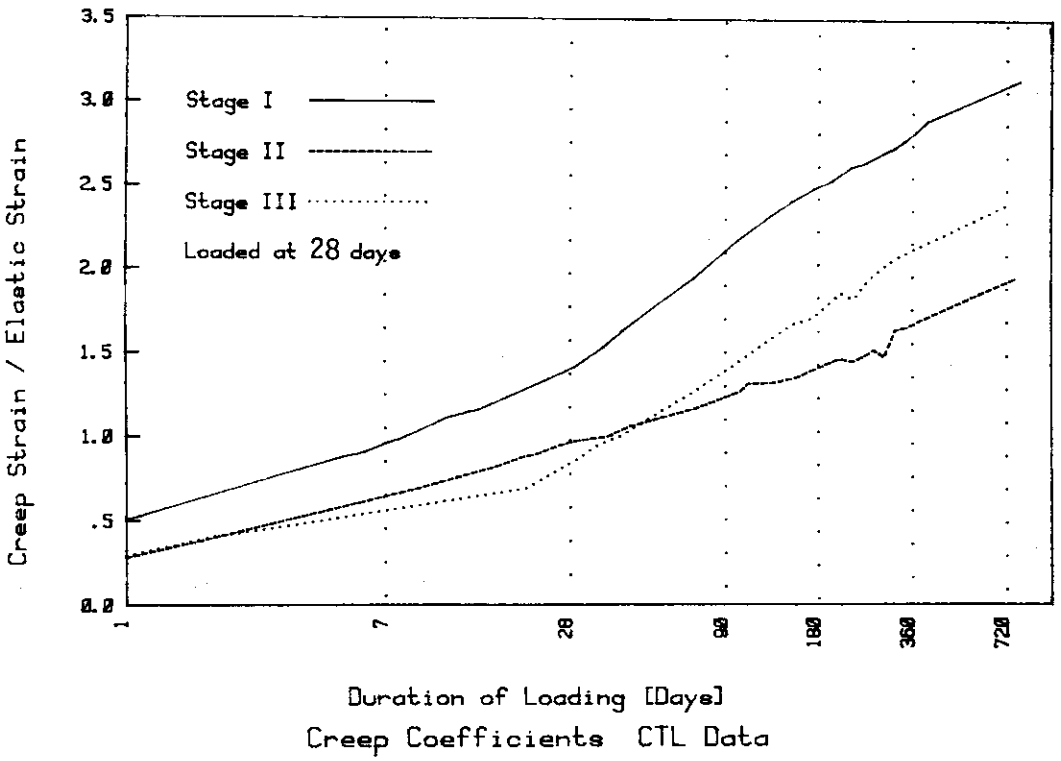

Figure 3.22. Time Development of Creep (CTL Data) Stage II

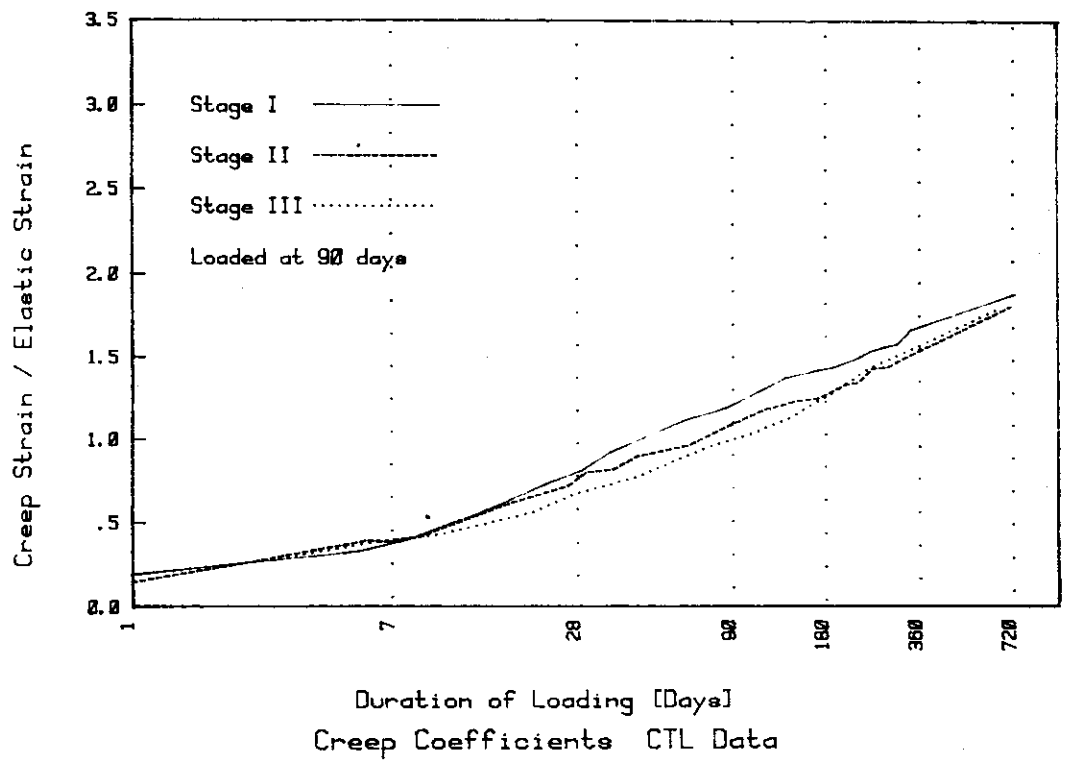

Figure 3.23. Time Development of Creep (CTL Data) Stage III

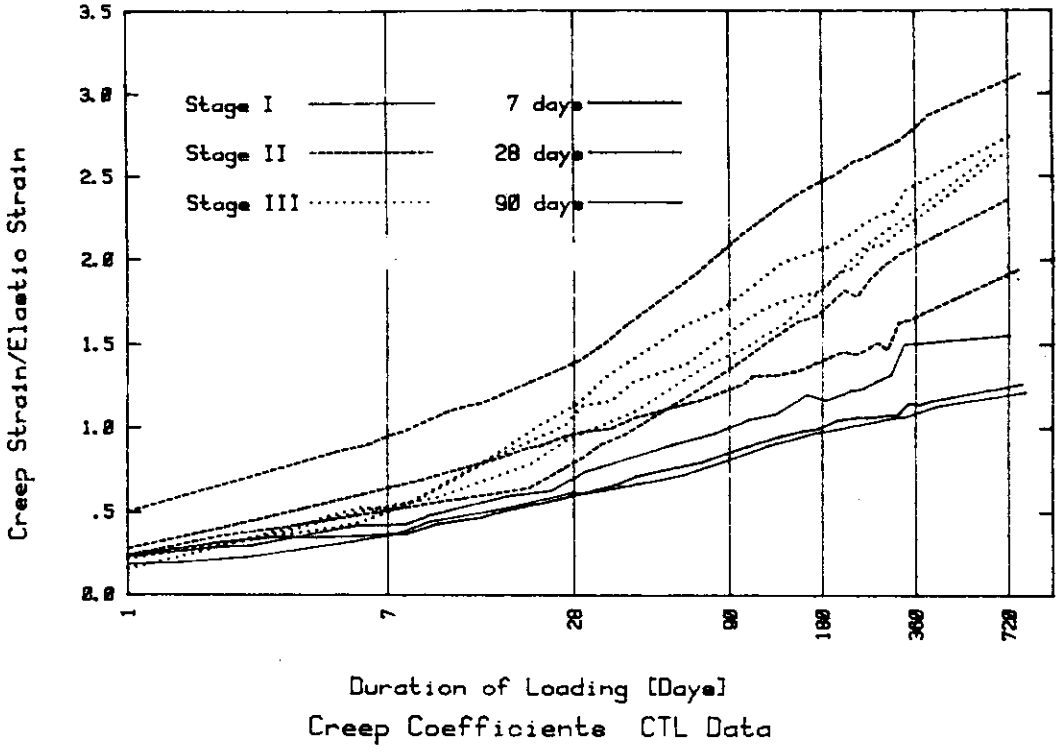

Figure 3.24. Time Development of Creep (CTL Data) Normalized by Equation 3.2 to Loading at 28 Days

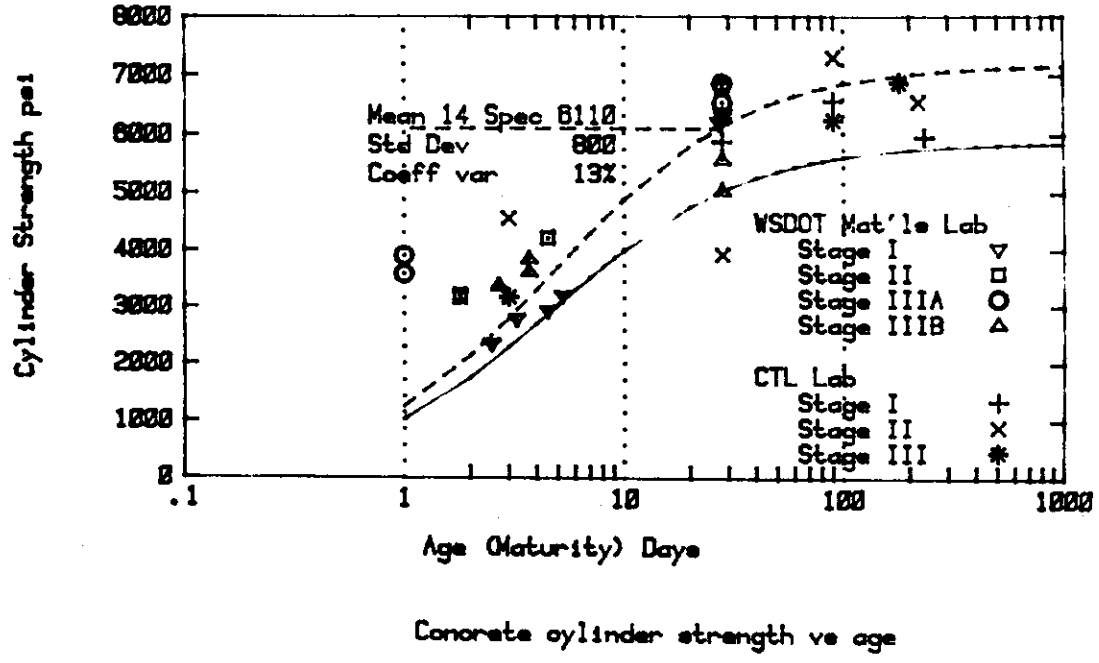

Figure 3.25. Time Development of Concrete Strength (CTL and WSDOT Data)

Table 3.6. Modulus of Elasticity (ksi)

	From Table 2 (CTL Report)	From Creep Data
Stage I loaded		
at 3 days	4240	
at 4 days		3770
at 28 days	3300	
at 27 days		4910
at 90 days	4610	3950
at 235 days	4500	
Stage II loaded		
at 3 days	4520	
at 5 days		4930
at 28 days	5470	4560
at 90 days	4830	
at 91 days		4390
at 220 days	4380	
Stage III loaded		
at 3 days	4430	
at 8 days		4430
at 28 days	4940	4440
at 90 days	4700	
at 92 days		4350
at 180 days	4510	

The development of concrete cylinder strength with time is shown in Figure 3.25 for all data reported by the CTL and the WSDOT Materials Laboratory. Also shown in Figure 3.25 are the results predicted by standard formulas (2.3). The Stage I and Stage II concrete for Span 4 contained a superplasticizer, Lomar-D. The mix design and aggregate gradation are shown in Table 3.7 for the concrete used in Spans 1 through 4 of the Denny Creek Viaduct. The contractor was unable to maintain adequate control of the quality of this mix and the mix was changed to one based on the use of Pozzolith 300N normal set water reducing admixture for later construction. It is believed that the data reported for Span 4 reflect the problems with mix

Table 3.7. Concrete Mix Design

Type: Concrete, Class W (with LOMAR D superplasticizer)

Ingredient	lb per cy	kg per m
Cement type I/II	660	390
Dry fine aggregate	1345	800
Dry coarse aggregate	1720	1020
Water (amount varied)	220	130
Air entrainment agent (amount varied)	7 oz	210 cm
Water reducing agent (amount varied)	140 oz	4140 cm

Coarse Aggregate Gradation (Representative)

No.	Sieve Opening (mm)	% Passing	Specification Min.	Specification Max.
3/4"	19.10	96	80	100
3/8"	9.52	16	10	40
1/4"	4.76	3	0	4

Fine Aggregate Gradation (Representative)

No.	Sieve Opening (mm)	Per Cent Passing	Per Cent Retained	Specification Min.	Specification Max.
4	4.76	98.3	1.7	95	100
6		89.4		82	98
8	2.38	79.0	21.0	68	86
16	1.19	53.7	46.3	47	65
30	0.59	31.2	68.8	27	42
50	0.297	13.5	86.5	9	20
100	0.149	4.6	95.4	0	7
200		2.0		0	2

319.7

Fineness modulus 3.20 (coarse sand)

consistency experienced on the job. Those problems may also be a significant factor in the differences between measured strains and those predicted by CTL. If the modulus of elasticity of the concrete is not known to better than ± 30 per cent accuracy, then no better agreement between measured and calculated strains can be expected. It is noted that in the shrinkage data, values for approximately 800 days are less than those for approximately 450 days. That variation could possibly be due to a disturbance of the reference, failure to maintain constant temperature and humidity conditions or some other explanation which is not a property of the concrete specimens tested. However, it is more likely to be a property of the specimens tested. The creep data were replotted after normalizing with respect to time using the formula proposed by Tadros, Ghali and Dilger (2.5).

$$k_d = \sqrt{\frac{t}{4.0 + 0.85t}} \quad \frac{10.29}{5 + \sqrt{t}} \tag{3.2}$$

where k_d = modifying factor on creep for age at first loading

and t = age at first loading modified as required for maturity to represent equivalent age at 70 degrees F

The resulting plots are shown in Figure 3.24. They do not show a significant improvement in the agreement for concrete loaded at different ages. This lack of agreement could be due to either inapplicability of the foregoing formula or inappropriate scatter in the data being normalized. The amount of data available is insufficient to discriminate between those two possibilities, but the weight of evidence suggests that the basic cause is a lack of consistency in the mix.

3.5. Comparison of Predicted and Measured CTL Strains

An attempt was made to circumvent the difficulties associated with the lack of precise knowledge on the stress history of the structure by examining

the differences in strain associated with a single significant event occuring early in the loading history. An event was chosen where the structural action was clear and it could be reasonably assumed that no extraneous or unknown loads were acting on the structure. Strain differences between Events 8 and 9 of Table 1 of the CTL report were calculated. Table 1 is reproduced in Appendix E of this report. Reading 8 was taken on day 21, prior to the casting of Stage I for Span 5. The results for that load case are listed in Table 3.8. Calculated values are those reported by CTL.

Table 3.8. Change in Strain (microstrain compression +) Between Events 8 & 9

	Section A		Section B		Section C	
Gage No.	Calc	Obsvd	Calc	Obsvd	Calc	Obsvd
1	-53	+59	-37	-64	-13	-27
2	-5	+4	+5	---	+1	-4
3	+100	+7	+104	+56	+37	-23
4	+77	+94	+97	+66	+35	+31
5	+100	-23	+104	+1	+37	0
6	-10	-14	+5	-44	+1	-27
7	-53	-8	-37	-11	-13	0
8	-82	+23	-64	-24	-23	-51
9	-82	-45	-64	-40	-23	-37
10	-82	+5	-64	-37	-23	-40

Comparison of the calculated and observed data shows that there are fundamental problems in either the observations or the calculations. Not only are the magnitudes different but even the character (tension or compression) is not consistent. Particularly noticeable are the results for gages 8, 9 and 10 at Section A. The observed magnitudes are considerably less than calculated magnitudes but more importantly, the sign (character) of the strain observed at gage 9 differs from that observed for gages 8 and 10. Those gages are all in the same relative position in the section. The differences could

be due to errors in the readings, errors in the gages, loads not properly accounted for in the calculations, or mistakes in the analysis of the observed data. It is not possible to check the reduction of the raw gage data as that material was not tabulated in the CTL report. Any construction loads that were not considered could probably be identified by reference to the WSDOT inspector's daily diaries. A thorough review should be undertaken of the CTL data, and construction records checked before any firm conclusions are drawn regarding redistribution of stress due to shrinkage and creep.

3.6. Concluding Remarks

This section of the study reviewed the data reported by CTL in their submission of August 1981 and examined the appropriateness of the procedures they adopted for predicting their results. Erection calculations supplied by WSDOT were also reviewed, the actual construction chronology compared with the sequence assumed for the erection calculations, and the data collected in this study used to extend the data collected by CTL.

There are several issues concerning CTL's comparison of predicted and observed strains which cannot be resolved with information currently available. Those issues could be partly resolved with further analyses. However, those analyses could be relatively costly and, when completed, still be inadequate to resolve several of those issues. On the limited basis of the observations made during the live load tests of 1981, it is concluded that it is safe to assume the cross-section functions as a complete unit in resisting applied live loads. However, the degree of redistribution of stress within the cross-section due to creep and shrinkage cannot be determined from the data available. In view of the uncertainties during design in the appropriate values for creep and shrinkage factors, it is recommended that alternate designs be prepared that account for variations of at least $\pm$ 33 per cent in

the assumed values. The testing of concrete samples representative of the mixes likely in the structure will help define the mean about which those variations should be taken but cannot significantly reduce the uncertainties which should be associated with those values.

4. LIVE LOAD STUDIES

This chapter describes the procedures and results of live load tests performed on the Denny Creek Bridge immediately prior to its opening to traffic. Those tests were performed on 23 July 1981. It was cool and overcast, or foggy, during the test period and on the preceding day. Thus, there were almost uniform temperature conditions in the bridge during the test period.

Static live loads, in the form of loaded gravel trucks, were applied at the expansion joint in Span 7 and at the center of Span 4 of the bridge (Figure 1.3). Truck weights and dimensions are listed in Table 4.1. Relative deflections across the expansion joint were measured in Span 7 and strains were measured at the three instrumented sections in Span 4.

The purpose of the test at the expansion joint in Span 7 was to measure deflections of the cantilever slabs and to relate those deflections to the deflections predicted from design data. The purpose of the load application at the center of Span 4 was to confirm that the stage constructed cross-section was acting monolithically in resisting the externally applied loads.

4.1. Test Procedures

4.1.1. Cantilever Slab Deflections at Expansion Joint

Static loads were positioned so as to produce the maximum deflection of the cantilever slab relative to the girder webs. Loads were applied first asymmetrically, then symmetrically, about the centerline of the box girder. The load pattern in illustrated in Figure 4.1 and is also apparent from the photographs of Figures 4.2, 4.3 and 4.4. Deflections were measured relative to the unloaded side of the expansion joint in seven locations spaced across the width of the bridge. Deflections were obtained using mechanical dial gages

Table 4.1 Truck Weights and Dimensions for Live Load Tests

Truck No.:	1 6E15-10	2 6E30	3 6E32	4 6E15-8
Rear axle(s) kips	25.0	19.3	20.75	26.5
Front axle kips	14.5	9.1	8.75	14.0
Wheel base inches	192	150	147	192
Distance between rear axles inches	50	--	--	50
Tread (outside) inches	92	91	92	92
Width of dual tires inches	21	20	21	20

Table 4.2. Cantilever Slab Deflections (0.001 inches)

Gage No:	1	2	3	4	5	6	7
Initial	298	486	664	555	200	477	579
Trucks 3,4	328	493	670	559	200	443	489
Deflection	+30	+ 7	+ 6	+ 4	0	-34	-90
Trucks 3,4	659*	493	670	559	200	443	489
Trucks 1,2	592	465	670	562	206	448	492
Add'l Defl.	-67	-28	0	+ 3	+ 6	+ 5	+ 3
Trucks 1-4	592	465	670	592	206	448	492
Final	652	486	664	819	199	477	577
Total Defl.	+60	+21	- 6	- 9	- 7	+29	+85

*Gage reset after being disturbed

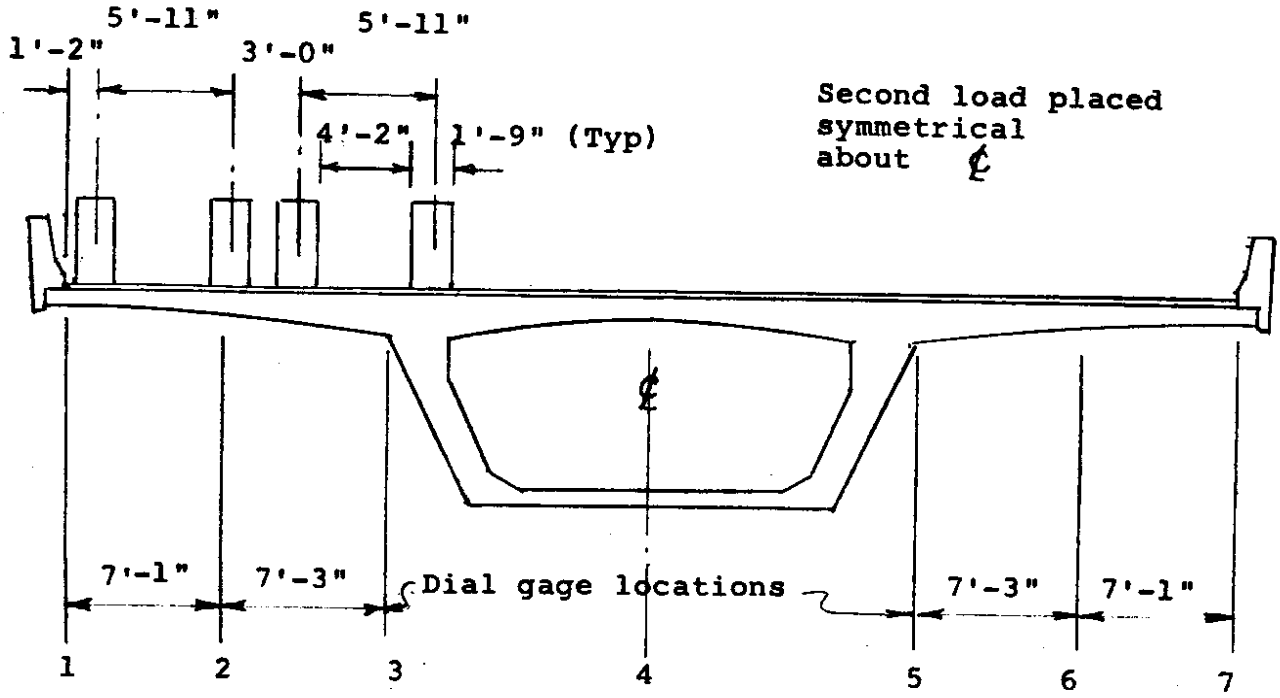

a) Transverse

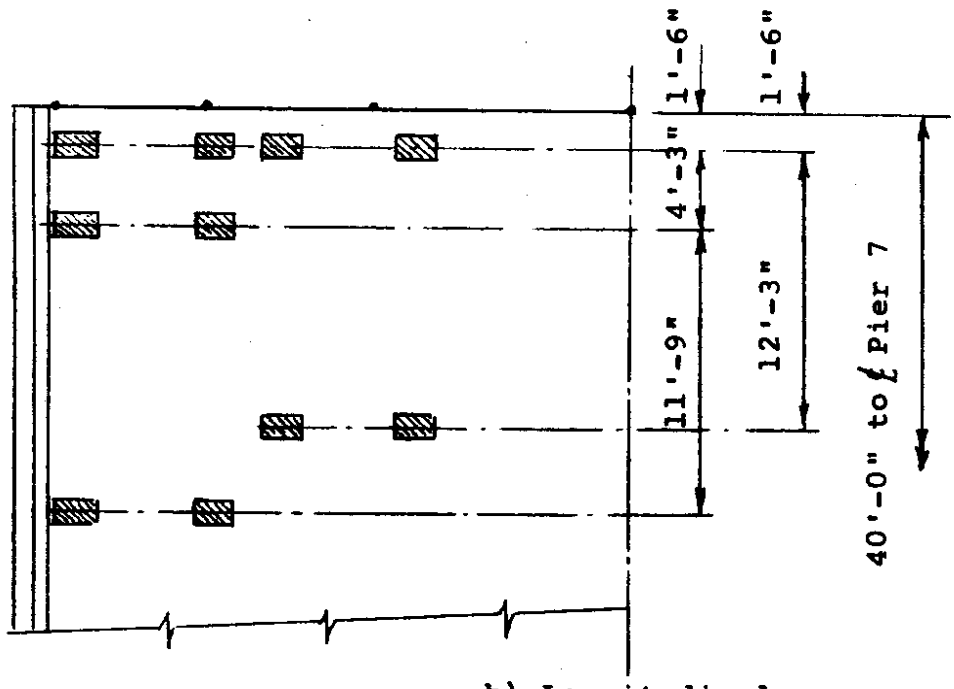

b) Longitudinal

Figure 4.1.
Cantilever Slab Deflection Test Load Pattern

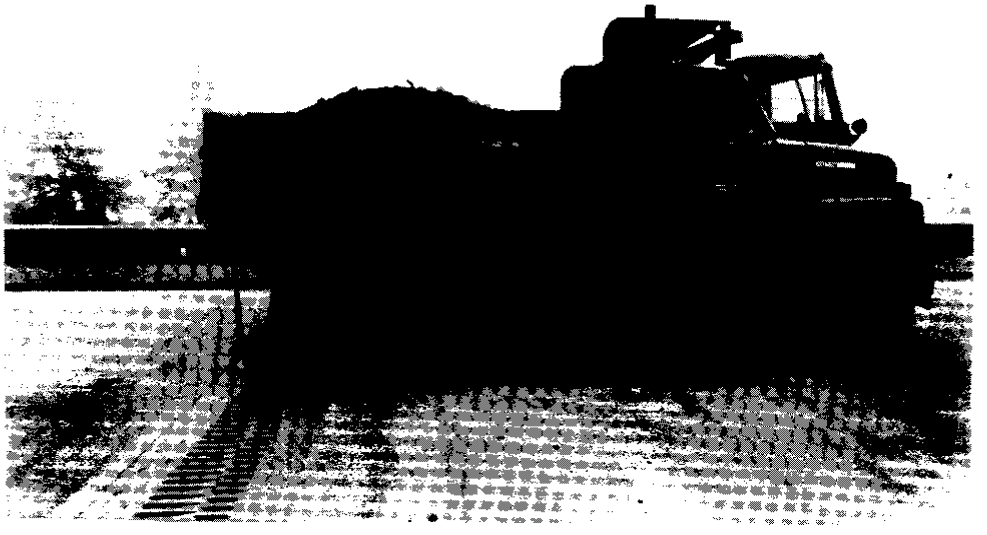

Figure 4.2. Longitudinal Placement of Trucks at Expansion Joint

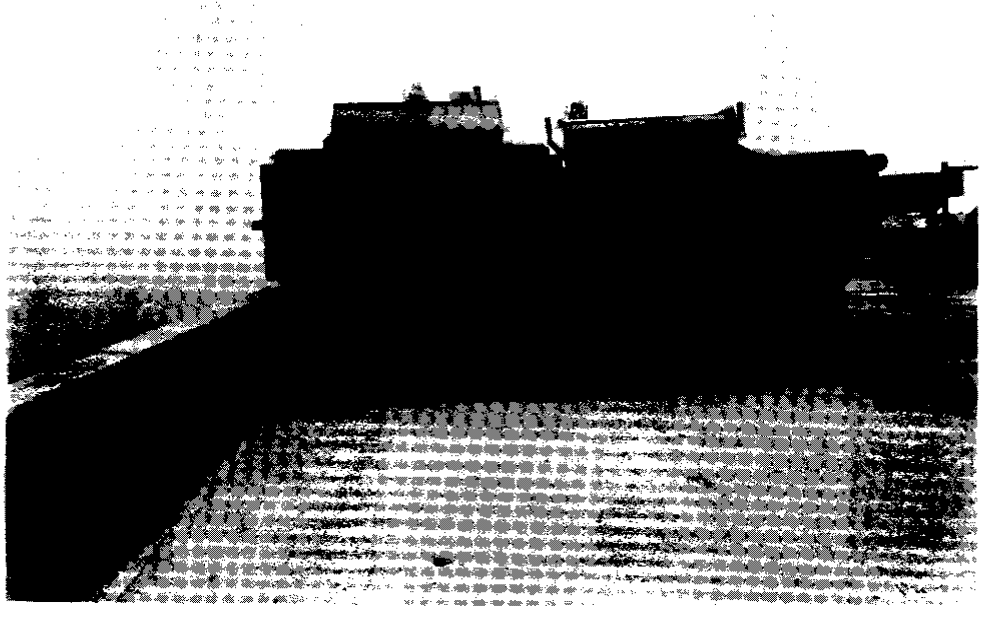

Figure 4.3. Cantilever Slab Loading, Transverse Placement of Trucks for Asymmetric Loading

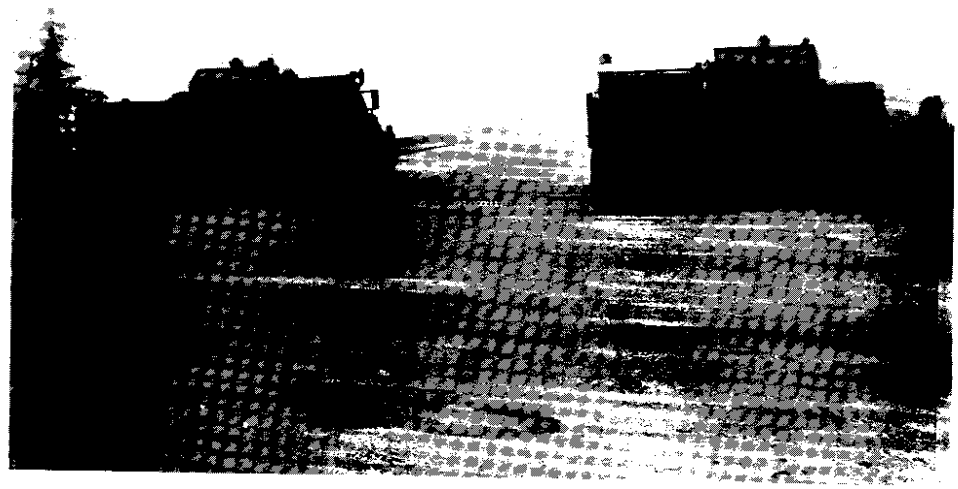

Figure 4.4. Cantilever Slab Loading, Transverse Placement of Trucks for Symmetrical Loading

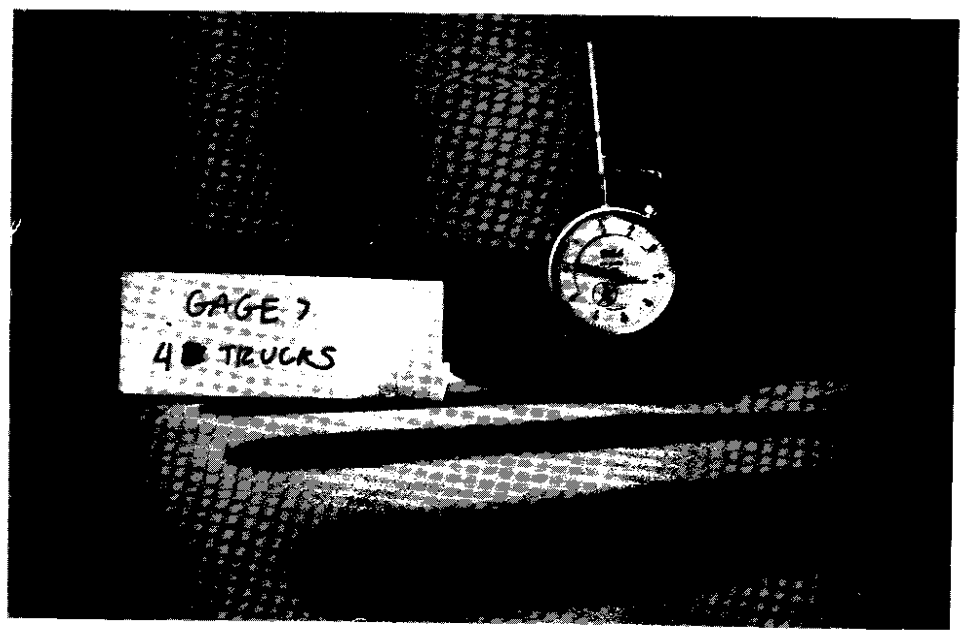

Figure 4.5. Set-Up for Typical Gage Reading at Expansion Joint

reading to a least value of 0.001 inch. The typical gage set-up is shown in Figure 4.5. Gages were read before positioning the loads, after positioning the loads, and after removing the loads. Results are shown in Table 4.2 and plotted in Figure 4.6.

4.1.2. Center Span Loading

Trucks were positioned so as to produce maximum positive momemt at the centerline of Span 4. The position of those trucks in the longitudinal direction is shown in Figure 4.7. The applied test load caused moments at the center of Span 4 calculated as equal to 65 per cent of standard AASHTO design live load moment without impact. The procedures used to calculate the shear and moments shown in Figure 4.7 are described in Section 4.2.2. Trucks were placed symmetrically about the longitudinal centerline of the box girder, in the same relation to the bridge centerline as shown in Figure 4.1. The Carlson gages and Whittemore gages mounted inside the box girder were read before positioning loads (initial), after positioning loads (loaded), and after removing the loads (final). Concrete surface temperatures and air temperatures were also measured. Results of these measurements are tabulated in Tables 4.3 and 4.4, and strains are shown in Figures 4.9 and 4.10. The deflection at the center of Span 4 was measured using a theodolite sighted down the interior of the box girder. The live load caused a deflection of 0.16 inches.

4.2. Calculated Deflections and Strains

4.2.1. Cantilever Slab

Deflection of the cantilever slab at the expansion joint in Span 7 was calculated using an empirical distribution of wheel loads similar to the distribution used in AASHTO Standard Specifications for Highway Bridges (1.1) with an empirical adjustment to account for the longitudinal discontinuity at

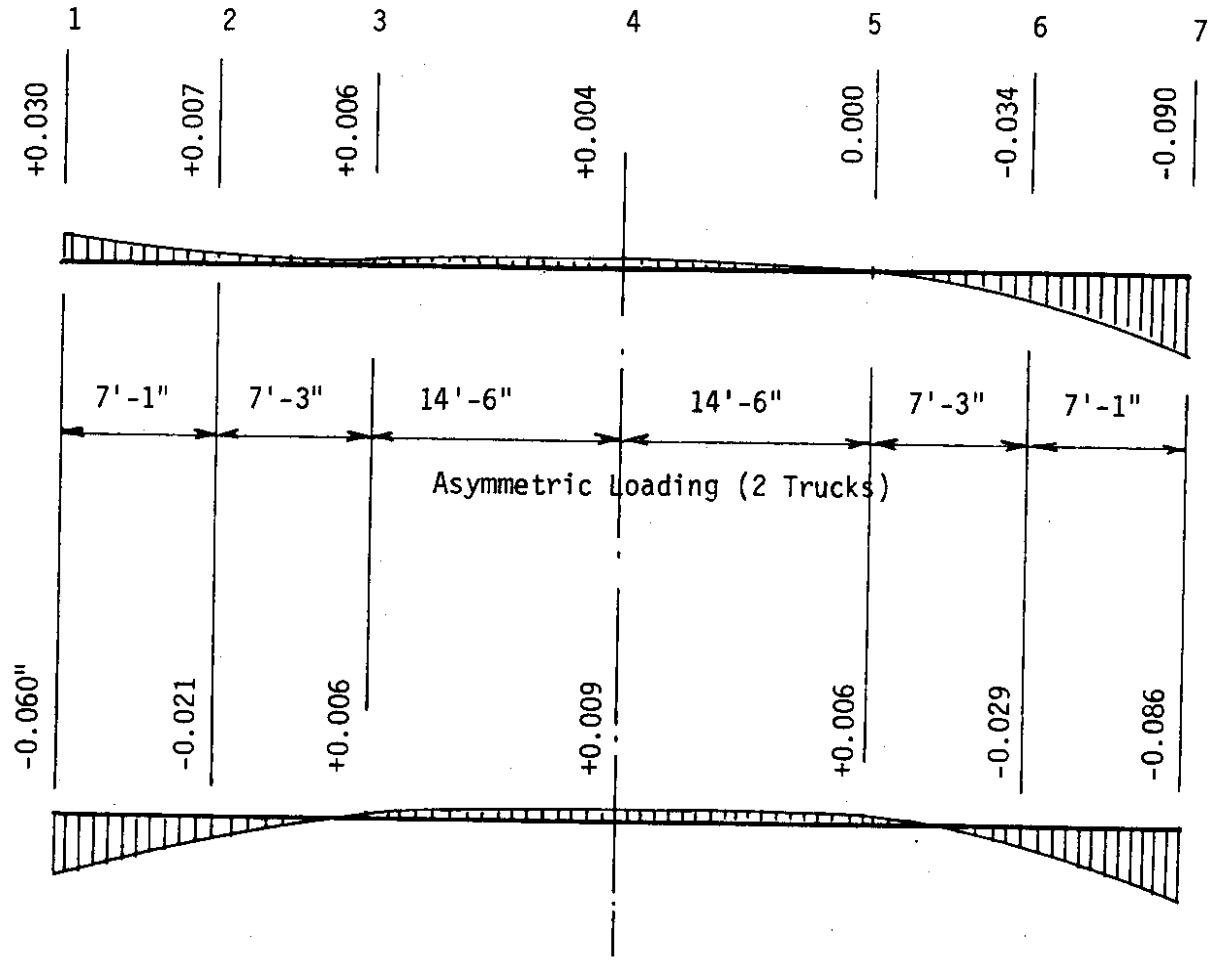

Figure 4.6. Relative Slab Deflections Across Expansion Joint, Span 7

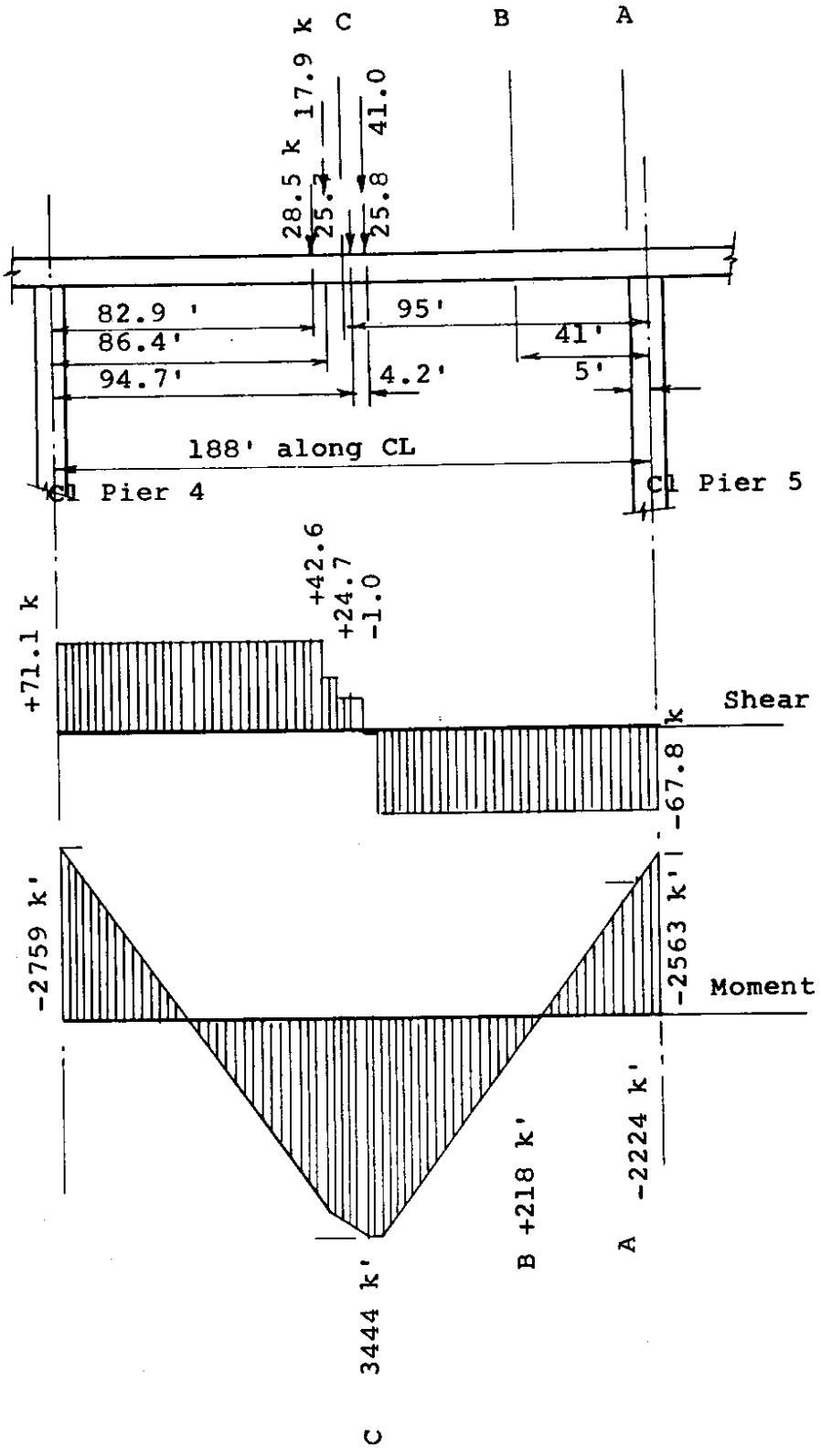

Figure 4.7. Live Loading at Center of Span 4

Table 4.3.

Live Load Test Strains at Carlson Gages

Microstrain

Section A					Section B					Section C				
Gage No.	Initial	Loaded	Final	LL Strain	Gage No.	Initial	Loaded	Final	LL Strain	Gage No.	Initial	Loaded	Final	LL Strain
A1	-719	-716	-717	2	B1					C1	-807	-813	-809	-5
2					2	-584	-583	-583	1	2	-645	-641	-645	4
3	-1132	-1143	-1124	-15	3	-612	-612	-612	0	3	-655	-625	-658	32
4	-457	-458	-455	-2	4	-386	-378	-383	7	4	-314	-282	-285	13
5	-1285	-1301	-1274	-22	5	-651	-651	-655	2	5	-669	-642	-673	29
6	-515	-512	-508	-1	6	-507	-510	-503	-5	6	-677	-677	-680	2
7	-491	-489	-490	2	7	-606	-604	-604	1	7	-658	-659	-659	-1
8					8	-201	-211	-204	-9	8	-188	-203	-195	-12
9	-187	-187	-191	2	9	-226	-229	-229	-2	9	-141	-155	-151	-9
10	-179	-172	-181	3	10	-312	-322	-322	-5	10	-278	-295	-286	-13
11	275	281	277	5	11	199	203	200	4	11	-26	-41	-34	-11
12	146	150	146	4	12	89	85	89	-4	12	116	110	121	-9
13	92	95	92	3	13	96	131	93	37	13	167	161	165	-5
14	174	174	174	0	14	78	77	77	-1	14	20	7	13	-10

Table 4.4.

Live Load Test Carlson Gage Temperature

Degrees Farenheit

Section A				Section B				Section C			
Gage No.	Initial	Loaded	Final	Gage No.	Initial	Loaded	Final	Gage No.	Initial	Loaded	Final
A1	61	61	61	B1				C1	68	67	67
2				2	62	61	61	2	59	59	59
3	57	57	57	3	57	57	57	3	57	57	57
4	61	60	60	4	59	59	58	4	58	57	57
5	58	58	58	5	58	58	58	5	57	57	57
6	59	59	59	6	59	59	59	6	59	59	59
7	62	62	61	7	61	61	61	7	62	61	61
8				8	62	62	62	8	62	62	62
9	61	61	61	9	61	62	62	9	61	61	62
10	62	63	63	10	61	62	62	10	61	61	61
11	58	58	58	11	60	60	60	11	59	60	59
12	60	59	59	12	58	59	58	12	58	57	57
13	61	61	61	13	58	58	58	13	58	58	58
14	58	58	58	14	61	61	61	14	60	60	60

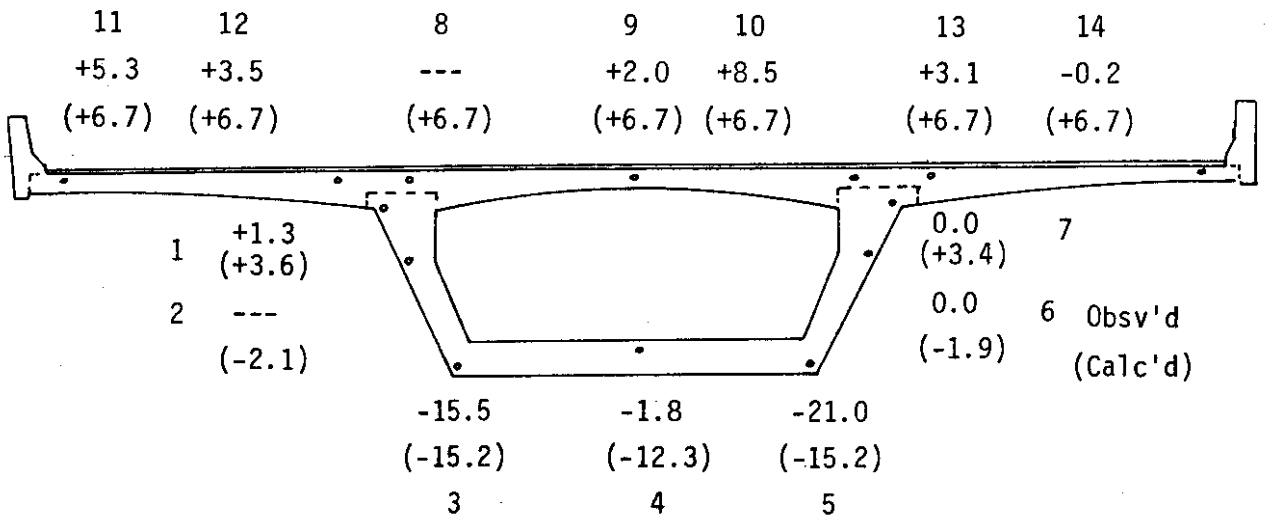

Figure 4.8. Live Load Test Strains, Section A Near Pier 5, Microstrain

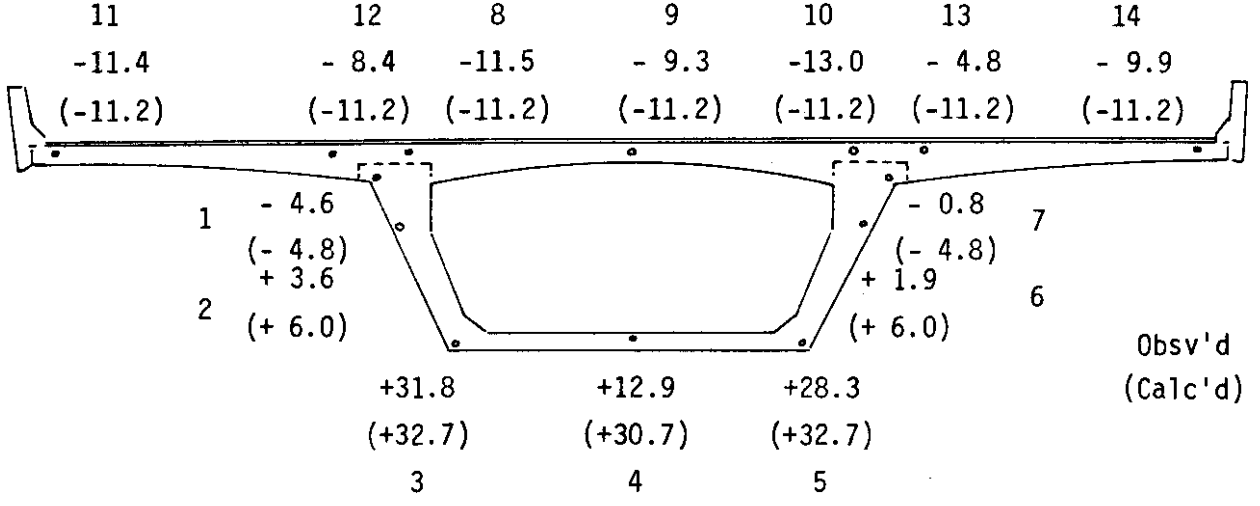

Figure 4.9. Live Load Strains, Section C Near Midspan, Microstrain

the expansion joint. Calculations were made for assumed wheel loads and positions which differed slightly from those actually applied in the test. The calculations of deflection were made using the gross section properties of the slab including the overlay. No provision was made for the effect of the barrier curb. Details of those calculations were presented in a previous interim report for this study. The calculated deflection at the curb under asymmetrical loading (2 trucks) was 0.129 inch due to slab deflection plus 0.010 inch due to rotation of the cross-section for a total deflection of 0.139 inch. The measured deflection at the curb line under the asymmetrical test loading was 0.090 inch.

4.2.2. Center Span

Strains at the Carlson gage locations were calculated using the following quantities:

1. End moments that were derived from a linear elastic displacement analysis using gross section properties;
2. Stresses that were calculated from those moments using transformed uncracked section properties for the cross-section and including the overlay assumed to act monolithically with the deck; and
3. A modulus of elasticity of the concrete at the time of test of 4500 ksi. That value was consistent with the values measured by CTL at ages of approximately 250 days.

Details of those calculations were given in a previous interim report for this study. Calculated strains are shown in parentheses in Figures 4.8 and 4.9.

4.4. Concluding Remarks

From the results of the live load tests it is apparent that:

1. AASHTO design procedures for live load are conservative for box girder bridges of the dimensions encountered here.
2. AASHTO slab design procedures for live load are conservative for the cantilever slabs of this box girder bridge.
3. The ability of the barrier curbs to distribute local wheel loads should be considered in the design of the bridge.
4. Assumption of full participation of the stage constructed section for resistance of live loads is justified.

5. THERMAL STRESS STUDIES

5.1. General Remarks

Design of a prestressed concrete box girder bridge for stresses induced by thermal gradients requires determination of the magnitude of the probable maximum thermal gradient (i.e., the total difference between the top and bottom surface temperatures of the section), the form of the resulting variation in temperature through the depth of the section, and the appropriate limit state. It is also necessary to determine appropriate combinations for thermally induced effects and effects caused by other loadings.

The magnitude of the total temperature difference between the top and bottom surfaces of the section and the variation in that temperature with depth must be related to the environmental parameters present at the site and the geometry and material properties of the structure. Once those parameters and properties are known, heat transfer theory can be used to predict the variation in tempeature over the depth of the section.

Once the temperature distribution is specified, the stresses caused by that distribution can be determined using customary methods of analysis. Generally, those analyses assume a homogeneous, isotropic, linear elastic material. The qualitative changes in the magnitude of the stresses caused by differences between the idealized conditions and those present in the actual structure should be considered in any interpretation of the results of such analyses. In particular, cracking of the concrete may lead to a significant change in the moments induced by thermally imposed curvatures.

Ideally, it is desirable that there be a relatively uniform risk of failure due to all loading combinations considered in the design of a bridge. Theoretically, that approach leads to the most economical design over the life of the structure. However, the consequences of the occurrence of the various

limit states which may be interpreted as "failure" are not of equal significance and therefore should not be given equal weighting. For example, the occurrence of the limit state of cracking is far less serious than the occurrence of the limit state of collapse. Nevertheless, cracking can lead to collapse, if that cracking affects the durability of the structure, or stress range, and therefore, the fatigue strength of the reinforcing steel. A quantitative determination of the loading combination appropriate for relating the significance of the thermally induced stresses to the stresses induced by other loads is beyond the scope of this study. However, that relation must be considered qualitatively in any interpretation of the results presented in this study.

This chapter describes the results of an investigation into the stresses caused in the Denny Creek Viaduct by variations in temperature over the depth of that bridge. The data collected during that investigation are described and related to environmental parameters given in standard weather data for the nearest official weather station. The analytical procedures available to predict the temperature distribution caused by those environmental parameters are then discussed and the temperatures measured in the Denny Creek Viaduct are compared to the results predicted by those procedures. The stresses resulting from a temperature distribution similar to that proposed by Priestley in Reference 1.6 are evaluated and the strains, assuming linear elastic behavior, compared with the strains measured in the bridge. The dominant overall concern in this study of the Denny Creek Viaduct was prediction of the stresses caused by thermal gradients.

5.2. Data Base

The original plan for this investigation called for the establishment of a weather station at the bridge site and a comparison of the results recorded

by that weather station with the nearest official weather station data. The objective was to see if the long-term data available for the official station were representative of the local weather conditions. The strains and concrete temperatures in the bridge and the site weather conditions were to be monitored by automatic recording equipment on a regular 2-hour schedule. The automatic data collection system failed to operate as planned and as a result, the strain and temperature data collected at the site were limited to 45 full sets of Carlson gage readings collected manually between 9 July and 14 August 1982. The Carlson gages were those installed previously by CTL. The 45 full sets of readings were supplemented by hourly readings on the gages of Section B taken on 5, 7, 13 and 14 August. Those hourly readings were taken during the day only. Ambient air temperatures inside and outside the the box girder and interior concrete surface temperatures were measured simultaneously with each set of Carlson gage readings. Inside air temperatures were measured with a laboratory type mercury thermometer graduated to 0.1 degree C. Outside air temperatures were measured with a pocket mercury themometer prior to 5 August 1982, and with a thermocouple after 5 August 1982. Both instruments gave readings to the nearest 1 degree Celsius. Concrete surface temperatures were measured with a thermocouple. The outside ambient air temperature readings were taken by suspending the thermometer, or the thermocouple probe, below the soffit of the bottom slab through a drainage hole located near Pier 4. That position was shielded from direct solar radiation. Outside air temperature and total wind run were measured continuously at a location approximately 300 feet southwest of Abutment No. 1 using a portable weather station furnished by WSDOT. This instrument included a spring-driven chart which could be read to the nearest 1 degree Farenheit. Wind velocity was obtained as the average run for a given hour or longer period. Measurements

of the overall expansion and contraction of the bridge at Abutment No. 1 were also made as described in Chapter 3.

5.3. Weather Data

Stampede Pass was the nearest national weather station site to the Denny Creek Viaduct site. Long term weather records for the Stampede Pass station were obtained from NOAA publications (5.1). The Stampede Pass weather station is situated at the top of a mountain pass adjacent to Snoqualmie Pass, is 12 miles SSE from the bridge site, and is at an elevation of 3958 feet above MSL. The instrumented span of the Denny Creek Viaduct is at an elevation of 2560 feet above MSL. The Stampede Pass station is subject to the same governing climatic influences as the bridge site, and therefore, the long-term range in climatic conditions for that site can be expected to be indicative of the same range for the bridge site. The weather conditions for the bridge site and Stampede Pass were correlated graphically for the time period covering the observations. This correlation is illustrated in Figure 5.1.

It was noted that while there were considerable differences in instantaneous wind and temperature conditions at the two sites due to the local variability of weather conditions in mountainous terrain, the mean trends for the two sites were similar. The validity of the use of the Stampede Pass data to represent long-term weather conditions for the Denny Creek Viaduct site can be judged with reference to the principal parameter used in this study, the deviations of the daily maximum or minimum air temperature from the 2-day running mean air temperature. Since this parameter is representative of the general weather conditions, it is used to derive the probable scenarios for extreme temperature conditions. The conditions of cloud cover and average wind velocity leading to these extreme conditions can

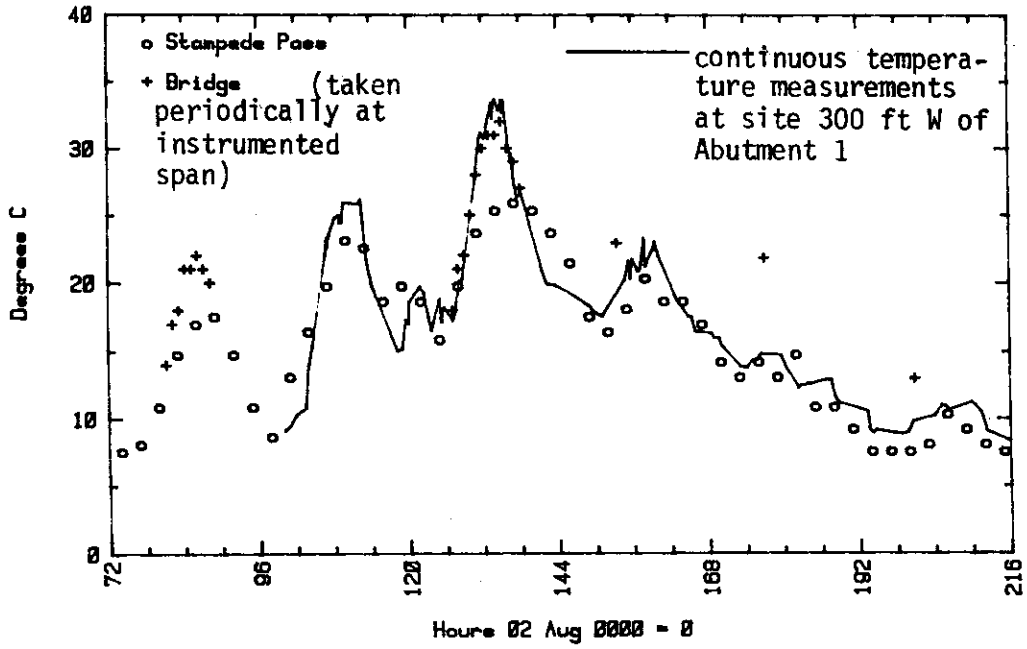

Figure 5.1.

Air Temperatures, 6 August 1200 to 10 August 2400

then be inferred from the conditions accompanying the extremes at the Stampede Pass station.

The deviations of the daily maximum and daily minimum air temperatures from the 2-day running mean air temperature at the Stampede Pass station for 1980 and 1981 are illustrated in Figures 5.2 through 5.5. The deviations of the daily maximum and minimum air temperatures from the 2-, 3- and 7-day running means for 9 July 1982 through 16 August 1982 are illustrated in Figures 5.6 and 5.7. It may be observed that, while there is little difference between the deviations from the 2-day and the 3-day running means, the deviations from the 7-day mean are considerably greater than those from the 2- and 3-day means. The results of the heat flow studies indicate that the deviation from the 2-day mean is the appropriate parameter for sections of the thickness generally encountered in bridges. The time period to be selected for the appropriate running mean is governed by the thickness of the sections considered. Since the running mean temperature defines the initial temperature values for the transient heat flow analysis, longer periods for the running means would be appropriate for thicker sections. In the limit, the deviations from the long-term mean annual temperature may be appropriate. The mean and extreme temperatures for the Stampede Pass station are illustrated in Figure 5.8, along with a curve representing the sine curve of best fit to the mean monthly temperatures for the 38 years of records at that station. From Figure 5.8 it can be concluded that the deviations of the extreme temperatures for each month are in the range of 3 to 4 times the difference between the mean maximum or mean minimum and the mean monthly temperature except for the month of December. That trend suggests that the deviation is a random variable. Examination of the detailed daily records for the dates of the December extremes shows that those temperatures occurred during periods when the running means were also at extreme values. It is

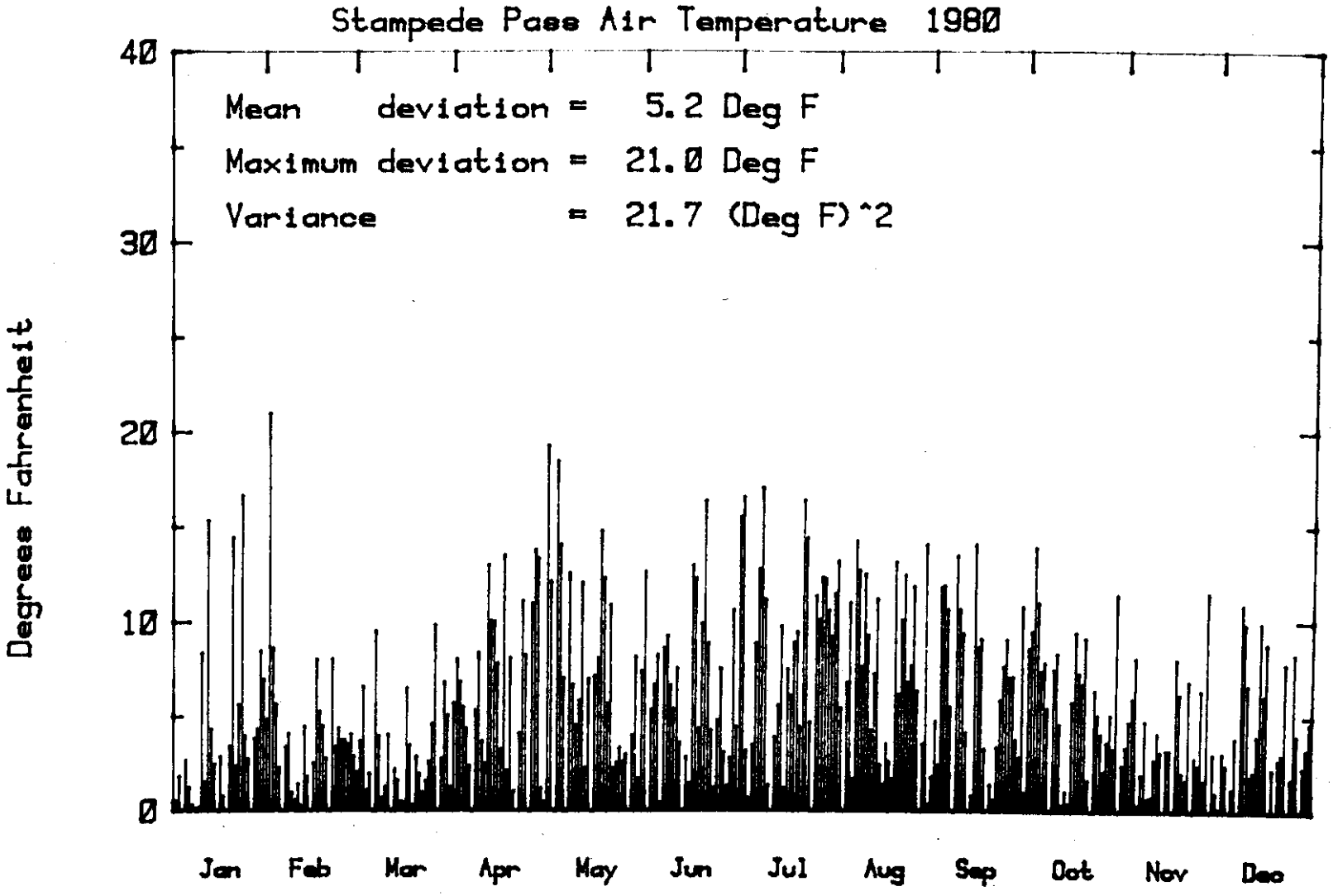

Figure 5.2. Deviation of daily maximum from 2 day running mean

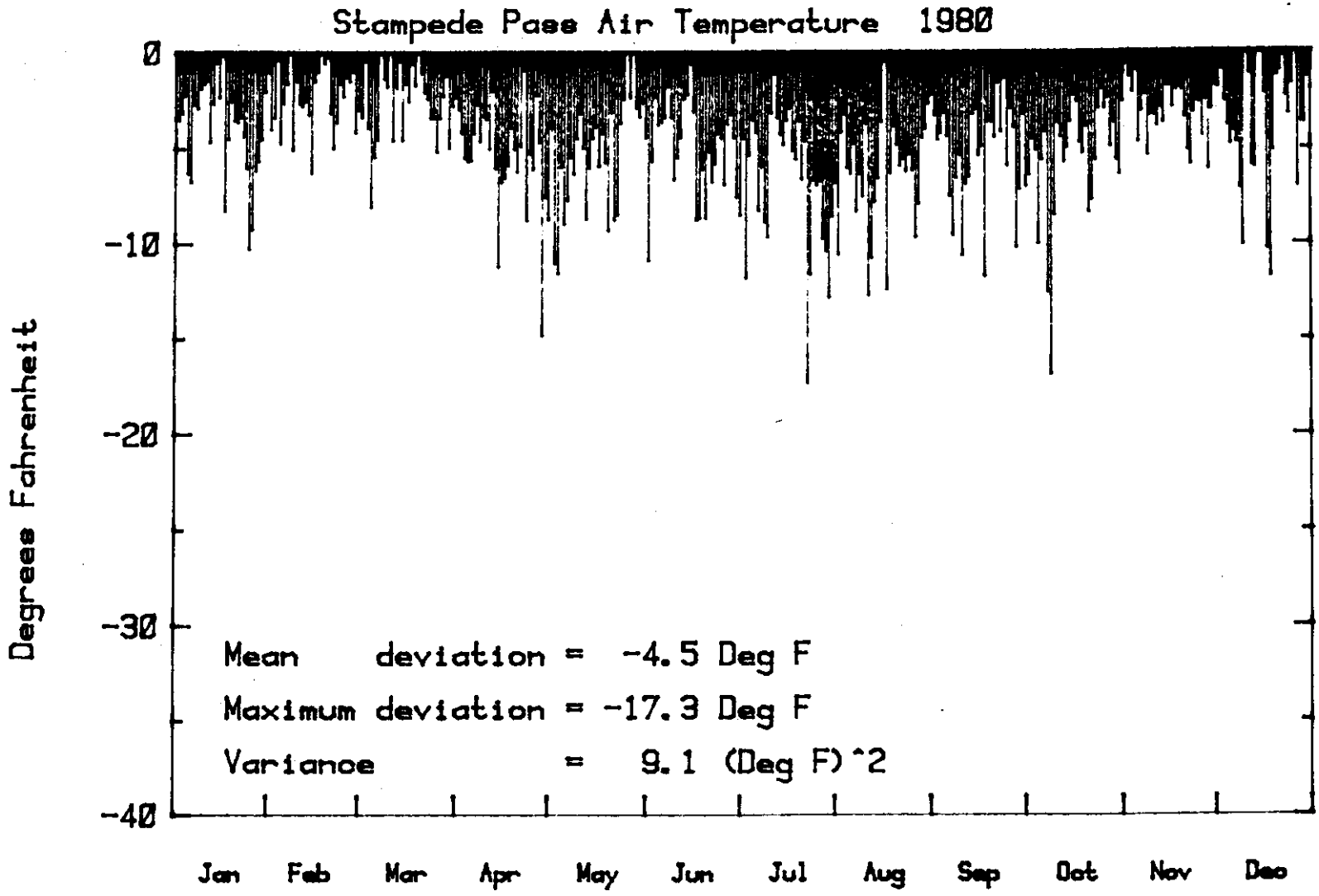

Figure 5.3. Deviation of daily minimum from 2 day running mean

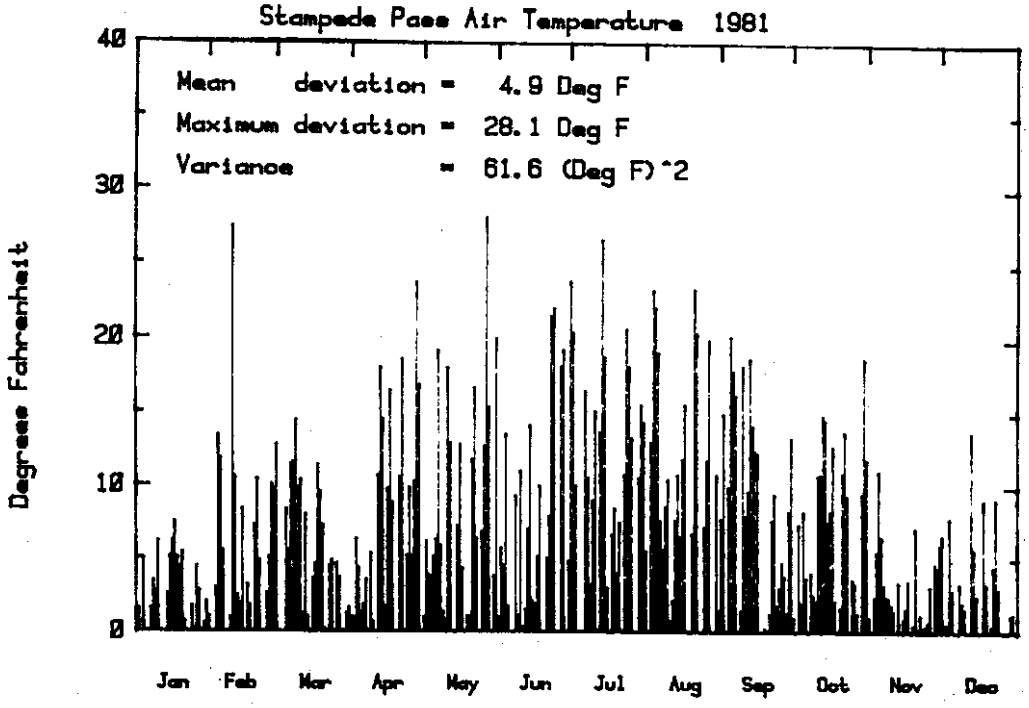

Figure 5.4. Deviation of Maximum Daily Air Temperature from 2 Day Running Mean, Stampede Pass 1981

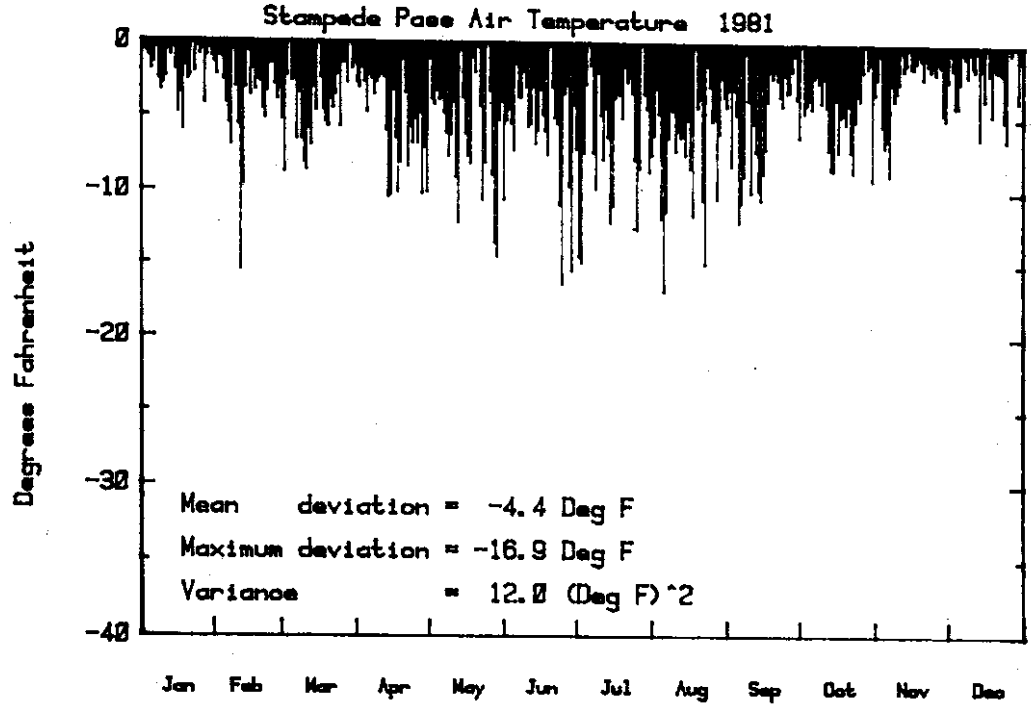

Figure 5.5. Deviation of Minimum Daily Air Temperature from 2 Day Running Mean, Stampede Pass 1981

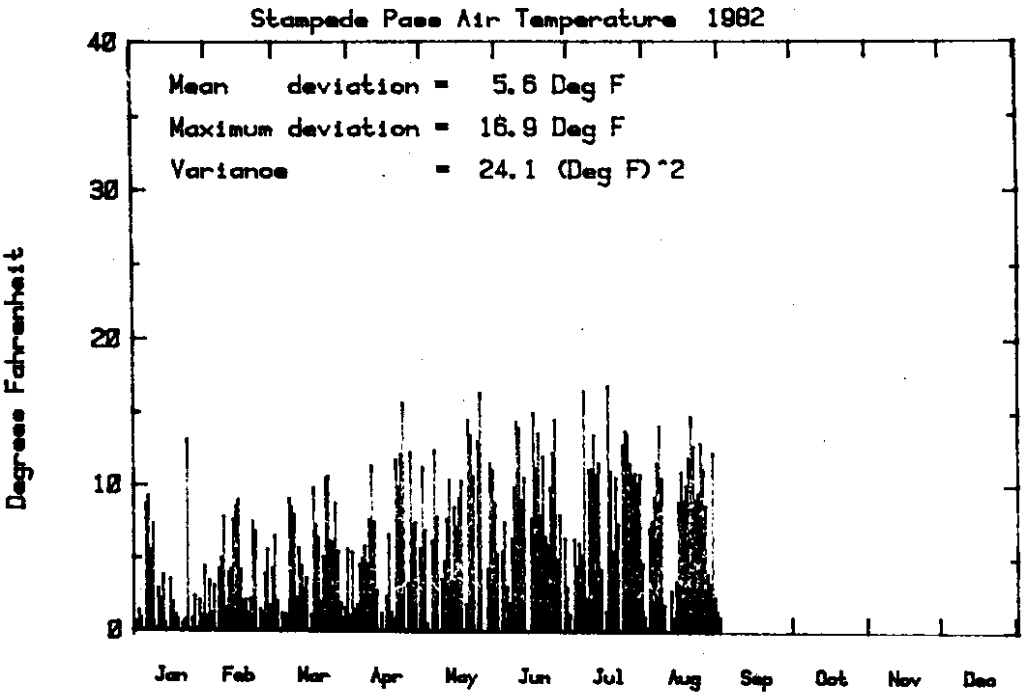

Figure 5.6. Deviation of Maximum Daily Air Temperature from 2 Day Running Mean, Stampede Pass 1982

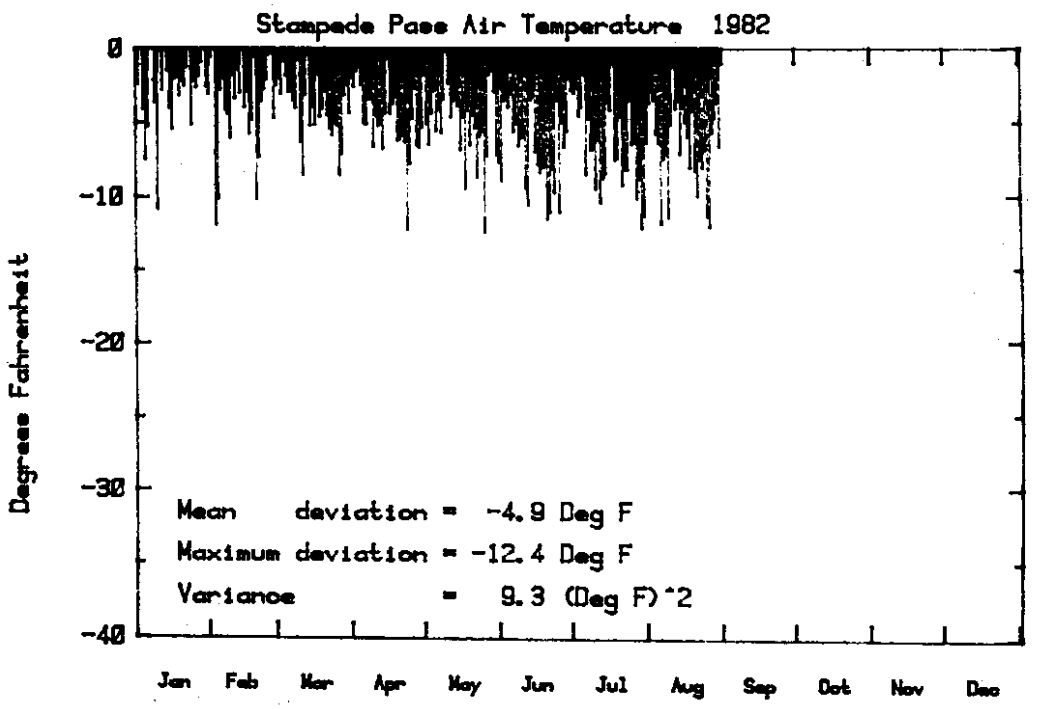

Figure 5.7. Deviation of Minimum Daily Air Temperature from 2 Day Running Mean, Stampede Pass 1982

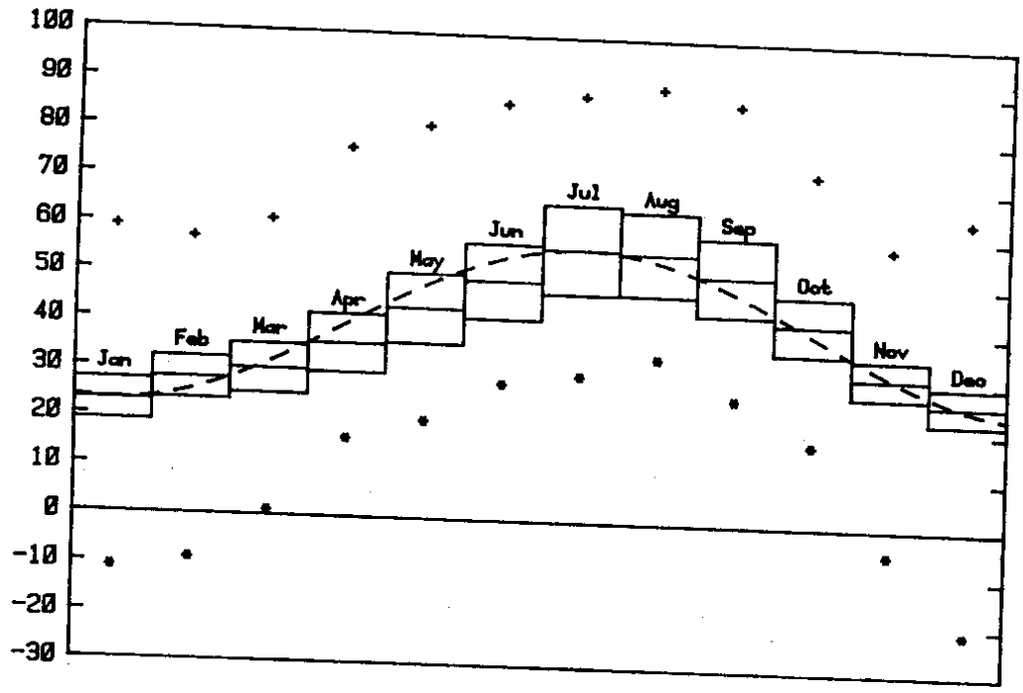

Figure 5.8.

Stampede Pass Mean and Extreme Temperatures
for Period of Record 1943-1981

\+ Extreme maximum

Mean daily maximum air temperature
Mean daily air temperature
Mean daily minimum air temperature

* Extreme minimum

therefore postulated that the deviation of the daily maximum or daily minimum temperature from the 2-day running mean air temperature may be taken as a random variable for purposes of estimating the probability of occurrence of a given value of that deviation.

From detailed examination of the long-term weather records for Stampede Pass and from consideration of the weather patterns characteristic of this area, it is apparent that there are two scenarios that can produce extreme differential temperature conditions in the Denny Creek Viaduct. The typical summer condition leading to the development of significant differential temperatures is the onset of warm clear weather following a period of cool overcast weather. That weather pattern is typical of the Cascade Mountains and occurs three to four times each summer. It was noted in this study that there is a significant daily variation in the pattern of bridge temperatures during clear summer weather due primarily to the influence of solar radiation. Since the rate of heat input at the deck is greater for solar radiation than for other means of heat transfer, it is clear that the summer conditions will produce a greater "positive" differential temperature, in the sense of the top surface being warmer than the bottom surface, than will weather patterns which occur at other times of the year.

By contrast, the worst "negative" differential temperature condition can be expected during winter months when the passage of a cold front causes relatively warm stormy conditions to be succeeded by clear cold conditions. This frontal passage is often accompanied by a sharp drop in the air temperature and strong winds. Even though the days are clear, they are short and therefore the solar radiation input is small compared to the input for summer conditions. Further, because of the longer nights, the radiative heat losses are at a maximum.

From the foregoing analysis of long-term weather records, it was concluded that there would be two extreme cases of input conditions for a heat flow analysis to determine the maximum probable differential temperature stresses in the bridge:

(1) Summer conditions result in a maximum positive differential temperature condition with the deck temperature greater than the bottom slab and web temperatures. This scenario starts with a uniform air temperature, overcast sky, and an outside air temperature varying between the daily minimum and the mean daily maximum temperature. The sky clears and the daily maximum air temperature then begins to increase, rising from the mean monthly temperature plus 1.5 times the deviation of the mean maximum from the mean monthly temperature on the first day to the mean plus 2.5 times the deviation on the second day and the mean plus 3.5 times the deviation on the third day. A minimum daily air temperature equal to the mean monthly minimum temperature occurs just before sunrise each morning. The maximum daily air temperature occurs at about 3:00 PM in the afternoon, local time. The sky remains clear and solar radiation is adjusted for the local topography, orientation and other site conditions. The wind velocity is 5 mph except for the influence of traffic on the deck, which must be considered by assuming a coefficient of surface heat transfer for the deck corresponding to a wind velocity of 40 mph.

(2) Winter conditions result in a negative differential temperature with the deck colder than the webs and bottom slab. This scenario also starts with overcast skies. The air temperature is near the mean monthly December temperature. The sky clears near sundown and the air temperature drops 10 degrees F per hour until a temperature equal to the mean monthly temperature less 3.5 times the deviation of the mean minimum from the monthly mean is reached. The wind velocity is 20 mph.

These two worst case scenarios represent extreme temperature conditions and result in changes in concrete temperature at the Denny Creek site similar to those reported by Priestley. The changes are a maximum of +40 degrees F and a minimum of -15 degrees F difference in temperature over the depth of the bridge for the positive and negative differential temperature cases, respectively. Those values are derived from the scenarios described above and are, a priori, applicable only to the Denny Creek site. For other sites, they should be verified or modified after a study of available weather data and local weather patterns before use in design.

5.4. Heat Flow Studies

5.4.1. Equations

The basic partial differential equation for heat flow in a homogeneous, isotropic solid is

$$\frac{\partial u}{\partial t} = \frac{1}{\kappa} \nabla^2 u \qquad (5.1)$$

where $u = u(x,y,z,t)$ = temperature at point x,y,z at time t

κ = diffusivity

$$\nabla^2 u = \left(\frac{\partial^2 u}{\partial x^2} + \frac{\partial^2 u}{\partial y^2} + \frac{\partial^2 u}{\partial z^2}\right)$$

The form of the bridge superstructure is such that the temperature distribution at any time can be taken as uniform along the length of the bridge since the cross-section is uniform except at the piers. Zichner (2.34) has shown that for bridges similar to the Denny Creek Viaduct, the variation in the temperature perpendicular to the longitudinal axis of the bridge is of significance only at the junction of the web and top flange. It is thus considered that the temperature distribution within a given cross-section can

be characterized by developing the unidimensional distribution through the depth of the structure for the three vertical sections shown in Figure 5.9.

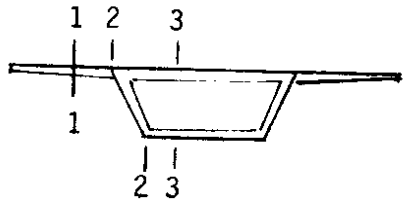

Figure 5.9. Sections for Temperature Distribution Calculations

Section 1-1 is taken at the mean thickness of the cantilever slab, Section 2-2 is taken at the web, and Section 3-3 is taken through the central box section. These assumptions reduce the governing partial differential equations to the unidimensional heat flow equation for a slab if, for Section 3-3, the response for the top and bottom slabs is considered separately, and the interior air temperature is taken as a known function of time. The unidimensional heat flow equation for a slab is

$$\frac{\partial u}{\partial t} = \kappa \frac{\partial^2 u}{\partial x^2} \qquad 0 < x < l \tag{5.2}$$

That equation is subject to the following boundary conditions:

$$-k \left.\frac{\partial u}{\partial x}\right|_{x=0} + h u_{x=0} = f_1(t) \tag{5.3a}$$

$$-k \left.\frac{\partial u}{\partial x}\right|_{x=l} \quad h u_{x=l} = f_2(t) \tag{5.3b}$$

and the following initial conditions:

$$u(x,0) = g(x) \tag{5.4}$$

where k = thermal conductivity
x = distance from the upper surface of the slab
l = slab thickness
h = surface coefficient of convective heat transfer
and f_1, f_2 = general functions of time

5.4.2. Closed Form Solutions

Closed form solutions to Equation 5.2 for various boundary conditions have been discussed by Carslaw and Jaeger (5.2). Solutions are available only for simple boundary conditions and even those solutions are lengthy expressions. Consider the case of a slab for which one face is maintained at a constant temperature while the temperature of the opposite face undergoes a sinusoidal variation with time. That situation is represented by the equation

$$u_t = \kappa u_{xx} \qquad 0 < x < 1$$

where $u(1,t) = \sin(\omega t + \varepsilon)$
$u(0,t) = 0$
$u(x,0) = 0$
t = time
ω = radian frequency = $2\pi/T$
T = period
and ε = arbitrary constant

This solution is valuable for gaining insight into the problem of developing a suitable solution for the bridge problem and identifying the influence of the differing variables that are part of the equations. Carslaw and Jaeger give the solution as

$$u(x,t) = A \sin(\omega t + \varepsilon + \phi) + 2\pi\kappa \sum_{n=1}^{\infty} \frac{n(-1)^n (\kappa n^2\pi^2 \sin\varepsilon - \omega l^2 \cos\varepsilon)}{\kappa^2 n^4 \Pi^4 + \omega^2 l^4} \times \sin\frac{n\pi x}{l}\, e^{-\kappa n^2\pi^2 t/l^2} \qquad (5.5)$$

where ϕ = time lag
A = amplitude

A further simplification in Equation 5.5 is possible by expressing the amplitude A and the time lag ϕ as the ratios of those quantities for a given depth from the unheated surface to the surface amplitudes for the same quantities for steady state conditions. The amplitude ratio, A, is given by

$$A = \left|\frac{\sinh\ (\hat{k}x(1+i)}{\sinh\ (\hat{k}l(1+i)}\right| = \sqrt{\frac{\cosh\ 2\hat{k}x\ -\ \cos\ 2\hat{k}x}{\cosh\ 2\hat{k}l\ -\ \cos\ 2\hat{k}l}} \qquad (5.6)$$

where $\hat{k} = \sqrt{\frac{\omega}{2\kappa}}$ = the "wave" number

and the time lag, ϕ, is given by

$$\phi = \arg\left\{\frac{\sinh\ (\hat{k}x(1+i)}{\sinh\ (\hat{k}l(1+i)}\right\} \qquad (5.7)$$

The velocity, v, of propagation of the peak temperature, or any other point on the cycle, through the depth is given by

$$v = \sqrt{2\omega\kappa} \qquad (5.8)$$

These concepts were applied to the top slab of the Denny Creek Viaduct. The mean thickness of that slab over the interior cell is approximately 0.40 m (15.7 in). The variation in the amplitude at the depth of the Carlson gages Nos. 8-14 in the slab (0.12 m) (4.7 in) to the surface amplitude, and the lag times at that depth were predicted to be as shown in Table 5.1 for a range of diffusivities. The period for the variation in surface temperatures was 24 hours. The values listed in Table 5.1 are not sensitive to the slab thickness for thicknesses greater than that assumed, and therefore temperature amplitude ratios and the phase lag for the top gages in the slab of the Viaduct should be able to be represented by such a calculation. The characterization of the top surface boundary condition as a sinusoidal variation in surface temperature and the lower surface boundary condition as a constant temperature is reasonably representative of the conditions for the Denny Creek Viaduct when weather conditions have been stable for three or four days.

Table 5.1.

Effect of Diffusivity on Amplitude Ratio and Time Lag

Diffusivity	at x/l = 0.28 m/0.40 m Amplitude Ratio	Time Lag
0.6 x 10 m^2/sec	0.395	-3.61 hrs
0.8 "	0.455	-3.13 hrs
1.0 "	0.502	-2.76 hrs
1.6 "	0.589	-2.02 hrs
2.4 "	0.641	-1.46 hrs
3.2 "	0.665	-1.13 hrs

The influence of the different variables on the resulting surface temperatures can be studied simplistically by considering the equation for steady state heat flow through a slab under the influence of a constant radiative heat input at the upper surface. Suppose the upper surface of the slab is in contact with a fluid at a given temperature and the lower surface is in contact with a fluid at another temperature. The variables for this condition are illustrated and defined in Figure 5.10.

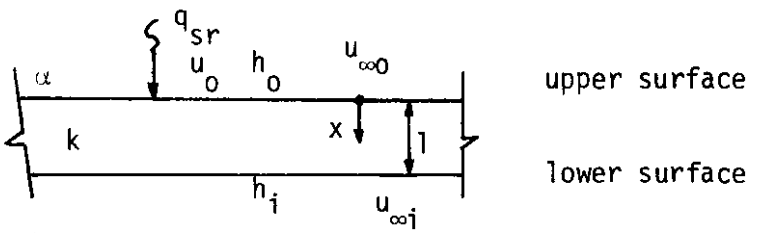

α=absorptivity; q_{sr}=solar radiation; u_o=temperature of upper surface; h=surface coefficient of convective heat transfer; u_{∞}= fluid temperature; k=conductivity.

Figure 5.10. Slab with Radiative Heat Input

The heat flow balance for the steady state condition can be expressed as

$$\alpha\, q_{sr} = h_o(u_o - u_{\infty o}) + U'(u_o - u_{\infty i}) \tag{5.9}$$

$$\text{where } U' = \frac{1}{\frac{1}{k} + \frac{1}{h_i}} = \frac{kh_i}{1 + 1h_i} \tag{5.10}$$

The heat absorbed at the upper surface is partly lost to the fluid at that surface by convection and partly conducted to the lower surface where it is lost to the fluid there by convection. It is assumed that the fluids are always separated by the slab and remain at a constant temperature.

Solving Equation 5.9 for the upper surface temperature gives:

$$u_o = \frac{\alpha\, q_{sr} + h_o u_{\infty o} + U' u_{\infty i}}{h_o + U'} \tag{5.11}$$

In the transient state, prior to achievement of steady state conditions, the temperature gradient at the upper surface will always be greater than the steady state gradient, and thus the heat flow rate into the slab will be a larger portion of the total radiative input than in the steady state. In any event, the surface temperature given by Equation 5.11 will be the maximum temperature attained under the stated conditions, and Equation 5.11 can be utilized to study the probable upper limit for surface temperature over the range of thermal properties and ambient conditions likely to be encountered. Temperatures given by Equation 5.11 will be greater than those observed in any real situation because the radiative heat input, due to solar radiation, is not constant over the times required to achieve steady state conditions for concrete bridge slabs, nor is the ambient air temperature constant over the same time span.

Closed form solutions to the unidimensional heat flow equation for simple boundary conditions and qualitative expressions obtained from steady state

heat flow balance considerations are useful for studying the relative influence of various parameters. However, those solutions and expressions are not adequate to address the differential temperature problem for bridges. In that case, the boundary conditions are not amenable to simple expressions, and they change with sufficient rapidity so that steady state conditions are not attained. To overcome those constraints, it is necessary to resort to a numerical solution of the partial differential equations as discussed in the next section.

5.4.3. Boundary Conditions for Denny Creek Viaduct

The numerical solution of the heat flow problem for the Denny Creek Viaduct first requires establishment of the boundary conditions. The boundary conditions influencing the heat flow into and through the slab for Section 3-3, Figure 5.9, of the Denny Creek Viaduct include the ambient air temperature at the upper and lower surfaces, the effective sky temperature, the solar radiation, the absorptivity and emissivity of the upper surface, and the surface coefficients of convective heat transfer. The absorptivity, emissivity and surface coefficients are also properties of the material but are discussed in this section because they influence the boundary conditions. The boundary condition at the upper surface of the slab is derived from the heat flow balance at the surface and is given by

$$h(u_{\infty} - u_{x=0}) + \alpha\ q_{sr} - \varepsilon\sigma(u^4_{x=0} - u^4_{sky}) = 0 - k\ \frac{\partial u}{\partial x} \qquad (5.12)$$

where k = surface coefficient of convective heat transfer at the upper surface

h = surface coefficient of convective heat transfer at the lower surface

α = adsorptivity of the upper surface (short wave radiation)

ε = emissivity of the upper surface (long wave radiation)

σ = Stephan-Boltzmann constant

q_{sr} = solar radiation (direct and diffuse)

and u_{sky} = effective sky temperature for long wave radiation

The outside ambient air temperature may be taken from measured values or prescribed as a continuous function of time. The inside air temperature may also be taken from measured values or prescribed as a continuous function of time. It was found in this study that the inside air temperature did not vary significantly on a daily basis and could be taken as the same as the 2-day running mean of the outside air temperature. It is apparent from Equation 5.11 that the maximum upper surface temperature is not sensitive to variations in the interior temperature for ranges of h likely to be encountered in concrete bridges. The ventilation rate or ratio of the total cell volume to the area of the openings in the cell walls, top and bottom, is the most important determinant of the relation between the inside and outside air temperatures. The ventilation rate for the average box girder bridge is very large, corresponding to little opportunity for exchange of air between inside and outside. The ventilation rate for Frame 1 (Abutment 1 to Expansion Joint 2) of the Denny Creek Viaduct was estimated as 7,100 ft^3/ft^2. One practical conclusion readily apparent from this study is that differential temperature effects could be reduced substantially by improving box girder ventilation. The Denny Creek Viaduct has a form ideal for application of that concept on ventilation. Since the bridge has a marked slope and a critical event is associated with a heated upper surface, and a cool interior box, ventilation at the lower and upper levels of the Viaduct would allow cold entrapped air to exit from the lower ventilation port and warm outside air to enter through the upper ventilation port.

The surface coefficient of convective heat transfer of the upper surface is dependent on the average wind velocity over the time period considered. That velocity can be a function of time if its variation is known. However, in this study it was observed that for the Denny Creek Viaduct, the traffic flow was such that during a summer time event, regardless of the ambient wind velocity, there was an almost constant stirring of the air immediately above the deck by the traffic. For the winter event, where weather conditions elsewhere may determine the traffic flow, there may not be the same degree of constant stirring. Most investigators of thermal stresses in bridges have assumed minimal wind velocities to derive maximum temperatures. The anticipated traffic volume should be considered in selecting the surface coefficient of convective heat transfer for the deck. Account should be taken of the average traffic speed and frequency of vehicle passage. It is recommended that the "apparent" wind velocity be the value intermediate between ambient wind velocity and the traffic speed. The surface coefficient of convective heat transfer for the upper surface may then be calculated using the expression given by Zichner (2.34).

The surface coefficients of convective heat transfer for the outside surfaces not influenced by traffic will depend upon the ambient wind velocity, the orientation of the surface (i.e., the direction of the outward pointing normal to the surface), and the expected direction of the heat flow. The values that have been reported by different investigators differ markedly with test conditions. It is recommended that the values given in Sucec (5.3), Holman (5.4), or ASHRAE (5.5) be used. The effects of these coefficients on the overall temperature distribution are not sufficient to warrant a detailed examination of their appropriate values. It is recommended that the value for a downward-facing horizontal surface for upward heat flow and moderate (5 mph)

wind velocity be used.

The absorptivity of the upper surface is the proportion of incoming radiation which is absorbed by, as opposed to reflected from, the slab. The absorptivity of a surface depends on the material, the texture, and the color of that surface. Higher values of absorptivity are associated with rough, dark-colored surfaces than with smooth, light-colored surfaces. Thus, the absorptivity of a concrete surface can be expected to increase with age as the concrete darkens. A light-colored curing sealer, such as the white pigmented curing compound frequently used on concrete bridge decks, can be expected to significantly reduce absorptivity at early ages. However, that sealer is worn off quickly by traffic. It is recommended that absorptivity values in the range between 0.5 and 0.85 be used for concrete surfaces. Those values are appropriate for the wave lengths of light, where most of the energy of solar radiation is concentrated.

The emissivity of a given surface is the ratio of the heat radiated by a unit area of the surface of that material to the heat radiated from a unit area of the surface of a perfect "black" body when both objects are radiating into space. For a bridge, the emissivity is dependent on the texture of the slab and on the wave length of the outgoing radiation. The wave length of the outgoing radiation lies in the infrared region of the spectrum for bodies at normal atmospheric temperatures. The emissivity of common building materials ranges from 0.75 to 0.95. Appropriate values for emissivity for different conditions are listed in Section (5.3).

The appropriate solar radiation input for any given site can be determined from the latitude, longitude, day of the year, orientation of the surface, and the atmospheric conditions prevalent at that site on a given day. All those parameters are deterministic except for the atmospheric conditions. The atmospheric condition with the dominant influence on solar radiation is

the amount of moisture in the atmospheric column. That moisture can be in the form of water vapor or clouds. Details of this influence are discussed by Raphael (5.6). Theoretical values for solar radiation that depend only on the geographic location, time of year, and the site elevation are given by Duffie and Beckman (5.7). The influence of the local topography must be considered in mountainous terrain such as the site of the Denny Creek Viaduct. The resulting net values of solar radiation, including outgoing long wave radiation, are shown in Figures 5.11 through 5.13 for Span 4 of the Denny Creek Viaduct for December 21, July 15 and August 5. These diagrams illustrate the large differences in the amount of daily heat input for a clear summer day and a clear winter day.

5.4.4. Numerical Solution

The complexity of closed form solutions to heat flow problems, and the limited range of boundary conditions for which such solutions are available, make numerical solutions the only practical procedure for heat flow studies for concrete bridges. There are in general two methods for solving the parabolic partial differential equations for heat flow by numerical means. These are the explicit and implicit methods described by Gerald (5.8).

The explicit method projects the situation at the next time step from the known conditions for the current time step. The explicit method is straightforward and relatively simple. The one-dimensional heat flow partial differential equation is solved by replacing the partial derivatives by finite-difference approximations:

$$u_i^{\,i+1} = \kappa\frac{\Delta t}{\Delta x^2}\left(u_{i+1}^{\,i} + u_{i-1}^{\,i}\right) + \left(1-2\kappa\frac{\Delta t}{\Delta x^2}\right) u_i^{\,i} \qquad (5.13)$$

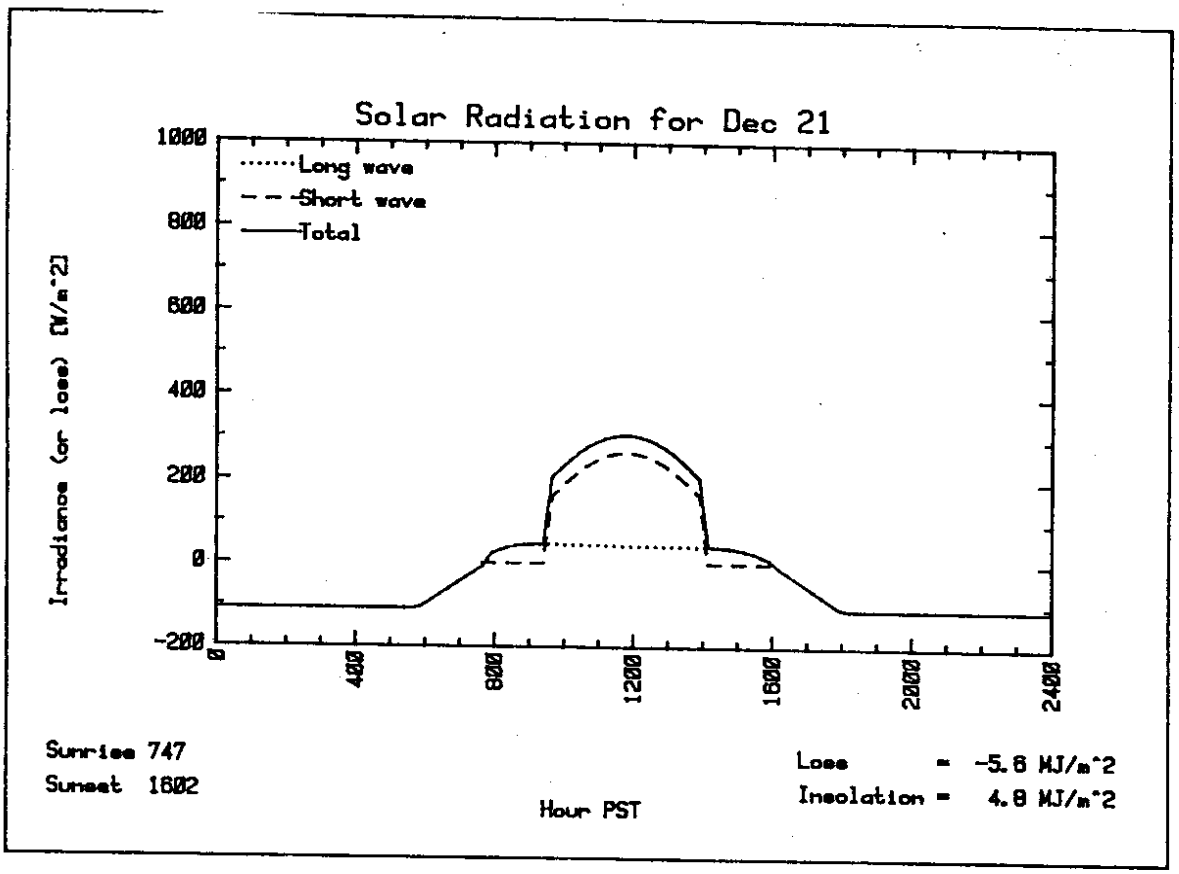

Figure 5.11.

Theoretical Solar Radiation for December 21

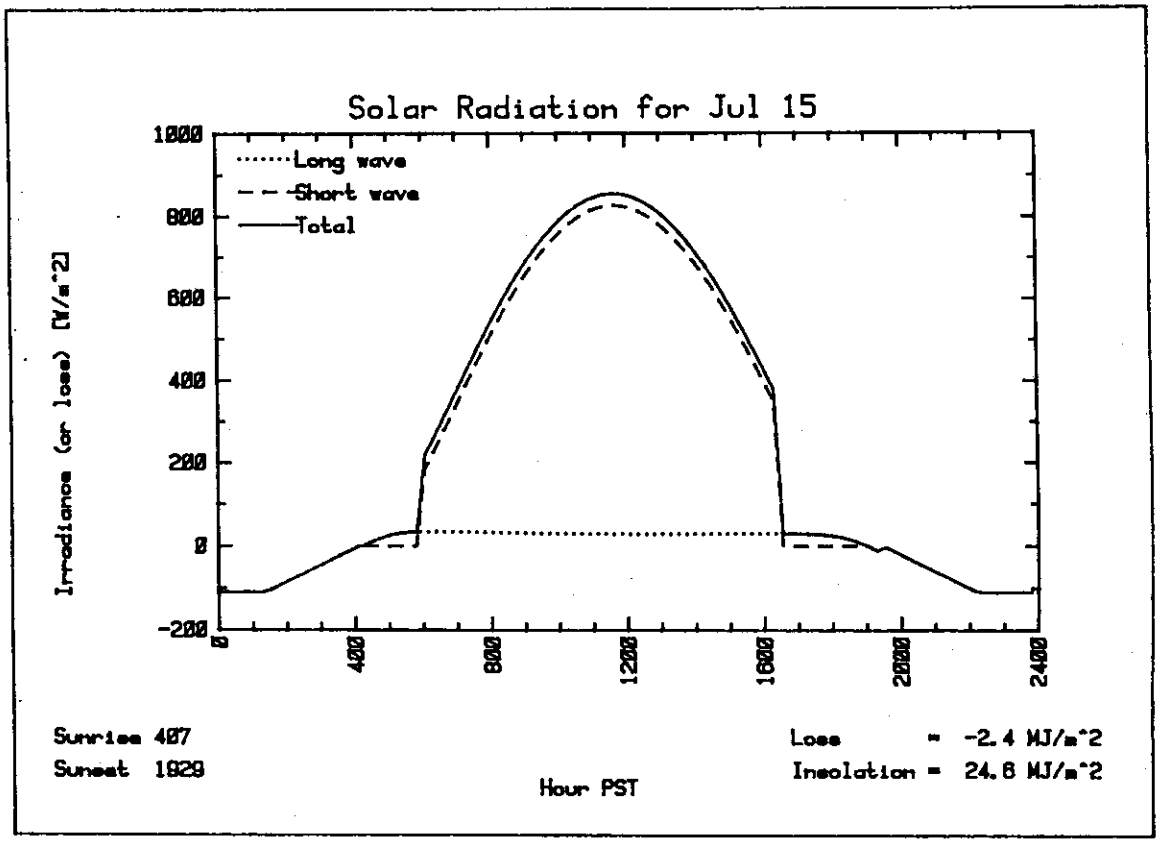

Figure 5.12.

Theoretical Solar Radiation for July 15

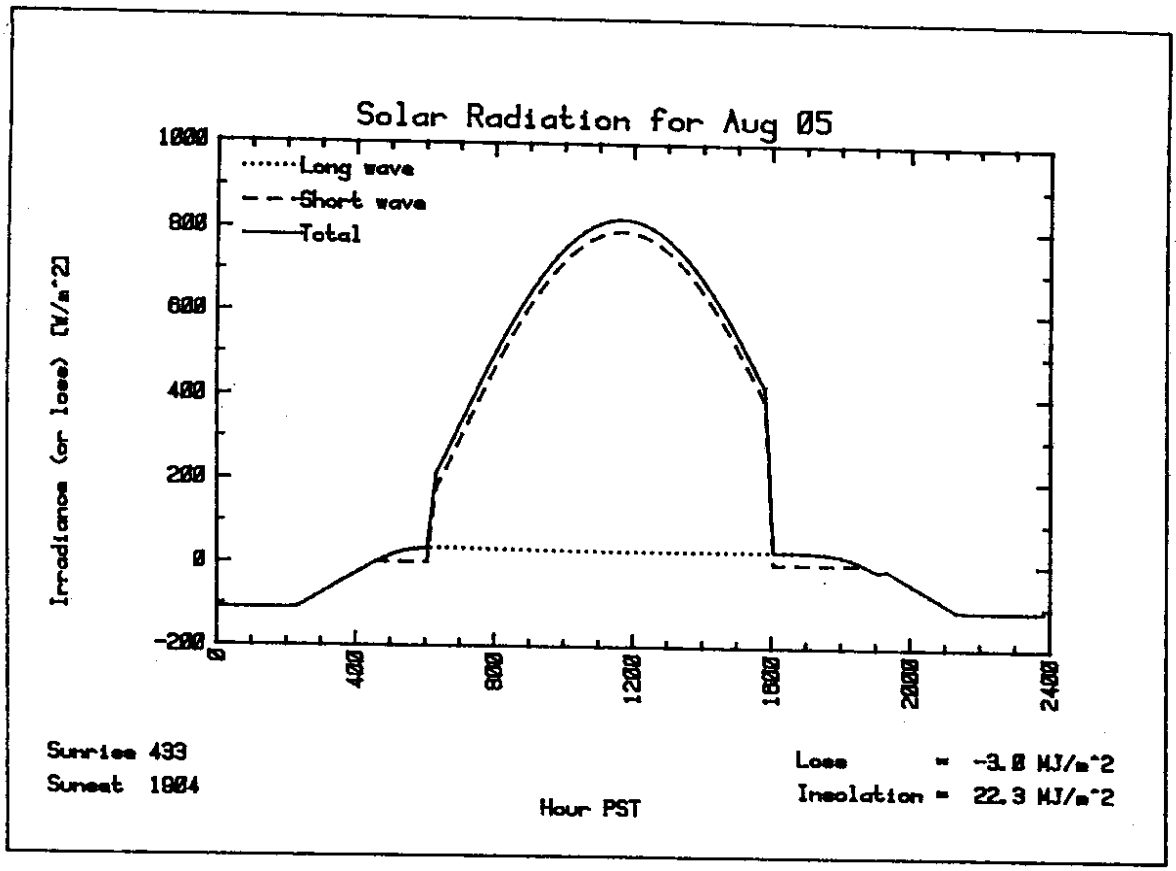

Figure 5.13.

Theoretical Solar Radiation for August 5

The superscripts (j) denote the time step and the subscripts (i) denote the spatial increment.

The stability of the explicit method is, however, dependent upon use of a sufficiently small time step. This time step is related to the size of the spatial increment and the thermal diffusivity of the material. The upper limit of the time step size for stability is

$$\Delta t = \frac{\Delta x^2}{2\kappa} \tag{5.14}$$

when there are prescribed temperatures on the boundaries and less when there are derivative boundary conditions. The small time step required for stability with the explicit method often makes that method too slow for economical solutions of practical problems, such as the one addressed in this study.

The Crank-Nicholson method is an implicit method in which the temperatures for the next time step appear in the heat flow equations as unknowns. This method entails the repeated solution of a set of linear equations to determine the temperatures at the end of the next time step. These equations are

$$- ru_{i-1}^{j+1} + (2 + 2r)\, u_i^{j+1} - ru_{i+1}^{j+1} = ru_{i-1}^{j} + (2 - 2r)u_i^{j} + ru_{i+1}^{j} \tag{5.15}$$

$$\text{where } r = \kappa \frac{\Delta t}{\Delta x^2}$$

The first and last equations are modified to account for derivative boundary conditions (i.e., the prescribed heat flow conditions).

Stability is guaranteed for any positive value of the ratio r, but the equations can be greatly simplified by the choice of r=1. This choice leads

to inconvenient values of the time step or spatial increment and is of no particular use when the equations are set up by a computer program. It is more convenient to choose an even time step and spatial increment. Gerald (5.8) has developed a computer program for solving the one-dimensional parabolic partial differential heat flow equation by the Crank-Nicholson method. That program was used for this study.

5.4.5. Thermal Properties of the Concrete

The relevant thermal properties for the concrete in the Denny Creek Viaduct were taken from the literature. Neville (5.9) gives a range of properties which are suitable for this study. The work of Brewer (5.10), Campbell-Allen and Thorne (5.11), Whiting, Litvin and Goodwin (5.12), Lentz and Monfore (5.13), Mitchell (5.14) and Rhodes (5.15) were consulted, but since data were not available on the mineralogical content of the aggregates, no better estimates than those given by Neville could be made. The relevant thermal properties for the concrete are the density, ρ, the conductivity, k, and the specific heat, c. These properties combine in the relation

$$\kappa = \frac{k}{\rho c} \qquad (5.16)$$

to give the diffusivity, κ. Except for density, direct measurement of these thermal properties requires specialized procedures. Facilities for making such tests are not generally available. Conservative values for those properties were therefore taken from the literature. That approach insures that the diffusivity is at a minimum.

The conductivity of concrete is a function of the mineralogical content of the aggregates, the moisture content, the paste to aggregate volume ratio, the type of cement, and the temperature of the concrete. The mineralogical

content is the single most important factor determining the conductivity. Neville (5.9) gives the following range for conductivity for normal weight concrete exposed to the weather:

$$1.44 < k \text{ W/(m}^2 \text{ deg C)} < 3.68$$

Mitchell (5.14) gives a range from 1.4 to 4.3 for conductivity.

According to Neville (5.9), the specific heat varies with the same parameters as follows:

$$0.8 < c \text{ KJ/(kg deg C)} < 1.2$$

The density of the concrete in the Denny Creek Viaduct was taken from the Resident Engineer's records and verified by weighing and measuring cylinders found at the site. The density was approximately 2.44 t/m^3 (152 lb per ft^3). Allowance for the weight of embedded reinforcing steel would raise this to 2.57 t/m^3 (160 lb per ft^3).

The parameters that determine the conductivity and specific heat also determine the diffusivity. However, the range in values for the diffusivity is less than that predicted from the ranges for conductivity and specific heat, since the factors which lead to a greater conductivity usually contribute to a greater density and specific heat. Therefore, for this study the diffusivity of the concrete in the Denny Creek Viaduct was taken as 0.7×10^{-6} m^2/second. That is the lower value of the range of values reported in the literature. Neville cites that range as

$$0.7 \times 10^{-6} < m^2/\text{sec} < 1.4 \times 10^{-6}$$

The smaller the conductivity and diffusivity values, the greater are the predicted thermal gradients.

5.4.6. Results of the Heat Flow Studies

Heat flow studies were made to predict the temperature distributions measured in the Denny Creek Viaduct. Those heat flow studies used as input

the environmental parameters discussed previously. The period from 2 August through 7 August 1982 was used for a calibration study. This period began with cool weather and overcast skies which produced nearly uniform temperatures throughout the bridge. The sky cleared on 4 August and remained substantially clear through 7 August. The daily range in air temperatures at the site rose from 6 degrees F on 1 August to 31 degrees F on 5 August, and remained at 30 degrees F for 6 and 7 August.

On the morning of 2 August the average measured bridge temperature was 52 degrees F (11.2 degrees C) and that value was taken as the initial temperature for the calibration study. The outside and inside air temperature boundary conditions were also taken from theoretical values, modified for cloud cover as reported by the Stampede Pass weather station. These boundary conditions were discussed previously in Section 5.4.3 and are illustrated in Figure 5.14 as a plot of these environmental parameters versus time. Differing values for the coefficients of conductive heat transfer for the deck and shaded surfaces and for the diffusivity were input in the numerical solution procedure, and those values which gave the best fit with the measured concrete temperatures for the top slab gages (Nos. 8-14) were determined. The variation in the measured and predicted concrete temperatures with time are shown in Figure 5.15. The predicted values are those for which best agreement was obtained with the test values for differing reasonable combinations of absorptivity, emissivity, and diffusivity. The values of the latter properties are shown in Figure 5.15. The peak temperature predicted for 5 August is in good agreement with the peak temperature observed , and the daily range predicted for both 5 August and 7 August is in good agreement with the observed range. However, the values of the observed temperatures for 7 August are from 4 to 6 degrees C less than the predicted temperatures. The results show that the concrete temperatures for the night of 6-7 August were surpris-

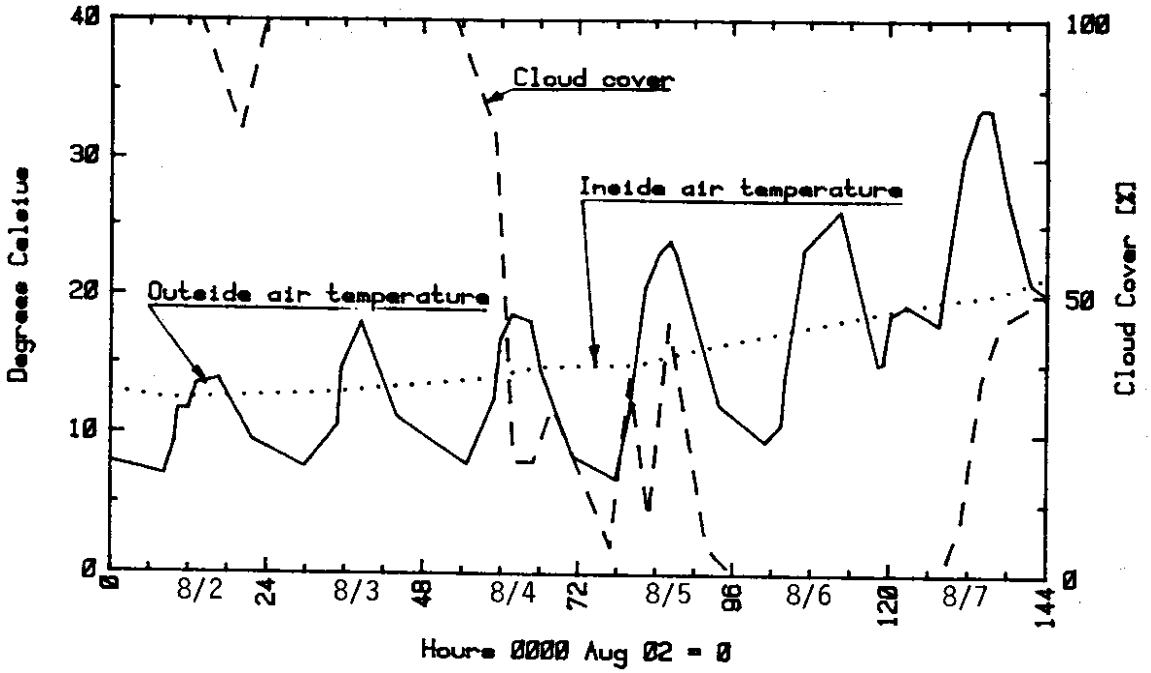

Figure 5.14. Boundary Conditions for Heat Flow Analysis for 2-7 August 1982

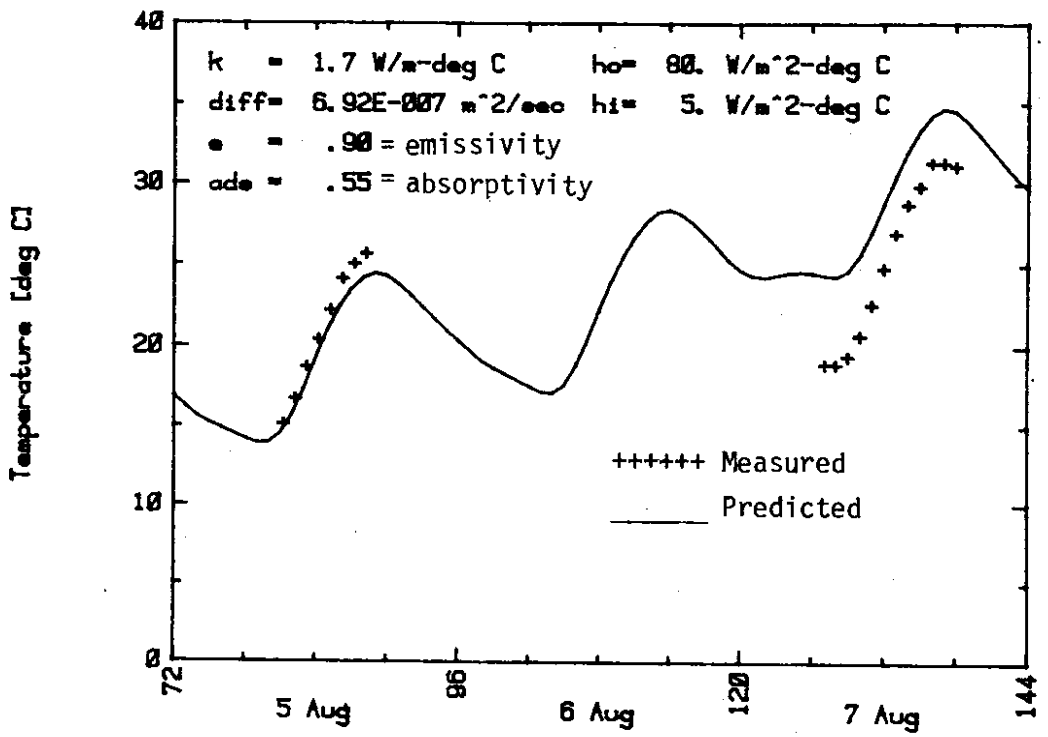

Figure 5.15. Comparison of Measured and Predicted Concrete Temperatures for 5-7 August 1982

ingly warm compared with those for the previous night. The occurrence of that anomaly was checked by examining the Stampede Pass air temperature record for 6-7 August. The occurrence of a warm night was also confirmed by that record. No explanation for the discrepancy between measured and predicted results for 7 August is apparent from the data. It should, however, be noted that the times of the measured maximum and minimum temperatures were in good agreement with the predictions for those times.

Based on the results of these calibration studies, it is concluded that the model developed here will predict temperature distributions in the Viaduct with sufficient accuracy for design purposes, once the controlling environmental boundary conditions are established.

5.5. Calculation of Thermal Stresses from a Given Temperature Distribution

There are many methods available for calculation of the stresses from a given temperature distribution. The CTL report utilized Mattock's procedure (2.2). Based on comparisons of the measured strains and measured temperatures, the use of Priestley's procedure (1.6) is recommended here. Mattock's procedure was developed originally to calculate stresses due to differential shrinkage between composite slabs and precast girders. Its use is discussed in the CTL report. The procedure requires calculation of the average temperature of the top slab and the average temperature of the webs and the bottom slab. The equivalent strain differential caused by those temperatures is then found by multiplying the difference between those two average temperatures by the coefficient of thermal expansion. The shear and moment required at the slab-web interface to maintain strain compatibility is then found and that shear and moment applied to the composite section. The stresses caused by that shear and moment are calculated with due consideration to support and continuity conditions and any relaxation with time. Mattock's

procedure can be expected to give reasonably accurate results for the stresses at the extreme bottom fiber if appropriate average temperatures are used for slab and webs, respectively. However, details of the stress distribution would not be correct. In particular, high stresses are predicted at the slab-web interface which are not present in an actual girder.

Priestley's method (1.6) assumes a linearly elastic, homogeneous, isotropic material for which plane sections before flexure remain plane sections after flexure. It also assumes a continuous but non-uniform temperature distribution through the depth of the section. The product of the temperature variation and the section width is integrated over the depth to give the "average" temperature (i.e., the effective temperature for overall longitudinal expansion or contraction). This "average" temperature is the temperature which influences stresses due to restraint of axial expansion and contraction. The product of temperature, section width, and distance from the neutral axis are integrated to give the "effective" gradient (i.e., the gradient which would be effective in producing curvature in a simple beam or generating streses due to flexural restraint in a fixed end beam). The restraint stresses, f_{c_1}, necessary to maintain plane sections plane, are then found as follows:

$$f_{c_1}(y) = -E\alpha[t(y) - t_{na} - y\Psi] \qquad (5.17)$$

where $t_{na} = \int t(y)b(y)dy/A$ = the "average" temperature

$t(y)$ = temperature at distance y from the neutral axis

$b(y)$ = section width at distance y from the neutral axis

y = distance from the neutral axis, positive above the neutral axis

E = modulus of elasticity

α = coefficient of thermal expansion

$\Psi = \int t(y)b(y)ydy/I$ = the "effective" temperature gradient

I = moment of inertia of section

The stresses, f_{c_2}, due to restraint of axial expansion, are determined from the expression:

$$f_{c_2} = E\alpha t_{na}\eta_a \qquad (5.18)$$

where η_a = degree of axial restraint

$\eta_a = 0$ if free

and $\eta_a = 1$ if built-in

The stresses, f_{c_3}, due to restraint of flexure, are found similarly from the expression:

$$f_{c_3} = -E\alpha\, y\psi\eta_f \qquad (5.19)$$

where η = degree of flexural restraint

Geometric terms in Equations 5.16-5.19 are illustrated in Figure 5.15.

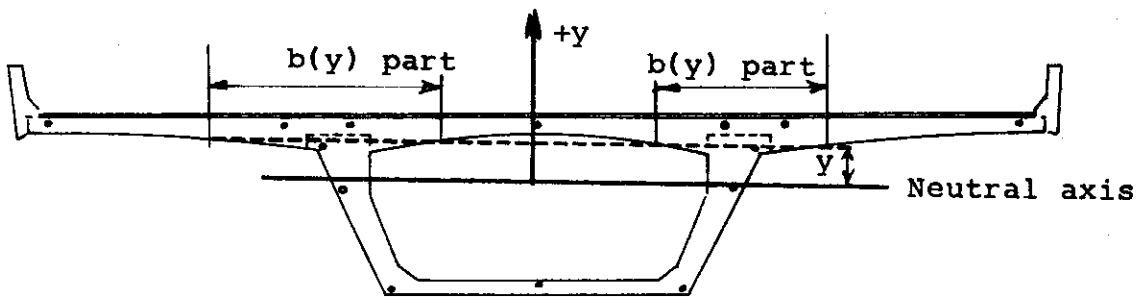

Figure 5.16. Geometric Terms for Calculation of Stresses due to Non-Linear Temperature Distribution

Priestley's method can be generalized to encompass different materials by including the modulus of elasticity under the integral sign and can also be extended to cover cracked sections by an iterative procedure that neglects the tensile strength of the concrete or utilizes a generalized moment curvature relationship.

The results obtained by Mattock's and Priestley's procedures were investigated for the Denny Creek Viaduct subjected to the temperature distribution shown in Figure 5.17. That distribution is Priestley's distribution for the upper surface of the deck being 40 degrees F warmer than webs, and the webs being 10 degrees F warmer than the soffit. That distribution represents the extreme positive event for the Viaduct postulated earlier. Temperature profiles are drawn in Figure 5.17 for each of the three sections shown on Figure 5.9. The eigenstresses (i.e., the temperature stresses necessary to maintain plane sections plane in a simply supported beam Radioli and Green ((1.7)) are shown in Figure 5.18 for stresses predicted using Priestley's method. Those stresses, combined with the flexural restraint stresses caused by the "effective" temperature gradient, are shown in Figure 5.19. The calculations from which Figures 5.18 and 5.19 were derived are shown in Appendix F. The eigenstresses for CTL's method are shown in Figure 5.20 and those stresses combined with the restraint stresses caused by those stresses are shown in Figure 5.21. The calculations for Figures 5.20 and 5.21 are also shown in Appendix F.

In a case where the top slab is cooling rapidly due to outgoing radiation on a clear, cold night, the resultant stress at the upper surface is predicted to be tensile by either method and opposite in form to that shown in Figure 5.17. The steep gradient at the surface means that the equivalent tensile force for which mild steel reinforcement might be added would be considerably less by Priestley's procedure than that by CTL's procedure. It should be noted that this equivalent force should be determined from the cumulative stress distribution found after superimposing all relevant service load cases.

The increase in soffit temperature predicted by Priestley's procedure reduces tensile stresses at the same location. That reduction is important since, for the positive moment region of a beam, the tensile stresses caused by temperature gradients at that location combine with tensile stresses caused by gravity loads.

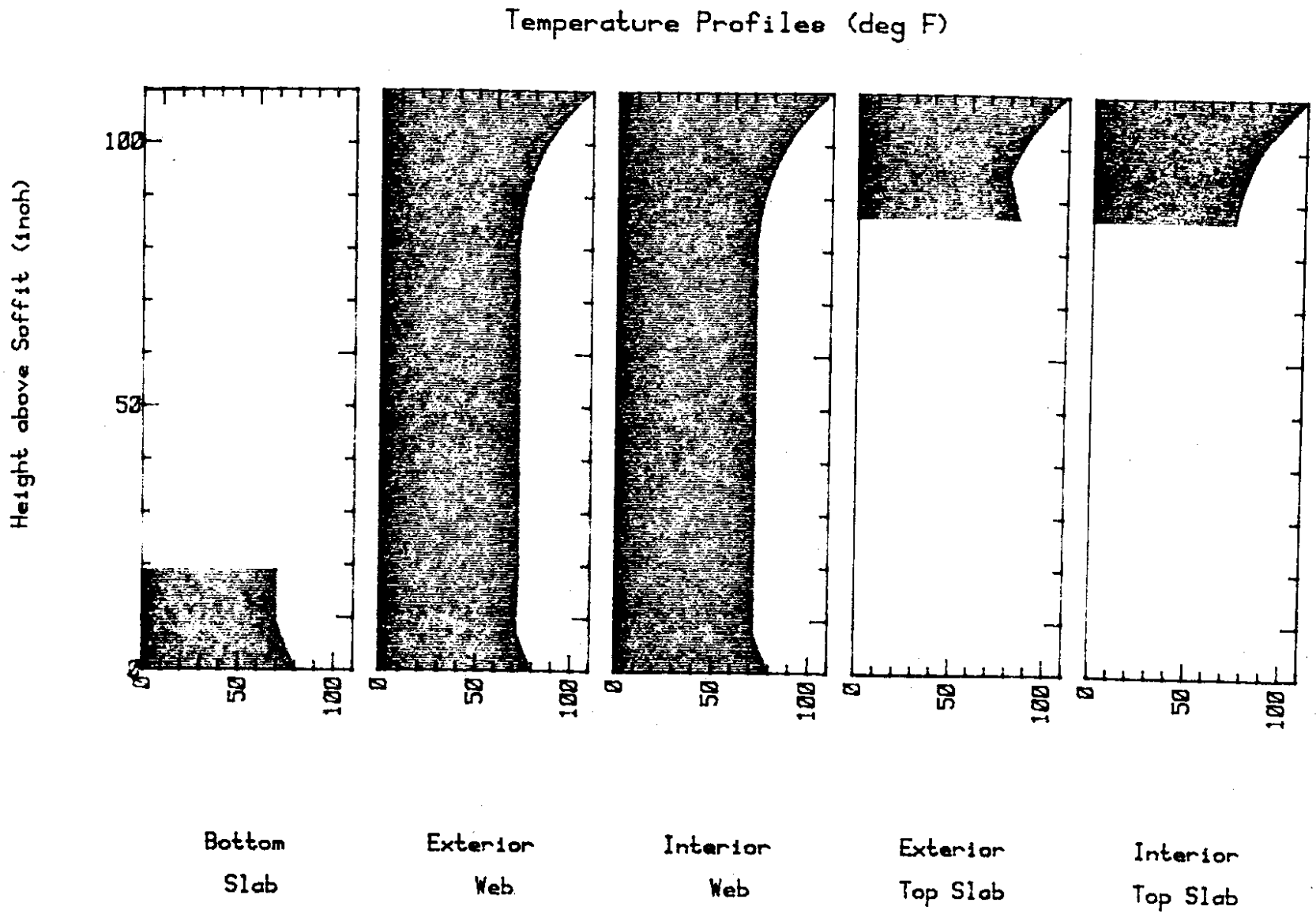

Figure 5.17. Temperature Distributions for Extreme Positive Differential Temperature Event

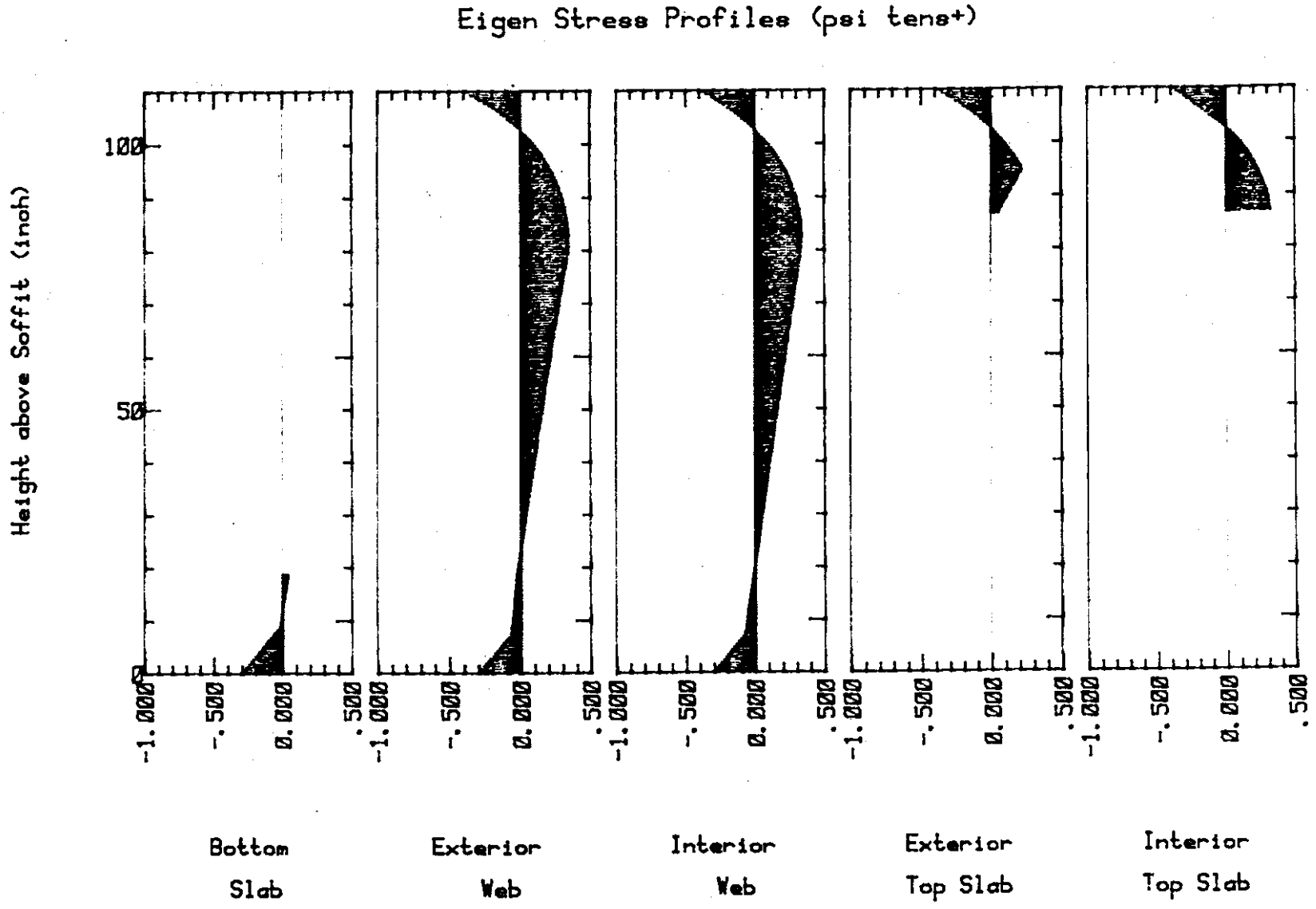

Figure 5.18. Thermal Stresses Predicted for Extreme Positive Differential Temperature Event by Priestley's Procedure, Eigenstresses Only

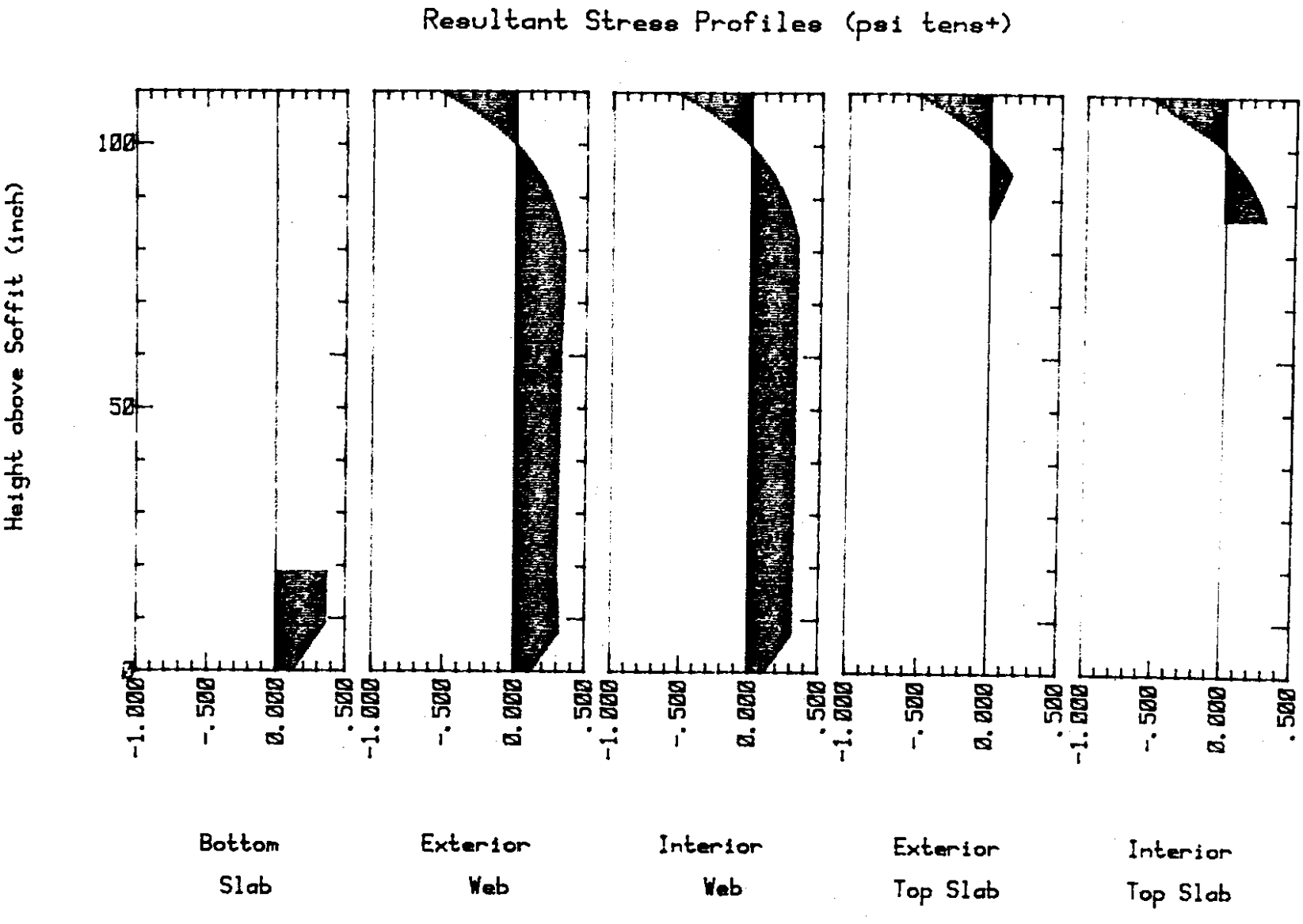

Figure 5.19. Thermal Stresses Predicted for Extreme Positive Differential Temperature Event by Priestley's Procedure, Resultant Stresses

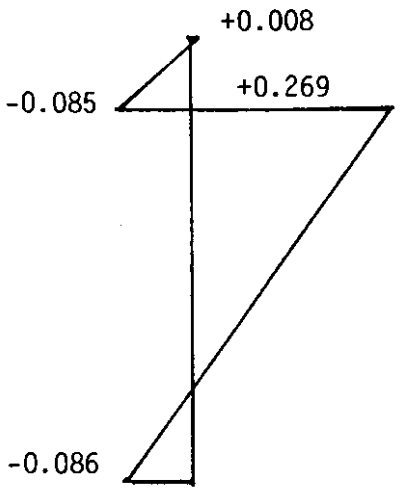

Figure 5.20. Thermal Stresses Predicted for Extreme Positive Differential Temperature Event by CTL Procedure, Eigenstress Only (psi tension +)

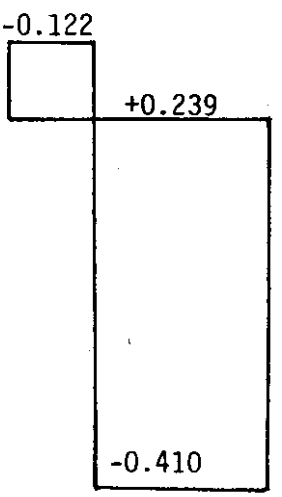

Figure 5.21. Thermal Stresses Predicted for Extreme Positive Differential Temperature Event by CTL Procedure, Resultant Stresses (psi tension +)

$\eta_f = 1$

6. RESEARCH METHODOLOGY

The original concept for the investigation envisaged sensors additional to those installed by CTL during the construction and the development of an intelligent, remote site automatic data collection and recording system. That system and the additional sensors failed to operate as planned for reasons discussed in this chapter. A block diagram with the various sensors originally planned for this study and the different components of the automatic recording system are shown in Figure 6.1.

6.1. Background

The Carlson gages installed by the CTL during construction were planned by WSDOT to provide specific information on the concrete stresses that developed during construction. The contract with CTL included only installation of the gages, assistance in data collection, and limited data analysis and interpretation. The investigators for this project did not become aware of the details of that instrumentation until after the CTL investigation was substantially complete. A proposal was made to WSDOT which included continued monitoring of these gages and subsequent analysis of the results in order to provide information on differential temperature effects. Later, it was decided to install other sensors and to automate the recording system in order to provide more continuous and comprehensive information. While that automated system and the additional sensors failed to operate as planned, the original objective of providing definitive information on differential temperature effects was still achieved using the Carlson gages installed by CTL.

The Carlson gage selected by CTL for this project was the Model A-10 strain gage. This gage consists essentially of a fine resistance wire so

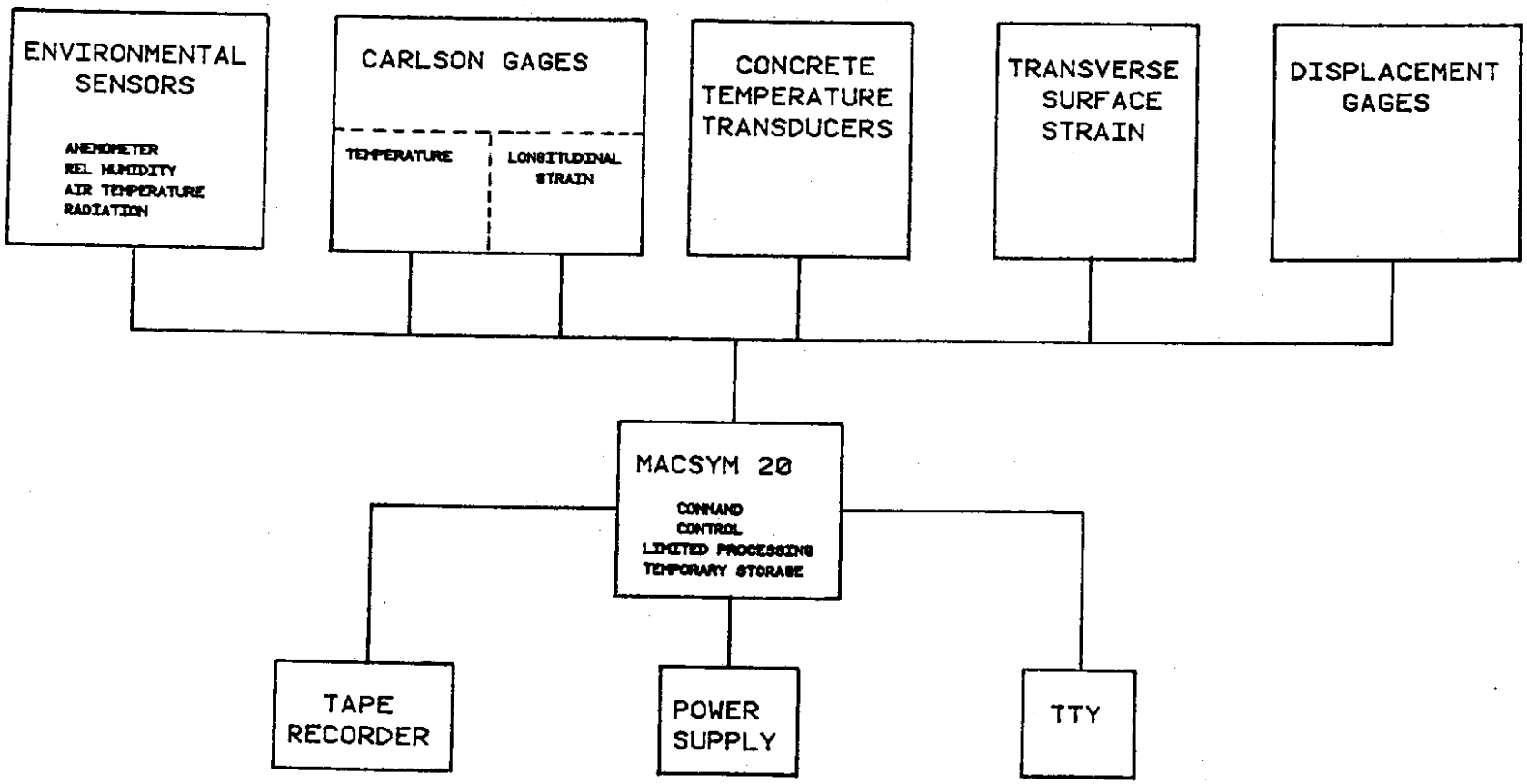

Figure 6.1. BLOCK DIAGRAM INSTRUMENTATION SYSTEM

fixed to the gage ends that, with change in the overall length of the gage, one-half of the wire lengthens and the other half shortens. A Carlson gage is shown in Figure 6.2. Four lead wires are run to each gage, one wire from each end of the gage wire, one lead wire from the center of the gage wire, and the fourth lead from one of the ends. Readings of the change in resistance in the gage wire and in the ratio between the resistance of the two halves of the gage wire are made by incorporating the gage wire as part of a Wheatstone bridge. When the two leads from opposite ends of the gage wire are used, the change in the total resistance of the gage is measured. This resistance change is used to compute the temperature of the gage wire. Connecting the three leads, including the center tap as two adjacent active arms of a Wheatstone bridge, measures the ratio of the resistance of the two halves, which is calibrated to strain. The two leads connected to the same end of the gage wire may be used to measure lead resistance if desired. The fixed gages, excitation source, and galvanometer, with an associated amplifier, are housed in a portable case. Knowledge of the temperature of the gage wire when a strain reading is made is necessary to correct for the difference in the coefficient of thermal expansion of the gage wire and the surrounding concrete. Self heating of the gage by the excitation current is avoided during manual readings by using a minimal excitation voltage (1 volt) and by using only momentary excitation to determine the value of the variable resistance necessary to null the bridge. The nulling technique makes knowledge of the actual excitation voltage unnecessary. Thus, to record both temperature and strains, two different Wheatstone bridge configurations are required. For temperature, two fixed resistors and one variable resistor are used with the gage and for strain, one variable and one fixed resistor, of approximately one-half the value of those used in the temperature bridge, are used with the two halves of the gage. The sensitivity of the Wheatstone bridge and the

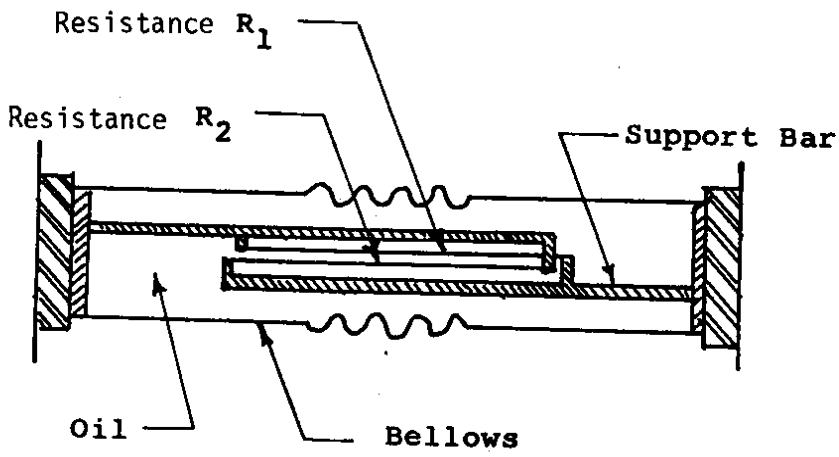

Figure 6.2.

Carlson Gage Schematic Diagram

manual readout system are such that differences in resistance of approximately 0.01 ohms can be measured. The temperature coefficient of resistance of the wire used in the gage is approximately 0.125 ohms per degree Fahrenheit. Thus, the least reading of the gage in the temperature configuration is equivalent to 0.04 degrees F, and the least reading in the strain configuration is equivalent to approximately 4 microstrain. That least reading of 4 microstrain is relatively large compared to the maximum reading obtained in the live load test, which was 28 microstrain.

6.2. Automation of Reading of Carlson Gages

In order to automate the reading of Carlson gages, it is necessary to replace the manual nulling procedure by a circuit that reads the voltage generated across the Wheatstone bridge by changes in the resistance of the Carlson gages. It is also necessary to insure that with the automated set-up, the changes in resistance due to other factors, such as lead wire resistance, and switching devices are smaller than the desired signal by at least one, and hopefully two, orders of magnitude. Temperature stability of the fixed resistors used in the bridge is also critical to the success of the automated procedure. When the unknown resistance in the Wheatstone bridge is computed from the signal appearing in the unbalanced condition, knowledge of the excitation voltage is also necessary. Noise in the excitation voltage is as much a signal as a change in the resistance. Thus, to automate the reading of the 40 Carlson gages in the Viaduct, a system of fixed resistors of high precision and relays of high resistance stability had to be devised and constructed. The specifications necessary in order for these components to satisfy the foregoing criteria made those components very expensive and necessitated a long lead time for acquisition. Decisions were required early in the project for ordering components and different decisions would have been

made later once the complete scope of the resistance, switching, and noise problems were identified. The circuit diagram developed for an automated Carlson gage switching network is shown in Figure 6.3.

6.3. Control

The data control and logging device chosen to operate the automatic recording system was a MACSYM 20 industrial process controller made by Analog Devices, Norwood, MA. This system is capable of multi-task analog to digital data conversion, signal amplification, limited data processing, and both digital and digital-to-analog control signalling. Data recording was to be done on a Quantex 1200 tape recorder. Data for one complete set of readings would be stored in the data buffers of the MACSYM 20 and output to the tape recorder at high speed. The choice of this system was based partially on compatibility with other available equipment and partially on successful use of a MACSYM 2 system on other Department of Civil Engineering, University of Washington, structural engineering research projects. As purchased, both the MACSYM 20 and the Quantex tape recorder required 120 volt AC power. The MACSYM 20 is designed to operate continuously over extended time periods and has the capability of having programs stored in EPROMS (electrically programmable read only memories) for unattended power-up starting.

Amplification of external analog signals prior to digital conversion was provided by the MACSYM 20 by a two-stage programmable gain amplifier system capable of a maximum gain of 2048, which gave a minimum resolution of approximately 2.4 microvolts. Theoretical strain resolution was thus approximately 0.4 microstrain for a bridge excitation voltage of 1 volt.

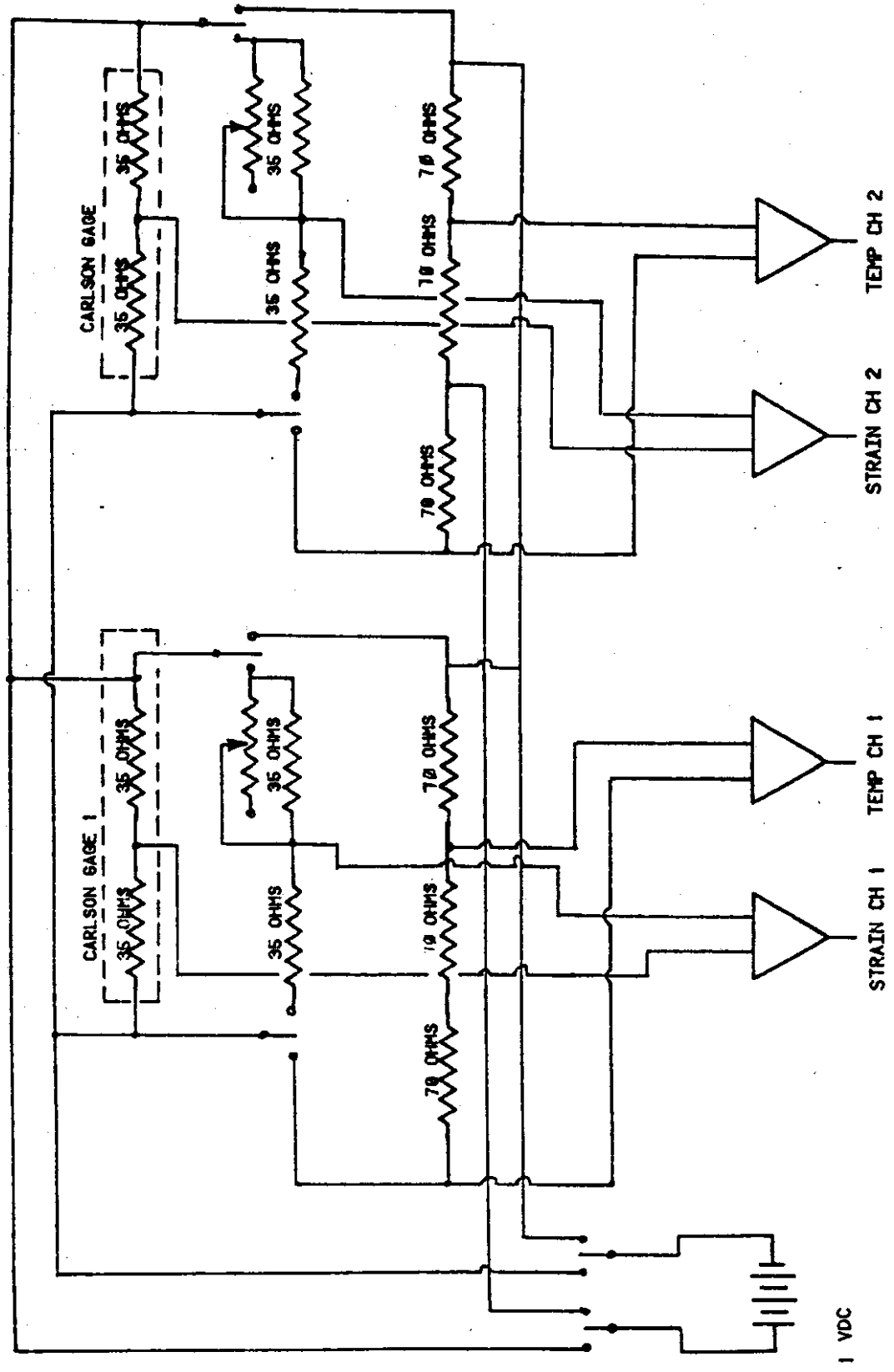

Figure 6.3. Proposed Automatic Switching Network for Carlson Gages

6.4. Operational Difficulties

During the early phases of the project, when the ordering of equipment and the development of switching devices was necessary, it was decided by WSDOT that AC power would not be available at the site during the time scheduled for data collection. Therefore, steps were made to convert the MACSYM 20 and Quantex tape recorder to operate on battery power. Marine storage batteries operating at 12 volts DC were chosen for the main power source. The batteries were to be charged by an AC powered battery charger driven by a gasoline-driven AC generator. Coversion of the MACSYM 20 to operate on DC required the installation of a DC to DC converter to supply the various voltages (+5 VDC, -5 VDC, +15 VDC, and -15 VDC) required by the computer. Excitation power for the Carlson gages and foil strain gages was supplied by rechargable Nicad batteries. This AC to DC conversion system was cumbersome and obviously not desirable in view of the resolution problems anticipated in the automated data collecting system.

Prior to installation of the data collection system in the bridge, AC power was installed, as well as telephone lines from Snoqualmie Pass, to Abutment No. 1. When difficulties were encountered with the resolution of the DC-powered data collection systems, an attempt was made to use that Abutment No. 1 source for powering the battery charger and the computer. However, the voltage drop over the distance from the abutment to the instrumented span was too great for successful operation of the charger or the computer. Further, during system checkout at the site, the gasoline-driven generator was stolen, indicating potential security problems for any important equipment left at the site.

While the automated data collection system was successfully completed and made operational, it was never able to obtain information with the required degree of resolution. Automatic data recording had to be abandoned due to

internal noise problems which completely swamped the Carlson gage signals. The minimum noise level which was achieved was approximately 2 to 10 millivolts of high frequency noise. The source of this noise centered on the DC to DC converter. However, there were also extraneous high frequency noises associated with bridge traffic and the power systems utilizing the bridge.

Another problem encountered during the site calibration phase was interconnection of the Carlson gage circuits through the inactive bridge, strain or temperature, such that a change of resistance on the active bridge affected all other circuits. This problem was overcome by the addition of blocking diodes in the circuits. However, even though this technique was successful in isolating the individual bridges from one another, it complicated the data reduction since the voltage drop through the diodes had to be measured and incorporated into the data reduction algorithm. This drop was slightly different for each diode but a constant once known. Rewiring the original switching circuit cards was required to add these isolation diodes. That rewiring was a relatively complicated task and detracted from the resolution of the individual card.

Data communication difficulties were experienced in interfacing the Quantex recorder with the MACSYM 20 and MACSYM 2 systems. These difficulties were overcome to the extent that the MACSYM 20 could write data to the recorder and information stored on the tapes could be read back through the MACSYM 20 to a teletype. The Quantex was not successfully interfaced with the MACSYM 2, which was the intended system for data reduction. The problem was believed to have been inherent in different "handshaking" routines employed by the two devices which were incompatible. Further software development would hae been necessary to overcome those "handshaking" difficulties.

The original plan called for supplementing the Carlson gages with foil strain gages mounted on the interior surfaces of the box girder and also on the deck. Holes were cored in the deck to carry the lead wires and to allow emplacement of integrated circuit temperature sensors at different depths in the deck slab. The foil gages on the deck and the holes in the deck were then sealed and protected with an epoxy patch immediately prior to the opening of the bridge to traffic in summer 1981. The epoxy patches failed over the first winter so that the foil gages were not operational during the main data collection period in August 1972. After the bridge was opened to traffic, a closure for sufficient time to replace damaged gages was impossible. The failure of the epoxy patches was aggravated by the extreme conditions on the deck where traffic included snowplows and vehicles with chains and studded tires. Failure of the epoxy seals at the top of holes allowed water to seep down into the deck and permanently damage the temperature sensors.

Problems were also experienced with the main power supply batteries. Six 12-volt batteries of 60 amp-hour (each) capacity were connected in parallel to provide power for approximately two weeks between charging. On one occasion during the system checkout, discharge of a single battery in the group rendered the total system inoperative. This same situation occurred again just prior to abandonment of the automated system. It was clear that this form of power supply would not have been sufficiently reliable for extended unattended operation.

6.5. Concluding Remarks

The instrumentation system for this project was originally conceived to be an "off-the-shelf, plug-in" system. However, that system consumed over 25 per cent of the project budget for materials, all the project budget for equipment, more than 50 per cent of the personnel time and 18 months of the

scheduled time for the project prior to its abandonment. In all, more than $50,000 of direct expenses (60% of the total direct expenses) was consumed in attempting to make the automated system operational. These concluding remarks are intended to provide guidance to others attempting automated measurement of strains on full-scale field projects.

(1) There is no substitute for thorough, detailed planning in the proposal stage. An early and conservative assessment of the difficulties of the proposed measurements with respect to the state-of-the-art of instrumentation capabilities is desirable. That assessment should start wiht a clear definition of the quantities that are expected for those measurements, and the resolution necessary for those measurements to be successful. It should take into account long-term difficulties in the stability of gages, in the attachment and waterproofing of those gages, and in the stability of the recording system.

(2) Project budget development should be very conservative where prior experience with application of a specific instrumentation system as a complete package is not available. In such cases, a two-phase budget program is strongly recommended where the first phase of the investigation is funded for detailed design and development of the instrumentation system prior to commitment to the project for which that system is intended. Since much state-of-the-art equipment requires considerable lead time for purchase, a rush to make selection of the equipment is undesirable since detailed evaluation during the waiting period will often suggest that inappropriate equipment has been ordered in the original rush.

(3) Instrumentation and data collection, recording, and processing equipment to be used in remote locations should be well-proven, commercially

available equipment. Compatibility of the various pieces of equipment, and particularly of any necessary power supplies, must be assured. Careful assessment should also be made of security requirements for remote location equipment and adequately controlled.

(4) Sensors which have critical signal to noise requirements, such as the Carlson gages, should be provided with separate signal conditioning on each channel. Preliminary investigations were made on this project for such a system which would have provided filtering and preamplification on each channel. However, the need for these investigations was not identified until the research project was well underway and all equipment ordered. The costs of filtering and preamplification were beyond the project budget and time did not permit further study of that approach. Two stage budgeting would probably have resulted in this difficulty being anticipated and the cost of the separate signal conditioning identified in the first stage.

(5) Review of project proposals by sponsoring agencies should include detailed review of any proposed instrumentation by agency personnel with the necessary requisite experience to identify any potential difficulties.

(6) The most effective instrumentation projects are likely to be projects developed in conjunction with the design and construction of new facilities. Sensor locations can be optimized and adequate protection provided to gages. Further, coordination between the designer and the researchers at that stage would lead to a better understanding of the questions which the designers need to have answered, the instrumentation required to collect the necessary data, and the capabilities required for the researchers in order to analyze that data and provide answers to the designers' questions. During

construction, there should be adequate time available for acquisition and laboratory verification of the stability and resolution of the instrumentation. Such instrumentation would seem highly desirable for any large scale facility incorporating new construction methods or subjected to imprecisely defined loading conditions.

REFERENCES

1.1. AASHTO, Standard Specifications for Highway Bridges, 12th Ed., American Association of State Highway and Transportation Officials, Washington, D.C., 1977.

1.2. Shiu, K.N., J.D. Aristizabal-Ochoa and H.G. Russell, "Instrumentation of Denny Creek Bridge," Construction Technology Laboratories of the Portland Cement Association, Skokie, IL, August 1981.

1.3. ACI-ASCE, "Analysis and Design of Reinforced Concrete Bridge Structures," ACI-ASCE Joint Committee 343 Report, Manual of Standard Practice, Part 4 - 1981, American Concrete Institute, Detroit, MI, 1981.

1.4. Hambly, E.C., "Temperature Distributions and Stresses in Concrete Bridges, The Structural Engineer, Vol. 56A, No. 5, May 1978, pp. 143-148.

1.5. Leonhardt, F., G. Kolbe and J. Peter, "Temperature unterschiede gefahren Spannbetonbrucke (temperature differences endanger prestressed concrete bridges)," Beton und Stahlbetonbau, Vol. 60, No. 7, July 1965, pp. 231-244.

1.6. Priestley, M.J.N., "Design of Concrete Bridges for Temperature Gradients," Journal of the American Concrete Institute, Proceedings, Vol. 75, No. 5, May 1978, pp. 209-217.

1.7. Radoli, M. and R. Green, "Thermal Stresses in Concrete Bridge Superstructure under Summer Conditions," Transportation Research Record, No. 547, 1975, pp. 23-36.

1.8. Reynolds, J.C. and J.H. Emanuel, "Thermal Stresses and Movements in Bridges," Journal of the Structural Division, American Society of Civil Engineers, Vol. 100, No. ST1, January 1974, pp. 63-78.

2.1. Ross, A.D., "Creep of Concrete under Variable Stress," Journal of the American Concrete Institute, Proceedings, Vol. 29, No. 9, March 1958.

2.2. Mattock, A.H. and P. Kaar, "Prestressed Concrete Bridges, Part 5, Creep and Shrinkage Studies," Journal of the Research and Development Division, Portland Cement Association, Skokie, IL, May 1961.

2.3. Branson, D.E., Deformation of Concrete Structures, McGraw-Hill, New York, 1977.

2.4. Tadros, M.K., A. Ghali and W. Dilger, "Time Dependent Analysis of Composite Frames," Journal of the Structural Division, American Society of Civil Engineers, Vol. 103, ST4, April 1977, pp. 871-884.

2.5. Tadros, M.K., A. Ghali and W. Dilger, "Segmental Erection of Concrete Bridges," Prestressed Concrete Institute Journal, Vol. 24, No. 4, July-August 1979.

2.6. CEB-FIP, "International Recommendations for the Calculations and Execution of Concrete Structures," Comite Europeen du Beton - Federation Internationale de la Precontrainte, Prague, June 1970.

2.7. CEB-FIP, "International Recommendations for the Calculations and Execution of Concrete Structures," Comite Europeen du Beton - Federation Internationale de la Precontrainte, Prague, 1978.

2.8. Chiorino, M.A., P. Napoli, F. Mola and M. Koprna, "CEB Design Manual, Structural Effects of Time-Dependent Behavior of Concrete," Bulletin d'Information No. 136, Comite Euro-International du Beton, Budapest, June 1980.

2.9. Kristek, V., Theory of Box Girders, John Wiley and Sons, New York, 1979.

2.10. Maisel, B.I., R.E. Rowe and R.A. Swann, "Concrete Box-Girder Bridges," The Structural Engineer, London, Vol. 51, No. 18, October 1973.

2.11. Hambly, E.C., Bridge Deck Behavior, John Wiley and Sons, New York, 1976.

2.12. Meyer, C. and A.C. Scordelis, "Computer Program for Non-Prismatic Plates with Plate and Beam Elements," Report No. SESM 71-23, University of California, Berkeley, CA, 1971.

2.13. Corley, W.G., J.C. Carpenter et al., "Design Ultimate Load Test of 1/10 Scale Micro-Concrete Model of the New Potomac River Crossing, I-266," Journal of the Prestressed Concrete Institute, Vol. 16, No. 6, November-December 1971, pp. 70-84.

2.14. Pucher, A., "Einfluss Flache fur Elastischen Platte (Influence Surfaces for Elastic Plates)," Springer-Verlag, Berlin, 1964.

2.15. Homberg, H. and W. Ropers, "Fahrbahnplatten mit verandlicher Dicke (Roadway Slabs with Variable Thicknesses), Springer-Verlag, Berlin, 1965.

2.16. Hildebrand, F.B., Advanced Calculus for Applications, 2nd Ed., Prentice-Hall, Englewood Ciffs, NJ, 1976, pp. 48-50.

2.17. Schlaich, J. and H. Scheef, "Concrete Box Girder Bridges," Structural Engineering Documents 1e, International Association for Bridge and Structural Engineers, Zurich, 1982.

2.18. Guyon, Y., Prestressed Concrete, Vol. II, John Wiley and Sons, New York, 1960, Chapter 34.

2.19. Kawai, T. and B. Thurlimann, "Influence Surfaces for Moments in Slabs Continuous over Flexible Cross-Beams," Proceedings, International Association for Bridge and Structural Engineers, Vol. 17, Zurich, 1957.

2.20. Bahkt, B., "Simplified Anaysis of Edge Stiffened Cantilever Slabs," Journal of the Structural Division, American Society of Civil Engineers, Vol. 107, ST3, March 1981.

2.21. Menn, C., "Brueckenbau I (Bridge Construction I)," Lecture Manuscript, ETH, Zurich, 1979.

2.22. Emerson, M., "The Calculation of the Distribution of Temperature in Bridges," Department of the Environment, Transportation Road Research Laboratory, Letter Report 561, Crowthorne, 1973.

2.23. Emerson, M., "Temperature Differences in Bridges: Basis of Design Requirements," Department of the Environment, Transportation Road Research Laboratory, Letter Report 765, Crowthorne, 1976.

2.24. Emerson, M., "Bridge Temperature Estimated from Shade Temperatures," Department of the Environment, Transportation Road Research Laboratory, Letter Report 696, Crowthorne, 1976.

2.25. Emerson, M., "Prediction of Bridge Temperatures in the Arabian Gulf, Theoretical Predictions," Transportation Road Research Laboratory, Supplementary Report No. 495, Crowthorne, 1979.

2.26. Jones, M.R., "Bridge Temperatures Calculated by a Computer Program," Department of the Environment, Transportation Road Research Laboratory, Letter Report 765, Crowthorne, 1976.

2.27. Priestley, M.J.N., "Temperature Gradients in Bridges--Some Design Considerations," New Zealand Engineering, Vol. 27, Part 7, July 1972, pp. 228-233.

2.28. Built, J.W., A.W. Smith and P.B. McKinnel, "The Newmarket Viaduct," New Zealand Engineering, December 1965, pp. 493-511.

2.29. White, I.G., "Non-Linear Differential Temperature Distributions in Concrete Bridge Structures: A Review of the Current Literature," Cement and Concrete Association Technical Report 525, London, May 1979.

2.30. Richmond, B., "The Creep-Temperature Mechanism in Concrete Bridges," Department of the Environment, Transportation Road Research Laboratory, Supplementary Report 442, Crowthorne, 1979.

2.31. Aguado, A., A. Mari and E. Penon, "Non-Linear Analysis for Thermal Effects and Support Displacement on Frame Concrete Structures," Comite Europeen du Beton - Feeration International de la Precontrainte, Pavia, October 1981.

2.32. Aparicio, A.C. and J.J. Arenas, "The Behavior of Continuous Reinforced and Prestressed Beams Subjected to a Thermal Gradient under Loads Increasing up to Failure," Comite Europeen du Beton - Federation Internationale de la Precontrainte, Pavia, October 1981.

2.33. Emerson, M., "The Influence of the Environment on Concrete Bridge Temperatures," Comite Europeen du Beton - Federation Internationale de la Precontrainte, Pavia, October 1981.

2.34. Zichner, T., "Thermal Effects on Concrete Bridges," Comite Europeen du Beton - Federation Internationale de la Precontrainte, Pavia, October 1981.

3.1. Leonhardt, F., Prestressed Concrete, Design and Construction, Wilhelm Ernst und Sohn, Berlin 1974, pp. 438-442.

5.1. NOAA, "Local Climtalogical Data, Stampede Pass, Washington, 1957 through August 1982," National Oceanic and Atmospheric Administration, Nashville, TN.

5.2. Carslaw, H.C. and J.C. Jaeger, Conduction of Heat in Solids, 2nd Ed., Oxford University Press, Amen House, London, 1959.

5.3. Sucec, J., Heat Transfer, Simon and Schuster, New York, 1975.

5.4. Holman, J.P., Heat Transfer, 4th Ed., McGraw-Hill Book Company, New York, 1976.

5.5. ASHRAE, "Guide and Data Book," American Society of Heating, Refrigerating and Air-conditioning Engineers, New York, 1963.

5.6. Raphael, J.M., "Prediction of Temperature in Rivers and Reservoirs," Journal of the Power Division, American Society of Civil Engineers, Vol. 88, 2 July 1962, pp. 157-181.

5.7. Duffie, J.A. and W.A. Beckman, Solar Engineering of Thermal Processes, John Wiley and Sons, New York, 1980.

5.8. Gerald, C.F., Applied Numerical Analysis, 2nd Ed., Addison-Wesley Publishing Company, Reading, MA, 1980.

5.9. Neville, A.M., Properties of Concrete, Pitman Publishing Company, New York, 1972.

5.10. Brewer, H.W., "General Relation of Heat Flow Factors to the Unit Weight of Concrete," Journal of the Portland Cement Association, Research and Development Department, Vol. 9, No. 1, January 1967, pp. 48-60.

5.11. Campbell-Allen, D. and C.P. Thorne, "The Thermal Conductivity of Concrete," Magazine of Concrete Research, Vol. 15, No. 43, March 1963, pp. 39-48.

5.12. Whiting, D., A. Litvin and S.E. Goodwin, "Specific Heat of Selected Concretes," Journal of the American Concrete Institute, July 1978, Paper No. 75-32.

5.13. Lentz, A.E. and G.E. Monfore, "Thermal Conductivities of Portland Cement Paste, Aggregate and Concrete Down to Very Low Temperatures," Journal of the Portland Cement Association, Research and Development Department, Vol. 8, No. 3, September 1966, pp. 27-33.

5.14. Mitchell, L.J., "Thermal Properties: Significance of Tests and Properties of Concrete and Concrete Making Minerals," American Society for Testing and Materials, STP 169A, 1966.

5.15. Rhodes, J.A., "Thermal Properties: Significance of Tests and Properties of Concrete and Concrete Making Materials," American Society for Testing and Materials, STP 169B, 1978.

APPENDIX A.

DETAILED CONSTRUCTION CHRONOLOGY

The following detailed construction chronology was taken from the WSDOT resident engineer's records for Contract 0200. The chronology starts with the casting of Stage I, Span 4. This was the instrumented section of the bridge. The chronology extends to the point where all direct loads have been applied to Span 4. Loads which are remote enough to be insignificant in the magnitude of their effect on the instrumented section are not included. In cases where the dates are not available from the record, the probable date has been estimated by consideration of the construction steps necessary. Dates for application of Stage I loads have been taken as the date of application of the post-tensioning to Stage I. Reading numbers from the CTL chronology (Table 1 of their report) have been indicated for comparison purposes in column 3 of this chronology.

Loading Description	Date	Day	System**	Remarks
	05/16/78	0-(1)*	7	Reference date
PT I Span 4	05/19/78	3-(2)	8	
DL I Span 4	05/19/78	3	8	Loading
-875k @ 4.17	05/23/78	7	9	
250k @ 5.17	05/24/78	8-(3)	9	
Move Stg II forms 3>4	05/26/78	10	9	Date estimated
	05/30/78	14-(4)		
DL II Span 4	05/31/78	15	9	
DL IIIB Span 1	06/01/78	16-(5)	9	
PT II Span 4	06/05/78	20-(6),(7)	10	
Move Stg III forms 1B>2A	06/06/78	21-(8)	10	Date estimated
625k @ 5.17	06/08/78	23	10	
DL IIIA Span 2	06/09/78	24-(9)	10	
DL I Span 5	06/14/78	29	11	
PT I Span 5	06/14/78	29-(10)	11	
Move Stg III forms 2A>2B	06/15/78	30	11	Date estimated
-875k @ 5.17	06/15/78	30	11	
Move Stg II forms 4>5	06/16/78	31	11	Date estimated
250k @ 6.17	06/16/78	31	11	
	06/19/78	34-(11)		
DL II Span 5	06/22/78	37-(12),(13)	11	
DL IIIB Span 2	06/23/78	38	11	
PT II Span 5	06/26/78	41-(14)	12	

*sequential structural system applicable
**CTL reading number (event)

Move Stg III forms 2B>3A	06/27/78	42-(15)	12	Date estimated
625k @ 6.17	06/30/78	45	12	
DL IIIA Span 3	07/05/78	50-(16)	12	
	07/06/78	51-(17)		
DL Span 6	07/07/78	52	13	
PT I Span 6	07/07/78	52	13	
-875k @ 6/17	07/10/78	55	13	
Move Stg II forms 5>6	07/11/78	56	13	Date estimated
250k @ 7.17	07/12/78	57	13	
Move Stg III forms 3A>3B	07/13/78	58	13	Date estimated
DL II Span 6	07/18/78	63	13	
DL IIIB Span 3	07/19/78	64-(18)	13	
	07/20/78	65-(19)		
PT II Span 6	07/21/78	66	14	
PT III Span 3	07/24/78	69	15	
Move Stg III forms 3B>4A	07/28/78	73	15	Date estimated
625k @ 7.17	08/04/78	80	15	
DL IIIA Span 4	08/07/78	83-(20)	15	
	08/08/78	84-(21)		
	08/10/78	86-(22)		
Move Stg II forms 4A>4B	08/14/78	90	16	Date estimated
DL IIIB Span 4	08/18/78	94-(23)	16	
	08/19/78	95-(24)		
Barrier Span 1	08/21/78	97-(25)	16	Begin
PT III Span 4	08/22/78	98	17	
	08/24/78	100-(26)		
DL I Span 7	09/06/78	113	17	Cast 8/10/78
PT I Span 7	09/06/78	113	17	Applied 8/10/78

-875k @ 7.17	09/06/78	113	17	
250k @ 8.17	09/07/78	114	17	
Move Stg II forms 6>7	09/08/78	115	17	Date estimated
Move Stg III forms 4B>5A	09/12/78	119	17	Date estimated
DL II Span 7	09/14/78	121	17	
Barrier Span 1	09/15/78	122	17	End
Pt II Span 7	09/18/78	125-(27)	18	
DL IIIA Span 5	09/19/78	126	18	
Barrier Span 2	09/19/78	126	18	Begin
	09/20/78	127-(28)		
625k @ 8.17	09/22/78	129	18	
Move Stg II forms 5A>5B	09/27/78	134	19	Date estimated
-875k @ 8.17	09/28/78	135	20	
DL I Span 8	09/28/78	135	20	
PT I Span 8	09/28/78	135	20	
Move Stg II forms 7>8	09/29/78	136	20	Date estimated
DL IIIB Span 5	10/03/78	140-(29)	20	Partial load
250k @ 9.17	10/03/78	140	20	
Barrier Span 2	10/05/78	142	20	End
DL II Span 8	10/06/78	143	20	
DL IIIB Span 5	10/09/78	146	21	Remainder of load
PT II Span 8	10/09/78	146	21	
Barrier Span 3	10/10/78	147	21	Begin
625k @ 9.17	10/13/78	150-(30)	22	
PT III Span 5	10/16/78	153	22	
PT I Span 9	10/17/78	154	22	
DL I Span 9	10/17/78	154	22	
Move Stg III forms 5B>6A	10/18/78	155	22	Date estimated

-875k @ 9.17	10/19/78	156	22	
250k @ 10.17	10/20/78	157	22	
Barrier Span 3	10/20/78	157	22	End
DL IIIA Span 6	10/23/78	160	22	
Barrier Span 4	10/25/78	162	22	Begin first half
DL II Span 9	10/26/78	163	23	
PT II Span 9	10/30/78	167	24	
Move Stg III form 6A>6B	11/02/78	170	24	Date estimated
Barrier Span 4	11/02/78	170	24	End first half
625k 10.17	11/03/78	171	25	
DL I Span 10	11/08/78	176	25	
DL IIIB Span 6	11/08/78	179	25	
PT III Span 7	11/13/78	181	26	
-875k @ 10/17	11/22/78	190	26	
250k @ 11.17	11/29/78	197	26	
Move Stg II forms 9>10	12/01/78	199	26	Date estimated
DL II Span 10	12/06/78	204	26	
PT II Span 10	12/11/78	209	27	
	12/14/78	211-(31)		
	04/26/79	345-(32)		
625k @ 11.17	05/11/79	360	27	
Barrier Span 4	06/27/79	407	30	Begin second half
Barrier Span 4	07/06/79	416	30	End second half
Barrier Span 5	07/06/79	416	30	Begin
Barrier Span 5	07/18/79	428	30	End
Barrier Span 6	07/18/79	428	30	Begin
	07/26/79	436-(33)		
Barrier Span 6	07/27/79	437	30	End

Barrier Span 7	07/30/79	440	30	Begin
Barrier Span 7	08/08/79	449	30	End
	10/18/79	520- (34)		
	01/22/80	616- (35)		
	04/23/80	708- (36)		
Overlay	07/15/80	791	30	Date estimated
	07/30/80	806- (37)		

APPENDIX B

STRAIN HISTORIES

List of Tables

List of Figures

APPENDIX B.

STRAIN HISTORIES

Carlson gage strain readings taken under this study have been used to extend the strain history plots presented in the CTL report. No changes have been made to the differential temperature corrections applied by CTL to their raw data. The strains taken in this study, and near the end of the plots, include readings taken both in the morning, when temperatures were relatively uniform throughout the section, a condition which corresponds to the conditions for the CTL data, and readings taken late in the evening, when temperatures were non-uniform on some days. The corrections for differential temperature after the casting of a new stage are given in Appendix D of the CTL report. Those data are included herein as Table B2. Those tables were derived by subtracting data given in a preliminary copy of the CTL report from the values shown in Tables A1, A3 and A5 of the final CTL report. Figures B1, B2 and B3 show correction stresses (eigenstresses only) calculated using Mattock's procedure for data tabulated in Table B3. Figures B4, B5 and B6 are plots of the corresponding stresses taken from the CTL report and Table 2. Those figures show the magnitude of the stress corrections applied for differential temperature at the time of casting a new stage. Strain corrections given in CTL Tables D4, D5 and D6 were derived from those stresses by dividing by the appropriate moduli of elasticity (4163 ksi for Stage I, 4800 ksi for Stage II and 4645 ksi for Stage III). It should be noted that the sign convention for the data derived in this study differs from that for the data derived in the CTL study.

Table B 1

Measured Strains for Section A
CTL data corrected for differential temperature at casting succeeding stage

No	Microstrain													
	1	2	3	4	5	6	7	8	9	10	11	12	13	14
1	+47	+23	+25	+23	+33	+18	+33	+0	+0	+0	+0	+0	+0	+0
2	+457	+332	+58	+35	+154	+238	+346	+0	+0	+0	+0	+0	+0	+0
3	+509	+384	+25	+33	+142	+273	+383	+0	+0	+0	+0	+0	+0	+0
4	+533	+389	+36	+49	+141	+286	+397	+0	+0	+0	+0	+0	+0	+0
5	+383	+316	+320	+36	+515	+220	+359	-116	-109	-54	+0	+0	+0	+0
6	+434	+418	+404	+105	+516	+242	+238	-69	-44	-33	+0	+0	+0	+0
7	+552	+520	+468	+86	+655	+349	+363	+3	+37	+74	+0	+0	+0	+0
8	+499	+485	+506	+139	+672	+350	+363	+18	+47	+61	+0	+0	+0	+0
9	+558	+481	+513	+233	+649	+336	+355	+41	+2	+66	+0	+0	+0	+0
10	+535	+548	+551	+217	+641	+351	+338	+41	+19	+66	+0	+0	+0	+0
11	+569	+507	+521	+198	+696	+337	+381	+74	+78	+78	+0	+0	+0	+0
12	+604	+583	+586	+237	+742	+410	+453	+139	+87	+148	+0	+0	+0	+0
13	+585	+570	+583	+235	+769	+399	+406	+89	+58	+126	+0	+0	+0	+0
14	+581	+629	+602	+271	+747	+399	+410	+89	+100	+130	+0	+0	+0	+0
15	+608	+596	+659	+250	+820	+412	+407	+99	+126	+129	+0	+0	+0	+0
16	+613	+599	+598	+277	+747	+425	+436	+120	+99	+149	+0	+0	+0	+0
17	+612	+608	+566	+258	+738	+403	+437	+113	+108	+143	+0	+0	+0	+0
18	+631	+615	+597	+261	+757	+436	+463	+152	+132	+185	+0	+0	+0	+0
19	+672	+613	+580	+238	+743	+415	+451	+127	+101	+158	+0	+0	+0	+0
20	+645	+662	+695	+282	+815	+419	+450	+133	+127	+158	+0	+0	+0	+0
21	+630	+663	+819	+287	+959	+424	+429	+96	+109	+119	+0	+0	+0	+0
22	+628	+663	+815	+296	+949	+513	+512	+185	+193	+203	+0	+0	+0	+0
23	+618	+653	+805	+314	+950	+421	+426	+104	+106	+126	+0	+0	+0	+0
24	+628	+653	+863	+324	+1020	+421	+433	+84	+92	+109	-76	-163	-135	-143
25	+644	+677	+895	+328	+1045	+434	+462	+106	+121	+145	-51	-159	-76	-82
26	+665	+706	+885	+345	+1040	+455	+457	+133	+142	+154	-37	-133	-85	-56
27	+656	+707	+880	+350	+1026	+452	+453	+134	+140	+156	-42	-147	-96	-72
28	+649	+701	+932	+357	+1087	+451	+443	+112	+125	+136	-26	-154	-101	-64
29	+654	+717	+945	+369	+1088	+462	+451	+112	+123	+135	-54	-154	-102	-96
30	+662	+721	+1195	+387	+1056	+463	+456	+119	+120	+139	-68	-155	-107	-103
31	+620	+680	+954	+365	+1106	+449	+435	+85	+93	+108	-84	-162	-117	-74
32	+631	+701	+992	+343	+1137	+446	+427	+63	+140	+137	-60	-185	-96	-69
33	+737	+856	+1168	+512	+1303	+552	+531	+176	+235	+229	+31	-87	-32	-4
34	+756	+854	+1134	+472	+1204	+501	+541	+150	+198	+192	-19	-80	-54	-22
35	+722	+867	+1208	+473	+1345	+523	+507	+133	+181	+195	+58	+13	-64	-32
36	+723	+827	+1165	+442	+1282	+417	+535	+0	+256	+218	+38	+8	-3	+7
37	+806	+1099	+1129	+540	+1288	+574	+556	+0	+261	+249	+125	+38	-1	+57

Table B 1 (cont.)

Measured Strains for Section A
UW data uncorrected for differential temperature at casting succeeding stage

	Microstrain													
No	1	2	3	4	5	6	7	8	9	10	11	12	13	14
38	+817	+1067	+1241	+553	+1362	+615	+577	+0	+241	+239	-204	-77	+4	-85
39	+718	+0	+1128	+456	+1279	+511	+490	+0	+189	+180	-276	-146	-92	-174
40	+745	+846	+1172	+455	+1334	+0	+484	+0	+271	+229	-249	-111	-62	-122
41	+716	+839	+1196	+445	+1326	+0	+483	+0	+251	+217	-254	-107	-61	-118
42	+742	+873	+1154	+503	+1288	+0	+508	+0	+191	+188	-288	-146	-90	-176
43	+736	+867	+1157	+496	+1298	+0	+503	+0	+201	+189	-273	-140	-89	-160
44	+708	+855	+1163	+468	+1316	+0	+477	+0	+269	+233	-218	-105	-57	-118
45	+736	+856	+1169	+482	+1323	+0	+504	+0	+217	+188	-240	-120	-73	-143
46	+737	+849	+1170	+471	+1328	+0	+501	+0	+211	+184	-243	-118	-55	-132
47	+734	+848	+1164	+473	+1325	+0	+504	+0	+204	+183	-257	-125	-75	-153
48	+708	+837	+1166	+449	+1327	+0	+478	+0	+271	+226	-204	-89	-46	-102
49	+737	+845	+1161	+467	+1320	+0	+503	+0	+211	+186	-258	-124	-77	-148
50	+714	+833	+1160	+450	+1322	+0	+482	+0	+266	+222	-213	-94	-53	-116
51	+745	+844	+1153	+478	+1305	+0	+510	+0	+201	+183	-281	-126	-78	-165
52	+723	+833	+1144	+468	+1292	+0	+498	+0	+222	+199	-274	-125	-72	-164
53	+744	+857	+1152	+489	+1292	+0	+509	+0	+196	+188	-295	-141	-88	-176
54	+714	+847	+1158	+463	+1308	+0	+484	+0	+270	+238	-234	-96	-50	-116
55	+745	+855	+1156	+485	+1299	+0	+509	+0	+206	+189	-284	-135	-84	-160
56	+714	+844	+1164	+458	+1318	+0	+477	+0	+268	+233	-221	-97	-52	-106
57	+737	+854	+1165	+470	+1319	+0	+504	+0	+210	+185	-268	-131	-83	-151
58	+709	+850	+1178	+441	+1341	+0	+474	+0	+278	+235	-186	-86	-43	-88
59	+737	+852	+1162	+461	+1328	+0	+505	+0	+206	+175	-260	-126	-80	-150
60	+712	+848	+1176	+436	+1343	+0	+479	+0	+271	+228	-203	-88	-48	-89
61	+741	+853	+1154	+457	+1334	+0	+505	+0	+201	+179	-261	-125	-80	-148
62	+712	+853	+1185	+408	+1357	+0	+478	+0	+278	+229	-175	-81	-40	-86
63	+738	+853	+1170	+449	+1341	+0	+501	+0	+211	+183	-262	-123	-77	-143
64	+713	+848	+1177	+424	+1356	+0	+477	+0	+273	+227	-190	-86	-41	-84
65	+748	+844	+1158	+458	+1325	+0	+506	+0	+196	+176	-267	-122	-81	-155
66	+723	+834	+1156	+443	+1321	+0	+484	+0	+251	+218	-233	-96	-58	-145
67	+743	+849	+1146	+464	+1307	+0	+506	+0	+197	+182	-290	-134	-86	-174
68	+745	+855	+1148	+475	+1297	+0	+509	+0	+198	+187	-289	-138	-86	-169
69	+746	+860	+1149	+486	+1294	+0	+511	+0	+198	+185	-292	-143	-91	-172
70	+745	+862	+1150	+498	+1283	+0	+509	+0	+202	+193	-287	-141	-85	-168
71	+744	+873	+1159	+501	+1300	+0	+509	+0	+204	+191	-277	-142	-85	-160
72	+746	+870	+1166	+502	+1307	+0	+507	+0	+210	+188	-261	-129	-78	-148
73	+757	+872	+1183	+510	+1328	+0	+525	+0	+243	+207	-234	-91	-53	-123
74	+713	+847	+1170	+466	+1325	+0	+480	+0	+276	+233	-196	-86	-41	-112

Table B 1 (cont)

Measured Strains for Section A
UW data uncorrected for differential temperature at casting succeeding stage

	Microstrain													
No	1	2	3	4	5	6	7	8	9	10	11	12	13	14
75	+759	+862	+1172	+491	+1315	+0	+511	+0	+215	+189	-266	-119	-74	-151
76	+715	+853	+1178	+460	+1333	+0	+481	+0	+266	+230	-218	-89	-49	-104
77	+746	+863	+1180	+472	+1343	+0	+510	+0	+205	+181	-249	-121	-72	-137
78	+714	+861	+1190	+439	+1358	+0	+480	+0	+271	+229	-195	-87	-44	-85
79	+746	+857	+1178	+461	+1342	+0	+505	+0	+210	+181	-241	-113	-71	-134
80	+747	+861	+1169	+469	+1329	+0	+507	+0	+202	+182	-265	-125	-82	-149
81	+751	+874	+1166	+491	+1311	+0	+513	+0	+197	+188	-287	-134	-83	-166
82	+746	+871	+1162	+493	+1304	+0	+507	+0	+205	+190	-279	-137	-85	-161
83	+778	+904	+1193	+525	+1325	+0	+529	+0	+228	+209	-250	-111	-65	-136
84	+744	+876	+1170	+499	+1306	+0	+510	+0	+210	+191	-263	-129	-80	-149
85	+737	+873	+1171	+496	+1310	+0	+504	+0	+216	+193	-250	-126	-75	-139
86	+744	+871	+1170	+506	+1304	+0	+510	+0	+213	+191	-265	-126	-81	-152
87	+744	+871	+1170	+506	+1304	+0	+510	+0	+213	+191	-265	-126	-81	-152
88	+744	+871	+1170	+506	+1304	+0	+510	+0	+213	+191	-265	-126	-81	-152
89	+744	+871	+1170	+506	+1304	+0	+510	+0	+213	+191	-265	-126	-81	-152

Table B 1 (cont.)

Measured Strains for Section B
CTL data corrected for differential temperature at casting succeeding stage

No	Microstrain													
	1	2	3	4	5	6	7	8	9	10	11	12	13	14
1	-5	+35	+24	+45	+24	+0	+32	+0	+0	+0	+0	+0	+0	+0
2	+99	+192	+198	+173	+223	+127	+200	+0	+0	+0	+0	+0	+0	+0
3	+114	+247	+211	+187	+213	+130	+278	+0	+0	+0	+0	+0	+0	+0
4	+96	+288	+227	+172	+224	+162	+276	+0	+0	+0	+0	+0	+0	+0
5	+117	+285	+202	+172	+229	+141	+303	-52	-39	-11	+0	+0	+0	+0
6	+232	+302	+222	+204	+280	+194	+344	-114	-84	+35	+0	+0	+0	+0
7	+278	+408	+297	+252	+387	+260	+405	-17	-18	+91	+0	+0	+0	+0
8	+318	+0	+338	+250	+406	+346	+427	-7	-10	+72	+0	+0	+0	+0
9	+254	+352	+394	+316	+407	+302	+416	-31	-50	+35	+0	+0	+0	+0
10	+319	+408	+405	+310	+397	+279	+379	-24	+0	+84	+0	+0	+0	+0
11	+308	+418	+381	+296	+368	+275	+411	+6	+15	+97	+0	+0	+0	+0
12	+314	+453	+397	+339	+431	+357	+490	+31	+41	+142	+0	+0	+0	+0
13	+345	+438	+431	+352	+448	+344	+449	+20	+63	+132	+0	+0	+0	+0
14	+314	+425	+437	+351	+472	+346	+434	+15	+56	+150	+0	+0	+0	+0
15	+330	+447	+453	+366	+469	+336	+464	+25	+100	+155	+0	+0	+0	+0
16	+358	+443	+463	+360	+484	+365	+469	+191	+48	+159	+0	+0	+0	+0
17	+322	+436	+446	+357	+495	+368	+486	+37	+63	+151	+0	+0	+0	+0
18	+376	+485	+437	+336	+473	+357	+473	+55	+66	+162	+0	+0	+0	+0
19	+381	+507	+434	+339	+479	+366	+503	+34	+60	+151	+0	+0	+0	+0
20	+376	+497	+474	+363	+505	+380	+514	+75	+87	+182	+0	+0	+0	+0
21	+392	+466	+480	+364	+536	+417	+553	+104	+144	+232	+0	+0	+0	+0
22	+509	+616	+617	+505	+646	+391	+525	+75	+97	+198	+0	+0	+0	+0
23	+391	+503	+471	+342	+493	+393	+518	+93	+106	+208	+0	+0	+0	+0
24	+389	+535	+448	+323	+467	+392	+548	+100	+110	+218	-214	-227	-104	-136
25	+437	+579	+477	+353	+496	+428	+613	+153	+159	+275	-160	-526	-18	-98
26	+420	+538	+501	+376	+535	+422	+545	+125	+184	+231	-171	-164	-20	-96
27	+425	+541	+501	+372	+539	+427	+544	+137	+133	+239	-173	-184	-40	-96
28	+415	+520	+521	+389	+556	+418	+532	+116	+132	+227	-185	-184	-33	-105
29	+427	+529	+538	+402	+581	+438	+540	+114	+119	+221	-180	-200	-53	-108
30	+436	+538	+549	+411	+584	+439	+543	+112	+114	+219	-183	-204	-62	-109
31	+394	+502	+505	+373	+556	+415	+512	+90	+80	+197	-197	-212	-60	-126
32	+0	+493	+486	+356	+535	+422	+507	+101	+145	+258	-203	-178	-28	-108
33	+0	+585	+628	+393	+646	+570	+624	+189	+187	+338	-103	-160	-39	-30
34	+0	+564	+629	+391	+668	+542	+682	+215	+170	+285	-116	-134	-12	-30
35	+0	+602	+619	+413	+663	+519	+612	+213	+156	+271	+161	-41	+28	-32
36	+0	+597	+547	+421	+630	+533	+632	+222	+218	+372	-103	+73	+17	-17
37	+0	+630	+667	+425	+753	+690	+675	+259	+267	+417	-18	+0	+72	+54

Table B 1 (cont.)

Measured Strains for Section B
UW data uncorrected for differential temperature at casting succeeding stage

No	Microstrain													
	1	2	3	4	5	6	7	8	9	10	11	12	13	14
38	+0	+690	+708	+471	+752	+580	+649	+251	+280	+361	-139	+89	+0	-15
39	+0	+532	+578	+321	+624	+461	+538	+233	+265	+365	-214	-97	-37	-93
40	+0	+584	+612	+384	+653	+505	+605	+202	+228	+317	-200	-89	-94	-78
41	+0	+550	+608	+349	+645	+488	+579	+232	+291	+378	-169	-32	-21	-65
42	+488	+551	+0	+342	+679	+482	+589	+261	+300	+428	-166	-67	-59	-46
43	+488	+549	+0	+339	+665	+481	+601	+258	+302	+432	-158	-68	-61	-41
44	+528	+578	+0	+380	+701	+529	+622	+216	+219	+345	-191	-77	-112	-60
45	+527	+574	+0	+380	+709	+529	+609	+224	+235	+365	-193	-73	-101	-65
46	+510	+541	+0	+339	+687	+496	+576	+274	+307	+443	-161	-52	-53	-35
47	+504	+570	+0	+372	+690	+503	+619	+220	+252	+365	-170	-56	-102	-51
48	+500	+572	+0	+374	+682	+495	+620	+215	+253	+362	-171	-57	-99	-50
49	+507	+569	+0	+371	+686	+498	+621	+217	+246	+364	-178	-61	-113	-57
50	+491	+540	+0	+336	+664	+470	+590	+269	+320	+441	-147	-31	-61	-31
51	+496	+570	+0	+364	+676	+487	+619	+219	+253	+368	-177	-64	-93	-57
52	+488	+544	+0	+336	+659	+475	+592	+262	+305	+433	-152	-38	-75	-19
53	+500	+580	+0	+374	+674	+497	+634	+214	+237	+355	-175	-76	-120	-54
54	+507	+563	+0	+363	+677	+496	+616	+238	+257	+390	-171	-80	-117	-45
55	+528	+578	+0	+373	+689	+515	+625	+216	+228	+360	-193	-93	-132	-65
56	+499	+527	+0	+112	+678	+493	+589	+272	+306	+443	-150	-65	-69	-32
57	+514	+575	+614	+370	+689	+505	+622	+221	+245	+372	-177	-82	-80	-57
58	+494	+525	+630	+336	+680	+482	+586	+270	+310	+450	-148	-49	-29	-34
59	+501	+539	+641	+364	+688	+500	+620	+217	+248	+373	-177	-72	-78	-62
60	+488	+492	+631	+328	+679	+476	+584	+271	+324	+455	-137	-28	-20	-27
61	+507	+515	+641	+366	+688	+493	+623	+208	+248	+363	-168	-68	-80	-59
62	+490	+471	+629	+331	+675	+469	+587	+263	+316	+448	-143	-38	-26	-32
63	+503	+480	+638	+363	+689	+494	+623	+207	+245	+364	-171	-67	-83	-60
64	+500	+417	+633	+326	+681	+476	+609	+267	+331	+456	-132	-17	-33	-28
65	+511	+428	+637	+356	+684	+489	+620	+211	+251	+373	-169	-70	-82	-63
66	+502	+409	+628	+328	+676	+477	+591	+264	+329	+457	-133	-33	-29	-32
67	+499	+411	+632	+368	+680	+490	+634	+206	+242	+354	-164	-67	-92	-57
68	+500	+255	+617	+335	+668	+479	+609	+254	+296	+428	-146	-65	-83	-44
69	+503	+0	+628	+361	+682	+501	+636	+216	+238	+368	-175	-86	-115	-63
70	+514	+0	+636	+370	+694	+512	+635	+220	+234	+364	-175	-80	-109	-59
71	+524	+0	+650	+381	+707	+525	+632	+218	+230	+359	-180	-80	-105	-61
72	+526	+0	+655	+383	+712	+527	+632	+222	+234	+364	-178	-75	-100	-58
73	+541	+0	+665	+388	+723	+531	+625	+224	+233	+364	-179	-68	-92	-61
74	+523	+611	+0	+386	+710	+521	+623	+220	+246	+365	-170	-60	-88	-53

Table B 1 (cont.)

Measured Strains for Section B
UW data uncorrected for differential temperature at casting succeeding stage

	Microstrain													
No	1	2	3	4	5	6	7	8	9	10	11	12	13	14
75	+517	+605	+0	+378	+704	+507	+621	+223	+253	+369	-167	-59	-93	-51
76	+502	+575	+0	+344	+687	+482	+592	+268	+319	+442	-133	-10	-62	-22
77	+521	+610	+0	+371	+701	+504	+621	+214	+247	+365	-172	-76	-96	-57
78	+500	+577	+0	+342	+695	+491	+591	+268	+317	+442	-136	-28	-42	-27
79	+510	+607	+655	+377	+706	+505	+632	+212	+251	+362	-159	-58	-78	-51
80	+499	+570	+647	+338	+702	+486	+592	+265	+325	+450	-130	-13	-33	-34
81	+504	+600	+0	+369	+692	+495	+627	+213	+255	+365	-155	-52	-79	-52
82	+511	+606	+0	+372	+699	+510	+630	+214	+244	+362	-163	-64	-98	-58
83	+537	+615	+0	+380	+711	+530	+635	+214	+232	+359	-171	-81	-114	-63
84	+535	+612	+0	+383	+718	+534	+627	+224	+244	+374	-152	+67	-105	-58
85	+537	+616	+669	+388	+724	+533	+630	+221	+238	+362	-168	-67	-103	-57
86	+536	+613	+0	+390	+728	+535	+626	+223	+246	+367	-167	-58	-93	-56
87	+532	+610	+0	+386	+728	+527	+618	+232	+256	+377	-156	-45	-80	-50
88	+531	+611	+0	+391	+723	+525	+626	+224	+246	+368	-164	-60	-96	-53
89	+514	+587	+0	+359	+707	+508	+593	+264	+300	+438	-151	-49	-72	-41

Table B 1 (cont.)

Measured Strains for Section C
CTL data corrected for differential temperature at casting succeeding stage

	Microstrain													
No	1	2	3	4	5	6	7	8	9	10	11	12	13	14
1	+39	+21	+40	+36	+30	+8	+25	+0	+0	+0	+0	+0	+0	+0
2	+255	+253	+497	+345	+455	+240	+252	+0	+0	+0	+0	+0	+0	+0
3	+314	+298	+565	+412	+544	+581	+302	+0	+0	+0	+0	+0	+0	+0
4	+305	+349	+606	+422	+560	+309	+303	+0	+0	+0	+0	+0	+0	+0
5	+421	+351	+484	+358	+482	+368	+447	-188	-207	-108	+0	+0	+0	+0
6	+484	+474	+545	+389	+496	+441	+497	-117	-132	-40	+0	+0	+0	+0
7	+525	+497	+594	+403	+586	+488	+495	-84	-132	-4	+0	+0	+0	+0
8	+512	+485	+622	+430	+605	+501	+500	-95	-114	-9	+0	+0	+0	+0
9	+485	+481	+599	+461	+605	+474	+500	-146	-151	-49	+0	+0	+0	+0
10	+516	+516	+651	+457	+593	+473	+492	-89	-55	-33	+0	+0	+0	+0
11	+553	+527	+617	+447	+564	+450	+495	-97	-103	-14	+0	+0	+0	+0
12	+555	+542	+648	+496	+655	+551	+561	-69	-52	+82	+0	+0	+0	+0
13	+528	+542	+654	+201	+649	+546	+539	-94	-72	+40	+0	+0	+0	+0
14	+556	+531	+712	+501	+674	+538	+565	-45	-44	+58	+0	+0	+0	+0
15	+546	+531	+676	+491	+679	+531	+544	-68	-39	+45	+0	+0	+0	+0
16	+557	+529	+667	+516	+709	+560	+580	-65	-68	+59	+0	+0	+0	+0
17	+549	+527	+733	+519	+707	+565	+575	-65	-48	+44	+0	+0	+0	+0
18	+587	+554	+703	+520	+696	+536	+539	-57	-57	+20	+0	+0	+0	+0
19	+598	+559	+710	+529	+715	+534	+555	-67	-54	+28	+0	+0	+0	+0
20	+600	+563	+688	+506	+688	+565	+568	-20	-1	+0	+0	+0	+0	+0
21	+653	+594	+666	+488	+666	+616	+618	+40	+45	+150	-354	-218	-118	-325
22	+680	+604	+631	+470	+629	+622	+623	+55	+11	+149	-328	-159	-115	-248
23	+657	+578	+641	+478	+648	+590	+599	+42	+14	+142	-321	-153	-110	-246
24	+693	+605	+646	+488	+657	+617	+628	+78	+47	+179	-304	-118	-76	-213
25	+691	+611	+658	+491	+666	+619	+630	+76	+45	+184	-287	-118	-77	-212
26	+676	+604	+671	+499	+675	+624	+616	+61	+28	+158	-305	-144	-122	-233
27	+682	+603	+664	+495	+673	+621	+623	+60	+31	+166	-306	-141	-170	-239
28	+667	+597	+669	+499	+674	+604	+613	+53	+36	+154	-304	-136	-152	-236
29	+683	+608	+681	+503	+683	+615	+619	+52	+25	+158	-313	-134	-161	-226
30	+688	+613	+678	+512	+684	+617	+627	+48	+23	+164	-309	-141	-175	-230
31	+676	+577	+619	+472	+635	+582	+620	+44	-10	+161	-332	-119	-206	-231
32	+694	+594	+666	+447	+658	+634	+636	+153	+91	+250	-265	-42	-82	-152
33	+786	+693	+716	+490	+689	+721	+669	+202	+155	+289	-215	+30	-13	-143
34	+791	+678	+700	+461	+738	+719	+683	+185	+119	+263	-213	+35	+48	-154
35	+747	+674	+707	+436	+759	+737	+696	+165	+142	+248	-180	+11	+63	-208
36	+766	+635	+669	+468	+726	+711	+698	+198	+91	+318	-125	+88	-21	-181
37	+905	+673	+791	+432	+769	+754	+736	+245	+254	+365	-153	+0	+100	-76

Table B 1 (cont.)

Measured Strains for Section C
UW data uncorrected for differential temperature at casting succeeding stage

	Microstrain													
No	1	2	3	4	5	6	7	8	9	10	11	12	13	14
38	+856	+717	+754	+590	+734	+757	+714	+258	+192	+341	+85	+136	-65	+49
39	+758	+618	+633	+247	+648	+642	+621	+207	+173	+322	+53	-148	-196	+5
40	+809	+645	+656	+295	+671	+678	+658	+182	+146	+282	+30	-118	-166	-16
41	+767	+631	+661	+341	+661	+658	+616	+231	+193	+327	+89	-87	-144	+22
42	+794	+631	+641	+465	+636	+658	+642	+240	+223	+361	+102	+0	-157	+57
43	+796	+631	+637	+466	+633	+654	+641	+248	+223	+364	+101	+0	-155	+55
44	+844	+678	+655	+496	+655	+702	+683	+224	+163	+304	+47	+0	-156	+1
45	+829	+669	+655	+492	+655	+693	+672	+210	+175	+313	+49	+0	-154	+9
46	+796	+645	+647	+481	+642	+665	+650	+254	+229	+376	+109	+0	-159	+62
47	+837	+647	+647	+487	+642	+672	+664	+210	+177	+306	+62	+0	-136	+12
48	+824	+640	+642	+486	+637	+668	+660	+208	+178	+300	+61	+0	-132	+12
49	+825	+646	+643	+487	+638	+674	+660	+209	+174	+305	+54	+0	-145	+11
50	+791	+623	+629	+463	+619	+648	+637	+254	+232	+368	+111	+0	-156	+62
51	+822	+639	+637	+484	+632	+664	+659	+213	+178	+306	+59	+0	-142	+15
52	+800	+624	+624	+470	+618	+652	+641	+253	+224	+367	+107	+0	-157	+56
53	+835	+646	+629	+494	+627	+673	+669	+211	+167	+296	+50	+0	-143	+1
54	+825	+642	+631	+487	+625	+669	+660	+229	+183	+324	+68	+0	-159	+26
55	+840	+673	+642	+500	+638	+686	+671	+211	+163	+304	+40	+0	-162	-1
56	+803	+642	+635	+484	+630	+658	+647	+262	+223	+369	+102	+0	-156	+51
57	+833	+652	+645	+507	+641	+673	+668	+210	+173	+309	+50	+0	-148	+9
58	+794	+634	+639	+482	+631	+655	+643	+258	+233	+373	+112	+0	-150	+60
59	+823	+648	+644	+501	+643	+669	+660	+205	+177	+304	+54	+0	-143	+11
60	+786	+632	+664	+507	+632	+646	+630	+261	+241	+376	+119	+0	-136	+67
61	+820	+646	+645	+511	+643	+667	+655	+202	+173	+298	+53	+0	-131	+5
62	+791	+633	+646	+496	+636	+646	+628	+252	+232	+364	+114	+0	-139	+62
63	+822	+646	+649	+527	+642	+667	+654	+202	+170	+299	+50	+0	-134	+5
64	+785	+634	+655	+504	+641	+649	+624	+257	+240	+370	+122	+0	-134	+62
65	+813	+642	+652	+543	+644	+663	+643	+208	+180	+307	+57	+0	-142	+12
66	+779	+633	+646	+520	+646	+647	+623	+259	+242	+372	+120	+0	-135	+63
67	+803	+630	+633	+553	+626	+659	+651	+203	+164	+288	+46	+0	-134	-6
68	+802	+631	+629	+508	+621	+652	+640	+249	+216	+353	+96	+0	-162	+43
69	+831	+653	+641	+542	+637	+680	+661	+215	+167	+303	+44	+0	-160	-2
70	+835	+663	+648	+558	+645	+684	+667	+217	+164	+302	+41	+0	-154	-2
71	+839	+669	+650	+565	+648	+693	+673	+212	+163	+300	+40	+0	-154	-2
72	+837	+664	+652	+554	+650	+691	+674	+217	+167	+305	+45	+0	-149	+0
73	+839	+676	+661	+553	+661	+696	+675	+211	+166	+301	+43	+0	-144	+3
74	+837	+662	+660	+551	+656	+686	+673	+211	+175	+302	+52	+0	-133	-10

Table B 1 (cont.)

Measured Strains for Section C
UW data uncorrected for differential temperature at casting succeeding stage

	Microstrain													
No	1	2	3	4	5	6	7	8	9	10	11	12	13	14
75	+835	+656	+653	+560	+645	+680	+675	+220	+185	+310	+66	+0	-131	+18
76	+798	+635	+639	+536	+631	+652	+646	+261	+236	+368	+111	+0	-141	+61
77	+832	+649	+642	+557	+641	+670	+664	+207	+175	+303	+53	+0	-143	+8
78	+799	+640	+650	+537	+642	+657	+648	+255	+233	+364	+111	+0	-136	+58
79	+833	+661	+663	+606	+657	+679	+666	+213	+181	+304	+61	+0	-113	+14
80	+789	+642	+665	+534	+654	+656	+633	+255	+242	+371	+120	+0	-122	+67
81	+819	+643	+653	+529	+646	+661	+651	+206	+177	+296	+60	+0	-120	+10
82	+829	+658	+656	+565	+650	+679	+660	+214	+170	+301	+57	+0	-131	+6
83	+837	+667	+654	+585	+652	+691	+671	+208	+161	+296	+41	+0	-149	-4
84	+834	+673	+660	+604	+655	+694	+672	+214	+170	+308	+48	+0	-149	+5
85	+842	+680	+669	+645	+662	+698	+679	+331	+171	+303	+51	+0	-137	+4
86	+843	+678	+673	+641	+670	+700	+679	+218	+178	+308	+59	+0	-129	+13
87	+833	+672	+666	+624	+662	+689	+673	+222	+185	+315	+65	+0	-128	+18
88	+841	+670	+665	+661	+661	+694	+680	+218	+179	+304	+59	+0	-129	+10
89	+813	+654	+652	+587	+648	+674	+661	+247	+226	+366	+102	+0	-151	+61

Table B2

Calculation of CTL Corrections for Differential Temperature
at Casting of Succeeding Stage

Denny Creek Stress Investigation 63-1080
Calculation of CTL Temperature Correction Factors Stage III
Microstrain (Compression +)

Day	Gage A-1	Gage A-2	Gage A-3	Gage A-4	Gage A-5	Gage A-6	Gage A-7	Gage A-8	Gage A-9	Gage A-10	Gage A-11	Gage A-12	Gage A-13	Gage A-14
83	598	638	669	269	782	401	416	162	154	166	0	0	0	0
20	645	662	695	282	815	419	450	133	127	158	0	0	0	0
Corr't'n	47	24	26	13	33	18	34	-29	-27	-8	0	0	0	0
95	581	629	838	310	986	403	400	113	118	117	0	0	0	0
24	628	653	863	324	1020	421	433	84	92	109	-76	-163	-135	-143
Corr't'n	47	24	25	14	34	18	33	-29	-26	-8	-76	-163	-135	-143
345	584	678	967	330	1104	428	393	92	167	145	-67	-162	-81	-51
32	631	701	992	343	1137	446	427	63	140	137	-60	-185	-96	-69
Corr't'n	47	23	25	13	33	18	34	-29	-27	-8	7	-23	-15	-18
16	335	293	295	23	482	203	226	0	0	0	0	0	0	0
5	383	316	320	36	515	220	259	-116	-109	0	0	0	0	0
Corr't'n	48	23	25	13	33	17	33	-116	-109	0	0	0	0	0

Table B2 (cont.)

Denny Creek Stress Investigation 63-1080
Calculation of CTL Temperature Correction Factors Stage III
Microstrain (Compression +)

Day	Gage B-1	Gage B-2	Gage B-3	Gage B-4	Gage B-5	Gage B-6	Gage B-7	Gage B-8	Gage B-9	Gage B-10	Gage B-11	Gage B-12	Gage B-13	Gage B-14
83	381	461	450	318	481	381	482	128	126	193	0	0	0	0
20	379	497	474	363	505	380	514	75	87	182	0	0	0	0
Corr't'n	-2	36	24	45	24	-1	32	-53	-39	-11	0	0	0	0
95	394	500	424	278	443	392	516	152	149	229	0	0	0	0
24	389	535	448	323	467	392	548	100	110	218	-214	-227	-104	-136
Corr't'n	-5	35	24	45	24	0	32	-52	-39	-11	-214	-227	-104	-136
345		457	462	311	511	422	476	153	184	269		-139	-25	-94
32		493	486	356	535	422	507	101	145	258	-203	-178	-28	-108
Corr't'n	0	36	24	45	24	0	31	-52	-39	-11		-39	-3	-14
'16	122	249	178	127	205	141	272	0	0	0	0	0	0	0
5	117	285	202	172	229	141	303	-52	-39	-11	0	0	0	0
Corr't'n	-5	36	24	45	24	0	31	-52	-39	-11	0	0	0	0

Table B2 (cont.)

Benny Creek Stress Investigation 63-1080
Calculation of CTL Temperature Correction Factors Stage III
Microstrain (Compression +)

Day	Gage C-1	Gage C-2	Gage C-3	Gage C-4	Gage C-5	Gage C-6	Gage C-7	Gage C-8	Gage C-9	Gage C-10	Gage C-11	Gage C-12	Gage C-13	Gage C-14
83	561	542	648	470	658	557	543	43	68		0	0	0	0
20	600	563	688	506	688	565	568	-20	-1		0	0	0	0
Corr't'n	39	21	40	36	30	8	25	-63	-69	0	0	0	0	0
84	614	573	625	451	636	608	593	103	114	188	0	0	0	0
21	653	594	666	488	666	616	618	40	45	150	-354	-218	-118	-325
Corr't'n	39	21	41	37	30	8	25	-63	-69	-38	-354	-218	-118	-325
345	665	573	625	411	621	626	611	216	160	288	-159		-54	-55
32	694	594	666	447	658	634	636	153	91	250	-265	-42	-82	-152
Corr't'n	39	21	41	36	30	8	25	-63	-69	-38	-106		-28	-97
16	382	330	443	322	452	359	422	0	0	0	0	0	0	0
5	421	351	484	358	482	368	447	-188	-207	-108	0	0	0	0
Corr't'n	39	21	41	36	30	9	25	-188	-207	-108	0	0	0	0

Table B 3

Corrections for differential temperature at casting of succeeding stage by CTL procedure, eigenstresses only

Element	Area ft2	ybcgc ft	Inertia ft4	kern^2 ft2	Mod of Elast ksf
Sections B and C					
Stage I	40.224	3.551	312.390	7.766	691,200.
Stage II	27.120	.424	3.618	.133	504,000.
Stage III	31.703	.435	4.038	.127	504,000.
Stage I+II	67.344	5.513	698.800	10.377	
Stage I+II+III	99.048	6.448	884.430	8.929	
Section A					
Stage I	50.545	3.057	360.490	7.132	691,200.
Stage II	27.120	.424	3.618	.133	504,000.
Stage III	31.703	.435	4.038	.127	504,000.
Stage I+II	77.665	4.931	870.880	11.213	
Stage I+II+III	109.369	5.947	1148.860	10.504	

Note: Modulus of elasticity of Stage I used for Stages I and II for Stage I+II > Stage III calculation

Shear and Moment to restore compatability for differential temp

Section and Stage	Diff deg F	Shear kips	Moment kip-ft
Stage I > II at A	-15	-355.6	-136.9
Stage I+II > III at A	-24	-1196.6	-506.0
Stage I > II at B	-19	-435.4	-166.9
Stage I+II > III at B	-28	-1362.3	-575.5
Stage I > II at C	-28	-641.6	-246.0
Stage I+II > III at C	-34	-1652.5	-698.1

Stresses to restore compatibility [psi compression +]

Section and Stage	fcbI	fctI	fcbII	fctII	fcbIII	fcbIII
Section A						
Stage I > II	-63.	229.	-102.	-76.		
Stage I+II > III	-57.	209.	209.	243.	-273.	-248.
Section B						
Stage I > II	-91.	283.	-126.	-92.		
Stage I+II > III	-77.	238.	238.	278.	-311.	-282.
Section C						
Stage I > II	-134.	417.	-186.	-135.		
Stage I+II > III	-93.	289.	289.	337.	-377.	-342.

Table B4

Concrete Ages at Date of Carlson Gage Readings (Events)

Reading Number	Date	Age Stage I	Age Stage II	Age Stage IIIA	Age Stage IIIB
1	16 May 78	3			
2	19 May 78	6			
3	24 May 78	11			
4	30 May 78	17			
5	1 Jun 78	19	1		
6	5 Jun 78	23	5		
7	5 Jun 78	23	5		
8	6 Jun 78	24	6		
9	9 Jun 78	27	9		
10	14 Jun 78	32	14		
11	19 Jun 78	37	19		
12	22 Jun 78	40	22		
13	22 Jun 78	40	22		
14	26 Jun 78	44	26		
15	27 Jun 78	45	27		
16	5 Jul 78	53	35		
17	6 Jul 78	54	36		
18	19 Jul 78	67	49		
19	20 Jul 78	68	50		
20	7 Aug 78	86	68		
21	8 Aug 78	87	69	1	
22	10 Aug 78	89	71	3	
23	18 Aug 78	97	79	11	
24	19 Aug 78	98	80	12	1
25	21 Aug 78	100	82	14	3
26	24 Aug 78	103	85	17	6
27	18 Sep 78	128	110	42	31
28	20 Sep 78	130	112	44	33
29	3 Oct 78	143	125	57	46
30	13 Oct 78	153	135	67	56
31	13 Dec 78	214	196	128	117
32	26 Apr 79	348	330	262	251
33	26 Jul 79	439	421	353	342
34	19 Oct 79	524	506	438	427
35	21 Jan 80	620	602	534	523
36	24 Apr 80	712	694	626	615
37	1 Aug 80	811	793	725	714

Table B 4 (cont.)

Concrete Ages at Date of Carlson Gage Readings

Reading Number	Date	Age Stage I	Age Stage II	Age Stage IIIA	Age Stage IIIB
38	24 Oct 80	895	877	809	798
39	8 Jul 81	1152	1134	1066	1055
40	23 Jul 81	1167	1149	1081	1070
41	9 Aug 81	1184	1166	1098	1087
42	9 Jul 82	1519	1501	1433	1422
43	12 Jul 82	1522	1504	1436	1425
44	15 Jul 82	1524	1506	1438	1427
45	16 Jul 82	1525	1507	1439	1428
46	16 Jul 82	1526	1508	1440	1429
47	17 Jul 82	1526	1508	1440	1429
48	18 Jul 82	1527	1509	1441	1430
49	19 Jul 82	1528	1510	1442	1431
50	19 Jul 82	1529	1511	1443	1432
51	20 Jul 82	1529	1511	1443	1432
52	20 Jul 82	1530	1512	1444	1433
53	21 Jul 82	1530	1512	1444	1433
54	21 Jul 82	1531	1513	1445	1434
55	22 Jul 82	1531	1513	1445	1434
56	22 Jul 82	1532	1514	1446	1435
57	23 Jul 82	1532	1514	1446	1435
58	23 Jul 82	1533	1515	1447	1436
59	24 Jul 82	1533	1515	1447	1436
60	24 Jul 82	1534	1516	1448	1437
61	25 Jul 82	1534	1516	1448	1437
62	25 Jul 82	1535	1517	1449	1438
63	26 Jul 82	1535	1517	1449	1438
64	26 Jul 82	1536	1518	1450	1439
65	27 Jul 82	1536	1518	1450	1439
66	27 Jul 82	1537	1519	1451	1440
67	28 Jul 82	1537	1519	1451	1440
68	28 Jul 82	1538	1520	1452	1441
69	29 Jul 82	1538	1520	1452	1441
70	30 Jul 82	1539	1521	1453	1442
71	31 Jul 82	1540	1522	1454	1443
72	1 Aug 82	1541	1523	1455	1444
73	2 Aug 82	1542	1524	1456	1445
74	3 Aug 82	1543	1525	1457	1446
75	4 Aug 82	1544	1526	1458	1447

Table B 4 (cont.)

Concrete Ages at Date of Carlson Gage Readings

Reading Number	Date	Age Stage I	Age Stage II	Age Stage IIIA	Age Stage IIIB
76	4 Aug 82	1545	1527	1459	1448
77	5 Aug 82	1545	1527	1459	1448
78	5 Aug 82	1546	1528	1460	1449
79	7 Aug 82	1547	1529	1461	1450
80	7 Aug 82	1548	1530	1462	1451
81	8 Aug 82	1548	1530	1462	1451
82	9 Aug 82	1549	1531	1463	1452
83	10 Aug 82	1550	1532	1464	1453
84	11 Aug 82	1551	1533	1465	1454
85	12 Aug 82	1552	1534	1466	1455
86	13 Aug 82	1553	1535	1467	1456
87	13 Aug 82	1554	1536	1468	1457
88	14 Aug 82	1554	1536	1468	1457
89	14 Aug 82	1555	1537	1469	1458

Table B5.

Concrete Temperatures at Each Reading (Event)

Temperature Data **Section A,B,C**

Degrees Celsius at Gage No

Event	1	2	3	4	5	6	7	8	9	10	11	12	13	14
42A	16.3	15.9	16.2	14.7	16.6	.	16.9	.	22.7	22.8	17.2	19.3	20.3	20.8
42B	15.9	16.8	16.2	15.3	16.7	16.1	16.7	23.7	23.6	24.9	20.1	17.4	21.4	21.1
42C	20.4	16.4	16.7	15.8	16.9	16.6	17.2	22.3	24.3	24.6	23.1	.	17.6	24.8
43A	19.4	18.3	17.7	17.7	18.4	.	20.1	.	25.6	26.2	20.0	22.7	23.7	24.2
43B	18.4	20.6	18.3	16.9	18.8	18.8	19.9	27.7	26.5	28.2	23.4	20.2	24.6	24.6
43C	24.2	18.8	18.6	18.6	19.2	19.2	20.3	25.6	26.9	27.5	25.9	.	20.5	27.5
44A	12.8	12.5	10.9	14.0	11.6	.	13.1	.	10.4	12.0	8.3	10.3	10.2	8.6
44B	12.1	12.3	10.4	11.1	10.9	12.3	12.7	10.8	10.4	11.4	10.4	8.6	8.6	10.9
44C	16.1	12.7	10.3	11.1	10.2	12.9	13.3	12.2	10.4	11.4	9.8	.	8.7	10.0
45A	11.6	11.9	11.0	12.6	11.7	.	11.9	.	10.7	11.8	9.2	9.7	9.9	9.4
45B	11.4	10.8	10.3	10.2	10.8	11.7	11.3	10.7	10.9	12.0	10.0	9.4	9.6	10.6
45C	14.4	12.0	10.3	10.6	10.2	12.2	11.9	12.1	11.1	12.1	10.2	.	9.1	11.1
46A	12.8	13.9	14.0	12.6	14.6	.	13.2	.	20.7	21.2	17.2	16.5	17.7	18.2
46B	13.6	12.3	13.4	11.8	13.9	13.8	12.7	21.5	21.2	23.2	17.2	15.8	18.3	17.9
46C	16.0	14.1	13.8	12.3	13.8	14.2	13.2	20.1	21.3	22.1	19.9	.	13.7	21.7
47A	14.9	13.6	13.4	14.0	13.9	.	15.3	.	15.5	15.7	14.5	14.7	15.3	14.3
47B	13.2	14.9	13.0	13.7	13.3	13.2	15.0	14.8	15.7	15.5	15.0	14.2	14.1	15.7
47C	18.3	13.6	13.0	13.8	13.0	13.6	15.3	15.4	15.9	15.4	15.0	.	14.6	15.7
48A	17.2	15.3	15.0	15.8	15.3	.	17.7	.	17.7	17.9	16.9	17.5	18.0	16.9
48B	14.9	17.8	14.9	15.9	15.2	14.8	17.4	17.4	17.9	17.7	17.7	16.8	16.7	18.4
48C	21.2	15.2	14.8	16.3	14.9	15.2	17.7	17.6	18.1	17.5	17.7	.	17.1	18.0
49A	17.1	15.4	14.6	16.1	15.1	.	17.6	.	16.8	17.5	15.7	16.7	17.2	15.6
49B	15.1	17.6	14.7	15.7	15.0	15.1	17.3	17.1	17.0	17.3	16.9	16.0	15.6	17.7
49C	21.1	15.5	14.7	16.0	14.8	15.6	17.6	17.4	17.3	17.3	16.8	.	15.7	17.4
50A	17.7	17.1	16.7	16.1	17.2	.	18.3	.	26.2	26.3	23.4	22.9	24.1	24.1
50B	16.8	18.5	16.9	16.7	17.3	16.9	18.1	27.7	26.6	27.8	23.3	22.2	23.7	24.4
50C	21.9	17.2	16.9	17.1	17.3	17.2	18.3	25.1	26.6	26.6	25.6	.	19.0	26.8
51A	18.2	16.1	15.2	16.7	15.5	.	18.7	.	18.6	19.1	16.7	18.0	18.5	17.2
51B	15.8	19.1	15.2	16.3	15.5	15.7	18.4	19.1	18.8	19.0	18.3	16.8	17.2	19.1
51C	22.6	16.2	15.2	16.7	15.3	16.1	18.7	18.9	18.9	18.8	18.2	.	16.9	18.7
52A	18.2	16.9	16.2	16.6	16.7	.	18.8	.	25.4	25.7	22.7	22.4	23.4	22.8
52B	16.7	19.1	16.4	16.7	16.8	16.8	18.6	26.8	25.7	27.1	22.8	21.9	22.6	19.6
52C	22.5	17.1	16.3	16.9	16.7	17.1	18.8	24.6	25.7	25.9	24.7	.	18.4	25.8
53A	17.2	14.5	12.8	16.4	13.6	.	17.8	.	15.6	16.7	13.4	16.1	16.4	14.1
53B	14.1	17.8	13.0	15.1	13.4	14.4	17.7	16.2	15.6	15.8	16.2	13.6	13.8	17.1
53C	21.3	14.6	12.7	15.3	12.9	14.9	17.9	16.9	15.6	15.8	15.2	.	14.6	15.2

Table B-5 (cont.)

Temperature Data — Degrees Celsius at Gage No — Section A,B,C

Event	1	2	3	4	5	6	7	8	9	10	11	12	13	14
54A	16.2	14.5	13.1	15.7	13.9	.	16.8	.	17.8	19.1	14.4	16.7	17.4	14.7
54B	14.2	16.6	13.2	14.2	13.7	14.6	16.6	19.1	17.8	19.1	17.0	13.6	14.8	18.1
54C	20.2	14.8	13.1	14.6	13.4	15.1	17.0	18.8	17.8	18.6	17.1	.	13.8	17.7
55A	14.8	13.5	12.0	14.8	12.3	.	15.1	.	12.6	14.3	9.7	12.4	12.7	10.3
55B	13.1	14.8	11.6	12.6	11.8	13.1	14.7	13.3	12.6	14.0	12.6	9.7	10.5	13.5
55C	18.5	13.7	11.5	13.1	11.3	13.7	15.3	14.4	12.9	14.0	12.1	.	10.9	12.7
56A	15.5	15.6	14.9	14.6	15.4	.	16.1	.	22.8	23.8	18.3	19.6	20.6	20.3
56B	15.2	15.6	14.6	14.0	15.0	15.3	15.7	24.5	22.9	24.8	19.8	16.1	20.3	21.0
56C	19.3	15.6	14.7	14.6	14.8	15.8	16.1	22.6	22.7	23.6	21.5	.	15.7	22.4
57A	15.5	13.9	12.9	14.9	13.3	.	15.8	.	14.5	15.5	11.5	13.7	14.1	12.9
57B	13.5	15.6	12.5	13.3	12.6	13.4	15.4	14.6	14.7	15.6	14.1	11.5	13.3	14.8
57C	19.3	14.1	12.6	13.9	12.4	14.1	15.8	15.4	15.0	15.6	14.2	.	13.1	14.8
58A	16.4	16.3	16.3	14.9	16.6	.	16.9	.	24.2	24.9	20.3	20.6	21.8	22.4
58B	16.2	16.7	15.9	15.1	16.4	16.1	16.6	25.7	24.6	26.7	21.1	19.3	22.4	22.2
58C	20.4	16.6	16.3	15.7	16.4	16.5	16.9	23.6	24.7	25.4	23.5	.	17.6	25.0
59A	17.2	15.8	15.2	15.9	15.7	.	17.7	.	17.1	17.7	14.8	16.3	16.8	16.1
59B	15.5	17.7	15.0	15.6	15.4	15.4	17.4	17.2	17.3	17.9	16.7	15.1	16.3	17.4
59C	21.4	15.9	15.2	16.1	15.3	15.9	17.7	17.4	17.6	17.7	16.8	.	16.2	17.4
60A	19.2	19.3	20.0	16.4	20.1	.	19.8	.	28.6	28.9	26.1	24.9	26.3	27.7
60B	19.3	20.1	19.8	18.6	20.1	19.1	19.6	30.4	29.1	30.6	25.5	24.9	27.3	26.6
60C	23.8	19.5	15.8	19.1	20.3	19.3	19.7	27.2	28.9	29.2	27.9	.	22.4	29.3
61A	19.8	17.9	17.6	17.9	17.8	.	20.3	.	19.6	20.0	18.1	19.3	19.9	19.2
61B	17.7	20.8	17.6	18.5	18.0	17.8	20.1	19.9	19.9	19.9	19.7	18.4	19.4	20.4
61C	24.5	18.1	17.6	19.0	18.0	18.1	20.3	19.7	20.2	19.8	19.6	.	19.6	20.1
62A	21.1	20.7	21.2	18.2	21.3	.	21.7	.	29.4	29.7	26.4	26.2	27.6	28.7
62B	20.6	22.2	21.2	20.3	21.7	20.6	21.4	31.4	30.1	31.4	26.7	25.3	28.6	27.8
62C	26.1	20.9	21.5	20.9	22.1	20.9	21.7	28.1	29.9	30.1	29.1	.	23.9	30.5
63A	21.5	19.6	19.1	19.6	19.2	.	21.9	.	20.8	21.4	19.4	20.9	21.4	20.4
63B	19.4	22.7	19.2	20.1	19.6	19.4	21.8	21.8	21.3	21.5	21.2	19.8	20.8	22.0
63C	26.6	19.8	19.2	20.7	19.7	19.8	22.1	21.3	21.6	21.4	21.1	.	21.0	21.7
64A	23.7	23.7	24.4	20.1	24.2	.	24.3	.	32.9	33.1	31.3	29.7	31.0	31.6
64B	23.6	25.2	24.4	23.1	24.7	23.4	19.9	35.4	33.5	34.6	30.2	30.0	30.9	31.1
64C	29.2	23.9	24.7	23.6	25.2	23.6	24.2	31.4	33.3	33.2	32.4	.	27.0	33.5
65A	23.8	22.0	21.6	21.4	21.9	.	24.3	.	24.4	24.9	21.9	23.8	24.3	23.7
65B	21.8	25.2	21.9	22.4	22.3	22.1	24.1	25.8	25.9	25.4	24.2	22.4	24.0	24.8
65C	29.4	22.3	22.0	23.2	22.8	22.4	24.4	24.4	25.3	25.0	24.6	.	23.6	25.3

Table B-5 (cont.)

Temperature Data — Section A,B,C

Degrees Celsius at Gage No

Event	1	2	3	4	5	6	7	8	9	10	11	12	13	14
66A	25.2	24.8	25.2	21.8	25.2	.	25.8	.	34.0	34.2	31.3	30.8	32.0	32.8
66B	24.7	27.0	25.5	24.5	25.8	24.8	25.6	36.8	34.7	35.9	31.2	30.0	32.6	32.2
66C	31.1	25.1	25.7	25.2	26.6	25.0	25.8	32.6	34.6	34.6	33.7	.	28.1	34.8
67A	24.3	21.4	20.1	22.5	20.2	.	24.6	.	22.6	23.6	21.2	23.7	23.8	21.9
67B	21.2	25.7	20.5	22.4	20.7	21.1	24.6	24.5	22.9	22.8	23.9	21.6	22.1	24.4
67C	29.9	21.7	20.2	23.0	20.7	21.6	24.8	23.7	22.9	22.8	22.9	.	22.8	22.7
68A	23.7	21.9	20.6	22.1	21.1	.	24.2	.	28.8	29.7	25.5	27.1	27.6	24.9
68B	21.7	24.4	21.2	21.9	21.6	21.9	24.2	31.8	29.4	30.8	27.4	23.7	25.1	28.2
68C	29.3	22.2	21.1	22.6	21.8	22.2	24.4	28.9	29.3	29.8	28.8	.	22.8	29.4
69A	21.9	19.6	17.6	21.1	18.4	.	22.4	.	20.0	21.5	17.2	20.2	20.5	17.8
69B	19.3	.	17.9	19.6	18.4	19.6	22.4	22.2	20.3	21.3	20.5	17.4	17.7	21.3
69C	27.1	19.9	17.7	20.3	18.4	20.2	22.7	21.9	20.5	21.3	19.9	.	18.2	20.2
70A	19.7	18.2	16.5	19.4	17.1	.	20.3	.	17.9	19.6	15.2	17.7	18.2	15.8
70B	17.8	.	16.2	17.5	16.7	18.0	20.1	19.7	17.9	18.9	17.9	15.3	15.6	18.9
70C	24.4	18.3	16.1	18.2	16.6	18.5	20.5	19.8	17.9	18.9	17.0	.	16.1	17.3
71A	17.1	16.2	14.4	17.7	15.3	.	17.6	.	14.8	16.4	12.4	14.6	14.9	13.0
71B	15.7	.	14.0	15.2	14.6	16.0	17.2	15.9	14.6	15.8	14.8	12.6	12.9	15.7
71C	21.2	16.2	13.8	16.0	14.2	16.5	17.7	16.6	14.7	15.7	13.8	.	13.4	14.3
72A	14.7	14.1	12.6	15.8	13.3	.	15.2	.	13.1	14.6	10.7	12.4	12.8	11.1
72B	13.5	.	12.1	13.0	12.6	13.8	14.8	13.6	12.8	13.9	12.7	10.8	11.1	13.6
72C	18.2	14.1	11.9	13.8	12.0	14.3	15.3	14.6	12.9	13.8	11.8	.	11.5	12.3
73A	13.2	13.3	12.3	14.3	13.0	.	13.6	.	11.6	12.8	10.0	10.9	11.3	10.3
73B	12.6	.	11.4	11.8	11.9	12.8	12.9	11.4	11.4	12.2	11.2	10.1	10.2	11.8
73C	16.2	13.1	11.4	12.6	11.4	13.3	13.6	12.7	11.5	12.1	10.6	.	10.5	11.1
74A	13.6	13.1	12.4	14.2	13.2	.	14.0	.	12.8	13.5	11.6	12.3	12.7	11.8
74B	12.4	13.3	11.8	12.4	12.2	12.6	13.4	12.3	12.7	12.9	12.6	11.7	11.7	13.2
74C	16.6	12.9	11.7	13.1	11.7	13.1	13.9	13.4	12.8	12.8	12.1	.	12.2	12.4
75A	14.7	13.4	12.9	14.6	13.6	.	15.2	.	14.7	15.1	13.1	14.2	14.6	13.2
75B	12.8	14.7	12.4	13.4	12.8	12.9	14.7	14.1	14.6	14.6	14.3	13.1	12.8	14.9
75C	18.1	13.3	12.4	14.1	12.4	13.3	15.0	14.9	14.8	14.5	14.1	.	13.4	14.4
76A	15.8	15.7	15.8	14.6	16.1	.	16.4	.	24.0	24.1	21.5	20.8	22.2	21.0
76B	15.2	16.3	15.4	15.0	15.7	15.1	16.1	24.6	24.3	25.1	21.2	22.4	20.3	22.4
76C	19.6	15.5	15.4	15.6	15.5	15.3	16.3	22.7	24.1	23.8	22.8	.	17.4	23.9
77A	15.7	14.1	13.6	15.1	13.9	.	16.0	.	15.0	15.5	12.7	14.4	14.8	13.5
77B	13.6	16.0	13.2	13.9	13.4	13.6	15.6	14.4	15.1	15.4	14.7	12.6	13.5	15.4
77C	19.4	14.1	13.2	14.7	13.2	14.0	16.0	15.2	15.3	15.2	14.5	.	13.7	15.1

Table B-5 (cont.)

Temperature Data

Degrees Celsius at Gage No

Section A,B,C

Event	1	2	3	4	5	6	7	8	9	10	11	12	13	14
78A	17.0	16.9	17.4	15.3	17.6	.	17.5	.	24.6	24.8	20.5	21.4	22.6	22.8
78B	16.7	17.6	17.0	16.2	17.3	16.6	17.1	25.4	24.8	25.9	21.8	21.3	22.7	22.8
78C	20.9	16.9	17.2	16.8	17.3	16.8	17.3	23.3	24.6	24.7	23.7	.	18.8	24.7
79A	19.6	18.0	17.8	17.7	18.0	.	20.1	.	18.9	19.3	18.2	19.1	19.6	19.0
79B	17.7	20.8	17.8	18.6	18.2	17.7	19.8	19.1	19.1	18.7	19.3	17.9	19.0	19.9
79C	24.1	18.1	17.7	19.5	18.2	18.0	20.0	19.1	19.1	18.6	18.6	.	19.7	18.9
80A	21.6	21.9	23.2	18.4	23.2	.	22.3	.	30.2	30.2	27.2	26.7	28.1	29.6
80B	21.9	23.3	23.0	21.3	23.4	21.9	21.9	31.8	30.6	31.7	27.3	28.2	29.2	28.2
80C	26.6	22.2	23.3	22.1	23.9	22.1	22.1	28.4	30.4	30.3	29.6	.	25.2	30.9
81A	22.2	20.3	20.0	20.2	20.0	.	22.7	.	22.2	22.5	21.6	22.4	22.9	22.6
81B	20.1	24.0	20.2	21.2	20.5	20.1	22.6	22.9	22.6	22.2	22.7	21.6	22.6	23.3
81C	27.2	20.3	20.1	21.8	20.7	20.3	22.7	22.2	22.6	22.0	22.4	.	22.9	22.8
82A	21.0	19.4	18.4	20.0	18.6	.	21.3	.	19.6	20.7	18.4	20.1	20.4	19.1
82B	19.2	22.5	18.7	19.7	18.9	19.2	21.2	20.9	19.9	20.2	20.3	18.4	19.2	20.9
82C	25.8	19.6	18.4	20.5	18.8	19.6	21.5	20.6	19.9	20.1	19.6	.	19.5	19.9
83A	17.5	16.6	15.0	18.0	15.7	.	17.9	.	14.9	16.5	13.0	15.2	15.3	13.4
83B	16.2	18.2	14.9	15.4	15.3	16.5	17.6	16.1	15.0	15.8	15.3	13.0	13.3	16.1
83C	21.6	16.8	14.7	16.7	15.1	17.0	18.1	16.6	15.0	15.8	14.4	.	14.0	14.7
84A	15.4	15.4	14.2	16.2	14.7	.	15.6	.	14.0	15.3	12.1	13.3	13.5	12.2
84B	14.9	15.6	13.6	13.9	13.9	14.8	15.1	14.6	13.9	15.0	9.3	12.3	12.2	14.2
84C	19.7	15.4	13.4	14.8	13.4	15.3	15.7	15.2	14.0	14.8	13.1	.	12.3	13.5
85A	14.1	14.1	13.2	15.1	13.6	.	14.3	.	12.2	13.3	10.8	11.9	12.0	11.0
85B	13.4	13.8	12.3	12.7	12.6	13.3	13.6	12.1	11.9	12.6	12.0	10.7	10.8	12.4
85C	17.2	13.8	12.2	13.8	12.1	13.8	14.2	13.2	12.1	12.5	11.3	.	11.3	11.6
86A	13.2	13.5	13.1	14.1	13.4	.	13.4	.	12.1	12.9	11.1	11.6	11.8	11.3
86B	12.9	12.8	12.2	12.2	12.5	12.9	12.8	11.7	11.9	12.4	11.8	11.2	11.2	12.3
86C	16.2	13.3	12.1	13.3	11.9	13.3	13.4	12.8	12.1	12.3	11.3	.	11.4	11.7
87A	13.1	13.4	12.9	13.9	13.4	.	13.3	.	13.1	13.9	12.5	12.5	12.8	12.6
87B	12.8	12.7	12.3	12.3	12.6	12.8	12.7	12.9	13.1	13.5	12.8	12.6	12.5	13.1
87C	16.0	13.2	12.2	13.2	12.1	13.2	13.2	13.6	13.1	13.3	12.5	.	12.0	12.9
88A	12.3	12.1	11.4	13.3	12.1	.	12.6	.	11.3	12.1	9.9	10.8	11.1	10.2
88B	11.5	11.7	10.8	11.3	11.1	11.6	11.9	10.6	11.2	11.4	11.1	10.0	10.1	11.6
88C	15.1	11.9	10.6	12.4	10.5	11.9	12.4	11.9	11.1	11.3	10.5	.	10.6	10.8
89A	12.6	13.1	12.9	13.1	13.6	.	12.9	.	18.3	18.4	13.2	14.5	15.4	15.2
89B	12.6	12.1	12.4	11.6	12.9	12.8	12.3	18.2	18.4	20.2	15.0	14.2	15.8	15.7
89C	15.5	12.9	12.6	12.4	12.6	13.2	12.8	17.3	18.5	19.1	17.3	.	12.0	18.9

Table B6.

Concrete Temperatures at Section B for Hourly Readings, August 1982

Date	Temperatures (Deg F) 1	2	3	4	5	6	7	TW	IAT
05 AUG 0915	56	61	56	57	56	56	60	58	59
05 AUG 1015	57	61	57	57	58	57	60	58	59
05 AUG 1115	58	61	58	58	59	59	61	59	59
05 AUG 1215	59	62	59	58	60	59	61	60	59
05 AUG 1315	60	62	60	59	61	60	61	61	59
05 AUG 1415	61	62	61	60	62	61	62	61	60
05 AUG 1515	62	63	62	60	63	62	62	62	60
05 AUG 1615	62	64	63	61	63	62	63	62	61
07 AUG 0705	64	69	64	65	65	64	68	66	67
07 AUG 0800	64	69	64	65	65	64	68	66	67
07 AUG 0900	64	69	64	65	65	65	67	66	67
07 AUG 1000	65	69	65	65	66	65	68	66	67
07 AUG 1100	66	70	67	66	68	66	68	67	67
07 AUG 1200	67	70	68	66	69	68	68	68	67
07 AUG 1300	68	71	70	67	71	69	69	69	67
07 AUG 1400	69	72	71	68	72	70	70	70	68
07 AUG 1500	70	73	72	69	73	71	70	71	67
07 AUG 1600	71	73	73	70	74	71	71	72	68
07 AUG 1635	71	74	73	70	74	71	71	72	68
07 AUG 1700	72	74	73	71	74	71	72	72	70
07 AUG 1800	72	75	73	71	74	71	72	73	71
08 AUG 0925	68	75	68	70	69	68	73	70	66
09 AUG 0900	67	72	66	67	66	67	70	68	59
10 AUG 0850	61	65	59	60	60	62	64	61	64
11 AUG 1000	59	60	56	57	57	59	59	58	59
12 AUG 0900	56	57	54	55	55	56	56	56	55
13 AUG 0750	55	55	54	54	55	55	55	55	54
13 AUG 0900	55	55	54	54	55	55	55	55	54
13 AUG 1000	55	55	54	54	55	55	55	55	55
13 AUG 1100	55	55	54	54	55	55	55	55	54
13 AUG 1200	55	55	54	54	55	55	55	55	54
13 AUG 1300	55	55	54	54	55	55	55	55	54
13 AUG 1400	55	55	54	54	55	55	55	55	54
13 AUG 1500	55	55	54	54	55	56	55	55	54
13 AUG 1615	55	55	54	54	55	55	55	55	54
13 AUG 1700	55	55	54	54	55	55	55	55	54
14 AUG 0740	53	53	51	52	52	53	54	53	53
14 AUG 0900	53	53	51	52	52	53	53	53	53
14 AUG 1000	53	53	52	52	52	53	53	53	53
14 AUG 1100	53	53	52	52	53	54	53	53	52
14 AUG 1200	54	53	53	52	54	54	54	53	52
14 AUG 1320	55	54	54	53	55	55	54	54	53
14 AUG 1415	61	62	61	60	62	61	62	61	60
14 AUG 1515	62	63	62	60	63	62	62	62	60

Table B 6 (cont)
Carlson Gage Readings at Section B 1/4 Point Span 4

Temperatures (Deg F)

Date	8	9	10	11	12	13	14	TD	OAT
05 AUG 0915	58	59	60	58	55	56	60	58	57
05 AUG 1015	61	62	63	60	55	59	61	60	63
05 AUG 1115	65	65	67	62	56	62	63	63	64
05 AUG 1215	68	68	71	64	57	65	65	65	70
05 AUG 1315	71	71	74	66	60	68	67	68	70
05 AUG 1415	75	74	77	68	66	70	70	71	72
05 AUG 1515	77	76	78	70	68	72	71	73	70
05 AUG 1615	78	77	79	71	70	73	73	74	68
07 AUG 0705	66	66	66	67	64	66	68	66	64
07 AUG 0800	66	66	66	67	64	66	68	66	70
07 AUG 0900	67	67	67	67	64	66	68	67	72
07 AUG 1000	69	69	70	67	64	68	69	68	77
07 AUG 1100	72	72	74	69	65	70	70	70	82
07 AUG 1200	76	76	78	71	66	73	72	73	86
07 AUG 1300	80	79	82	74	69	77	75	77	88
07 AUG 1400	84	82	85	76	74	79	78	80	88
07 AUG 1500	86	84	87	78	79	82	80	82	90
07 AUG 1600	89	87	89	80	82	84	82	85	86
07 AUG 1635	89	87	89	81	83	85	83	85	86
07 AUG 1700	89	87	89	82	83	85	83	86	81
07 AUG 1800	89	87	88	82	84	84	84	86	81
08 AUG 0925	73	73	72	73	71	73	74	73	73
09 AUG 0900	70	68	68	69	65	67	70	68	71
10 AUG 0850	61	59	61	60	55	56	61	59	55
11 AUG 1000	58	57	59	49	54	54	58	56	52
12 AUG 0900	54	54	55	54	51	52	54	53	50
13 AUG 0750	53	54	54	53	52	52	54	53	52
13 AUG 0900	53	54	54	53	52	52	54	53	54
13 AUG 1000	53	54	55	53	53	53	54	54	52
13 AUG 1100	54	54	55	54	53	53	54	54	52
13 AUG 1200	54	55	55	54	54	53	54	54	52
13 AUG 1300	55	55	56	54	54	54	55	55	52
13 AUG 1400	55	56	57	55	55	54	55	55	52
13 AUG 1500	55	56	57	55	55	55	55	55	50
13 AUG 1615	55	56	56	55	55	55	56	55	50
13 AUG 1700	55	55	56	55	54	54	56	55	50
14 AUG 0740	51	52	53	52	50	50	53	52	46
14 AUG 0900	51	52	53	52	51	50	53	52	48
14 AUG 1000	53	54	55	52	52	51	53	53	52
14 AUG 1100	56	57	59	54	53	54	55	55	55
14 AUG 1200	59	60	63	56	54	57	57	58	59
14 AUG 1320	65	65	68	59	57	60	60	62	59
14 AUG 1415	75	74	77	68	66	70	70	71	72
14 AUG 1515	77	76	78	70	68	72	71	73	70

Table B7.

Strains at Section B for Hourly Readings, August 1982

Date	Strains (microstrain)						
	1	2	3	4	5	6	7
05 AUG 0915	-522	-610	+0	-371	-701	-505	-621
05 AUG 1015	-512	-602	+0	-367	-701	-502	-616
05 AUG 1115	-505	-594	+0	-359	-702	-503	-608
05 AUG 1215	-507	-590	+0	-353	-703	-501	-603
05 AUG 1315	-501	-585	+0	-348	-700	-495	-599
05 AUG 1415	-503	-580	+0	-341	-697	-493	-593
05 AUG 1515	-501	-578	+0	-341	-696	-492	-592
05 AUG 1615	-499	-577	+0	-342	-695	-491	-591
07 AUG 0705	-511	-607	-656	-377	-706	-505	-632
07 AUG 0800	-510	-603	-656	-377	-706	-505	-629
07 AUG 0900	-513	-600	-650	-369	-705	-504	-625
07 AUG 1000	-508	-596	-648	-362	-702	-502	-617
07 AUG 1100	-502	-591	-649	-357	-703	-499	-612
07 AUG 1200	-503	-582	-649	-348	-703	-496	-604
07 AUG 1300	-504	-577	-649	-342	-703	-493	-598
07 AUG 1400	-508	-575	-649	-340	-703	-494	-597
07 AUG 1500	-506	-569	-646	-334	-701	-489	-591
07 AUG 1600	-496	-567	-644	-332	-699	-487	-589
07 AUG 1635	-499	-570	-647	-338	-702	-487	-592
07 AUG 1700	-499	-569	-647	-337	-698	-483	-591
07 AUG 1800	-495	-568	-643	-339	-695	-483	-594
08 AUG 0925	-504	-600	+0	-369	-692	-495	-628
09 AUG 0900	-511	-606	+0	-372	-699	-510	-630
10 AUG 0850	-537	-615	+0	-380	-711	-530	-635
11 AUG 1000	-535	-612	+0	-383	-718	-534	-627
12 AUG 0900	-537	-616	-669	-388	-724	-533	-630
13 AUG 0750	-536	-613	+0	-390	-728	-535	-626
13 AUG 0900	-536	-609	+0	-390	-728	-535	-622
13 AUG 1000	-535	-609	+0	-390	-731	-535	-622
13 AUG 1100	-535	-609	+0	-387	-727	-535	-622
13 AUG 1200	-535	-610	+0	-387	-727	-531	-618
13 AUG 1300	-532	-606	+0	-386	-727	-531	-618
13 AUG 1400	-531	-606	+0	-383	-727	-527	-614
13 AUG 1500	-528	-606	+0	-382	-723	-526	-618
13 AUG 1615	-532	-610	+0	-386	-728	-527	-618
13 AUG 1700	-533	-607	+0	-387	-724	-528	-618
14 AUG 0740	-531	-611	+0	-391	-723	-525	-626
14 AUG 0900	-527	-611	+0	-387	-719	-525	-618
14 AUG 1000	-519	-600	+0	-376	-714	-517	-611
14 AUG 1100	-507	-589	+0	-361	-709	-512	-603
14 AUG 1200	-505	-581	+0	-360	-710	-510	-598
14 AUG 1320	-514	-587	+0	-359	-707	-508	-593
14 AUG 1415	-503	-580	+0	-341	-697	-493	-593
14 AUG 1515	-501	-578	+0	-341	-696	-492	-592

Table B 7 (cont)
Carlson Gage Readings at Section B 1/4 Point Span 4

Strains (microstrain)

Date	8	9	10	11	12	13	14
05 AUG 0915	-214	-247	-365	+172	+76	+96	+57
05 AUG 1015	-225	-259	-382	+167	+80	+87	+56
05 AUG 1115	-234	-273	-399	+165	+86	+80	+55
05 AUG 1215	-244	-285	-413	+159	+84	+67	+50
05 AUG 1315	-254	-296	-428	+153	+71	+63	+46
05 AUG 1415	-261	-308	-439	+147	+44	+50	+38
05 AUG 1515	-263	-312	-443	+140	+34	+47	+33
05 AUG 1615	-268	-317	-442	+136	+28	+42	+27
07 AUG 0705	-212	-252	-361	+159	+58	+78	+51
07 AUG 0800	-209	-248	-358	+162	+58	+82	+57
07 AUG 0900	-210	-250	-361	+169	+69	+87	+63
07 AUG 1000	-216	-259	-377	+168	+70	+79	+62
07 AUG 1100	-226	-271	-394	+164	+72	+81	+60
07 AUG 1200	-235	-281	-410	+162	+78	+69	+59
07 AUG 1300	-247	-295	-426	+153	+70	+62	+52
07 AUG 1400	-253	-307	-438	+148	+45	+50	+45
07 AUG 1500	-258	-312	-444	+142	+30	+45	+41
07 AUG 1600	-263	-322	-450	+136	+12	+35	+36
07 AUG 1635	-265	-325	-450	+130	+13	+33	+34
07 AUG 1700	-264	-325	-447	+132	+11	+33	+30
07 AUG 1800	-261	-321	-444	+126	+8	+36	+25
08 AUG 0925	-213	-255	-365	+155	+52	+79	+52
09 AUG 0900	-214	-244	-362	+163	+64	+98	+58
10 AUG 0850	-214	-232	-359	+171	+81	+114	+63
11 AUG 1000	-225	-244	-374	+152	+67	+105	+58
12 AUG 0900	-221	-238	-363	+168	+67	+103	+57
13 AUG 0750	-223	-246	-367	+167	+58	+93	+56
13 AUG 0900	-222	-245	-367	+167	+55	+93	+56
13 AUG 1000	-226	-248	-370	+163	+56	+90	+56
13 AUG 1100	-225	-248	-369	+164	+53	+91	+56
13 AUG 1200	-224	-247	-372	+164	+50	+91	+57
13 AUG 1300	-227	-250	-374	+165	+49	+89	+58
13 AUG 1400	-229	-252	-377	+162	+46	+87	+55
13 AUG 1500	-228	-251	-376	+163	+46	+84	+53
13 AUG 1615	-232	-256	-377	+156	+45	+80	+50
13 AUG 1700	-229	-252	-374	+159	+48	+83	+50
14 AUG 0740	-224	-246	-368	+163	+60	+96	+53
14 AUG 0900	-220	-237	-359	+171	+65	+103	+59
14 AUG 1000	-224	-249	-376	+168	+60	+99	+57
14 AUG 1100	-227	-256	-386	+176	+64	+97	+61
14 AUG 1200	-244	-274	-410	+161	+59	+85	+53
14 AUG 1320	-264	-300	-438	+151	+49	+72	+41
14 AUG 1415	-261	-308	-439	+147	+44	+50	+38
14 AUG 1515	-263	-312	-443	+140	+34	+47	+33

Figure B1. Calculated Eigenstresses for Differential Temperature at Casting of Succeeding Stage, Section A

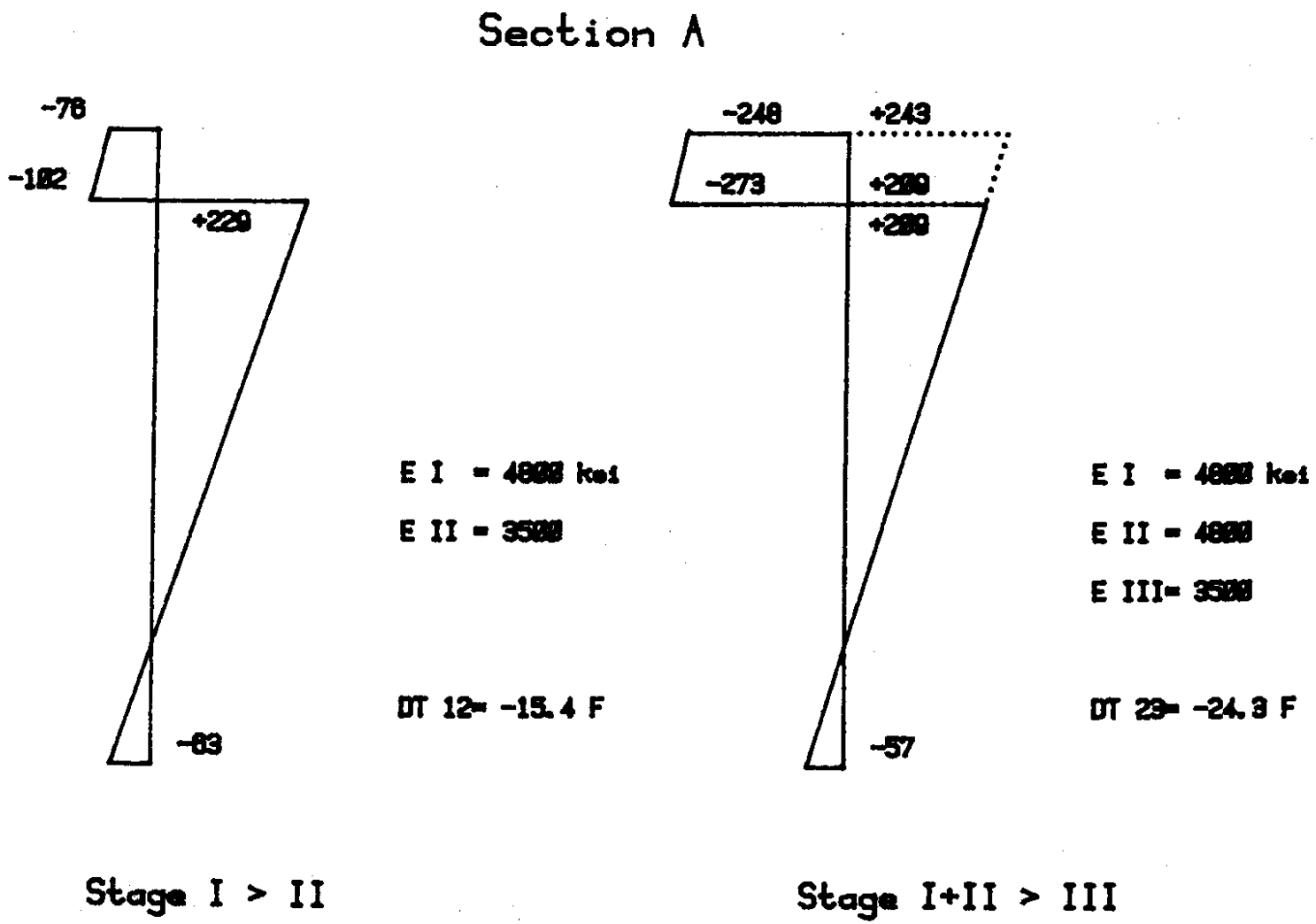

Figure B2. Calculated Eigenstresses for Differential Temperature at Casting of Succeeding Stage, Section B

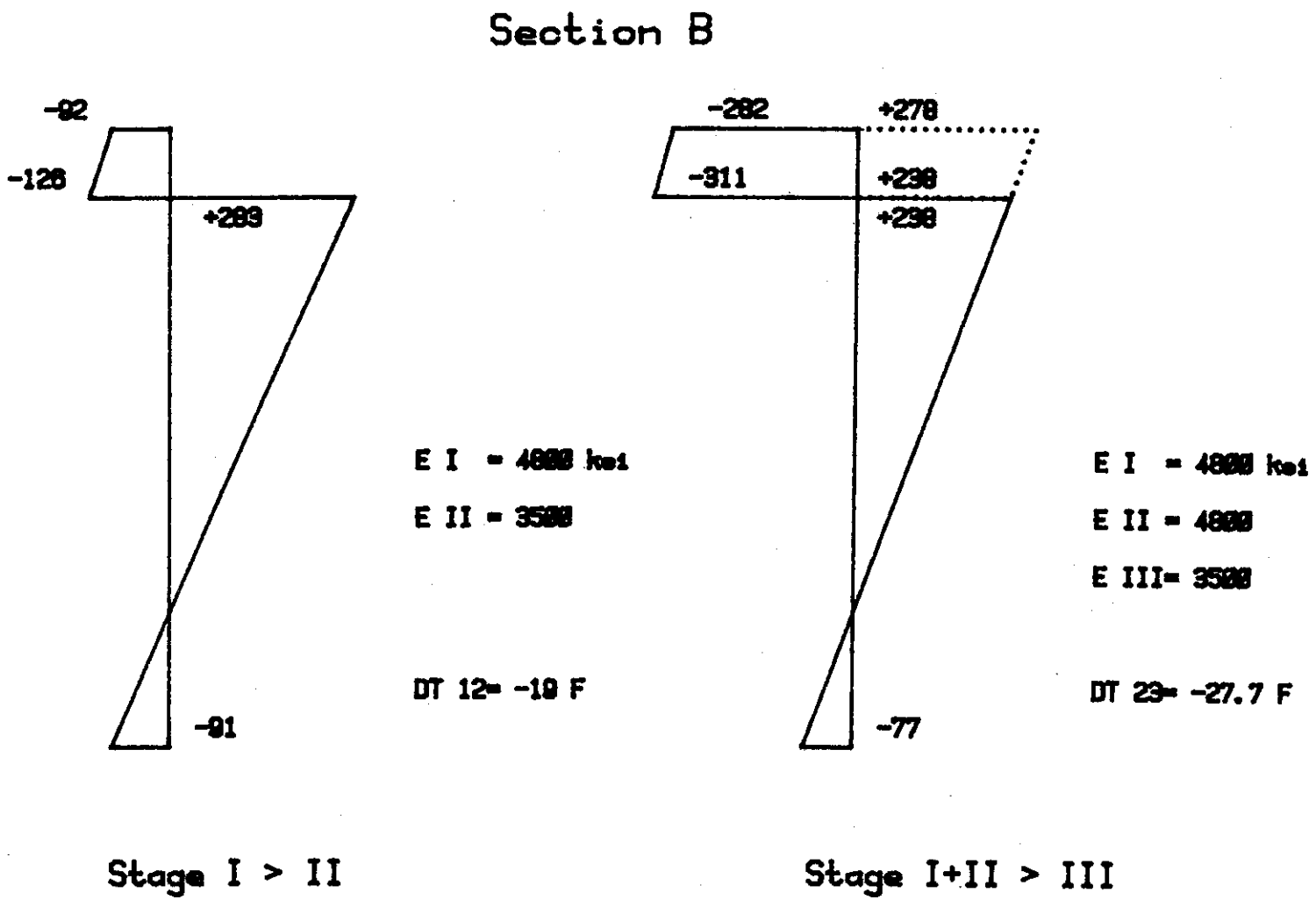

Figure B3. Calculated Eigenstresses for Differential Temperature at Casting of Succeeding Stage, Section C

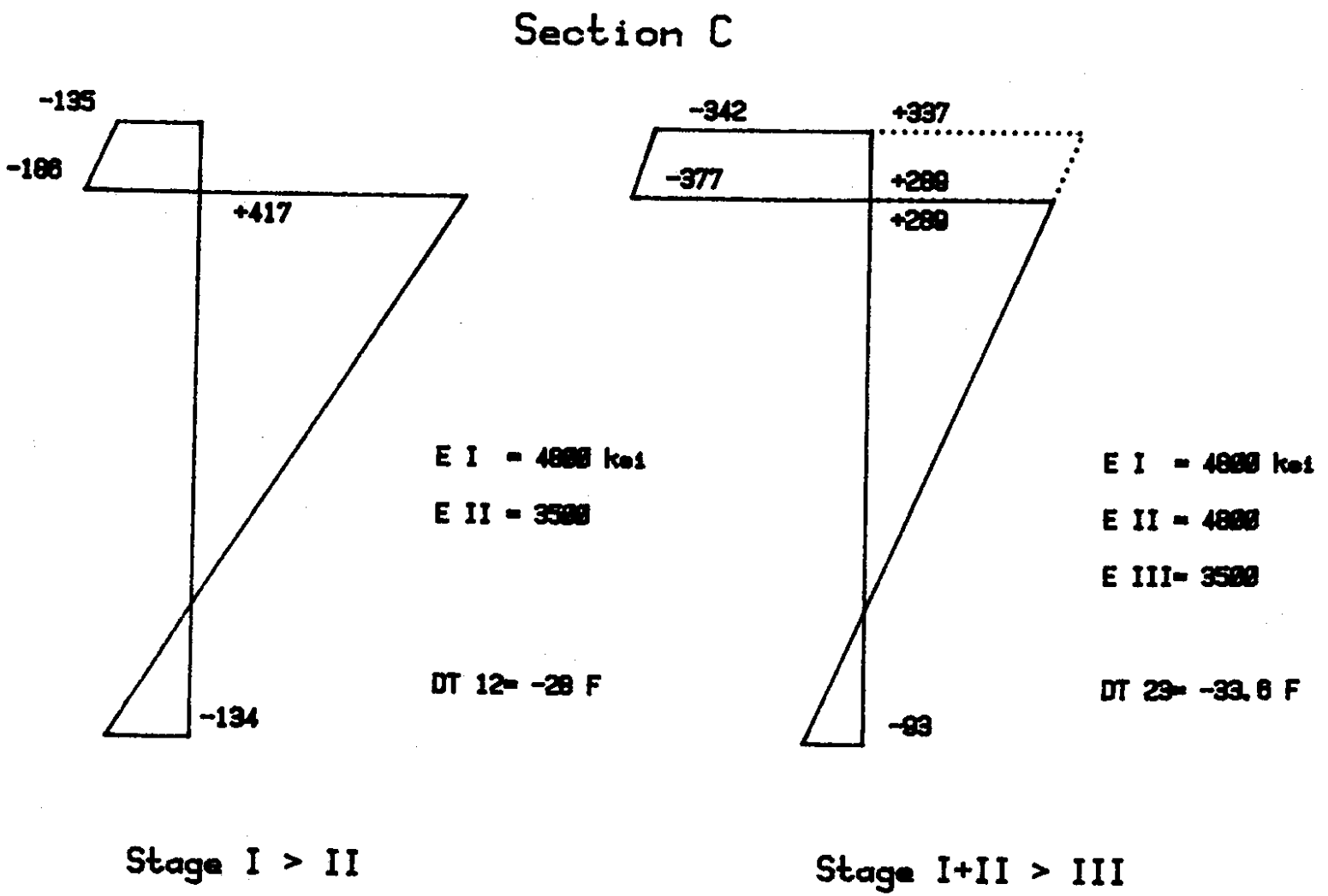

Figure B4. Eigenstresses from CTL Strain Data, Section A

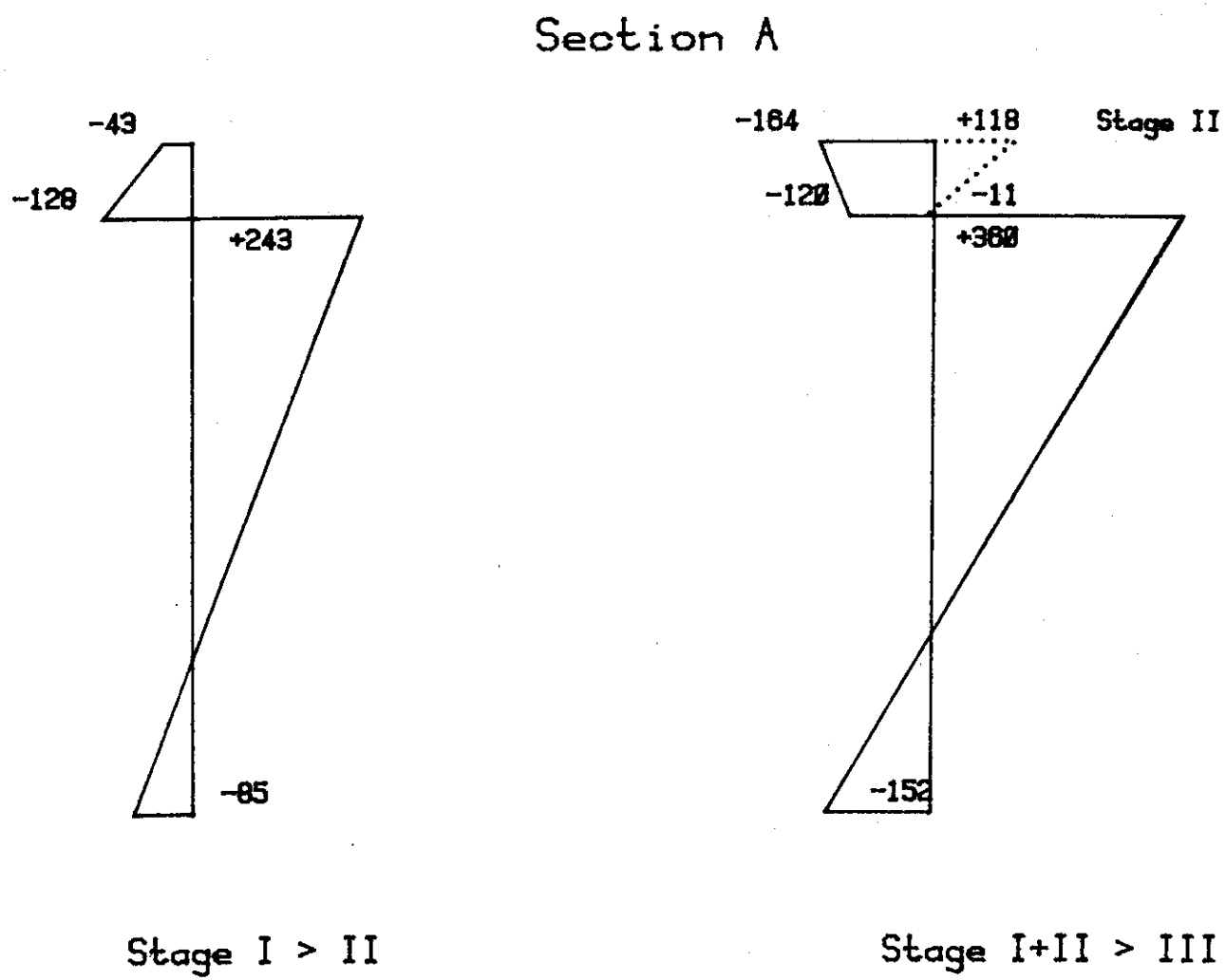

Figure B5. Eigenstresses from CTL Strain Data, Section B

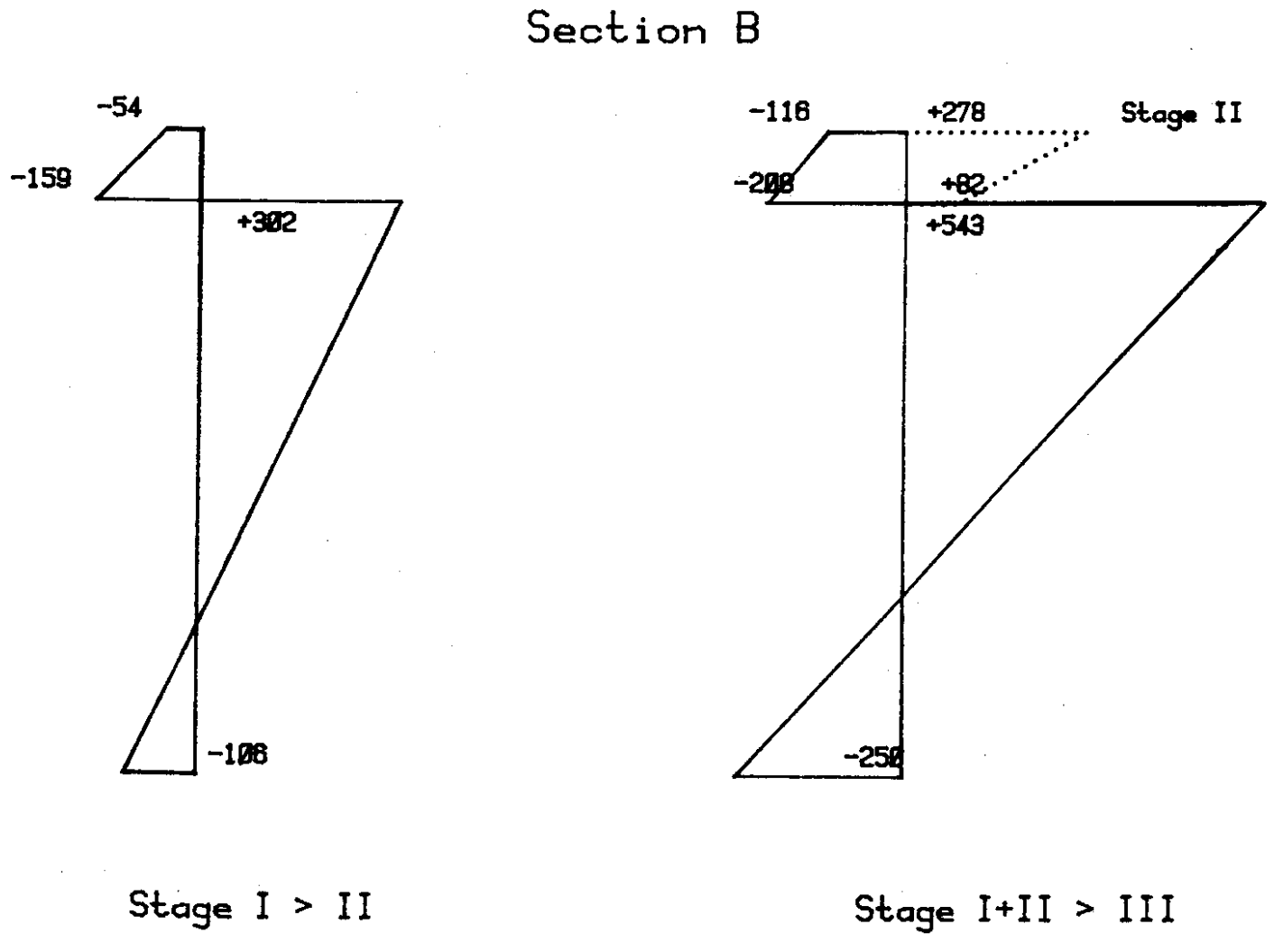

Figure B6. Eigenstresses from CTL Strain Data, Section C

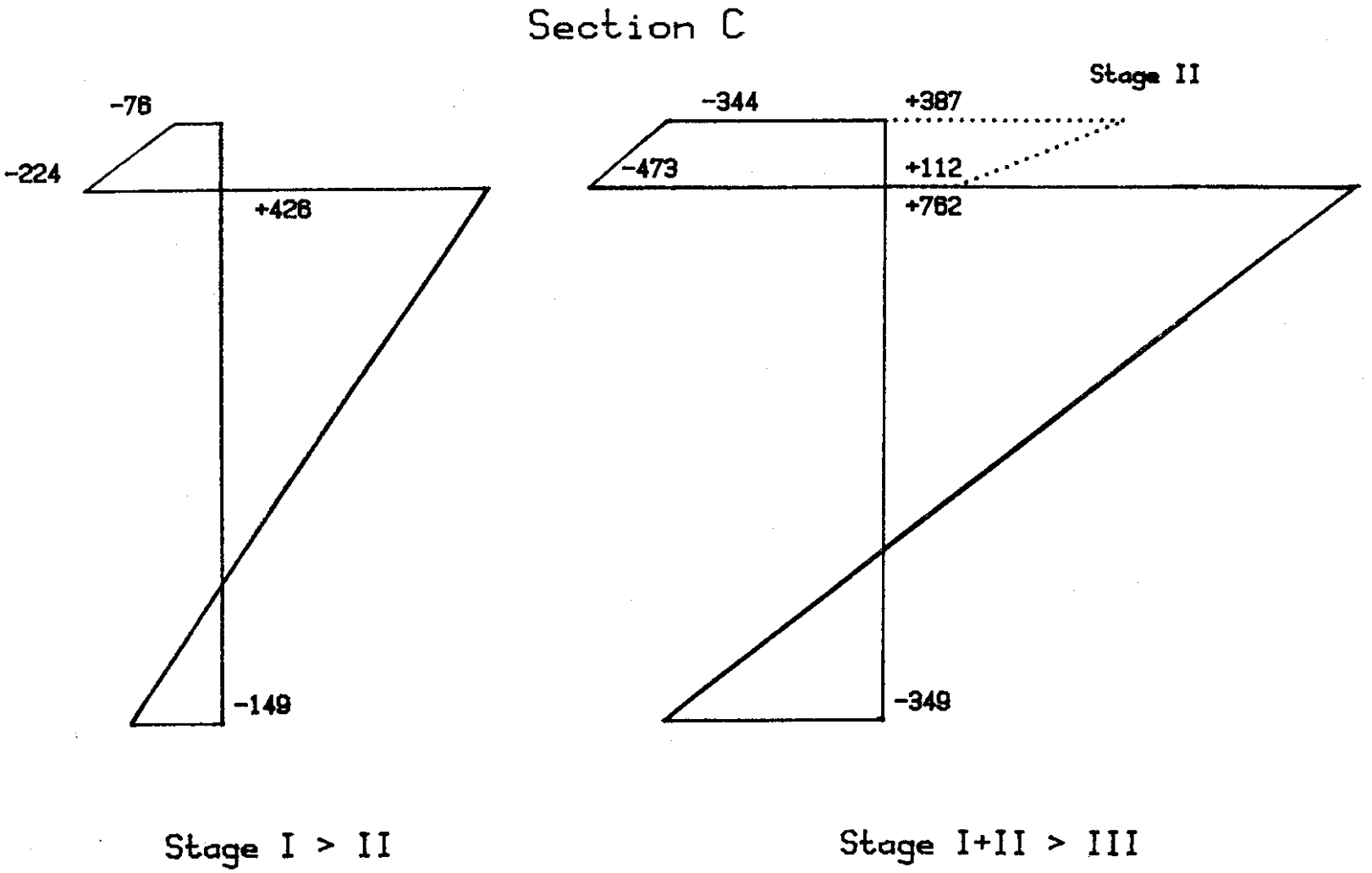

APPENDIX C.

EXPANSION JOINT MOVEMENT DATA

Movements of the superstructure with respect to the abutment were measured at Abutment 1 as shown in Figure 3-17. Interpretation of those data are subject to uncertainties in the location of the fixed point for expansion and contraction as discussed in the body of the report. Figure 3.18 shows the total data set corrected to a constant temperature of 73 degrees F. Figure 3.19 is a plot of the uncorrected data for a period during the present study when clear and sunny weather conditions prevailed. Data were corrected to equivalent movements at 73 degrees F by the following relation:

$$d = d + (73-T)(5E-06)(x) \qquad \text{where}$$

d = distance at constant temperature of 73 degrees F

d = distance at temperature of T degrees F

x = distance from Abut 1 to fixed point = 672 ft = 205 m for measurements after December 1978

This Appendix lists measured values for the superstructure movements and the same values, corrected as described above, to a temperature of 73 degrees F. The columns headed "Difference" are the changes from the previous readings.

Table C 1

Expansion joint movement at Abutment No 1

Date	Day	Temp	Measured Distance		Distance at 73 Deg F		Difference* in Distance	
		Deg F	East mm	West mm	East mm	West mm	East mm	West mm
20 Aug 77	-269	60	57	57	47	47		
16 Nov 77	-181	32	54	67	21	34	-26	-13
12 Dec 77	-155	35	57	70	26	39	5	5
20 Dec 77	-147	30	64	76	29	41	3	2
06 Jan 78	-130	25	76	86	37	47	8	6
23 Jan 78	-113	30	76	83	41	48	4	1
06 Feb 78	-99	35	76	86	45	55	4	7
22 Feb 78	-83	40	79	86	52	59	7	4
13 Mar 78	-64	34	79	86	48	55	-4	-4
04 Apr 78	-42	40	76	89	49	62	1	7
14 Dec 78	212	35	133		94		45	
08 Jan 79	237	10	152	156	88	92	-6	
26 Jan 79	255	28	133		87		-1	
22 Feb 79	282	29	127		82		-5	
20 Dec 79	583	35	140		101		19	
21 Apr 80	706	45	127		98		-3	
16 Nov 80	884	40	129		95		-3	
13 Jan 81	973	40	132		98		3	
16 Nov 81	1249	50	127		104		6	
09 Jul 82	1518	65	112	123	104	115	0	
12 Jul 82	1521	70	98	108	95	105	-9	-10
15 Jul 82	1524	53	118	131	98	111	3	6
16 Jul 82	1525	52	123	134	102	113	4	2
17 Jul 82	1526	58	115	125	100	110	-2	-3
18 Jul 82	1527	62	109	120	98	109	-2	-1
19 Jul 82	1528	61	109	120	97	108	-1	-1
20 Jul 82	1529	63	107	118	97	108	0	0
21 Jul 82	1530	60	110	121	97	108	0	0
22 Jul 82	1531	56	117	127	100	110	3	2
23 Jul 82	1532	58	115	126	100	111	0	1
24 Jul 82	1533	62	110	121	99	110	-1	-1
25 Jul 82	1534	67	104	115	98	109	-1	-1
26 Jul 82	1535	70	100	111	97	108	-1	-1
27 Jul 82	1536	74	94	104	95	105	-2	-3
28 Jul 82	1537	73	93	105	93	105	-2	0
29 Jul 82	1538	68	99	110	94	105	1	0
30 Jul 82	1539	64	104	115	95	106	1	1
31 Jul 82	1540	60	112	122	99	109	4	3
01 Aug 82	1541	56	118	128	101	111	2	2

* Difference from previous reading at 73 deg F

Table C 1 (cont)

Expansion joint movement at Abutment No 1

Date	Day	Temp	Measured Distance		Distance at 73 Deg F		Difference* in Distance	
			East	West	East	West	East	West
		Deg F	mm	mm	mm	mm	mm	mm
01 Aug 82	1542	54	122	132	103	113	2	2
03 Aug 82	1543	55	120	131	102	113	-1	0
04 Aug 82	1544	57	113	123	97	107	-5	-6
05 Aug 82	1545	58	116	127	101	112	4	5
07 Aug 82	1547	66	106	117	99	110	-2	-2
08 Aug 82	1548	71	98	109	96	107	-3	-3
09 Aug 82	1549	68	102	112	97	107	1	0
10 Aug 82	1550	61	111	122	99	110	2	3
11 Aug 82	1551	58	116	127	101	112	2	2
12 Aug 82	1552	54	119	130	100	111	-1	-1
13 Aug 82	1553	55	121	132	103	114	3	3
14 Aug 82	1554	53	123	134	103	114	0	0

* Difference from previous reading at 73 deg F

APPENDIX D

CREEP AND SHRINKAGE DATA FROM CTL REPORT

List of Tables

APPENDIX D.

CREEP AND SHRINKAGE DATA PLOTS

Data presented in Appendix B to the CTL report are retabulated herein and specific creep values are converted to creep factors (i.e., ratio of creep to elastic strain). The creep factors were normalized as discussed in the main body of this report. The resulting creep factors are plotted with time on a logarithmic scale. Shrinkage data from Appendix B to the CTL report are also retabulated and plotted. In addition, data comparing the shrinkage measured from the shrinkage specimens is compared to shrinkage data from the companion specimens to the creep specimens.

Table D-1

Analysis of CTL creep data
Stage I concrete loaded at 4 days to 1200 psi
Modulus of Elasticity calculated from this data 3774 ksi

Calculation of creep coefficient for loading at t and at 28 days

Load Dur'n	Total Strain	Shrink Strain	Creep Strain	Creep Coefficient for Load at 4	Load at 28
0	318	0	318	0.000	0.000
1	456	33	423	.330	.165
2	513	66	447	.406	.203
3	559	91	468	.472	.236
6	656	128	528	.660	.330
8	708	153	555	.745	.373
10	771	171	600	.887	.444
17	873	223	650	1.044	.522
28	1003	293	710	1.233	.617
31	1013	306	707	1.223	.612
37	1057	332	725	1.280	.640
45	1100	357	743	1.336	.668
52	1140	383	757	1.381	.690
65	1206	426	780	1.453	.727
94	1318	476	842	1.648	.824
122	1384	494	890	1.799	.900
150	1463	546	917	1.884	.942
171	1496	559	937	1.947	.974
195	1503	556	947	1.978	.989
218	1524	564	960	2.019	1.010
250	1561	588	973	2.060	1.030
275	1576	593	983	2.091	1.046
313	1576	581	995	2.129	1.065
334	1624	626	998	2.138	1.069
359	1641	629	1012	2.182	1.092
390	1656	631	1025	2.223	1.112
420	1670	631	1039	2.267	1.134
811	1673	581	1092	2.434	1.217

Table D-2

Analysis of CTL creep data
Stage I concrete loaded at 27 days to 1900 psi
Modulus of Elasticity calculated from this data 4910 ksi

Calculation of creep coefficient for loading at t and at 28 days

Load Dur'n	Total Strain	Shrink Strain	Creep Strain	Creep Coefficient for Load at 27	Load at 28
0	387	0	387	0.000	0.000
1	583	0	583	.506	.502
5	755	29	726	.876	.869
6	763	25	738	.907	.900
7	797	39	758	.959	.951
8	814	43	771	.992	.984
11	865	49	816	1.109	1.099
13	891	60	831	1.147	1.138
14	904	69	835	1.158	1.148
22	987	94	893	1.307	1.297
29	1053	119	934	1.413	1.402
36	1129	149	980	1.532	1.520
42	1180	163	1017	1.628	1.615
71	1350	213	1137	1.938	1.922
99	1457	231	1226	2.168	2.150
127	1567	283	1284	2.318	2.299
148	1614	296	1318	2.406	2.386
172	1639	293	1346	2.478	2.458
196	1665	301	1364	2.525	2.504
228	1722	324	1398	2.612	2.591
253	1737	329	1408	2.638	2.617
291	1750	318	1432	2.700	2.678
312	1805	363	1442	2.726	2.704
337	1825	366	1459	2.770	2.747
368	1850	368	1482	2.829	2.806
398	1874	368	1506	2.891	2.868
789	1920	318	1602	3.140	3.114

Table D-3

Analysis of CTL creep data
Stage I concrete loaded at 90 days to 2000 psi
Modulus of Elasticity calculated from this data 3953 ksi

Calculation of creep coefficient for loading at t and at 28 days

Load Dur'n	Total Strain	Shrink Strain	Creep Strain	Creep Coefficient for Load at 90	Load at 28
0	506	0	506	0.000	0.000
1	581	-12	593	.172	.256
5	670	2	668	.320	.477
6	670	-8	678	.340	.506
8	725	18	707	.397	.591
15	837	34	803	.587	.874
22	921	48	873	.725	1.080
29	975	60	915	.808	1.203
36	1008	36	972	.921	1.371
64	1161	88	1073	1.121	1.668
85	1208	101	1107	1.188	1.768
109	1256	98	1158	1.289	1.918
133	1306	106	1200	1.372	2.042
165	1351	130	1221	1.413	2.103
190	1368	135	1233	1.437	2.139
228	1385	123	1262	1.494	2.224
249	1450	168	1282	1.534	2.283
274	1466	171	1295	1.559	2.321
305	1478	173	1305	1.579	2.351
335	1521	173	1348	1.664	2.477
726	1580	123	1457	1.879	2.798

Table D-4

Analysis of CTL creep data
Stage II concrete loaded at 5 days to 1500 psi
Modulus of Elasticity calculated from this data 4934 ksi

Calculation of creep coefficient for loading at t and at 28 days

Load Dur'n	Total Strain	Shrink Strain	Creep Strain	Creep Coefficient for Load at 5	Load at 28
0	304	0	304	0.000	0.000
1	465	26	439	.444	.243
2	522	38	484	.592	.324
3	557	56	501	.648	.355
4	571	72	499	.641	.351
8	625	114	511	.681	.373
10	677	135	542	.783	.429
11	689	140	549	.806	.441
14	729	164	565	.859	.470
17	770	180	590	.941	.515
25	837	214	623	1.049	.574
32	901	248	653	1.148	.628
39	951	274	677	1.227	.672
45	990	288	702	1.309	.717
74	1109	360	749	1.464	.801
102	1186	388	798	1.625	.890
130	1271	440	831	1.734	.949
151	1316	468	848	1.789	.980
175	1322	463	859	1.826	.999
199	1361	475	886	1.914	1.048
231	1401	505	896	1.947	1.066
256	1414	518	896	1.947	1.066
294	1417	513	904	1.974	1.080
315	1476	571	905	1.977	1.082
340	1489	546	943	2.102	1.151
371	1509	570	939	2.089	1.144
401	1519	568	951	2.128	1.165
792	1536	528	1008	2.316	1.268

Table D-5

Analysis of CTL creep data
Stage II concrete loaded at 28 days to 1200 psi
Modulus of Elasticity calculated from this data 4563 ksi

Calculation of creep coefficient for loading at t and at 28 days

Load Dur'n	Total Strain	Shrink Strain	Creep Strain	Creep Coefficient for Load at 28	Load at 28
0	263	0	263	0.000	0.000
1	342	9	333	.266	.266
2	365	0	365	.388	.388
9	480	35	445	.692	.692
14	518	47	471	.791	.791
16	539	60	479	.821	.821
20	555	60	495	.882	.882
22	573	75	498	.894	.894
26	600	88	512	.947	.947
30	618	98	520	.977	.977
37	646	120	526	1.000	1.000
44	647	105	542	1.061	1.061
72	758	188	570	1.167	1.167
100	841	245	596	1.266	1.266
107	835	226	609	1.316	1.316
128	865	255	610	1.319	1.319
152	868	250	618	1.350	1.350
176	893	261	632	1.403	1.403
208	938	291	647	1.460	1.460
233	948	305	643	1.445	1.445
271	961	300	661	1.513	1.513
292	1008	358	650	1.471	1.471
317	1025	333	692	1.631	1.631
348	1053	356	697	1.650	1.650
378	1061	355	706	1.684	1.684
769	1089	315	774	1.943	1.943

Table D-6

Analysis of CTL creep data
Stage II concrete loaded at 91 days to 2000 psi
Modulus of Elasticity calculated from this data 4386 ksi

Calculation of creep coefficient for loading at t and at 28 days

Load Dur'n	Total Strain	Shrink Strain	Creep Strain	Creep Coefficient for Load at 91	Load at 28
0	456	0	456	0.000	0.000
1	570	47	523	.147	.220
2	586	25	561	.230	.344
6	660	25	635	.393	.587
7	695	62	633	.388	.580
9	680	34	646	.417	.623
16	748	20	728	.596	.891
26	841	59	782	.715	1.068
30	900	80	820	.798	1.193
37	918	90	828	.816	1.219
44	936	72	864	.895	1.337
65	996	100	896	.965	1.442
89	1048	95	953	1.090	1.629
113	1091	98	993	1.178	1.760
145	1146	128	1018	1.232	1.842
170	1166	141	1025	1.248	1.865
208	1200	136	1064	1.333	1.993
229	1265	195	1070	1.346	2.012
254	1278	170	1108	1.430	2.137
285	1305	193	1112	1.439	2.150
315	1325	191	1134	1.487	2.222
706	1431	151	1280	1.807	2.700

Table D-7

Analysis of CTL creep data
Stage III concrete loaded at 8 days to 1200 psi
Modulus of Elasticity calculated from this data 4428 ksi

Calculation of creep coefficient for loading at t and at 28 days

Load Dur'n	Total Strain	Shrink Strain	Creep Strain	Creep Coefficient for Load at 8	Load at 28
0	271	0	271	0.000	0.000
1	355	9	346	.277	.181
2	405	11	394	.454	.297
3	430	33	397	.465	.304
6	476	29	447	.649	.425
8	537	88	449	.657	.430
10	569	98	471	.738	.483
17	667	148	519	.915	.599
24	712	180	532	.963	.631
31	764	185	579	1.137	.744
59	932	287	645	1.380	.904
80	1004	332	672	1.480	.969
104	1049	342	707	1.609	1.053
128	1089	367	722	1.664	1.090
160	1170	400	770	1.841	1.206
185	1174	418	756	1.790	1.172
223	1195	415	780	1.878	1.230
244	1255	470	785	1.897	1.242
269	1267	464	803	1.963	1.285
300	1290	470	820	2.026	1.326
330	1364	470	894	2.299	1.505
721	1346	430	916	2.380	1.558

Table D-8

Analysis of CTL creep data
Stage III concrete loaded at 29 days to 2000 psi
Modulus of Elasticity calculated from this data 4444 ksi

Calculation of creep coefficient for loading at t and at 28 days

Load Dur'n	Total Strain	Shrink Strain	Creep Strain	Creep Coefficient for Load at 29	Load at 28
0	450	0	450	0.000	0.000
1	623	40	583	.296	.300
2	641	6	635	.411	.417
3	670	15	655	.456	.463
20	781	20	761	.691	.702
30	918	76	842	.871	.885
34	980	106	874	.942	.957
41	1028	126	902	1.004	1.020
69	1180	166	1014	1.253	1.273
93	1260	176	1084	1.409	1.431
117	1343	201	1142	1.538	1.561
149	1435	235	1200	1.667	1.692
174	1471	253	1218	1.707	1.733
212	1533	250	1283	1.851	1.880
233	1571	305	1266	1.813	1.841
258	1613	299	1314	1.920	1.950
289	1656	304	1352	2.004	2.035
319	1681	304	1377	2.060	2.092
710	1785	265	1520	2.378	2.414

Table D-9

Analysis of CTL creep data
Stage III concrete loaded at 92 days to 2000 psi
Modulus of Elasticity calculated from this data 4348 ksi

Calculation of creep coefficient for loading at t and at 28 days

Load Dur'n	Total Strain	Shrink Strain	Creep Strain	Creep Coefficient for Load at 92	Load at 28
0	460	0	460	0.000	0.000
1	545	0	545	.185	.277
1	545	0	545	.185	.277
2	568	-6	574	.248	.372
3	596	3	593	.289	.434
6	641	5	636	.383	.574
10	663	5	658	.430	.646
20	725	6	719	.563	.845
27	776	10	766	.665	.998
44	846	31	815	.772	1.158
76	966	65	901	.959	1.438
101	1015	83	932	1.026	1.539
139	1061	80	981	1.133	1.699
160	1150	135	1015	1.207	1.810
185	1173	129	1044	1.270	1.905
216	1218	134	1084	1.357	2.035
246	1250	134	1116	1.426	2.139
637	1378	95	1283	1.789	2.684

Table D10

Analysis of CTL shrinkage data
Stage I concrete loaded at 4 days to 1200 psi

Comparison of shrinkage from creep data with basic shrinkage data

Age	Load Dur'n	Creep Data	Shrink Data	Ratio c/s
5	1	33	6	5.249
6	2	66	17	3.883
7	3	91	35	2.628
10	6	128	62	2.063
12	8	153	78	1.953
14	10	171	94	1.818
21	17	223	141	1.577
32	28	293	201	1.460
35	31	306	209	1.466
41	37	332	239	1.391
49	45	357	264	1.352
56	52	383	294	1.302
69	65	426	326	1.305
98	94	476	378	1.260
126	122	494	395	1.251
154	150	546	442	1.235
175	171	559	452	1.236
199	195	556	451	1.233
222	218	564	460	1.226
254	250	588	482	1.219
279	275	593	485	1.222
317	313	581	483	1.202
338	334	626	520	1.204
363	359	629	523	1.203
394	390	631	525	1.203
424	420	631	527	1.197

Table D11

Analysis of CTL shrinkage data
Stage I concrete loaded at 27 days to 1900 psi

Comparison of shrinkage from creep data with basic shrinkage data

Age	Load Dur'n	Creep Data	Shrink Data	Ratio c/s
28	1	0	7	0.000
32	5	29	22	1.324
33	6	25	24	1.046
34	7	39	26	1.509
35	8	43	32	1.347
38	11	49	49	.995
40	13	60	56	1.075
41	14	69	59	1.170
49	22	94	84	1.115
56	29	119	114	1.040
63	36	149	136	1.098
69	42	163	147	1.112
98	71	213	198	1.076
126	99	231	215	1.075
154	127	283	262	1.080
175	148	296	272	1.087
199	172	293	271	1.080
223	196	301	281	1.071
255	228	324	303	1.070
280	253	329	305	1.078
318	291	318	306	1.040
339	312	363	340	1.066
364	337	366	343	1.067
395	368	368	345	1.067
425	398	368	348	1.057

Table D12

Analysis of CTL shrinkage data
Stage I concrete loaded at 90 days to 2000 psi

Comparison of shrinkage from creep data with basic shrinkage data

Age	Load Dur'n	Creep Data	Shrink Data	Ratio c/s
91	1	-12	3	-4.064
95	5	2	22	.091
96	6	-8	24	-.335
98	8	18	29	.631
105	15	34	43	.783
112	22	48	56	.850
119	29	60	48	1.238
126	36	36	45	.793
154	64	88	92	.955
175	85	101	102	.989
199	109	98	101	.969
223	133	106	111	.956
255	165	130	133	.981
280	190	135	135	1.000
318	228	123	136	.907
339	249	168	170	.986
364	274	171	173	.988
395	305	173	175	.990
425	335	173	178	.972

Table D13

Analysis of CTL shrinkage data
Stage II concrete loaded at 5 days to 1500 psi

Comparison of shrinkage from creep data with basic shrinkage data

Age	Load Dur'n	Creep Data	Shrink Data	Ratio c/s
6	1	26	11	2.353
7	2	38	20	1.864
8	3	56	28	1.966
9	4	72	40	1.820
13	8	114	71	1.603
15	10	135	84	1.604
16	11	140	89	1.565
19	14	164	107	1.538
22	17	180	123	1.468
30	25	214	151	1.415
37	32	248	174	1.421
44	39	274	196	1.401
50	45	288	217	1.329
79	74	360	281	1.282
107	102	388	320	1.212
135	130	440	361	1.219
156	151	468	381	1.227
180	175	463	380	1.219
204	199	475	394	1.204
236	231	505	422	1.196
261	256	518	432	1.200
299	294	513	442	1.162
320	315	571	480	1.189
345	340	546	464	1.175
376	371	570	484	1.177
406	401	568	486	1.168

Table D14

Analysis of CTL shrinkage data
Stage II concrete loaded at 28 days to 1200 psi

Comparison of shrinkage from creep data with basic shrinkage data

Age	Load Dur'n	Creep Data	Shrink Data	Ratio c/s
29	1	9	-5	-1.997
30	2	0	7	0.000
37	9	35	39	.897
42	14	47	55	.856
44	16	60	61	.982
48	20	60	75	.798
50	22	75	82	.920
54	26	88	98	.897
58	30	98	116	.848
65	37	120	133	.902
72	44	105	146	.720
100	72	188	196	.958
128	100	245	213	1.152
135	107	226	226	1.000
156	128	255	257	.993
180	152	250	265	.944
204	176	261	266	.981
236	208	291	284	1.024
261	233	305	297	1.026
299	271	300	292	1.027
320	292	358	303	1.180
345	317	333	334	.996
376	348	356	337	1.056
406	378	355	338	1.050

Table D15

Analysis of CTL shrinkage data
Stage II concrete loaded at 91 days to 2000 psi

Comparison of shrinkage from creep data with basic shrinkage data

Age	Load Dur'n	Creep Data	Shrink Data	Ratio c/s
92	1	47	-11	-4.273
93	2	25	1	20.460
97	6	25	22	1.121
98	7	62	25	2.520
100	9	34	29	1.177
107	16	20	44	.458
117	26	59	51	1.149
121	30	80	38	2.123
128	37	90	46	1.970
135	44	72	59	1.222
156	65	100	90	1.115
180	89	95	98	.971
204	113	98	99	.989
236	145	128	117	1.093
261	170	141	130	1.083
299	208	136	125	1.086
320	229	195	136	1.430
345	254	170	167	1.016
376	285	193	170	1.135
406	315	191	171	1.117

Table D16

Analysis of CTL shrinkage data
Stage III concrete loaded at 8 days to 1200 psi

Comparison of shrinkage from creep data with basic shrinkage data

Age	Load Dur'n	Creep Data	Shrink Data	Ratio c/s
9	1	9	6	1.577
10	2	11	21	.524
11	3	33	24	1.401
14	6	29	46	.625
16	8	88	61	1.443
18	10	98	69	1.417
25	17	148	100	1.480
32	24	180	132	1.365
39	31	185	157	1.182
67	59	287	206	1.393
88	80	332	279	1.190
112	104	342	312	1.096
136	128	367	334	1.097
168	160	400	350	1.142
193	185	418	358	1.167
231	223	415	391	1.061
252	244	470	402	1.169
277	269	464	401	1.157
308	300	470	438	1.073
338	330	470	434	1.083

Table D17

Analysis of CTL shrinkage data
Stage III concrete loaded at 29 days to 2000 psi

Comparison of shrinkage from creep data with basic shrinkage data

Age	Load Dur'n	Creep Data	Shrink Data	Ratio c/s
30	1	40	15	2.667
31	2	6	18	.333
32	3	15	20	.748
49	20	20	84	.237
59	30	76	125	.607
63	34	106	134	.791
70	41	126	148	.854
98	69	166	197	.841
122	93	176	206	.853
146	117	201	251	.800
178	149	235	270	.870
203	174	253	271	.934
241	212	250	293	.854
262	233	305	302	1.009
287	258	299	301	.993
318	289	304	304	1.000
348	319	304	340	.895

Table D18

Analysis of CTL shrinkage data
Stage III concrete loaded at 92 days to 2000 psi

Comparison of shrinkage from creep data with basic shrinkage data

Age	Load Dur'n	Creep Data	Shrink Data	Ratio c/s
93	1	0	14	0.000
93	1	0	14	0.000
94	2	-6	27	-.222
95	3	3	30	.101
98	6	5	36	.138
102	10	5	45	.110
112	20	6	64	.093
119	27	10	54	.184
136	44	31	72	.429
168	76	65	108	.600
193	101	83	107	.774
231	139	80	124	.643
252	160	135	139	.970
277	185	129	143	.900
308	216	134	133	1.004
338	246	134	177	.755

APPENDIX E.

OBSERVATIONS, FINDINGS AND RECOMMENDATIONS OF CTL REPORT

AND SELECTED EXTRACTS FROM CTL REPORT

Report to

STATE OF WASHINGTON
DEPARTMENT OF TRANSPORTATION
Agreement Y-1837

INSTRUMENTATION OF

DENNY CREEK BRIDGE

by

K. N. Shiu
J. D. Aristizabal-Ochoa
H. G. Russell

Submitted by

CONSTRUCTION TECHNOLOGY LABORATORIES
A Division of the Portland Cement Association
5420 Old Orchard Road
Skokie, Illinois 60077

August 1981

TABLE OF CONTENTS

TABLE OF CONTENTS (continued)

Observations

1. In the first 100 days, longitudinal deformations in the bridge were caused primarily by instantaneous strains.
2. After the casting of Stage III, measured strains indicated that the bridge behaved as a monolithic homogeneous structure.
3. Temperature differentials as large as 5°F were measured across construction joints.
4. Large shear lag strains were recorded in the bottom slab of the box girder especially at Section A. The measured strains at the corners of the bottom slab were substantially larger than those measured at the center of the slab.
5. For Stage I, approximately 90% of the measured deformations at 500 days were instantaneous strains. For Stages II and III, creep and shrinkage strains made up more than 50% of the total deformation.
6. In the first 200 days, small tensile strains were recorded in Stage III construction at Bridge Section C. Subsequently, tensile strains decreased steadily. At age 500 days, all strain meters indicated compressive strains in concrete.
7. Field data measured with Carlson strain meters at each section yielded consistent strain histories.

Findings

1. Strains caused by temperature induced stresses had to be considered in determining the total calculated strain.
2. Temperature gradients occurred across construction joints when concrete of a new stage was placed. Consequently, internal stresses were induced as the concrete temperatures became equalized. When the temperature gradients were higher than 30F, induced temperature stresses were probably large enough to exceed the tensile strength of the concrete.
3. Strain differentials between the corners and the midsection of the bottom slab occurred at all instrumented sections. However, differentials were less for sections further away from the pier. This effect was attributed to the presence of prestressing tendons in the bottom slabs in sections away from the pier. No prestressing was located in the bottom slab close to the pier.
4. A simplified method of analysis was used to calculate deformations caused by creep, shrinkage, and temperature. With the exception of strains at the corners of the bottom slab, excellent agreement between measured and calculated values was obtained.
5. Based on comparison between measured and calculated strain histories, it can be concluded that stress levels in the Denny Creek Bridge were reasonably predicted by the designer's stress analysis. However,

temperature-induced stresses were not considered. Temperature-induced stresses between 475 psi tension and 426 psi compression were calculated from measured temperature differentials.

Recommendations

Based on the results and findings of this investigation, the following recommendations are made for design of bridges by the three stage method of construction.

1. Use of concretes with comparable elastic properties will minimize strain or stress redistribution within cross-sections.
2. Since instantaneous strains are a major portion of the total deformation, accurate estimates of dead weight and post-tensioning stresses are necessary to accurately predict deformations in the bridge.
3. Attention and care should be given to control of concrete temperature during casting. Temperature of concrete to be placed should be as close as practical to the temperature of the old concrete. In addition, heat of hydration should also be considered. If large temperature differentials are unavoidable, analyses should be made to determine the effect of the temperature differentials.
4. Collecting of field data should continue since very little information about long-term creep and shrinkage behavior of box girders exists at present.

5. The information contained in this report should be developed into a procedure that can be used directly for design of other bridges.

TABLE 1 - SEQUENCE OF FIELD READINGS

Reading No.	Date	Event	Time Days
		Stage I	
1	May 16, 78	Zero reading before first post-tensioning	0
2	" 19, "	After post-tensioning	3
3	" 24, "	Truss moved to next span, 250 kip load on	8
4	" 30, "	One day prior to Stage II casting of Span 4	14
		Stages I and II	
5	June 1, 78	One day after casting Stage II of Span 4	16
6	" 5, "	Just prior to post-tensioning Stage II of Span 4	20
7	" 5, "	Just after post-tensioning Stage II of Span 4	20
8	" 6, "	Truss load on cantilever	21
9	" 9, "	After casting Stage I of Span 5	24
10	" 14, "	After post-tensioning Stage I of Span 5	29
11	" 19, "	After moving truss from Span 5, 250 kip load on	34
12	" 22, "	Before casting Stage II of Span 5	37
13	" 22, "	After casting Stage II of Span 5	37
14	" 26, "	Before post-tensioning Stage II of Span 5	41
15	" 27, "	After post-tensioning Stage II of Span 5	42
16	July 5, "	Before casting Stage IIIA of Span 3	50
17	" 6, "	After casting Stage IIIA of Span 3	51
18	" 19, "	Before casting Stage IIIB of Span 3	64
19	" 20, "	After casting Stage IIIB of Span 3	65
20	Aug. 7, "	Before casting Stage IIIA of Span 4	83
		Stages I, II and III	
21	" 8, 78	After casting Stage IIIA of Span 4	84
22	" 10, "	After post-tensioning Stage IIIA of Span 4	86
23	" 18, "	Before casting Stage IIIB of Span 4	94
24	" 19, "	After casting Stage IIIB of Span 4	95
25	" 21, "	Before post-tensioning Stage IIIB of Span 4	97
26	" 24, "	After post-tensioning Stage IIIB of Span 4	100
27	Sept. 18, "	Before casting Stage IIIA of Span 5	125
28	" 20, "	After casting Stage IIIA of Span 5	127
29	Oct. 3, "	Before casting Stage IIIB of Span 5	140
30	" 13, "	After casting Stage IIIB of Span 5	150
31	Dec. 13, "	After winter shutdown of 1978	211
32	April 26, 79	Restart work of 1979	345
33	July 26, "		436
34	Oct. 19, "		520
35	Jan. 23, 80		616
36	April 24, 80		708
37	Aug. 1, 80		806

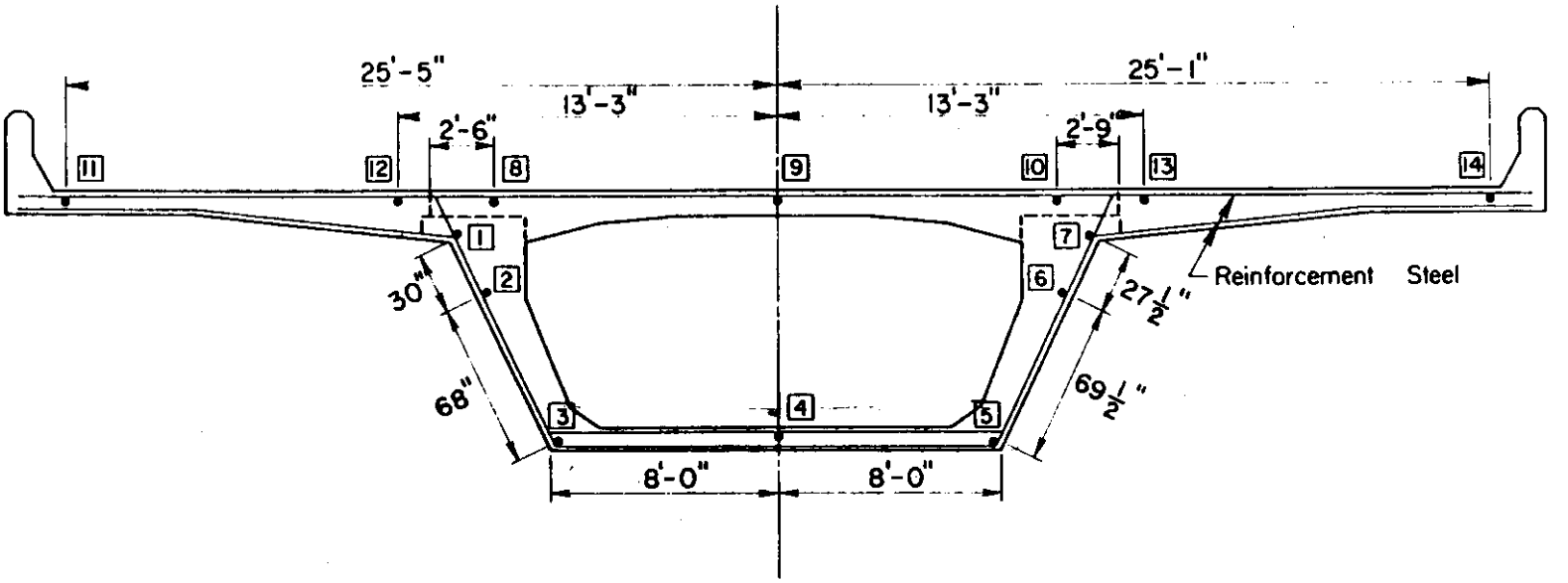

Note: All Strain Gages were Tied to Reinforcement Cage

Fig. A1 - Locations of Carlson Strain Gages in Building Section A

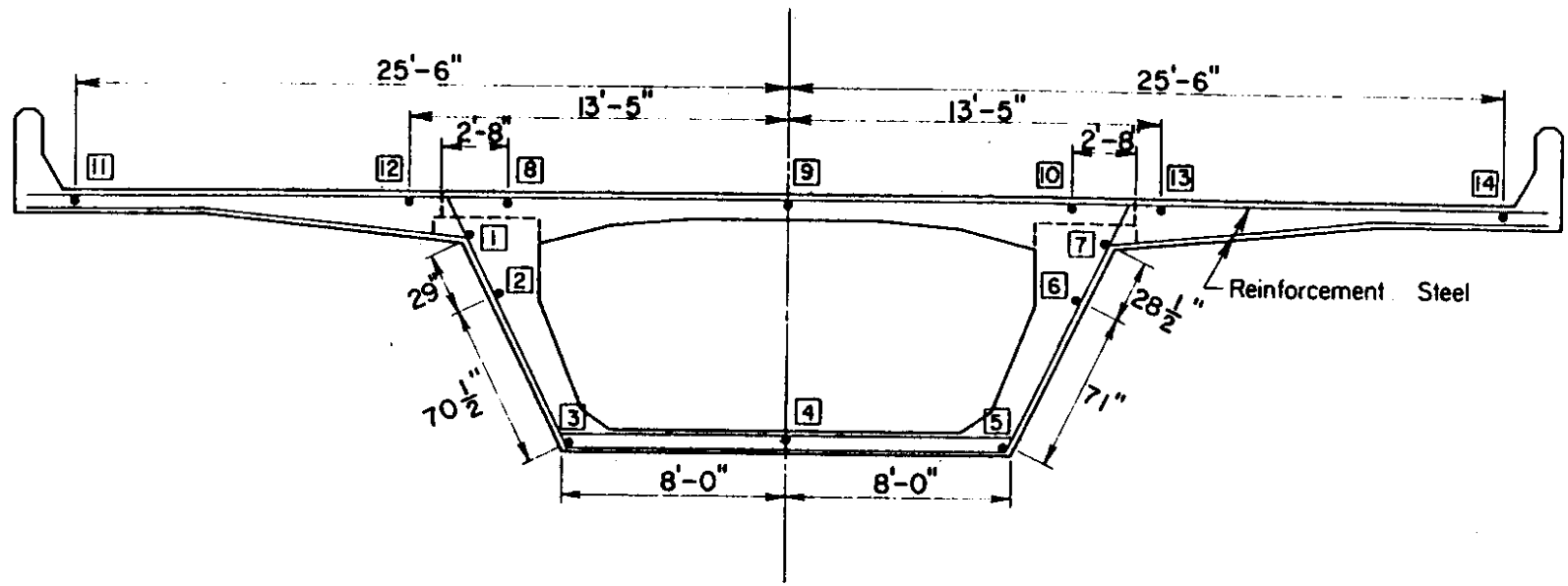

Note: All Strain Gages were Tied to Reinforcement Cage

Fig. A3 - Locations of Carlson Strain Gages in Building Section C

Variations of specific creep of concrete with time for each construction stage are shown in Fig. 10. Specific creep is defined as the amount of creep strain under unit stress expressed in millionths/psi. Concrete shrinkage was excluded from creep strain. Different curves in the figure represent specific creep of concrete loaded at different ages.

The relationships of drying shrinkage versus time for each construction stage are shown in Fig. 11. Shrinkage tests were started at nominal concrete ages of 3 days.

DATA ANALYSIS

To investigate stress redistribution in the box girder of Denny Creek Bridge, time-dependent behavior of selected sections was analyzed. Measured strains cannot be used directly to calculate stress levels because of the time-dependent behavior and redistribution of stresses caused by different end conditions. Therefore, an iterative procedure was developed to estimate stress levels in the box girder.

First, a set of stress histories were assumed for the instrumented bridge sections. Corresponding strain histories were calculated including time-dependent strain components such as creep and shrinkage. In addition, significant secondary deformations caused by temperature-induced stresses were also included. The resulting strain history was then compared with the actual measured data. If reasonable agreement was achieved, assumed stress history was a good estimate of the actual stress conditions in the bridge. Otherwise, stress history had to be modified and the analysis repeated.

Method of Analysis

Generally, long-term deformations of concrete structures can be analyzed in terms of four major components:

1. Instantaneous deformation
2. Creep deformation
3. Shrinkage deformation
4. Secondary deformation

Total deformation is the sum of the instantaneous, creep, shrinkage, and secondary strains. A significant secondary component considered in this report is the deformation induced by internal temperature differentials. Other secondary components are differential shrinkage between construction stages and restraint moments due to supporting conditions. However, only temperature differentials were considered in the present analysis.

Calculated deformations at different bridge sections were based on stress histories supplied by the State of Washington. These stresses had been calculated using Dyckerhoff and Widmann Computer Program dated June 1977.

A computer program was developed in CTL to calculate effects of creep and shrinkage. Creep and shrinkage properties of concrete were obtained from laboratory tests. Laboratory results were expressed as a logarithmic function of time. Functions obtained were then used as input for the computer program to estimate creep and shrinkage in the bridge.

It has been shown that inelastic deformations can be adequately predicted[5-8] from the properties of 6x12-in. diameter plain concrete cylinders.

Instantaneous Deformation

Instantaneous deformations were calculated using the modulus of elasticity of concrete together with the stress history. Modulus of elasticity of concrete for different construction stages at different ages was measured by laboratory tests.

As listed in Table 2, variation of modulus of elasticity of concrete with time was relatively small. Therefore, average value of the modulus for four different concrete ages was used in the analysis. Modulus values of 4163 ksi, 4800 ksi, and 4645 ksi were used for Stages I, II, and III respectively.

Stress histories used in the analysis of Sections A, B, and C were based on the output of the Dyckerhoff and Widmann Computer Program, dated June 1977. Dead loads and construction loads induced before and after significant events were included in the calculations. Detailed explanation of the assumptions and the accuracy of the listed stress histories are given in Appendix C.

The stress histories of Sections A, B, and C are listed in Tables C1, C2, and C3, respectively.

Creep Deformation

Superposition method[9] of calculating creep under variable stresses was used. This method used the assumption that creep strains produced by an increment of stress are independent of the effects of any other stresses applied at a different time. Other assumptions are as follows:

1. Concrete creeps in tension at the same rate as in compression.
2. Creep is linearly proportional to the applied stress.

With these assumptions, the time-dependent relationship between applied stress and creep strain can be written in the following form.

$$\varepsilon_{cr}(t) = f_o\, \varepsilon_{cru}(t, t_o) + \sum_{t_o}^{t} F(t_i)\, \varepsilon_{cru}(t, t_i) \qquad (1)$$

where:

f_o = initial stress in concrete at the time of first loading, t_o,

$\varepsilon_{cru}(t, t_o)$ = specific creep strain at time t, for concrete loaded at the age t_o,

$F(t_i)$ = additional stress increments or decrements applied at time $t_o < t_i < t$,

$\varepsilon_{cru}(t, t_i)$ = specific creep strain at time t, for concrete loaded at age $t_i > t_o$.

Specific creep strain, ε_{cru}, used in the expression was obtained from tests of concrete in the laboratory. Specific creep curves given in Fig. 9 were used. Effects of age of loading on creep were taken into consideration. Specific creep strains loaded at a given age were estimated by linear interpolation between the experimental creep curves.

The creep values obtained were modified for size effects. It has been shown by Hansen and Mattock[8,10] that effects of size on creep are related to volume-to-surface-area ratio of members. Modification factors used for a 6x12-in. concrete cylinders in relation to other volume-to-surface-area ratios of a structure are shown in Fig. 12.

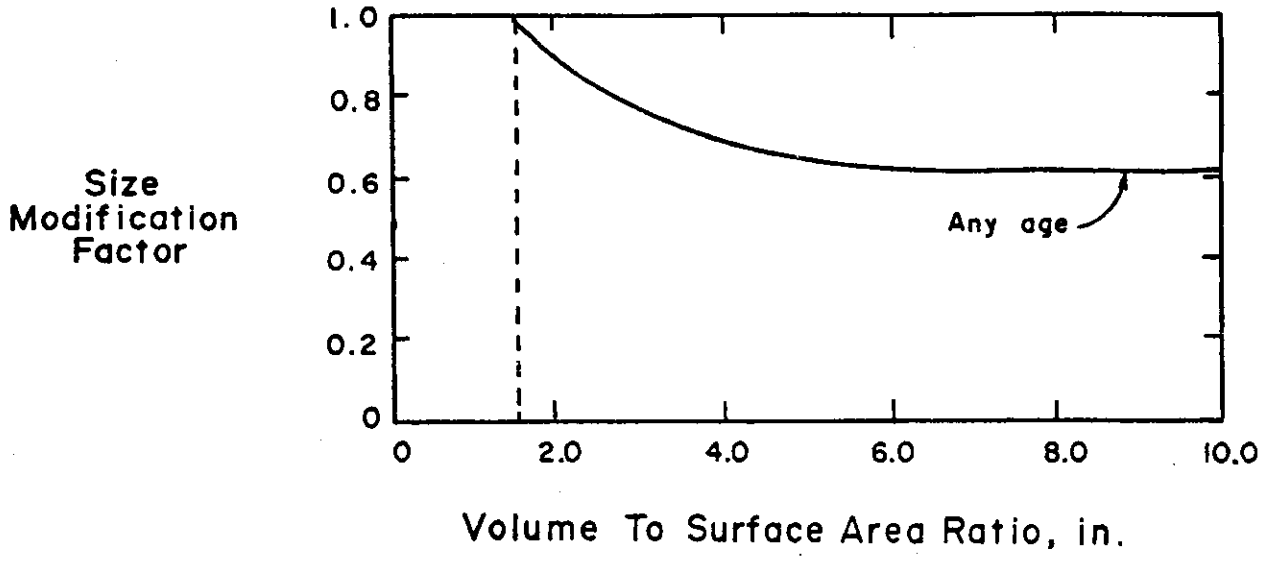

Fig. 12 Size Modification Factors for Creep of Plain Concrete

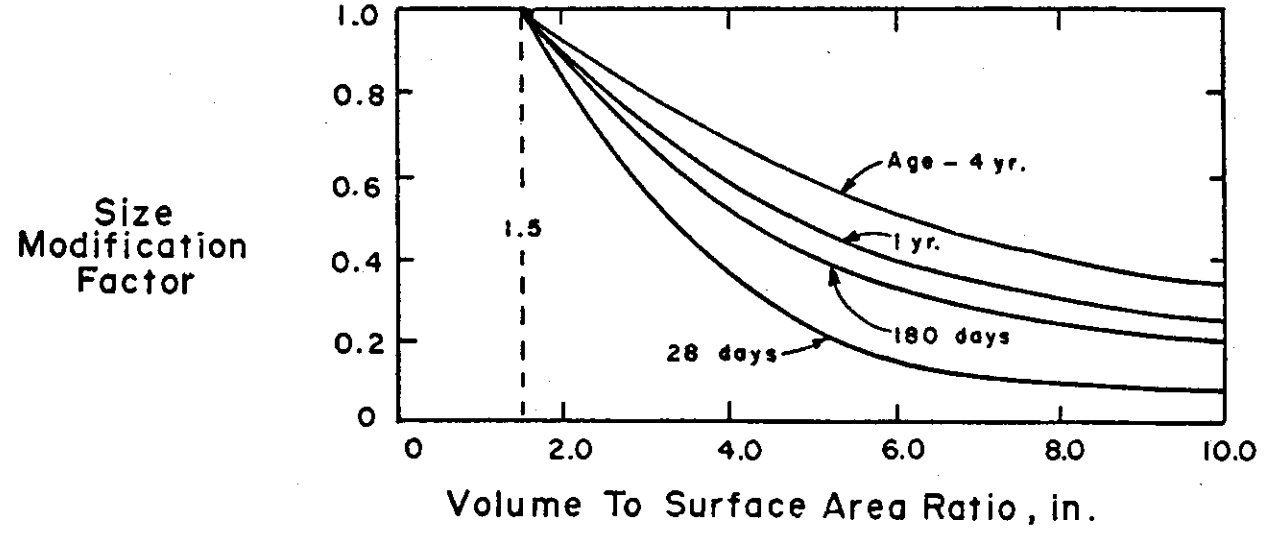

Fig. 13 Size Modification Factors for Shrinkage of Plain Concrete

Two sets of volume to surface area ratios for each section were calculated. The ratios were first calculated by including both the inside and outside surface areas. Then ratios were checked by considering the outside area only. The ratios thus obtained ranged from 7.6 in. to 8.3 in. and 10.2 in. to 11.2 in. corresponding to conditions with and without the inclusion of inside surface areas respectively. From Fig. 12, it is seen that size modification factor for creep is independent of volume to surface ratios when the ratio is greater than 6 in. Therefore, the bridge section can be considered either as a solid or hollow section for size correction. Size modification factor of 0.62 was used throughout the analysis.

Creep values were further modified for the effects of reinforcement with the equation suggested by Dischinger[11,12,13]

$$\varepsilon_{cr} = \frac{f_o}{E_s \rho_g} (1 - e^{-\alpha C E_c}) \qquad (2)$$

where:

ε_{cr} = creep strain

C = specific creep of unreinforced concrete with the same volume-to-surface-area ratio as the bridge

E_c = modulus of elasticity of concrete

E_s = modulus of elasticity of steel

ρ_g = percentage of reinforcement

$\alpha = \frac{\rho_g n}{1 + \rho_g n}$

$n = \frac{E_s}{E_c}$

Creep calculations were made by assuming stresses to be applied in increments. The stress histories listed in Tables C1, C2, and C3, for the three selected sections were used in the analysis.

Shrinkage Deformation

Shrinkage deformations were obtained from the laboratory tests started after approximately three days curing. Shrinkage values were modified for volume-to-surface-area effects by using the appropriate correction factors shown in Fig. 13. Volume-to-surface-area ratios ranging from 7.6 in. to 8.3 in. were used. Dischinger's equation was used to account for the presence of reinforcement.

$$\varepsilon_s = \frac{S}{CE_s \rho_g} (1 - e^{-\alpha CE_c}) \qquad (3)$$

where:

ε_s = shrinkage strain

S = shrinkage of unreinforced concrete with the same volume-to-surface-area ratio as the bridge

In contrast to the creep calculations, shrinkage was calculated for different ages in only one increment.

Internal Temperature Deformation

Concrete temperature data for Sections A, B, and C are listed in Tables A2, A4, and A6, respectively. Temperature differentials across construction joints of 20F to 50F were observed after concrete casting. The new concrete had the higher temperature. If free movements were allowed, relative temperature deformations would result across cold joints

between construction stages. However, in reality, fresh concrete was restrained by the relatively cool adjacent concrete surfaces. Temperature stresses were thus induced.

Induced temperature stresses at construction joints were calculated as follows:

$$\sigma_t = \delta t \, \mu \, E_c \qquad (4)$$

where:

σ_t = internal temperature stress

δt = temperature differential

μ = coefficient of thermal expansion

E_c = concrete modulus of elasticity

It was assumed that induced temperature stresses were applied to the restraining concrete surface as additional compressive force. Because of equilibrium, an equal tensile force also existed in the new concrete. The stress condition can be illustrated by the free body diagram in Fig. 14.

With the presence of temperature stresses, cross-sections of Stages I and II would attain a certain curvature. Because of compatibility of deformations, the curvature of Stages I and II should be the same and deformations across construction joints should be equal. Using these two conditions, moment and shear at construction joints were calculated. Stresses at selected locations in both sections were then determined. This method was first derived and used by Mattock.[14] Calculation details are given in Appendix D. The resulting temperature stresses after redistribution for Sections A, B, and C are summarized in Tables D1, D2, and D3 of Appendix D, respectively.

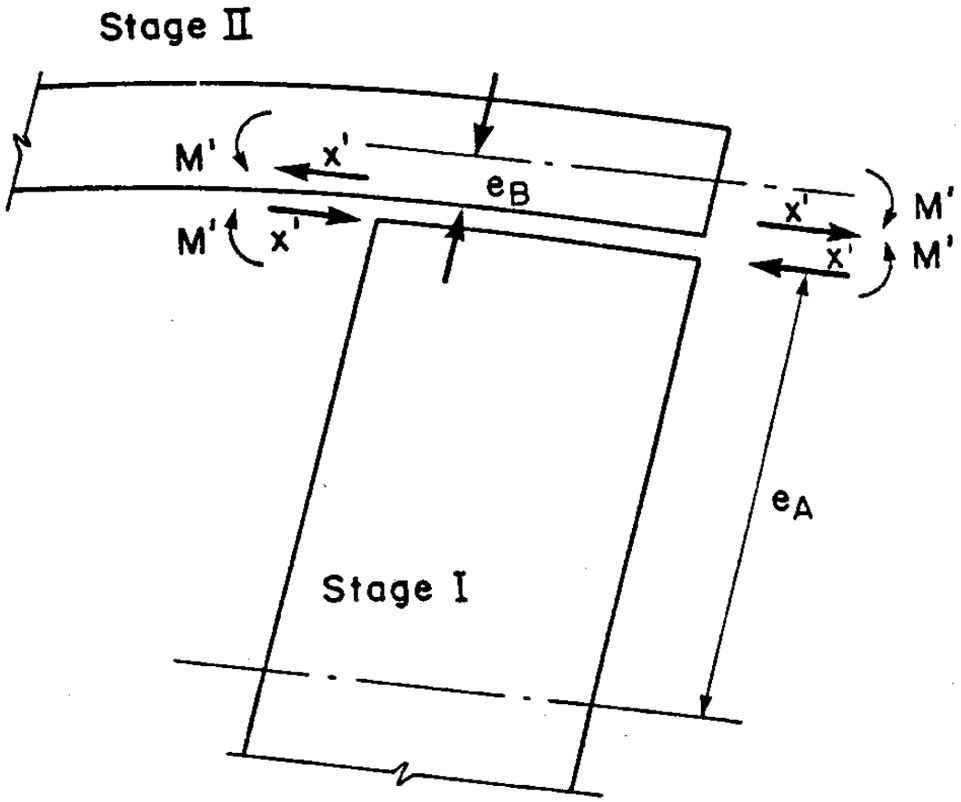

Fig. 14 Free Body Diagram of Stage I and Stage II Construction

To study time-dependent effects of induced temperature stresses, stress-relaxation of concrete was considered. Stress relaxation is the long-term decrease of stresses in a member at constant strain. A simple rate of creep formula developed by Mattock[14] was used for calculating stress relaxation. The relaxation function is given as follows:

$$R = (1 - e^{-\theta}) \frac{1}{\theta} \qquad (5)$$

where:

R = residual stress factor

$\theta = \frac{\varepsilon_c}{\varepsilon_e}$ = creep strain ratio

ε_c = creep strain

ε_e = elastic strain

Creep strain ratio, θ, in Equation (5) was calculated based on laboratory creep data. The relationship of residual stress factor after relaxation versus the creep strain ratio is illustrated in Fig. 15. Using this function, temperature induced stresses were reduced continually with time. Induced temperature strains were then calculated based on the reduced stresses.

The estimated temperature strains for sections A, B, and C are listed in Tables D4, D5, and D6 of Appendix D, respectively. It is noted that stress-relaxation of concrete had little effect on the estimation of temperature strains and thus can be neglected.

Data Interpretation

In this section, comparisons between measured field data and calculated strains are made. Observations and findings from the comparisons are presented.

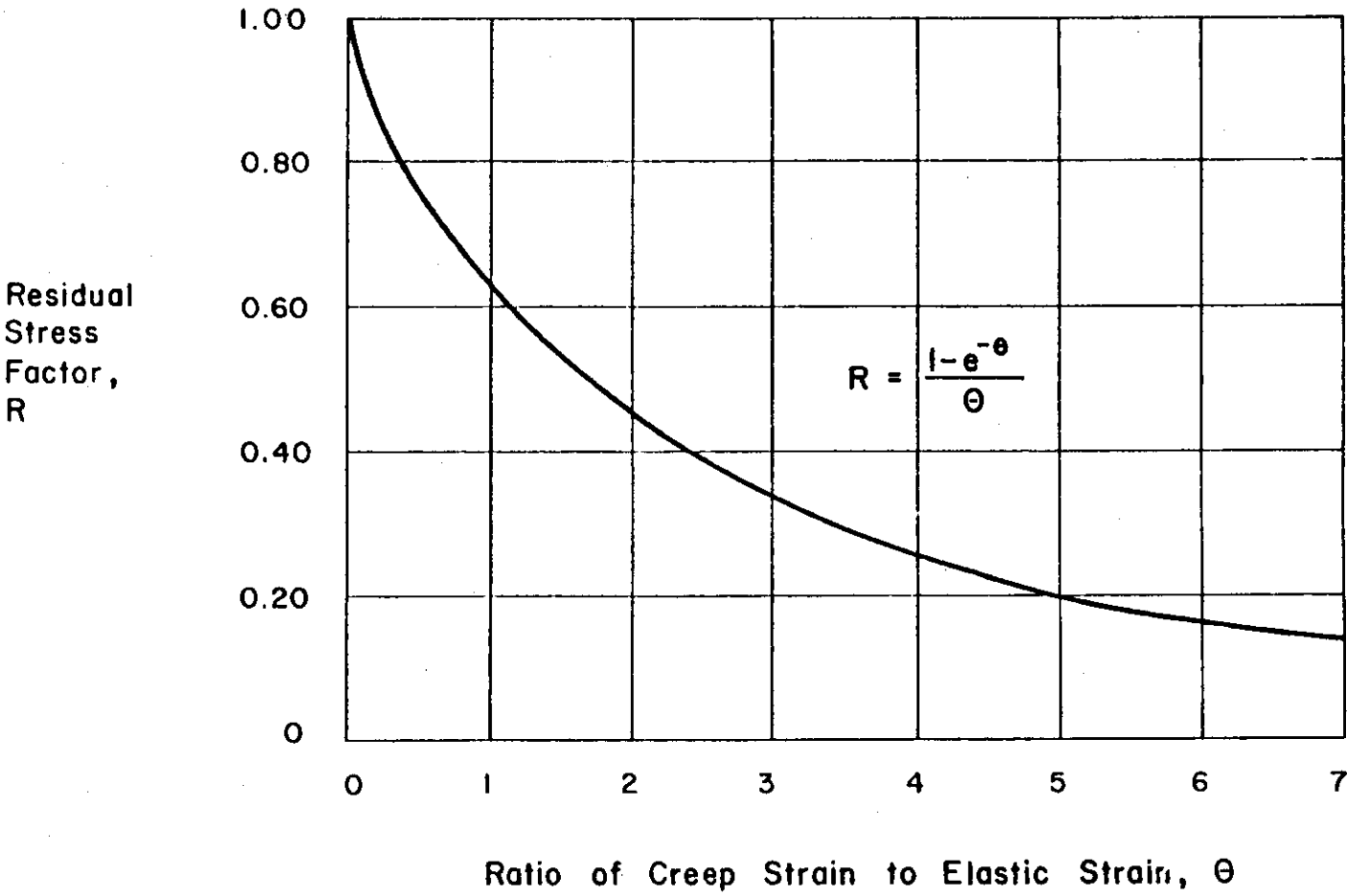

Fig. 15 Relationship of Residual Stress Factor versus Ratio of Creep Strain to Elastic Strain

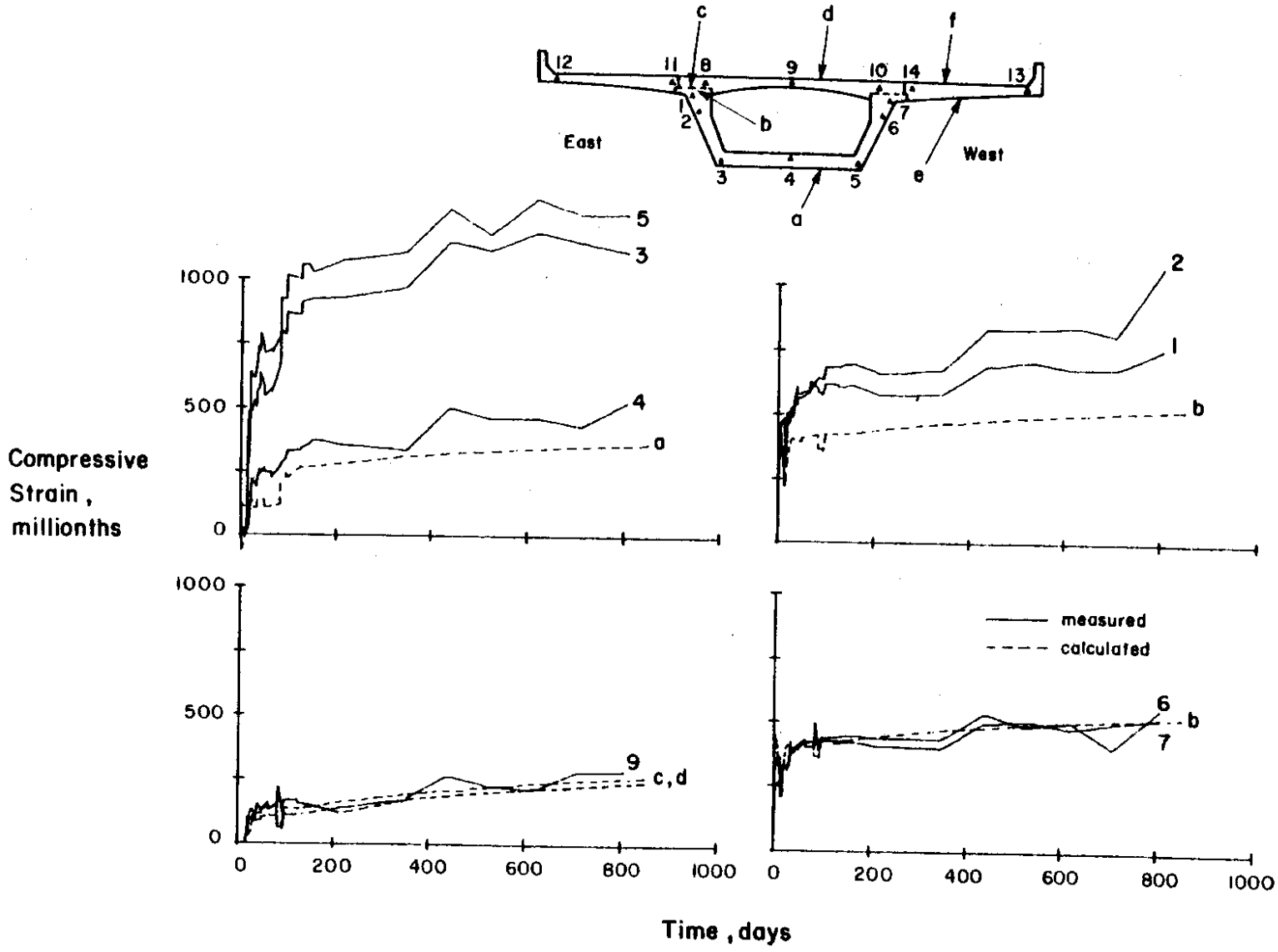

Fig. 21 Measured and Calculated Strain Histories of Section A

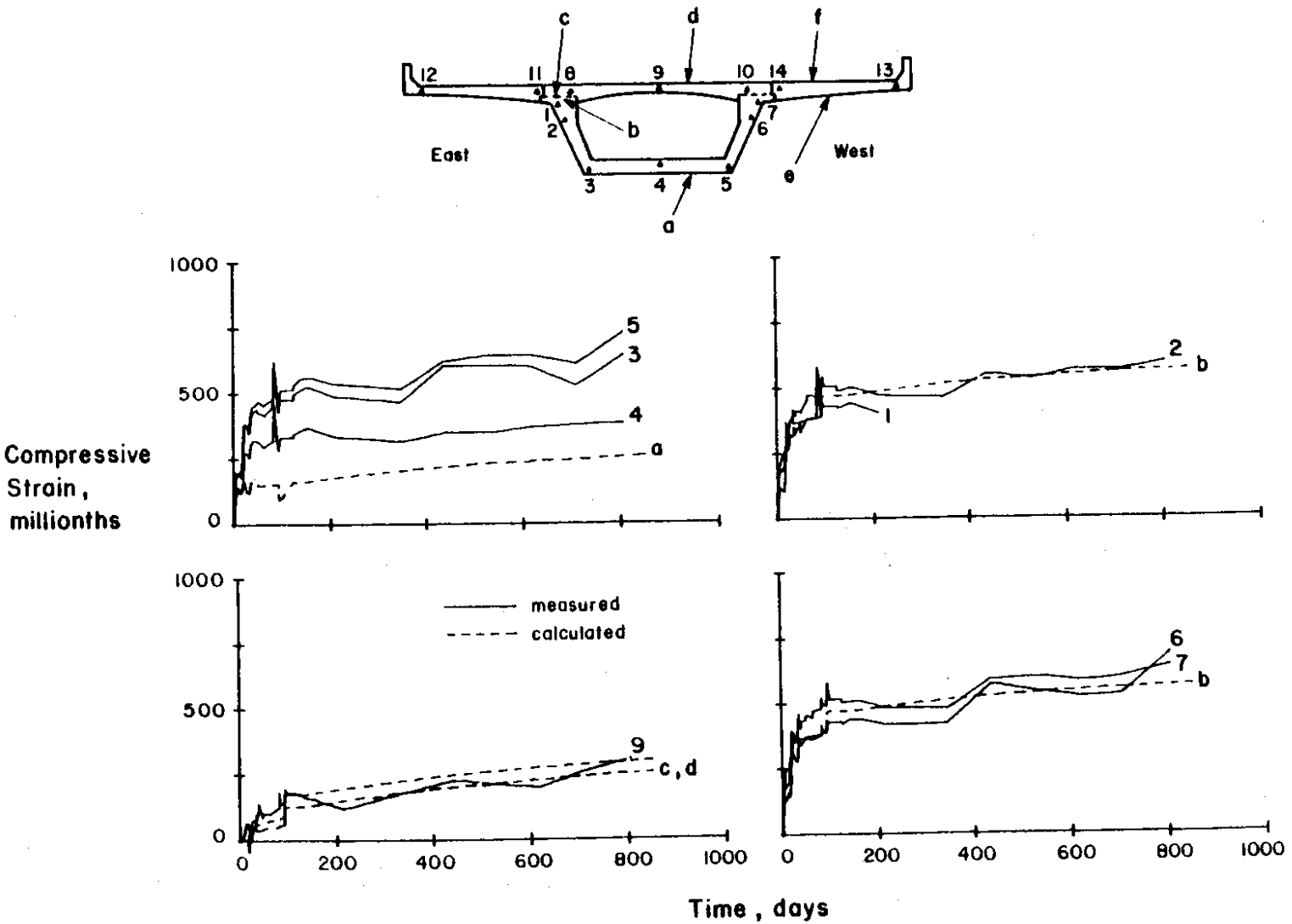

Fig. 22 Measured and Calculated Strain Histories of Section B

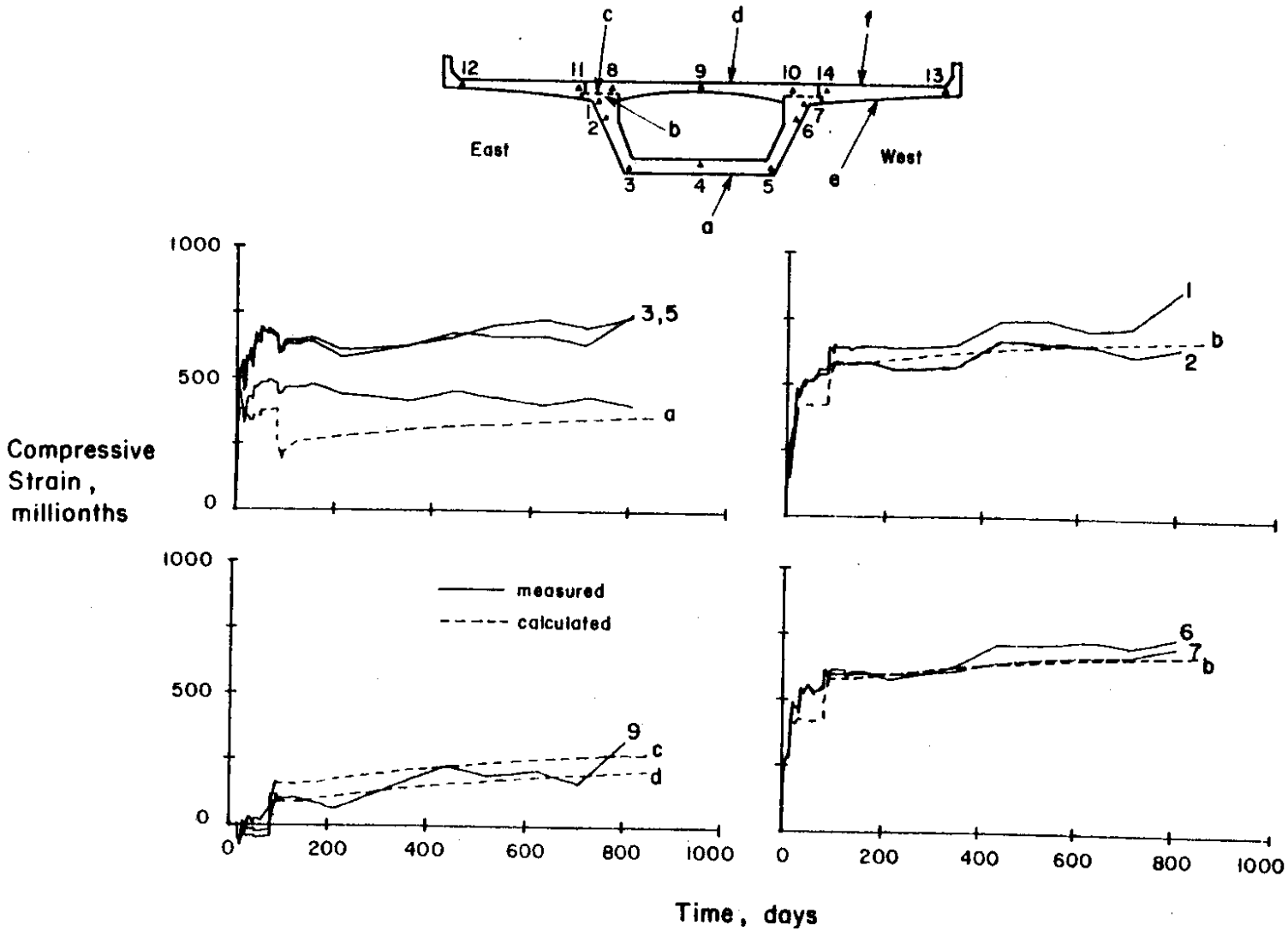

Fig. 23 Measured and Calculated Strain Histories of Section C

APPENDIX C - STRESS ANALYSIS DATA

In this Appendix, computed stress histories of the three instrumented sections are presented. Locations of the computed stresses are given in Fig. C1. The computed stresses of each section at different stages are listed in Tables C1 to C3.

Data were furnished by the Washington State Department of Transportation upon request. In a letter dated February 28, 1979, C.S. Gloyd, Bridge and Structures Engineer pointed out the following facts concerning the stress values.

> "The stress values at Sections B & C have been obtained by interpolating between different sections in the designer's computer output. We checked some of these values using the post-tensioning sub-contractor computer output. The correlation was only fair with variations up to 15%."

However, these computed values were used only as a basis for comparison with the field readings.

Assumptions made in the stress analysis are:

1. The structure behaves as a plane frame. Horizontal curve is not considered.
2. Creep and shrinkage is not considered for construction loadings.
3. Changes in sectional properties are considered (such as at supports).

4. Prestressing and construction loads are considered to act on the existing box section at the time of the prestress or load application. As construction proceeds, stresses resulting from additional prestress and construction loads are calculated based on the sectional properties at the time of application. These stresses are then superimposed on existing stresses.
5. A computer program is used to calculate deformations and forces.
6. Stress is proportional to deformation for instantaneous deformations.
7. A plane section before loading remains a plane section after loading.
8. Stresses are assumed to vary in a straight line between sections.
9. No change in prestress force was included in the calculations.

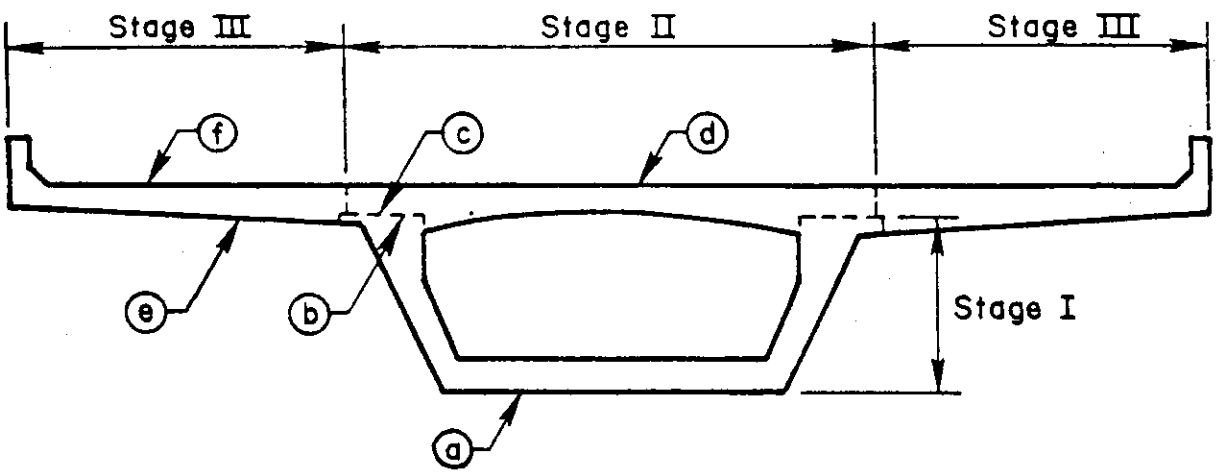

ⓐ Bottom of Stage I

ⓑ Top of Stage I

ⓒ Bottom of Stage II

ⓓ Top of Stage II

ⓔ Bottom of Stage III

ⓕ Top of Stage III

Fig. C1 Stress Locations

TABLE C1 - STRESS HISTORY FOR SECTION A

Reading No.		Location (psi) a	b	c	d	e	f	Time (days)
After Releasing Truss	Span 4	- 264	+1857	-	-	-	-	3
After Launching Truss (250k)	Span 4	- 121	+1614	-	-	-	-	8
After Casting Stage II	Span 4	+ 420	+ 765	-	-	-	-	16
After Casting Stage I	Span 5	+ 636	+1213	+457	+477	-	-	24
After Releasing Truss	Span 5	+ 450	+1336	+571	+638	-	-	29
After Launching Truss (250k)	Span 5	+ 462	+1326	+561	+625	-	-	34
After Casting Stage II	Span 5	+ 602	+1236	+471	+507	-	-	37
Before Casting Stage IIIA	Span 3	+ 557	+1262	+498	+542	-	-	50
After Casting Stage IIIA	Span 3	+ 450	+1321	+556	+627	-	-	51
Before Casting Stage IIIB	Span 3	+ 442	+1327	+562	+629	-	-	64
After Casting Stage IIIB	Span 3	+ 478	+1306	+541	+601	-	-	65
Before Casting Stage IIIA	Span 4	+ 476	+1308	+543	+604	-	-	83
After Casting Stage IIIA	Span 4	+ 887	+1063	+298	+277	-	-	84
Before Casting Stage IIIB	Span 4	+ 887	+1065	+300	+279	-	-	94
After Casting Stage IIIB	Span 4	+ 943	+1028	+263	+230	-	-	95
After P.T. Stage IIIB	Span 4	+ 924	+1198	+433	+423	+170	+193	100
After Casting Stage IIIA	Span 5	+1069	+1146	+381	+346	+119	+117	125
After Casting Stage IIIB	Span 5	+1028	+1160	+396	+368	+133	+139	127
After P.T. Stage IIIB	Span 5*	+1028	+1160	+396	+368	+133	+139	140

(+) Compression
(-) Tension
(*) Secondary effects of Post-Tensioning Stage IIIB, Span 5 are neglected.

TABLE C2 - STRESS HISTORY FOR SECTION B

Reading No.		Location (psi) a	b	c	d	e	f	Time (days)
After Releasing Truss	Span 4	+383	+ 840	-	-	-	-	3
After Launching Truss	Span 4	+506	+ 671	-	-	-	-	8
After Casting Stage II	Span 4	+436	+ 787	-	-		-	16
After Casting Stage I	Span 5	+733	+1076	+288	+286	-	-	24
After Releasing Truss	Span 5	+535	+1172	+384	+420	-	-	29
After Launching Truss (250k)	Span 5	+541	+1167	+379	+412	-	-	34
After Casting Stage II	Span 5	+715	+1086	+298	+300	-	-	37
Before Casting Stage IIIA	Span 3	+670	+1104	+317	+326	-	-	50
After Casting Stage IIIA	Span 3	+611	+1124	+336	+355	-	-	51
Before Casting Stage IIIB	Span 3	+602	+1127	+340	+360	-	-	64
After Casting Stage IIIB	Span 3	+619	+1122	+334	+352	-	-	65
Before Casting Stage IIIA	Span 4	+620	+1122	+335	+352	-	-	83
After Casting Stage IIIA	Span 4	+610	+1138	+351	+372	-	-	84
Before Casting Stage IIIB	Span 4	+612	+1138	+351	+372	-	-	94
After Casting Stage IIIB	Span 4	+493	+1191	+403	+445	-	-	95
After P.T. Stage IIIB	Span 4	+519	+1217	+429	+471	+26	+26	100
After Casting Stage IIIA	Span 5	+771	+1154	+367	+370	-36	-74	125
After Casting Stage IIIB	Span 5	+728	+1165	+378	+387	-25	-57	127
After P.T. Stage IIIB	Span 5*	+728	+1165	+378	+387	-25	-57	140

(+) Compression
(-) Tension
(*) Secondary Effects of Post-Tensioning Stage IIIB, Span 5 are neglected.

TABLE C3 - STRESS HISTORY FOR SECTION C

Reading No.		Location (psi) a	b	c	d	e	f	Time (days)
After Releasing Truss	Span 4	+1783	+ 616	-	-	-	-	3
After Launching Truss (250k)	Span 4	+1800	+ 582	-	-	-	-	8
After Casting Stage II	Span 4	+1325	+1204	-	-	-	-	16
After Casting Stage I	Span 5	+1491	+1183	+ 21	+ 44	-	-	24
After Releasing Truss	Span 5	+1393	+1234	+ 30	+ 25	-	-	29
After Launching Truss (250k)	Span 5	+1382	+1236	+ 32	+ 29	-	-	34
After Casting Stage II	Span 5	+1480	+1190	- 14	- 36	-	-	37
Before Casting Stage IIIA	Span 3	+1464	+1195	- 9	- 27	-	-	50
After Casting Stage IIIA	Span 3	+1542	+1152	- 52	- 86	-	-	51
Before Casting Stage IIIB	Span 3	+1540	+1154	- 51	- 84	-	-	64
After Casting Stage IIIB	Span 3	+1505	+1171	- 33	- 61	-	-	65
Before Casting Stage IIIA	Span 4	+1513	+1169	- 36	- 64	-	-	83
After Casting Stage IIIA	Span 4	+ 927	+1445	+241	+320	-	-	84
Before Casting Stage IIIB	Span 4	+ 933	+1444	+240	+319	- 2	- 2	94
After Casting Stage IIIB	Span 4	+1068	+1411	+207	+265	-34	- 56	95
After P.T. Stage IIIB	Span 4	+1068	+1411	+207	+265	-28	-49	100
After Casting Stage IIIA	Span 5	+1199	+1374	+170	+203	-71	-114	125
After Casting Stage IIIB	Span 5	+1180	+1378	+174	+214	-67	-106	127
After P.T. Stage IIIB	Span 5*	+1180	+1378	+174	+214	-67	-106	140

(+) Compression
(-) Tension
(*) Secondary Effects of Post-Tensioning Stage IIIB, Span 5 are neglected.

APPENDIX D - INTERNAL TEMPERATURE STRESS AND STRAIN DATA

In this appendix, procedure for calculating internal temperature stresses is given. Temperature induced stresses and strains are presented.

As illustrated in Fig. D1, the two equations for compatibility of curvatures and deformations as derived in Reference 14 are as follows:

$$X' = \varepsilon_S E_A I_A \frac{B}{BF - C^2} \tag{D1}$$

$$M' = \varepsilon_S E_A I_A \frac{C}{C^2 - BF} \tag{D2}$$

where: X' = shear stress at construction joint

M' = moment at construction joint

ε_s = temperature induced deformation

$= \mu\delta_t$

μ = coefficient of thermal expansion

δ_t = temperature differential

E_A = modulus of elasticity of Stage I concrete

I_A = moment of inertia of Stage I concrete

$B = (1 + m')$

$$m' = \frac{E_A I_A}{E_B I_B}$$

E_B = modulus of elasticity of Stage II concrete

I_B = moment of inertia of Stage II concrete

$F = e_A^2 + r_A^2 + m' e_B^2 + m' r_B^2$

$C = (e_B - m' e_A)$

r_A = radius of gyration of Stage I concrete

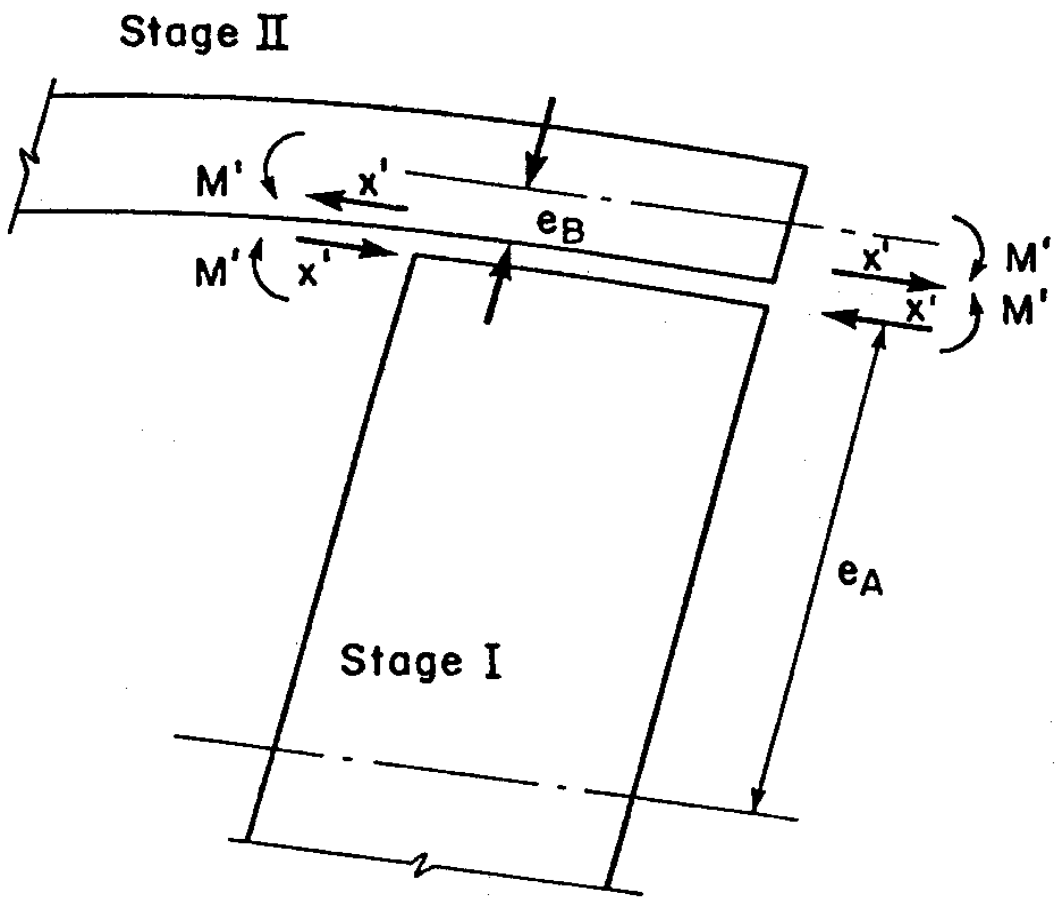

Fig. D1 Free Body Diagram of Stage I and Stage II Construction

r_B = radius of gyration of Stage II concrete

e_A and e_B = distances from construction joint to centroid of Stage I and Stage II concrete respectively.

The temperature induced deformations were calculated from the measured temperature differentials. From Equations D1 and D2, shear and moment at construction joint were calculated. Next, stresses at top and bottom of each construction stage were calculated. The resulting stresses for Sections A, B, and C are listed in Tables D1, D2 and D3 respectively.

Allowing for the time-dependent relaxation properties, temperature induced strains for Sections A, B, and C were calculated and are listed in Tables D4, D5 and D6 respectively.

TABLE D1 - CALCULATED TEMPERATURE STRESSES FOR SECTION A

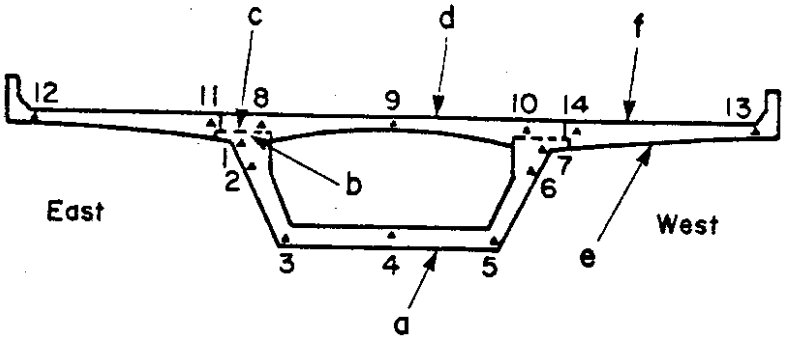

Time, days	Concrete Stress, psi					
	Location No.					
	a	b	c	d	e	f
0	0	0	0	0	0	0
3	0	0	0	0	0	0
8	0	0	0	0	0	0
16	0	0	0	0	0	0
24	-85	243	-128	-43	0	0
53	-85	243	-128	-43	0	0
58	-85	243	-128	-43	0	0
61	-85	243	-128	-43	0	0
74	-85	243	-128	-43	0	0
75	-85	243	-128	-43	0	0
88	-85	243	-128	-43	0	0
89	-85	243	-128	-43	0	0
107	-85	243	-128	-43	0	0
108	-85	243	-128	-43	0	0
118	-85	243	-128	-43	0	0
119	-85	243	-128	-43	0	0
124	-152	360	-11	118	-120	-164
251	-152	360	-11	118	-120	-164
264	-152	360	-11	118	-120	-164
274	-152	360	-11	118	-120	-164
335	-152	360	-11	118	-120	-164
469	-152	360	-11	118	-120	-164
560	-152	360	-11	118	-120	-164
644	-152	360	-11	118	-120	-164
740	-152	360	-11	118	-120	-164
832	-152	360	-11	118	-120	-164
974	-152	360	-11	118	-120	-164

TABLE D2 - CALCULATED TEMPERATURE STRESSES FOR SECTION B

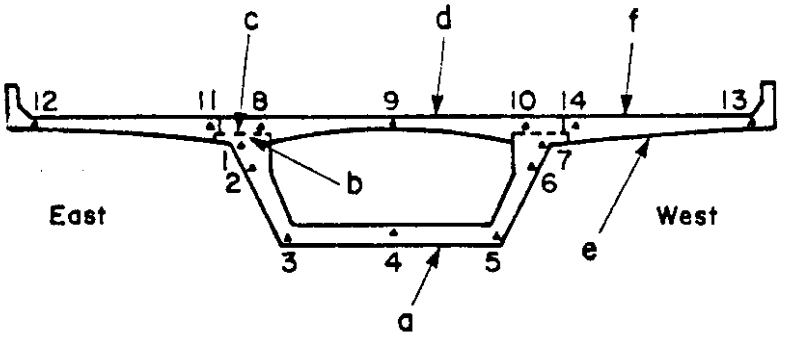

Time, days	Concrete Stress, psi					
	Location No.					
	a	b	c	d	e	f
0	0	0	0	0	0	0
3	0	0	0	0	0	0
8	0	0	0	0	0	0
16	0	0	0	0	0	0
24	-106	302	-159	-54	0	0
53	-106	302	-159	-54	0	0
58	-106	302	-159	-54	0	0
61	-106	302	-159	-54	0	0
74	-106	302	-159	-54	0	0
75	-106	302	-159	-54	0	0
88	-106	302	-159	-54	0	0
89	-106	302	-159	-54	0	0
107	-106	302	-159	-54	0	0
108	-106	302	-159	-54	0	0
118	-106	302	-159	-54	0	0
119	-250	543	82	278	-208	-116
219	-250	543	82	278	-208	-116
244	-250	543	82	278	-208	-116
246	-250	543	82	278	-208	-116
259	-250	543	82	278	-208	-116
269	-250	543	82	278	-208	-116
330	-250	543	82	278	-208	-116
464	-250	543	82	278	-208	-116
555	-250	543	82	278	-208	-116
735	-250	543	82	278	-208	-116
827	-250	543	82	278	-208	-116
919	-250	543	82	278	-208	-116

TABLE D3 - CALCULATED TEMPERATURE STRESSES FOR SECTION C

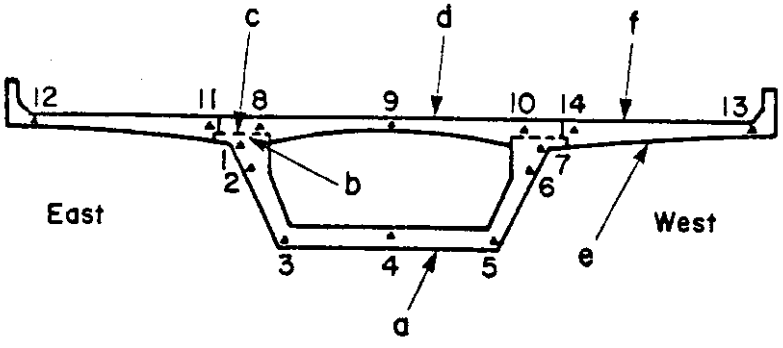

Time, days	Concrete Stress, psi					
	Location No.					
	a	b	c	d	e	f
0	0	0	0	0	0	0
3	0	0	0	0	0	0
8	0	0	0	0	0	0
16	0	0	0	0	0	0
24	-149	426	-224	-76	0	0
53	-149	426	-224	-76	0	0
58	-149	426	-224	-76	0	0
61	-149	426	-224	-76	0	0
74	-149	426	-224	-76	0	0
75	-149	426	-224	-76	0	0
88	-149	426	-224	-76	0	0
89	-149	426	-224	-76	0	0
107	-149	426	-224	-76	0	0
108	-149	426	-224	-76	0	0
118	-349	762	112	387	-478	-344
213	-349	762	112	387	-478	-344
219	-349	762	112	387	-478	-344
240	-349	762	112	387	-478	-344
245	-349	762	112	387	-478	-344
258	-349	762	112	387	-478	-344
268	-349	762	112	387	-478	-344
329	-349	762	112	387	-478	-344
463	-349	762	112	387	-478	-344
554	-349	762	112	387	-478	-344
734	-349	762	112	387	-478	-344
826	-349	762	112	387	-478	-344
958	-349	762	112	387	-478	-344

TABLE D4 - CALCULATED TEMPERATURE STRAINS FOR SECTION A

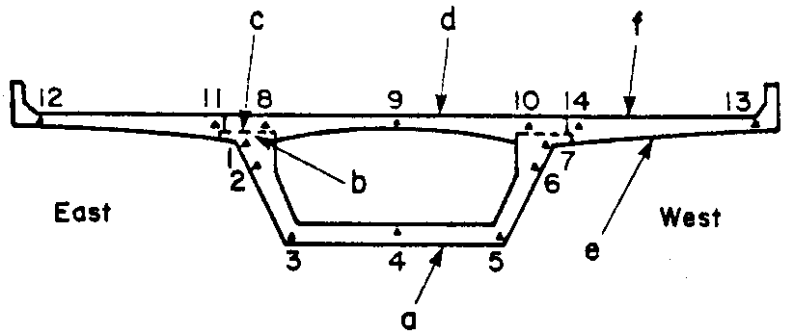

Time, days	Strain, millionths					
	Location No.					
	a	b	c	d	e	f
0	0.0	0.0	0.0	0.0	0.0	0.0
3	0.0	0.0	0.0	0.0	0.0	0.0
8	0.0	0.0	0.0	0.0	0.0	0.0
16	0.0	0.0	0.0	0.0	0.0	0.0
24	-20.5	58.4	-26.7	-9.0	0.0	0.0
29	-20.5	58.4	-26.6	-9.0	0.0	0.0
34	-20.4	58.4	-26.6	-9.0	0.0	0.0
37	-20.4	58.4	-26.6	-9.0	0.0	0.0
50	-20.4	58.4	-26.6	-9.0	0.0	0.0
51	-20.4	58.4	-26.6	-9.0	0.0	0.0
64	-20.4	58.3	-26.6	-9.0	0.0	0.0
65	-20.4	58.3	-26.6	-9.0	0.0	0.0
80	-20.4	58.3	-26.6	-9.0	0.0	0.0
84	-20.4	58.3	-26.6	-9.0	0.0	0.0
94	-20.4	58.3	-26.6	-9.0	0.0	0.0
95	-20.4	58.3	-26.6	-9.0	0.0	0.0
100	-36.5	86.4	-42.2	44.6	-25.8	-35.3
127	-36.4	86.3	-42.2	44.5	-25.8	-35.2
140	-36.4	86.3	-42.2	44.5	-25.8	-35.2
150	-36.3	86.3	-42.2	44.5	-25.7	-35.2
211	-36.3	86.3	-42.2	44.5	-25.7	-35.2
345	-36.3	86.2	-42.2	44.5	-25.7	-35.2
406	-36.2	86.2	-42.2	44.5	-25.7	-35.2
520	-36.2	86.2	-42.2	44.5	-25.7	-35.2
616	-36.2	86.2	-42.2	44.5	-25.7	-35.2
700	-36.2	86.2	-42.2	44.5	-25.7	-35.2
850	-36.2	86.2	-42.2	44.5	-25.7	-35.2

TABLE D5 - CALCULATED TEMPERATURE STRAINS FOR SECTION B

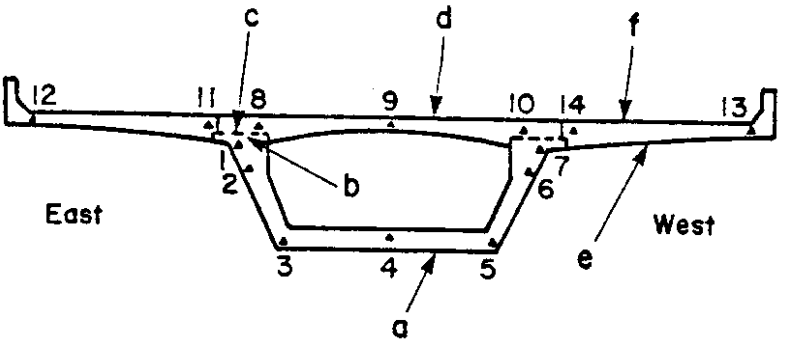

Time, days	Strain, millionths					
	Location No.					
	a	b	c	d	e	f
0	0.0	0.0	0.0	0.0	0.0	0.0
3	0.0	0.0	0.0	0.0	0.0	0.0
8	0.0	0.0	0.0	0.0	0.0	0.0
16	0.0	0.0	0.0	0.0	0.0	0.0
24	-25.5	72.6	-33.1	-11.3	0.0	0.0
29	-25.5	72.6	-33.1	-11.2	0.0	0.0
34	-25.5	72.6	-33.0	-11.2	0.0	0.0
37	-25.4	72.6	-33.0	-11.2	0.0	0.0
50	-25.4	72.5	-33.0	-11.2	0.0	0.0
51	-25.4	72.5	-33.0	-11.2	0.0	0.0
64	-25.4	72.5	-33.0	-11.2	0.0	0.0
65	-25.4	72.5	-33.0	-11.2	0.0	0.0
83	-25.4	72.5	-33.0	-11.2	0.0	0.0
84	-25.4	72.5	-33.0	-11.2	0.0	0.0
94	-25.4	72.5	-33.0	-11.2	0.0	0.0
95	-60.0	130.4	17.2	58.0	-44.8	-25.0
100	-59.9	130.4	17.2	57.9	-44.7	-24.9
125	-59.9	130.3	17.1	57.9	-44.7	-24.9
127	-59.9	130.3	17.1	57.9	-44.7	-24.9
140	-59.9	130.3	17.1	57.9	-44.7	-24.9
150	-59.9	130.3	17.2	57.9	-44.7	-24.9
211	-59.8	130.2	17.2	58.0	-44.7	-24.9
345	-59.8	130.2	17.2	58.0	-44.6	-24.8
436	-59.7	130.2	17.2	58.0	-44.6	-24.8
616	-59.7	130.1	17.2	58.0	-44.6	-24.8
708	-59.7	130.1	17.2	58.0	-44.6	-24.8
850	-59.7	130.1	17.2	58.0	-44.6	-24.8

TABLE D6 - CALCULATED TEMPERATURE STRAINS FOR SECTION C

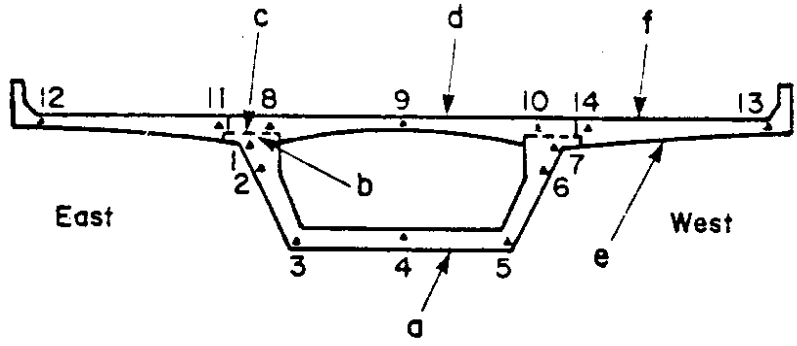

Time, days	Strain, millionths					
	Location No.					
	a	b	c	d	e	f
0	0.0	0.0	0.0	0.0	0.0	0.0
0	0.0	0.0	0.0	0.0	0.0	0.0
0	0.0	0.0	0.0	0.0	0.0	0.0
0	0.0	0.0	0.0	0.0	0.0	0.0
24	-85.0	102.2	-46.6	-15.8	0.0	0.0
29	-85.0	102.2	-46.6	-15.8	0.0	0.0
34	-85.0	102.2	-46.6	-15.8	0.0	0.0
37	-85.0	102.2	-46.6	-15.8	0.0	0.0
50	-85.0	102.2	-46.6	-15.7	0.0	0.0
51	-85.0	102.2	-46.6	-15.7	0.0	0.0
64	-85.0	102.2	-46.6	-15.7	0.0	0.0
65	-85.0	102.2	-46.6	-15.7	0.0	0.0
80	-85.0	102.2	-46.6	-15.7	0.0	0.0
84	-85.0	102.2	-46.6	-15.7	0.0	0.0
95	-85.0	102.2	-46.6	-15.7	0.0	0.0
100	-85.0	102.2	-46.6	80.7	-101.8	-74.0
125	-85.0	102.2	-46.6	80.7	-101.8	-74.0
127	-85.0	102.2	-46.6	80.7	-101.8	-74.0
140	-85.0	102.2	-46.6	80.7	-101.8	-74.0
150	-85.0	102.2	-46.6	80.7	-101.8	-74.0
211	-85.0	102.2	-46.6	80.7	-101.7	-74.0
245	-85.0	102.2	-46.6	80.7	-101.7	-73.9
426	-85.0	102.2	-46.6	80.7	-101.7	-73.9
516	-85.0	102.2	-46.6	80.7	-101.7	-73.9
700	-85.0	102.2	-46.6	80.7	-101.7	-73.9
850	-85.0	102.2	-46.6	80.7	-101.7	-73.9

APPENDIX F

CALCULATION OF THE DIFFERENTIAL TEMPERATURE STRESSES BY PRIESTLEY'S PROCEDURE AND MATTOCK'S (CTL) PROCEDURE

Calculation of differential temperature stresses

Priestley's temperature distribution (modified)

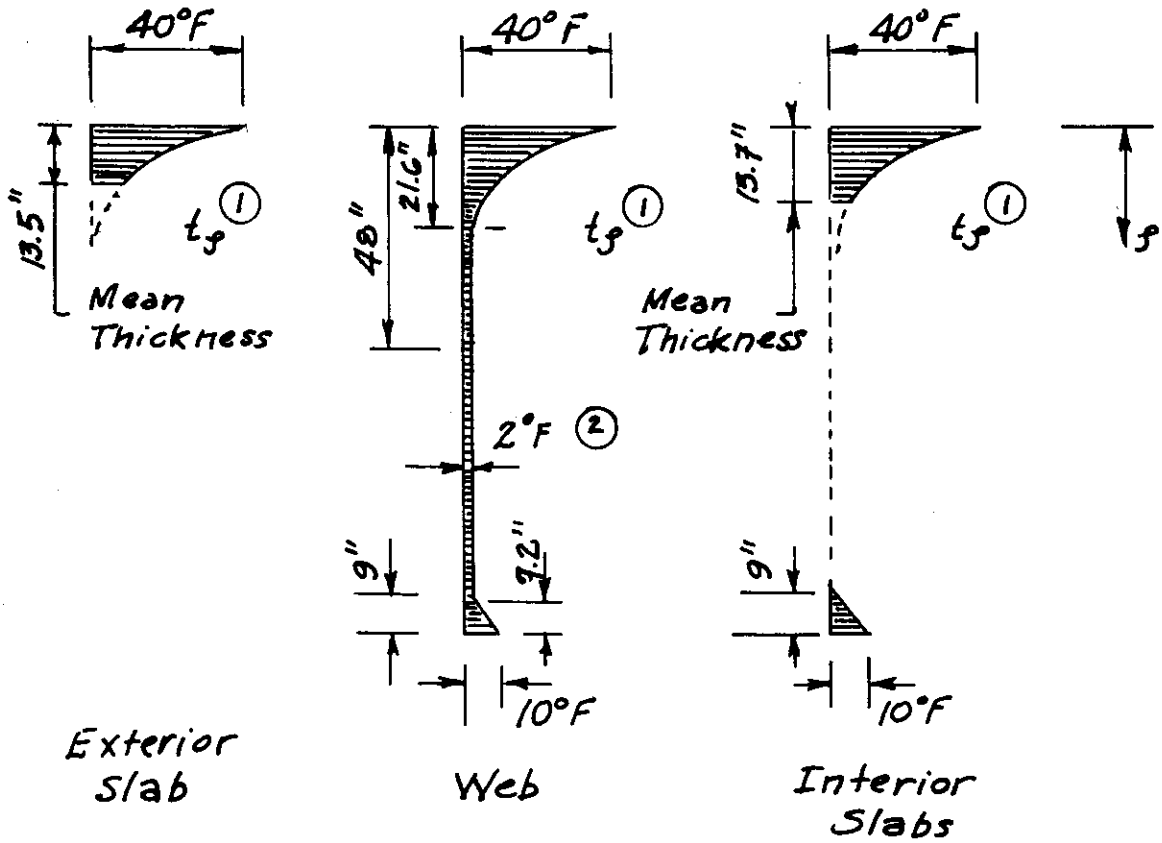

① $t_y = 40°F \left(\frac{48" - y}{48"}\right)^5$

② Distribution similar to that for bottom slab averaged over average web width

$$t_{web} = \frac{(1/2)(10°F)(9")}{(20.9")} \cong 2°F$$

Priestley's method

"Average" temperature $t_{na} = \int_0^d t(y)\,b(y)\,dy \,/ A$

$$\int_{98}^{110} 40\left(\frac{y-62}{48}\right)^5 322.375\ dy = 84,799.7\ \square''\,°F$$

$$\int_{88.4}^{98} 40\left(\frac{y-62}{48}\right)^5 32\ dy = 1,539.1$$

$$\int_{88.4}^{98} 40\left(\frac{y-62}{48}\right)^5 280\left(1-\sqrt{\frac{98-y}{11}}\right) dy = 6,336.2$$

$$\int_{87}^{88.4} 2\left[280\left(1-\sqrt{\frac{98-y}{11}}+32\right)\right] dy = 115.1$$

$$\int_{63}^{87} 2\left[20.414 + \frac{42}{87}(y-63)\right]\ dy = 1,257.9$$

$$\int_{18}^{63} 2\left[15.000 + \frac{5.414}{54}(y-9)\right] dy = 1,634.2$$

$$\int_{9}^{18} 2\left[24 - \frac{8.098}{9}(y-9)\right]\ dy = 39.9$$

$$\int_{7.2}^{9} 2\left[96 + \frac{42}{87}y\right]\ dy = 359.7$$

$$\int_{0}^{7.2} 10\left(\frac{9-y}{9}\right)\left[96 + \frac{42}{87}y\right]\ dy = 4,205.6$$

$$100,287.4\ \square''\,°F$$

$$t_{na} = \frac{100,287.4\ \square''\,°F}{7756.4\ \square''} = 12.9°F$$

Priestleys Method (cont)

"Effective" linear gradient $\psi = \int_0^d t(y)\, b(y)\, y\, dy / I$

$$\int_{98}^{110} 40 \left(\frac{y-62}{48}\right)^5 322.375\, y\, dy = 8,935,336.\ \text{in}^3\,°\text{F}$$

$$\int_{88.4}^{98} 40 \left(\frac{y-62}{48}\right)^5 32\, y\, dy = 145,244.$$

$$\int_{88.4}^{98} 40 \left(\frac{y-62}{48}\right)^5 280 \left(1-\sqrt{\frac{98-y}{11}}\right) y\, dy = 605,574.$$

$$\int_{87}^{88.4} 2 \left[280 \left(1-\sqrt{\frac{98-y}{11}}\right)+32\right] y\, dy = 10,100.$$

$$\int_{63}^{87} 2 \left[20.414 + \frac{42}{87}(y-63)\right] y\, dy = 95,457.$$

$$\int_{18}^{63} 2 \left[15.000 + \frac{5.414}{54}(y-9)\right] y\, dy = 67,709.$$

$$\int_{9}^{18} 2 \left[24 - \frac{8.098}{9}(y-9)\right] y\, dy = 527.$$

$$\int_{7.2}^{9} 2 \left[96 + \frac{42}{87} y\right] y\, dy = 2,914.$$

$$\int_{0}^{7.2} 10 \left(\frac{9-y}{9}\right) \left[96 + \frac{42}{87} y\right] y\, dy = 13,511.$$

$$9,876,372.\ \text{in}^3\,°\text{F}$$

$$\psi = \frac{9,876,372\ \text{in}^3\,°\text{F} - 79.94''\,(100,287.4\ \text{in}\,°\text{F})}{9,795,160\ \text{in}^4} = 0.1898\ \frac{°\text{F}}{\text{in}}$$

Priestley's Method (cont)

"Eigenstress" i.e. stresses to maintain plane sections plane in simple beam.

y in	$t(y)$ °F	$t_{N.A}$ °F	$y_{N.A}$ in	$\phi y_{N.A}$ °F	$t_1(y)$ °F	$\sigma_1(y)$* psi
110	40	12.9	30.06	5.7	21.4	-513
108	32.3	"	28.06	5.3	14.1	-338
106	25.9	"	26.06	4.9	8.1	-193
104	20.5	"	24.06	4.6	3.0	-73
102	16.1	"	22.06	4.2	-1.0	+24
100	12.4	"	20.06	3.8	-4.3	+103
98	9.5	"	18.06	3.4	-6.8	+164
96	7.1	"	16.06	3.0	-8.8	+212
96	5.3	"	14.06	2.7	-10.3	+246
92	3.8	"	12.06	2.3	-11.4	+273
90	2.7	"	10.06	1.9	-12.1	+291
88.4	2.0	"	8.46	1.6	-12.5	+300
87	"	"	7.06	1.3	-12.2	+294
63	"	"	-16.94	-3.2	-7.7	+184
45	"	"	-34.94	-6.6	-4.3	+102
18	"	"	-61.94	-11.8	+0.9	-21
9	"	"	-70.94	-13.5	+2.6	-62
7.2	2.0	"	-72.74	-13.8	+2.9	-70
0	10.0	12.9	-79.94	-15.2	+12.3	-295

* For $E = 4800$ ksi & $\alpha = 5 \times 10^{-6} \frac{in/in}{°F}$

Priestley's Method (cont)

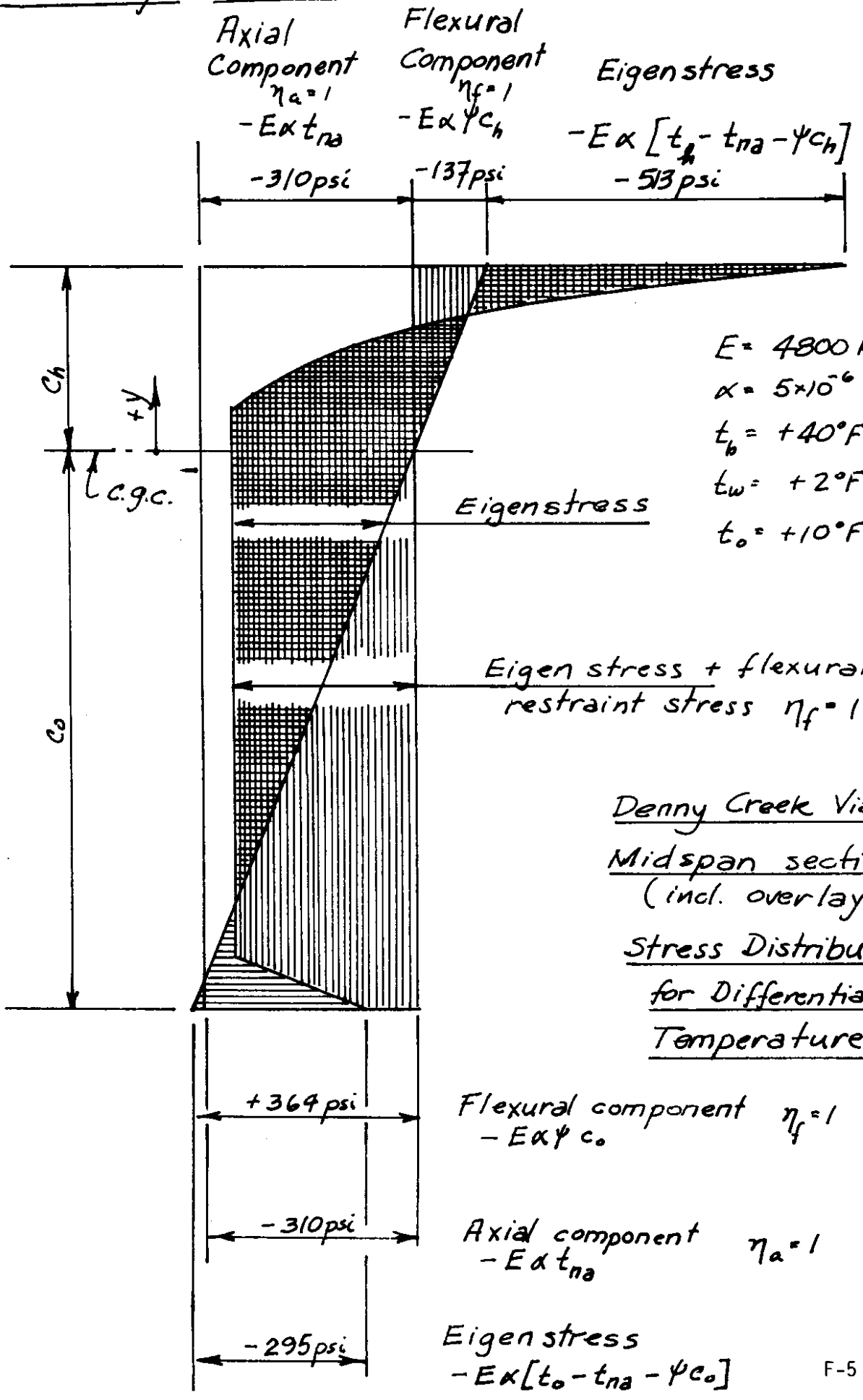

$E = 4800$ ksi

$\alpha = 5\times10^{-6}\ \frac{in/in}{°F}$

$t_b = +40°F$

$t_w = +2°F$

$t_o = +10°F$

Denny Creek Viaduct

Midspan section (incl. overlay)

Stress Distribution for Differential Temperature

Denny Creek Bridge Stress Investigation — 16 Jan 83

Section Properties — Stage III — Est NA= 77.31

Element	Width in	Height in	Area in2	y NA in	Ay in3	Ay^2 in4	Io in4
Top slab (ext)	184.38	10.00	1843.75	25.69	47368.29	1216952	15365
	174.00	11.00	638.00	17.39	11095.63	192967	4080
Top slab (int)	106.00	10.00	1060.00	25.69	27232.75	699644	8833
	106.00	11.00	388.67	17.39	6759.41	117555	2486
Top slab (web)	32.00	21.00	672.00	20.19	13568.54	273966	24696
			4602.42	23.04	106024.63	2501084	55460
Web	27.32	9.69	264.78	4.85	1283.03	6217	2072
	4.68	9.69	22.67	6.46	146.47	946	118
Sums above est NA			4889.87	21.97	107454.13	2508248	57651
Web	20.41	14.31	292.10	-7.15	-2089.76	14951	4984
	6.91	14.31	49.42	-4.77	-235.71	1124	562
	15.00	54.00	810.00	-41.31	-33460.07	1382193	196830
	5.41	54.00	146.17	-32.31	-4722.64	152583	23680
Sums web partial			1297.69	-31.22	-40508.18	1550850	226056
Bottom slab	9.00	9.00	40.50	-65.31	-2645.00	172742	182
	4.34	9.00	19.55	-71.31	-1394.21	99419	88
	96.00	9.00	864.00	-72.81	-62906.74	4580159	5832
Sums bottom slab			924.05	-72.45	-66945.95	4852320	6102
Sums below est NA			2221.74	-48.36	-107454.1	6403170	232158
Sums Section B/C			7111.61	1.1305E-7	0.00	8911418	289809
			ybcgc=	77.308723		289809	
						0	
					Io=	9201227	
Add for Section A							
	12.44	9.00	55.99	-62.31	-3488.75	217380	252
	76.34	9.00	687.10	-63.81	-43843.19	2797578	4638
Sums addition			743.09	-63.70	-47331.94	3014958	4890
Sums below est NA			2964.83	-52.21	-154786.1	9418128	237048
			7854.70	-6.03	-47331.94	11926376	294699
			ybcgc=	71.282785		294699	
						-285219	
					Io=	11935855	

Denny Creek Bridge Stress Investigation — 16 Jan 83

Section Properties — Stage III w/overlay — Est NA= 79.94

Element	Width in	Height in	Area in2	y NA in	Ay in3	Ay^2 in4	Io in4
Top slab (ext)	184.38	12.00	2212.50	24.06	53225.95	1280453	26550
	174.00	11.00	638.00	14.76	9414.92	138935	4080
Top slab (int)	106.00	12.00	1272.00	24.06	30600.41	736152	15264
	106.00	11.00	388.67	14.76	5735.53	84639	2486
Top slab (web)	32.00	23.00	736.00	18.56	13657.90	253449	32445
			5247.17	21.47	112634.71	2493628	80826
Web	28.59	7.06	201.78	3.53	711.97	2512	837
	3.41	7.06	12.02	4.70	56.55	266	33
Sum above est NA			5460.97	20.77	113403.24	2496406	81696
Web	20.41	16.94	345.87	-8.47	-2930.07	24822	8274
	8.18	16.94	69.29	-5.65	-391.34	2210	1105
	15.00	54.00	810.00	-43.94	-35593.89	1564105	196830
	5.41	54.00	146.17	-34.94	-5107.71	178479	23680
Sum web partial			1371.34	-32.10	-44023.01	1769616	229889
Bottom slab	9.00	9.00	40.50	-67.94	-2751.69	186959	182
	4.34	9.00	19.55	-73.94	-1445.71	106901	88
	96.00	9.00	864.00	-75.44	-65182.81	4917592	5832
Sum bottom slab			924.05	-75.08	-69380.22	5211451	6102
Sum below est NA			2295.39	-49.40	-113403.2	6981067	235991
Sum Section B/C			7756.36	2.7436E-7	0.00	9477473	317688
			ybcgc=	79.943072		317688	
						0	
					Io=	9795161	
Add for Section A							
	12.44	9.00	55.99	-64.94	-3636.25	236149	252
	76.34	9.00	687.10	-66.44	-45653.26	3033343	4638
Sum addition			743.09	-66.33	-49289.52	3269492	4890
Sum below est NA			3038.48	-53.54	-162692.8	10250560	240881
			8499.45	-5.80	-49289.51	12746966	322577
			ybcgc=	74.143931		322577	
						-285837	
					Io=	12783706	

Section Properties w/ overlay

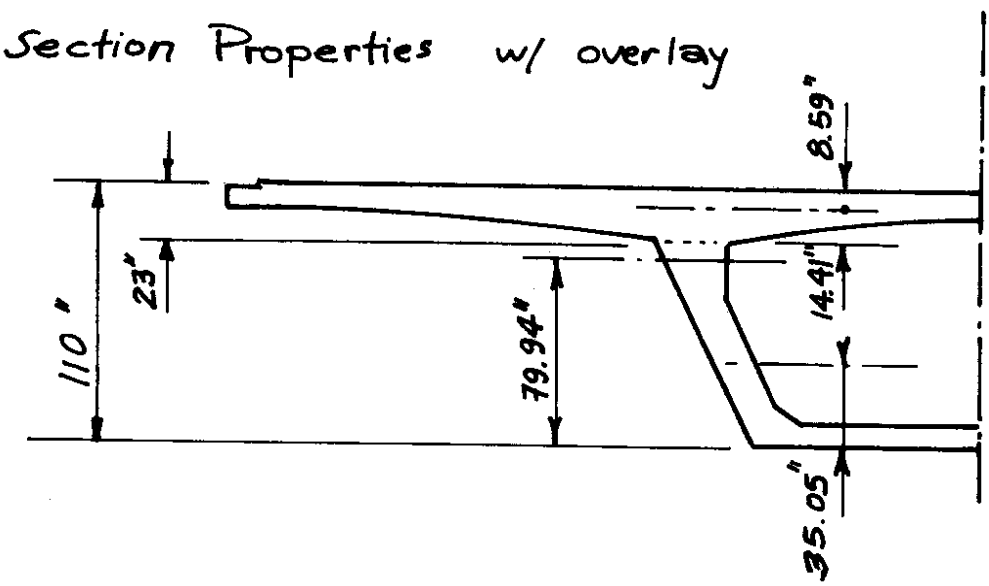

Area*	y_b	I_o*	c_{top}	c_{bot}	
5247.2 in²	101.41"	156,500 in⁴	8.59"	14.41"	Top Slab
2509.2 in²	35.05"	2,164,650 in⁴	51.95"	35.05"	Web & Bot. Slab
7756.4 in²	79.94	9,795,160 in⁴	30.06"	79.94"	Σ

* For ½ bridge

CTL Method for same temperature distribution

Average slab temperature

$$t_s = \int_{87}^{110} t(y)\, b(y)\, dy \Big/ A_{slab}$$

$$= \frac{115.1\ in^2 °F + 6336.2\ in^2 °F + 1539.1\ in^2 °F + 84,799.7\ in^2 °F}{5247.17\ in^2}$$

$$= 17.7°F$$

Average web & bottom slab temperature

$$t_w = \int_{0}^{87} t(y)\, b(y)\, dy \Big/ (A_{web} + A_{bottom\ slab})$$

$$= \frac{4205.6\ in^2 °F + 359.7\ in^2 °F + 39.9\ in^2 °F + 1634.2\ in^2 °F + 1257.9\ in^2 °F}{1585.14\ in^2 + 924.05\ in^2}$$

$$= 3.0°F$$

$\therefore\ \Delta t = 17.7°F - 3.0°F = 14.7°F$

$\alpha \Delta t = 14.7°F\ (5 \times 10^{-6}\ in/in/°F) = 73.5 \times 10^{-6}\ in/in$

Assume $E = 4800$ ksi

See previous sheet for section properties

Subscript 1 refers to top slab

" 2 " " web + bottom slab

CTL Method (cont)

$$m' = \frac{E_2 I_2}{E_1 I_1} = \frac{(4800\,ksi)(2{,}164{,}650\,in^4)}{(4800\,ksi)(156{,}500\,in^4)} = 13.83$$

$$B = 1 + m' = 14.83$$

$$C = e_2 - m' e_1 = 51.95'' - 13.83(14.41'') = -147.35''$$

$$F = e_2^2 + r_2^2 + m' e_1^2 + m' r_1^2$$

$$= (51.95'')^2 + \frac{2{,}164{,}650\,in^4}{2509.2\,in^2} + 13.83\left[(14.41'')^2 + \frac{156{,}500\,in^4}{5247.2\,in^2}\right]$$

$$= 6845.8\,in^2$$

$$BF - C^2 = (14.83)(6845.8\,in^2) - (-147.35'')^2 = 79810\,in^2$$

$$\frac{C}{B} = \frac{-147.35''}{14.83} = -9.94''$$

Then interface shear

$$X' = \alpha\,\Delta t\,E_2 I_2\left(\frac{B}{BF - C^2}\right)$$

$$= (73.5\times10^{-6})(4800\,ksi)(2{,}164{,}650\,in^4)\left(\frac{14.83}{79810\,in^2}\right)$$

$$= 141.9^k$$

and interface moment

$$M = \alpha\,\Delta t\,E_2 I_2\left(\frac{C}{C^2 - BF}\right)$$

$$= (73.5\times10^{-6})(4800\,ksi)(2{,}164{,}650\,in^4)\left(\frac{-147.35''}{-79810\,in^2}\right)$$

$$= (141.9^k)(9.94'') = 1410^{k''}$$

CTL Method (cont)

Flexural restraint stresses

For simple beam the end rotation for a prismatic beam

$$\theta = \frac{M^* \ell}{2EI_2} \qquad \text{where } M^* = Xe_{/2} + M$$

& for full flexural restraint, $\eta_f = 1$ the fixed end moment generated by this rotation is

$$M^F = +k_{sym}\,\theta \qquad \text{where } k_{sym} = \frac{2EI_{cs}}{\ell}$$

I_{cs} = moment of inertia of composite section

then $$M^F = +\frac{2EI_{cs}}{\ell} \cdot \frac{M^* \ell}{2EI_2} \cdot \eta_f = +M^* \frac{I_{cs}}{I_2}\eta_f$$

$$M^F = +\left[(141.9^k)(51.95'') + 1410^{k''}\right]\left(\frac{9,795,160^{in^4}}{2,164,650^{in^4}}\right)(1)$$

$$= +37,738^{k''}$$

& the restraint stresses are

$$f_{c_t}^{slab} = \left(\frac{+37,738^{k''}}{9,795,160^{in^4}}\right)(-30.06'') = -0.122 \text{ ksi}$$

$$f_{c_t}^{web} = (\quad " \quad)(-7.06) = -0.029 \text{ ksi}$$

$$f_{c_b}^{web} = (\quad " \quad)(79.94) = +0.324 \text{ ksi}$$

CTL Method (cont)

"Eigenstresses" (stresses req'd for strain & curvature compatibility at slab-web interface)

Note that since slab is warmer than the web, the interface shear acts in the sense that produces compression in the slab & tension in the girder

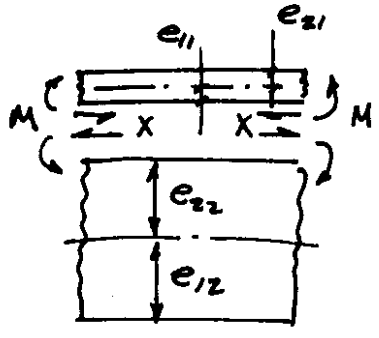

$$f_{c_t}^{slab} = -\frac{X}{A_1} + \frac{X e_{11} - M}{I_1} e_{21}$$

$$f_{c_b}^{slab} = -\frac{X}{A_1} - \frac{X e_{11} - M}{I_1} e_{11}$$

$$f_{c_t}^{web} = +\frac{X}{A_2} + \frac{X e_{22} + M}{I_2} e_{22}$$

$$f_{c_b}^{web} = +\frac{X}{A_2} - \frac{X e_{22} + M}{I_2} e_{12}$$

CTL Method (cont)

Eigenstresses

$$f_{c_t}^{slab} = -\frac{141.9^k}{5247.2^{in^2}} + \left[\frac{(141.9^k)(14.41") - 1410^{k"}}{156500 in^4}\right] 8.59" =$$

$$= +0.008 ksi$$

$$f_{c_b}^{slab} = -\frac{141.9^k}{5247.2^{in^2}} - \left[\frac{(141.9^k)(14.41") - 1410^{k"}}{156500 in^4}\right] 14.41" =$$

$$= -0.085 ksi$$

$$f_{c_t}^{slab} = +\frac{141.9^k}{2509.2^{in^2}} + \left[\frac{(141.9^k)(51.95") + 1410^{k"}}{2,164,650 in^4}\right] =$$

$$+0.267 ksi$$

$$f_{c_b}^{slab} = +\frac{141.9^k}{2509.2^{in^2}} - \left[\frac{(141.9^k)(51.95") + 1410^{k"}}{2,164,650 in^4}\right] =$$

$$-0.086 ksi$$

CTL Method (cont)

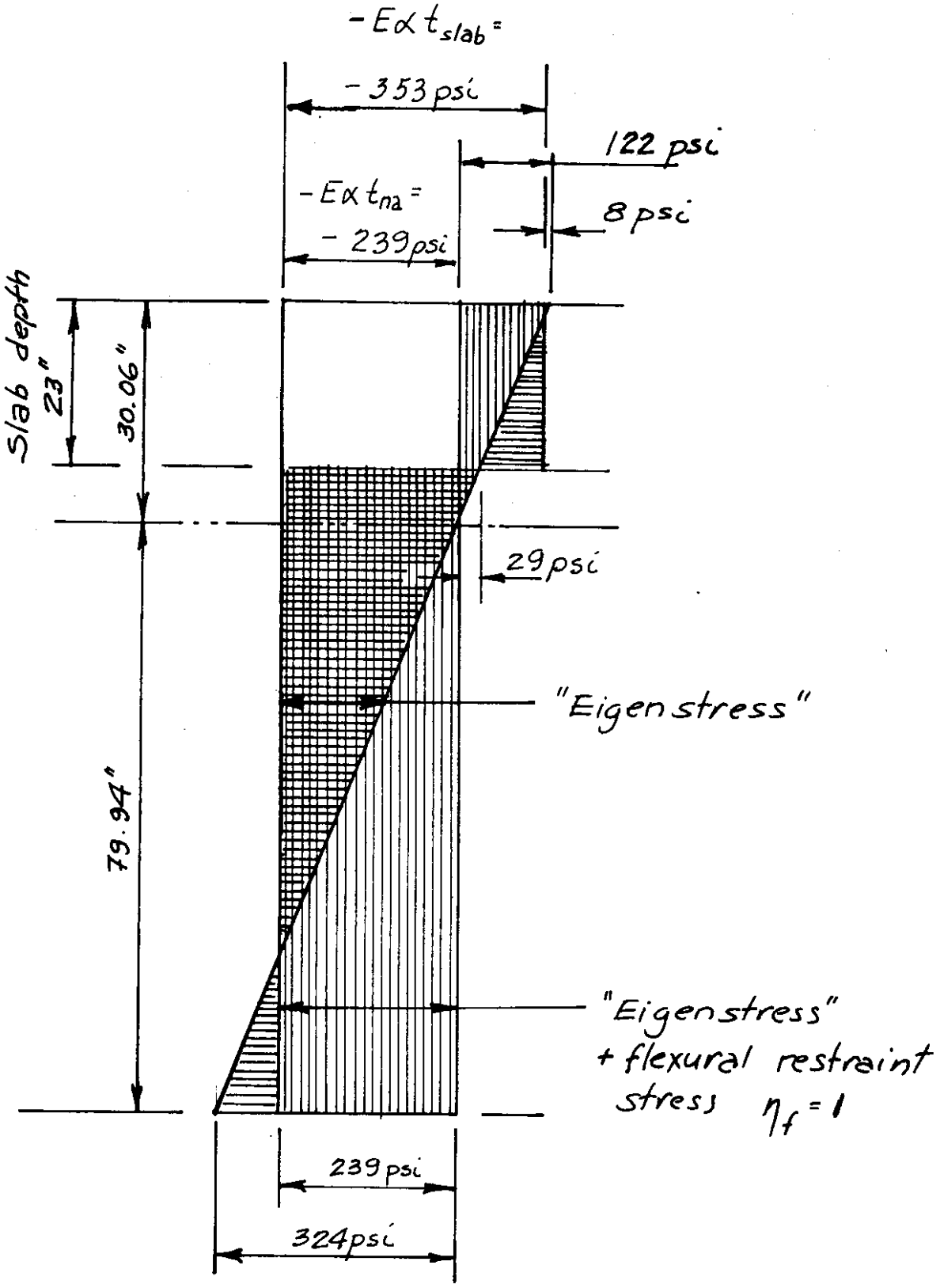

```
100 ! Stresses due to temperature distributions in the vertical direction
120 ! for Denny Creek Bridge          JH Clark        15 Jan 83
140 ! ************************************************************
160 ! Define box girder dimensions [inches]
180 DIM S5$[30]
200 SHORT W(5,220),T(5,220),FCA(220),FCF(220),FC1(5,220),FC2(5,220),Y(220)
220 X1=96 @ Y1=0 ! Soffit edge
240 X2=76.3445 @ Y2=9 ! Top of bottom slab at beginning of slab haunch
260 X3=88.7874 @ Y3=18 ! Top of bottom slab at end       of slab haunch
280 X4=106 @ Y4=63 ! Bottom of web/top slab fillet inside
300 X5=106 @ Y5=87 ! Top    of web/top slab fillet inside
320 X6=138 @ Y6=87 ! Top    of web/top slab fillet outside
340 X7=312 @ Y7=98 ! Bottom of top slab at end of exterior haunch
360 X8=322.375 @ Y8=98 ! Bottom of top slab at outside edge
380 X9=322.375 @ Y9=110 ! Top    of top slab at outside edge
400 X0=0 @ Y0=98 ! Bottom of top slab at centerline bridge
420 Swo=42/87 ! Slope of exterior web surface H/V
440 Sh=12.4429/9 ! Slope of bottom slab haunch H/V
460 Swi=17.2126/45 ! Slope of interior web surface H/V
480 Yt=48 !  Penetration of top slab parabolic distribution
500 ! ************************************************
520 DISP "Select printer" @ INPUT PNTR@ IF PNTR<> 701 THEN PNTR=1 @ PRINTER IS P
NTR
540 DISP "Selct plotter" @ INPUT PLTR@ IF PLTR<> 305 THEN PLTR=1
560 DISP "Plot section ? [Y] or [N]" @ INPUT Y$@ IF Y$="N" OR Y$="n" THEN GOTO N
P01
580 PLOTTER IS PLTR @ SETGU @ IF PLTR=1 THEN GCLEAR
600 SHOW 350,0,-.01,110.01
620 MOVE 0,0
640 DRAW X1,Y1
660 DRAW X6,Y6
680 MOVE X6,Y6
700 FOR Y=Y6 TO Y7 STEP (Y7-Y6)/32
720   DRAW FNWID4(Y)+X6,Y
740 NEXT Y
760 DRAW X7,Y7
780 DRAW X8,Y8
800 DRAW X9,Y9
820 DRAW 0,Y9
840 DRAW X0,Y0
860 FOR Y=Y0 TO Y5 STEP (Y5-Y0)/32
880    DRAW X5-FNWID5(Y),Y
900 NEXT Y
920 MOVE X5,Y5
940 DRAW X4,Y4
960 DRAW X3,Y3
980 DRAW X2,Y2
1000 DRAW 0,Y2
1020 DRAW 0,0
1040 ! DUMP GRAPHICS @ PRINT CHR$ (12)
1060 NP01: ! ************************************************
1080 DISP "Enter temperatures [Deg F]"
1100 DISP "      Top surface " @ INPUT Tts
1120 DISP "      Interior of box" @ INPUT Tint
1140 DISP "      Bottom surface" @ INPUT Tbs
1160 DISP "      Reference temperature" @ INPUT Tref
1180 DISP "Enter stiffness characteristics [ksi-inch-deg F units]"
1200 DISP "      Modulus of elasticity [ksi] " @ INPUT EL
1220 DISP "      Coefficient of thermal expansion " @ INPUT CTE
1240 DISP "      Axial restraint stiffness [k/in]" @ INPUT KA
```

```
1260 DISP "       Flexural   do      do  left [k-in/rad]" @ INPUT KFL
1280 DISP "       Flexural   do      do  right [k-in/rad]" @ INPUT KFR
1300 DISP "Enter distance of section from left end [ft]" @ INPUT XC
1320 DISP "Enter span length [ft]" @ INPUT XSP
1340 ! ********************************************
1360 FOR I=0 TO 220 @ FOR J=0 TO 5 @ T(J,I)=Tref @ NEXT J @ NEXT I
1380 ! Echo print basic input values
1400 PRINT CHR$ (27)&"&k9S"
1420 PRINT CHR$ (27)&"&l60F"
1440 PRINT CHR$ (27)&"&l1L"
1460 GOSUB HDR
1480 PRINT
1500 PRINT "      Section is Denny Creek Bridge at midspan with overlay"
1520 PRINT "      Temperatures [Deg F]"
1540 PRINT "            Top surface    : ";Tts
1560 PRINT "            Interior       : ";Tint
1580 PRINT "            Bottom surface : ";Tbs
1600 PRINT "            Reference      : ";Tref
1620 PRINT
1640 PRINT "            Young's modulus: ";EL;" ksi"
1660 PRINT "            Exp coeff      : ";CTE;" per deg F"
1680 PRINT
1700 PRINT "            Axial restraint: ";KA;" kips/inch"
1720 PRINT "            Flexural do lft: ";KFL;" kip-in/rad"
1740 PRINT "            Flexural do rht: ";KFR;" kip-in/rad"
1760 PRINT
1780 ! ************************************************************************
1800 ZX=TIME
1820 ! Calculate integrals
1840 S1,S2,S3,S4,S5=0
1860 NP=220 @ DY=(Y9-Y1)/NP
1880 FOR I=1 TO NP-1
1900   Y(I)=Y1+(Y9-Y1)*I/NP+.5*DY @ Y=Y(I)
1920   DS=0
1940   DS=FNTMP1(Y)*FNWID1(Y)*DY
1960   W(1,I)=FNWID1(Y) @ T(1,I)=FNTMP1(Y) ! Bottom slab
1980   DS=DS+FNTMP2(Y)*FNWID2(Y)*DY
2000   W(2,I)=FNWID2(Y) @ T(2,I)=FNTMP2(Y) ! Exterior webs
2020   DS=DS+FNTMP3(Y)*FNWID3(Y)*DY
2040   W(3,I)=FNWID3(Y) @ T(3,I)=FNTMP3(Y) ! Interior webs
2060   DS=DS+FNTMP4(Y)*FNWID4(Y)*DY
2080   W(4,I)=FNWID4(Y) @ T(4,I)=FNTMP4(Y) ! Exterior top slab
2100   DS=DS+FNTMP5(Y)*FNWID5(Y)*DY
2120   W(5,I)=FNWID5(Y) @ T(5,I)=FNTMP5(Y) ! Interior top slab
2140   S1=S1+DS
2160   S2=S2+DS*(Y+.5*DY)
2180   DA=0
2200   DA=FNWID1(Y)*DY
2220   DA=DA+FNWID2(Y)*DY
2240   DA=DA+FNWID3(Y)*DY
2260   DA=DA+FNWID4(Y)*DY
2280   DA=DA+FNWID5(Y)*DY
2300   S3=S3+DA
2320   S4=S4+DA*(Y+.5*DY)
2340   S5=S5+DA*(Y+.5*DY)^2
2360 ENDLP: NEXT I @ Y(0)=Y0 @ Y(NP)=Y9
2380 DS=(FNTMP1(.25*DY)*FNWID1(.25*DY)+FNTMP2(.25*DY)*FNWID2(.25*DY))*.5*DY
2400 DA=(FNWID1(.25*DY)+FNWID2(.25*DY))*.5*DY
2420 S1=S1+DS
2440 S2=S2+DS*.125*DY
```

```
2460 S3=S3+DA
2480 S4=S4+DA*.125*DY
2500 S5=S5+DA*(.125*DY)^2
2520 Z=Y9-.25*DY
2540 DA=(FNWID2(Z)+FNWID3(Z)+FNWID4(Z)+FNWID5(Z))*.5*DY
2560 DS=(FNTMP2(Z)*FNWID2(Z)+FNTMP3(Z)*FNWID3(Z)+FNTMP4(Z)*FNWID4(Z)+FNTMP5(Z)*F
NWID5(Z))*.5*DY
2580 S1=S1+DS
2600 S2=S2+DS*(Y9-.125*DY)
2620 S3=S3+DA
2640 S4=S4+DA*(Y9-.125*DY)
2660 S5=S5+DA*(Y9-.125*DY)^2
2680 TNA=S1/S3
2700 YNA=S4/S3
2720 INA=S5-S3*YNA*YNA
2740 DT=(S2-YNA*S1)/INA
2760 S1$="Area" @ S2$="Moment of inertia" @ S3$="Ybcgc" @ S4$="Temperature at NA
"
2780 S5$="Effective differential" @ U1$=" in2" @ U2$=" in4" @ U3$=" in"
2800 U4$="Deg F" @ U5$="Deg F/in"
2820 ZY=TIME
2840 DISP "Time to calculate integrals : ";ZY-ZX
2860 PRINT USING F02 ; S1$,S3,U1$
2880 PRINT USING F02 ; S2$,INA,U2$
2900 PRINT USING F02 ; S3$,YNA,U3$
2920 PRINT USING F02 ; S4$,TNA,U4$
2940 PRINT USING F02 ; S5$,DT,U5$
2960 F02: IMAGE 5X,22A,1X,1D.4DE,8A
2980 ! ********************************************************
3000 NUA=KA/(1+KA*XSP/(S1*EL))
3020 NUF=KFL*(1-XC/XSP)+KFR*XC/XSP @ NUF=NUF/(1+NUF*XSP/INA*EL)
3040 PRINT USING F02 ; "Axial restraint";NUA
3060 PRINT USING F02 ; "Flexural restraint";NUF
3080 FOR I=0 TO NP
3100   Y(I)=Y9*I/NP+.5*DY @ Y=Y(I)
3120   FCA(I)=-(EL*CTE*(TNA-Tref)*(1-NUA))
3140   FCF(I)=-(EL*CTE*DT*(Y-YNA)*(1-NUF))
3160   FOR J=1 TO 5
3180     FC1(J,I)=-(EL*CTE*(T(J,I)-Tref-(TNA-Tref)-DT*(Y-YNA)))
3200     FC2(J,I)=-(EL*CTE*(T(J,I)-Tref-(TNA-Tref)*(1-NUA)-DT*(Y-YNA)*(1-NUF)))
3220   NEXT J
3280 NEXT I
3300 KYLBL: ! ************************************************
3320 ON KEY# 1,"PNT TMP" GOTO PNTTMP
3340 ON KEY# 2,"PLT TMP" GOTO PLTTMP
3360 ON KEY# 3,"PNT STR" GOTO PNTSTR
3380 ON KEY# 4,"PLT STR" GOTO PLTSTR
3400 ON KEY# 5,"DEVICE " GOTO DVCE
3420 KEY LABEL
3440 WAIT 500 @ GOTO 3440
3460 ! ********************************************************
3480 PNTTMP: ! Print temperatures in different portions at all heights
3500 GOSUB HDR
3520 PRINT USING F144 ; "Height";"Temperature deg F"
3540 F144: IMAGE 5X,6A,15X,25A
3560 PRINT USING F145 ; " above";"Bottom";"Exterior";"Interior";"Exterior";"Inte
rir"
3580 F145: IMAGE 5X,6A,5(1X,8A)
3600 PRINT USING F145 ; "soffit";" slab ";"  web   ";"   web  ";"top slab";"top
slab"
```

```
3620 PRINT
3640 F147: IMAGE 5X,3D.3D,5(3X,M3D.D)
3660 FOR I=0 TO NP
3680   PRINT USING F147 ; Y(I),T(1,I),T(2,I),T(3,I),T(4,I),T(5,I)
3700 NEXT I
3720 GOTO KYLBL
3740 ! ******************************************************
3760 DVCE: DISP "Select printer CRT [1] or LPT [701] " @ INPUT PNTR
3780       DISP "Select plotter CRT [1] or 7225A [305] " @ INPUT PLTR
3800 GOTO KYLBL
3820 ! ************************************************************
3840 PLTTMP: ! Plot temperatures profiles for various parts
3860 IF PLTR=1 THEN GCLEAR
3880 LX1=15 @ LX2=35 @ LY1=25 @ LY2=80
3900 GOSUB PRFSET
3920 MOVE 0,0
3940 FOR I=0 TO Y3\DY+1
3960   MOVE 0,Y(I)
3980   DRAW T(1,I),Y(I)
4000 NEXT I
4020 LX1=37.5 @ LX2=57.5
4040 GOSUB PRFSET
4060 MOVE 0,0
4080 FOR I=0 TO NP
4100   MOVE 0,Y(I)
4120   DRAW T(2,I),Y(I)
4140 NEXT I
4160 LX1=60 @ LX2=80
4180 GOSUB PRFSET
4200 MOVE 0,0
4220 FOR I=0 TO NP
4240   MOVE 0,Y(I)
4260   DRAW T(3,I),Y(I)
4280 NEXT I
4300 LX1=82.5 @ LX2=102.5
4320 GOSUB PRFSET
4340 MOVE 0,0
4360 FOR I=(Y5-DY)\DY TO NP
4380   MOVE 0,Y(I)
4400   DRAW T(4,I),Y(I)
4420 NEXT I
4440 LX1=105 @ LX2=125
4460 GOSUB PRFSET
4480 MOVE 0,0
4500 FOR I=(Y5-DY)\DY TO NP
4520   MOVE 0,Y(I)
4540   DRAW T(5,I),Y(I)
4560 NEXT I
4580 SETGU @ DEG @ LDIR 0 @ CSIZE 4.5 @ MOVE 70,95 @ LORG 4
4600 LABEL "Denny Creek Bridge Stress Investigation"
4620 CSIZE 3.5 @ MOVE 70,86 @ LABEL "Temperature Profiles (deg F)"
4640 MOVE 25,8 @ CSIZE 3 @ LABEL "Bottom" @ MOVE 25,4 @ LABEL " Slab"
4660 MOVE 47.5,8 @ LABEL "Exterior" @ MOVE 47.5,4 @ LABEL "  Web"
4680 MOVE 70,8 @ LABEL "Interior" @ MOVE 70,4 @ LABEL "  Web"
4700 MOVE 92.5,8 @ LABEL "Exterior" @ MOVE 92.5,4 @ LABEL "Top Slab"
4720 MOVE 115,8 @ LABEL "Interior" @ MOVE 115,4 @ LABEL "Top Slab"
4740 LDIR 90 @ MOVE 4,55 @ LABEL "Height above Soffit (inch)"
4760 GOTO KYLBL
4780 ! ************************************************
4800 PRFSET: LOCATE LX1,LX2,LY1,LY2 @ CSIZE 3 @ FXD 0,0
```

```
4820 SCALE 0,Tts,0,Y9
4840 IF LX1=15 THEN LAXES 10,10,0,0,5,5,3 ELSE LAXES 10,0,0,0,5,0,3
4860 AXES 10,10,Tts,Y9,5,5,3 @ RETURN
4880 ! ************************************************************************
4900 PNTSTR: ! Print stresses at all levels for each part
4920 DISP "Select eigenstresses [0] or resultant stresses [1] " @ INPUT FLG1
4940 GOSUB HDR
4960 IF FLG1=0 THEN Z$="Eigen" ELSE Z$="Resultant"
4980 PRINT TAB (6);"Height "&Z$&"  Stresses (psi tens+)"
5000 PRINT USING F177 ; " above";"Bottom";"Exterior";"Interior";"Exterior";"Inte
rir";"Axial";"Flexural"
5020 F177: IMAGE 5X,6A,5(1X,8A),5X,2(1X,8A)
5040 PRINT USING F177 ; "soffit";" slab ";"  web   ";"   web  ";"top slab";"top
slab";"Restrnt";"Stress"
5060 PRINT
5080 F179: IMAGE 5X,3D.2D,5(3X,SD.3D),5X,2(3X,SD.3D)
5100 IF FLG1=1 THEN GOTO 5200
5120 FOR I=0 TO NP
5140   PRINT USING F179 ; Y(I),FC1(1,I),FC1(2,I),FC1(3,I),FC1(4,I),FC1(5,I),FCA(
I),FCF(I)
5160 NEXT I
5180 GOTO KYLBL
5200 FOR I=0 TO NP
5220   PRINT USING F179 ; Y(I);FC2(1,I);FC2(2,I);FC2(3,I);FC2(4,I);FC2(5,I)
5240 NEXT I
5260 ! ************************************************
5280 HDR: ! Page heading subroutine
5300 PRINT " " ! Page eject
5320 PRINT @ PRINT @ PRINT
5340 PRINT USING "5X,K" ; "Denny Creek Bridge Stress Investigation
63-1080"
5360 PRINT USING "5X,K" ; "Stresses due to given temperature distribution  "
5380 PRINT USING "5X,K" ; "Homogeneous elastic section
   15 Jan 83"                                                              JHC
5400 PRINT
5420 RETURN
5440 ! ************************************************
5460 ! Define width as function of height above soffit
5480 DEF FNWID1(y) = X2*(y<Y2) !      Width of bottom slab between haunch and CL
5500 DEF FNWID2(y) !                  Width of exterior web
5520    Xo=X1+Swo*y
5540    IF y>Y6 THEN Xo=X6
5560    Xi=X2+Sh*(y-Y2)*(y>Y2)
5580    IF y>Y3 THEN Xi=X3+Swi*(y-Y3)
5600    IF y>Y4 THEN Xi=X4
5620    FNWID2=Xo-Xi
5640 ! ************************************************
5660 FN END
5680 DEF FNWID3(y) = 0 !              Width of interior webs
5700 DEF FNWID4(y) !                  Width of exterior top slab
5720    IF y>Y7 THEN Xo=X8
5740    IF y>Y7 THEN GOTO 5780
5760    Xo=X6+(X7-X6)*(1-((Y7-y)/(Y7-Y6))^.5)
5780    Xi=X6
5800    FNWID4=(Xo-Xi)*(y>Y6)
5820 FN END
5840 ! ************************************************************
5860 DEF FNWID5(y) !                  Width of interior top slab
5880    Xo=X5
5900    IF y>Y0 THEN Xi=X0
```

```
5920     IF y>Y0 THEN GOTO 5960
5940     Xi=(X5-X0)*((Y0-y)/(Y0-Y5))^.5
5960     FNWID5=(Xo-Xi)*(y>Y5)
5980 FN END
6000 ! ************************************************************
6020 ! Define temperatures as function of height above soffit
6040 ! Priestly's slab distribution
6060 DEF FNTMP1(y) = Tref+(Tbs-Tref)*(1-y/Y2)*(y<Y2) ! Bottom slab
6080 ! ************************************************************
6100 DEF FNTMP2(y) !                                    Exterior web
6120   TY1=Tref+(Tbs-Tref)*(1-y/Y2)*(y<Y2)
6140   TY2=Tref+(Tbs-Tref)*(.5*Y2/FNWID2(y))
6160   IF Tbs>Tref THEN TY2=MAX (TY2,TY1) ELSE TY2=MIN (TY2,TY1)
6180   IF y<Yt THEN TY3=TY2 @ GOTO 6240
6200   TY3=Tref+(Tts-Tref)*((y-Yt)/(Y9-Yt))^5
6220   IF Tts>Tref THEN TY3=MAX (TY3,TY2) ELSE TY3=MIN (TY3,TY2)
6240   FNTMP2=TY3
6260 FN END
6280 ! ************************************************************
6300 DEF FNTMP3(y) !                                    Interior web
6320   TY1=Tref+(Tbs-Tref)*(1-y/Y2)*(y<Y2)
6340   TY2=Tint
6360   IF Tbs>Tref THEN TY2=MAX (TY2,TY1) ELSE TY2=MIN (TY2,TY1)
6380   IF y<Yt THEN TY3=TY2 @ GOTO 6440
6400   TY3=Tref+(Tts-Tref)*((y-Yt)/(Y9-Yt))^5
6420   IF Tts>Tref THEN TY3=MAX (TY3,TY2) ELSE TY3=MIN (TY3,TY2)
6440   FNTMP3=TY3
6460 FN END
6480 ! ************************************************************
6500 DEF FNTMP4(y) !                          Exterior top slab
6520   Q=.5*(Y9-Y8)*(X9-X6)^2+(Y7-Y6)*(X7-X6)^2/12
6540   Q4=Q/((Y9-Y8)*(X9-X6)+(Y7-Y6)*(X7-X6)/3) ! D4 is slab depth at centroid
6560   D4=Y9-Y8+(Y8-Y6)*((X7-X6-Q4)/(X7-X6))^2
6580   TY1=Tref+(Tbs-Tref)*(1-(y-Y9+D4)/D4) !          for parabolic haunch
6600   TY2=Tref+(Tts-Tref)*((y-Yt)/(Y9-Yt))^5
6620   IF Tts>Tref THEN TY2=MAX (TY1,TY2) ELSE TY2=MIN (TY1,TY2)
6640   FNTMP4=TY2
6660 FN END
6680 ! ************************************************************
6700 DEF FNTMP5(y) !                          Interior top slab
6720   Q=.5*(Y9-Y0)*X5^2+(Y0-Y5)*(X5-X0)^2/12
6740   Q5=Q/((Y9-Y0)*X5+(Y0-Y5)*(X5-X0)/3) !       Q is slab depth at centroid
6760   D5=Y9-Y0+(Y0-Y5)*((X5-X0-Q5)/(X5-X0))^2
6780   TY1=Tint+(Tts-Tint)*(y-Y9+D5)/D5*(y-Y9+D5>0) !    for parabolic haunch
6800   TY2=Tref+(Tts-Tref)*((y-Yt)/(Y9-Yt))^5
6820   IF Tts>Tref THEN TY2=MAX (TY1,TY2) ELSE TY2=MIN (TY1,TY2)
6840   FNTMP5=TY2
6860 FN END
6880 ! ************************************************************
6900 PLTSTR: ! Plot stresses
6920 DISP "Select eigenstresses [0] or resultant stresses [1] " @ INPUT FLG1
6940 IF PLTR=1 THEN GCLEAR
6960 LX1=15 @ LX2=35 @ LY1=25 @ LY2=80
6980 GOSUB PRFSET2
7000 MOVE 0,0
7020 FOR I=0 TO Y3\DY+1
7040   MOVE 0,Y(I)
7060   IF FLG1=0 THEN DRAW FC1(1,I),Y(I) ELSE DRAW FC2(1,I),Y(I)
7080 NEXT I
7100 LX1=37.5 @ LX2=57.5
```

```
7120 GOSUB PRFSET2
 .40 MOVE 0,0
7160 FOR I=0 TO NP
7180   MOVE 0,Y(I)
7200   IF FLG1=0 THEN DRAW FC1(2,I),Y(I) ELSE DRAW FC2(2,I),Y(I)
7220 NEXT I
7240 LX1=60 @ LX2=80
7260 GOSUB PRFSET2
7280 MOVE 0,0
7300 FOR I=0 TO NP
7320   MOVE 0,Y(I)
7340   IF FLG1=0 THEN DRAW FC1(3,I),Y(I) ELSE DRAW FC2(3,I),Y(I)
7360 NEXT I
7380 LX1=82.5 @ LX2=102.5
7400 GOSUB PRFSET2
7420 MOVE 0,0
7440 FOR I=(Y5-DY)\DY TO NP
7460   MOVE 0,Y(I)
7480   IF FLG1=0 THEN DRAW FC1(4,I),Y(I) ELSE DRAW FC2(4,I),Y(I)
7500 NEXT I
7520 LX1=105 @ LX2=125
7540 GOSUB PRFSET2
7560 MOVE 0,0
7580 FOR I=(Y5-DY)\DY TO NP
7600   MOVE 0,Y(I)
7620   IF FLG1=0 THEN DRAW FC1(5,I),Y(I) ELSE DRAW FC2(5,I),Y(I)
7640 NEXT I
7660 SETGU @ DEG @ LDIR 0 @ CSIZE 4.5 @ MOVE 70,95 @ LORG 4
7680 ! LABEL "Denny Creek Bridge Stress Investigation"
7700 IF FLG1=0 THEN Z$="Eigen" ELSE Z$="Resultant"
7720 CSIZE 3.5 @ MOVE 70,86 @ LABEL Z$&" Stress Profiles (psi tens+)"
7740 MOVE 25,8 @ CSIZE 3 @ LABEL "Bottom" @ MOVE 25,4 @ LABEL " Slab"
7760 MOVE 47.5,8 @ LABEL "Exterior" @ MOVE 47.5,4 @ LABEL "  Web"
7780 MOVE 70,8 @ LABEL "Interior" @ MOVE 70,4 @ LABEL "  Web"
7800 MOVE 92.5,8 @ LABEL "Exterior" @ MOVE 92.5,4 @ LABEL "Top Slab"
7820 MOVE 115,8 @ LABEL "Interior" @ MOVE 115,4 @ LABEL "Top Slab"
7840 LDIR 90 @ MOVE 4,55 @ LABEL "Height above Soffit (inch)"
7860 GOTO KYLBL
7880 PRFSET2: LOCATE LX1,LX2,LY1,LY2 @ FXD 3,0
7900 SCALE -1,.5,0,Y9 @ CSIZE 3
7920 IF LX1=15 THEN LAXES .1,10,-1,0,5,5,3 ELSE LAXES .1,0,-1,0,5,0,3
7940 AXES .1,10,.5,Y9,5,5,3 @ RETURN
7960 END
```